# The role of the PI3K/AKT signalling pathway during infectious bronchitis virus infection

Thesis submitted in accordance with the requirements of the University of Liverpool for the degree of Doctor in Philosophy by Ambalika Batra

September 2016

# The Role of the PI3K/AKT signalling pathway during infectious bronchitis virus infection

Ambalika Batra

## Abstract

Infectious bronchitis is a highly contagious respiratory disease that results in reduced egg production and can be fatal in young birds. It has recently been identified as the most economically detrimental disease to the poultry industry. It is caused by the gammacoronavirus infectious bronchitis virus (IBV), which is endemic in most countries worldwide. All viruses modulate cellular processes to establish themselves within the cell. The cellular PI3K/AKT signalling pathway is often modified by viruses and plays a crucial role in the regulation of many cellular processes. In this project the activation of the PI3K/AKT signalling pathway and downstream processes such as apoptosis, translation and macropinocytosis were investigated during IBV infection. Techniques such as western blotting, immunofluorescence, flow cytometry and protein expression were used to determine the effect of IBV infection on modulation of the signalling pathway, as well as the downstream cellular effects of the modulation. This study demonstrates that IBV requires an active PI3K/AKT pathway for efficient replication, and that infection with IBV induces phosphorylation of AKT in a PI3K-dependent manner in mammalian and avian cells. This activation occurs late during infection in mammalian cells. However, in avian cells activation occurs in a biphasic manner at both an early and late time point during infection. To summarise the findings, a model is presented to describe the role of the PI3K/AKT signalling pathway during IBV infection.

This study highlights the importance of the PI3K/AKT signalling pathway during IBV infection and may be applied to other human and livestock coronaviruses for development of therapeutics or novel vaccines.

# Acknowledgements

I would like to thank my supervisory team for all of their guidance and advice over the years. Mark, thank you for being supportive (even when I wasn't particularly rational) and for always finding time for me. Helena, thank you for all of the support and patience you have shown me. You are a fantastic role model to women in science and I wish you all the best in your new adventure. Julian, thanks for the input over the years and for giving me a university to graduate from!

Thank you to everyone in the Avian Programme at The Pirbright Institute who have offered advice, direction and friendship over the years. Thank you to the Genetics and Genomics group (past and present). Particularly Karen whose unfailing kindness, support and humour helped me through the 4 years. Thank you also to everyone in the avian endemic viruses group for having me in your lab, answering my questions and putting up with me popping in, making a mess and leaving!

To all of the old Compton students, Tom P, Joe, Tom W and Phoebe thank you for the friendships and amazing times we had. Ross, I promise I'll always try to live somewhere interesting for you. To all the new Pirbright students, thanks for helping me through the last year and distracting me with wine, good food and fantastic friendships.

Finally, I'd like to thank my family for all of their love and support. To my little brothers, I will now only respond if called Dr Ambi! To my sister and best friend who has found success despite having a less cool and geeky sister. Thank you for putting up with me, not replacing me and always being there to remind me of the things that matter the most. To Papa and Rina, thank you for believing in me. Papa, even when you didn't have my hand you always had my back. To Mum, the love, support, guidance and opportunities you have given me throughout my life have allowed me write this epic book. I hope you think it was worth it! Thank you for being the amazing, strong and inspirational role model that every woman needs.

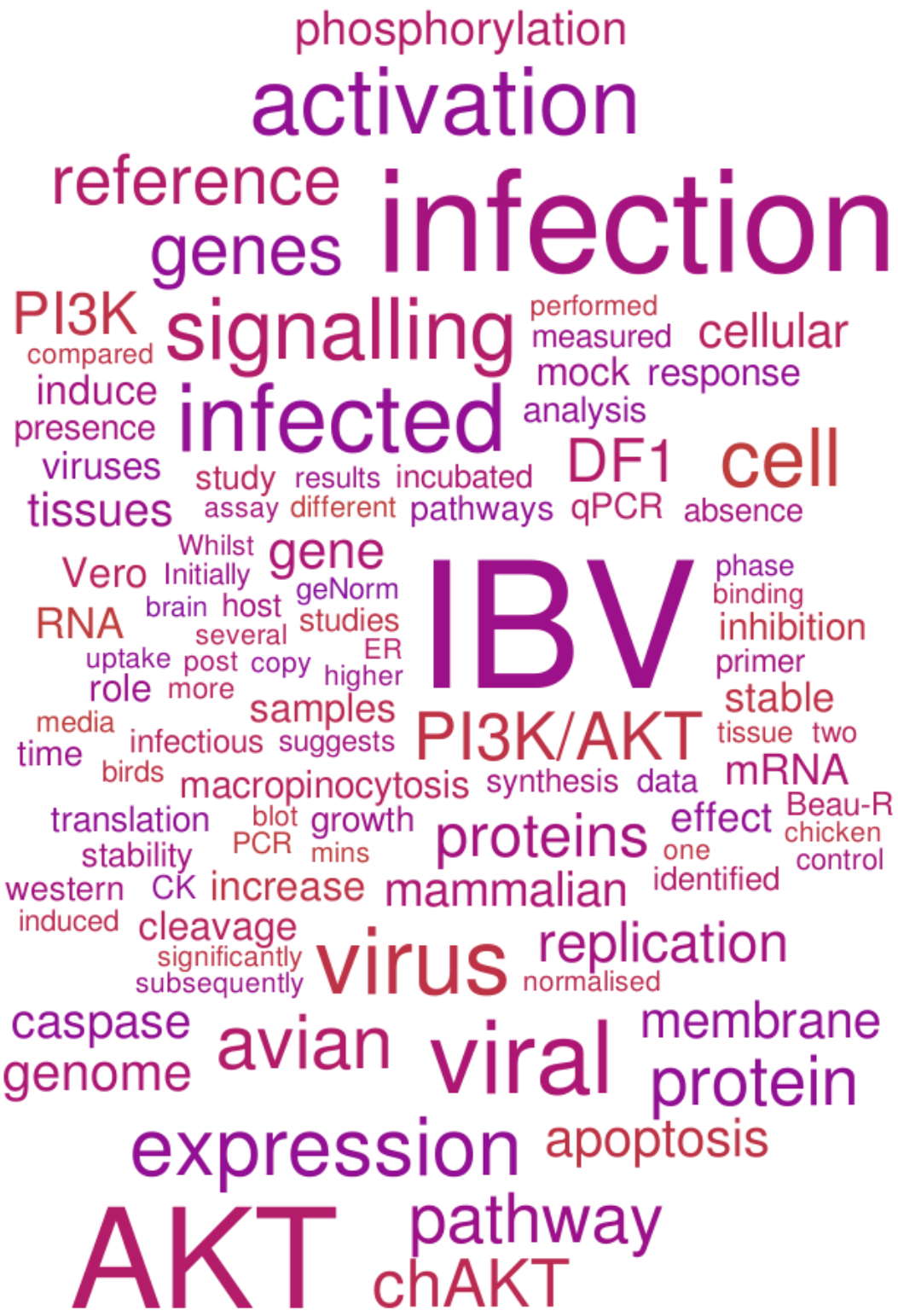
phosphorylation
activation
reference
infection
genes
PI3K
signalling
performed
measured
cellular
compared
induce
infected
mock
response
presence
analysis
viruses
DF1
cell
study
results
incubated
tissues
assay
different
pathways
qPCR
absence
Whilst
gene
Vero
Initially
IBV
phase
binding
geNorm
brain
host
RNA
studies
inhibition
several
ER
uptake
post
copy
primer
higher
role
more
stable
samples
media
PI3K/AKT
tissue
two
infectious
suggests
time
mRNA
birds
macropinocytosis
synthesis
data
translation
blot
growth
proteins
effect
Beau-R
chicken
PCR
one
stability
control
western
CK
increase
mammalian
identified
induced
cleavage
replication
virus
significantly
subsequently
normalised
caspase
membrane
avian
viral
genome
protein
expression
apoptosis
AKT
pathway
chAKT

# Table of Contents

# List of Figures

**CHAPTER 1**

**CHAPTER 3**

**CHAPTER 4**

**CHAPTER 6**

# List of Tables

**CHAPTER 2**



**CHAPTER 3**



**CHAPTER 5**

# Abbreviations

4E-BP1 – eIF4E-Binding Protein 1

ANOVA – Analysis Of Variance

Apaf-1 – Apoptotic Protease Activating Factor -1

APN – Aminopeptidase N

ATF6 – Activating Transcription Factor 6

Bad – Bcl-2 Associated Death Promoter

Bcl-2 – B-Cell Lymphoma 2

BEI – Binaryethylemine

BES – N,N-Bis(2-Hydroxyethyl)Taurine

BSA – Bovine Serum Albumin

CAD – Caspase-Activated Deoxyribonuclease

cDNA – Complementary DNA

CK Cells – Chick Kidney Cells

CPE – Cytopathic Effect

Cq – Quantitation Cycle

DAPI – 4',6-Diamidino-2-Phenylindole

DISC – Death-Inducing Signalling Complex

DMEM – Dulbeccos Minimum Essential Medium

DMSO – Dimethyl Sulfoxide

DNA – Deoxyriobonucleic Acid

Dpi – Days Post Infection

dsRNA – Double-Stranded RNA

E – Viral Envelope Protein

EGF – Epidermal Growth Factor

eIF2α – Eukaryotic Translation Initiation Factor 2α

eIF4A – Eukaryotic Translation Initiation Factor 4A

eIF4E – Eukaryotic Translation Initiation Factor 4E

eIF4F – Eukaryotic Translation Initiation Factor 4F

eIF4G – Eukaryotic Translation Initiation Factor 4G

ER – Endoplasmic Reticulum

ERGIC – ER-Golgi Intermediate Compartment

FADD – Fas Associated Via Death Domain

FCS – Foetal Calf Serum

FITC – Fluorescin Isothiocyanate

FOXO1 – Forkhead Box Protein O1

GC – Guanine-Cytosine

gDNA – Genomic DNA

GSK-3β – Glycogen Synthase Kinase 3 Beta

HIV – Human Immunodeficiency Virus

Hpi – Hours Post Infection

IAV – Influenza A Virus

IBDV – Infectious Bursal Disease Virus

IBV – Infectious Bronchitis Virus

IFN – Interferon

IRE1 – Inositol-Requiring Enzyme 1

LPS – Lipopolysaccharide

M – Viral Membrane Protein

MDA5 – Melanoma Differentiation-Associated Protein 5

MEM – Minimum Essential Medium

MERS-Cov – Middle East Respiratory Syndrome Coronavirus

MIQE – Minimum Information for the Publication of Quantitative Real-Time PCR Experiments

mRNA – Messenger RNA

mTOR – Mechanistic Target of Rapamycin

mTORc – Mammalian Target of Rapamycin Complex

N – Viral Nucleocapsid Protein

NF-κB – Nuclear Factor- κB

No-RT – No Reverse Transcriptase Control

NS1 – Influenza Non-Structural Protein 1

Nsp – Non-Structural Protein

NTC – No Template Control

ORF – Open Reading Frame

pAKT – Phosphorylated AKT

PBSa – Phosphate Buffered Saline A

PCR – Polymerase Chain Reaction

PDK1 – Protein Kinase 1

PERK – Protein Kinase R-Like ER Kinase

PGDF – Platelet-derived growth factor

PH-Domain – Pleckstrin Homology Domain

PI – Propidium Iodide

PI3K – Phosphatidylinositol-3-Kinase

$PIP_2$ – Phosphatidylinositol 4,5-Biphosphate

$PIP_3$ – Phosphatidylinositol 3,4,5-Trisphosphate

PKB – Protein Kinase B

PKC – Protein Kinase C

PMA – Phorbol Myristate Acetate

PRRSV – Porcine Respiratory and Reproductive Syndrome Virus

PS – Phosphatidylserine

PTEN – Phosphatase and Tensin Homolog

qPCR – Quantitative Polymerase Chain Reaction

RdRp – RNA-Dependent RNA Polymerase

RLU – Relative Light Units

RNA – Ribonucleic Acid

Rq – Relative Quantities

RTK – Receptor Tyrosine Kinase

S – Viral Spike Protein

SARS-Cov – Severe Acute Respiratory Syndrome Coronavirus

SDS-PAGE – Sodium Dodecyl Sulphate-Polyacrylamide Gel Electrophoresis

SEM – Standard Error of the Mean

sgRNA – Sub-Genomic RNA

SNX – Sorting Nexin Protein 5

TBE – Tris/Borate/EDTA Buffer

TCID – Tissue Culture Infectious Dose

TEM – Transmission Electron Microscopy

TLR3 – Toll-Like Receptor 3

TUNEL – Terminal Deoxynucleotidyl Transferase dUTP Nick End Labelling

TM – Transmembrane Domain

TNF – Tumour Necrosis Factor

TOC – Tracheal Organ Culture

TRS – Transcription-Regulating Sequence

UPR – Unfolded Protein Response

Vpg – Viral Genome-Linked Protein

VSVG – Vesicular Stomatitis Virus Glycoproteins

WT – Wild Type

ZAP – Zinc-Finger Antiviral Protein

# Publications and Presentations

## Publications

Batra, A., Maier, H. J. & Fife, M. S. 2016. Selection of reference genes for gene expression analysis by real-time qPCR in avian cells infected with infectious bronchitis virus. *Avian Pathology***,** 1-20

Staines, K.*, Batra, A.*, Mwangi, W.*, Maier, H. J., Van Borm, S., Young, J. R., Fife, M.** & Butter, C.** 2016. A Versatile Panel of Reference Gene Assays for the Measurement of Chicken mRNA by Quantitative PCR. *PLoS ONE,* 11**,** e0160173.

Batra, A., Maier, H.J., Fife, M.S., 2016. Activation of PI3K/AKT signalling pathway by avian infectious bronchitis virus. JVI *(In preparation)*

## Presentations

Batra, A., Maier, H.J., Fife, M.S., 2016. Infectious Bronchitis and the PI3K/AKT signalling pathway. 9th International Symposium on Avian Corona- and Pneumoviruses and Complicating Pathogens, Utrecht, The Netherlands *(Oral presentation)*

Batra, A., Maier, H.J., Hiscox, J.A., Fife, M.S., 2016. The role of AKT activation during infectious bronchitis virus infection. Microbiology Society Annual conference, Liverpool, UK *(Oral presentation)*

Batra, A., Maier, H.J., Hiscox, J.A., Fife, M.S., 2015. PI3K/AKT signalling during infectious bronchitis virus infection. Annual Infection and Global Health (IGH) Day, University of Liverpool. UK. *(Oral presentation)*

Batra, A., Maier, H.J., Hiscox, J.A., Fife, M.S., 2015. PI3K/AKT signalling during infectious bronchitis virus infection. Food Security: Improving Approaches to Prevent and Control Viral Diseases of Livestock and Poultry, British Council Research Links Workshop, Istanbul, Turkey *(Oral presentation)*

Batra, A., Maier, H.J., Britton, P., Hiscox, J.A., Fife, M.S., 2015. The role of AKT activation during infectious bronchitis virus infection. Society of General Microbiology Annual conference, Liverpool, UK *(Poster presentation)*

Batra, A., Maier, H.J., Britton P., Hiscox, J.A., Fife, M.S., 2014. AKT activation during infectious bronchitis virus infection. XIIIth International Nidovirus Symposium, Salamanca, Spain *(Poster presentation)*

Batra, A., Maier, H.J., Britton, P., Hiscox, J.A., Fife, M.S., 2014. AKT activation during infectious bronchitis virus infection. Society of General Microbiology Annual conference, Liverpool, UK *(Poster presentation)*

# Chapter 1

# Introduction

## 1.1 The Poultry Industry and Avian Diseases

Domestic chickens (*Gallus gallus domestica*) belong to the genus *Gallus* of the family *Phasianidae* and order *Galliformes* (Figure 1.1). Their closest relative is the red junglefowl (*Gallus gallus*) native to Asia, and present in Indonesia right through to China (Kan et al., 2010). There are 281 recognized species of game birds, divided amongst 81 genera, in the order *Galliformes* (Jourdan et al., 2012, Westneat, 1992). The current form of egg layer came about through years of domestication of the wild Red Junglefowl (Moiseyeva et al., 2003). In 2004, the chicken became the first agricultural animal and the first bird to have its genome sequenced (ICGSC, 2004). The genome of the chicken is less than half the size of a mouse at 1.07 Gb. It consists of 38 autosomes and 2 sex chromosomes referred to as Z and W, with the females carrying the ZW chromosomes (Figure 1.2). Their chromosomes vary much more in size than that of mammals, ranging from 200 Mb to 5 Mb (Romanov et al., 2009). The distribution of chicken breeds around the globe can be significantly attributed to human movement, as they lack the ability to fly or swim for long distances. This wide distribution highlights how important their trade has been throughout history. The British poultry industry itself produces around 875 million chickens a year, in over 2,500 poultry farms across the UK (BPC, 2016). Poultry is the staple protein in the diet of many communities worldwide, where other forms of protein such as pork or beef may be prohibited by religion or law. It is because of this, and the relatively low production costs, that levels of consumption have been increasing yearly. Consumption of poultry has risen from 81 to 89 million metric tons in the last four years (FAS, 2012). Those numbers, when compared to the consumption of beef and veal at only 59 million metric tons, show how vital the poultry industry is.

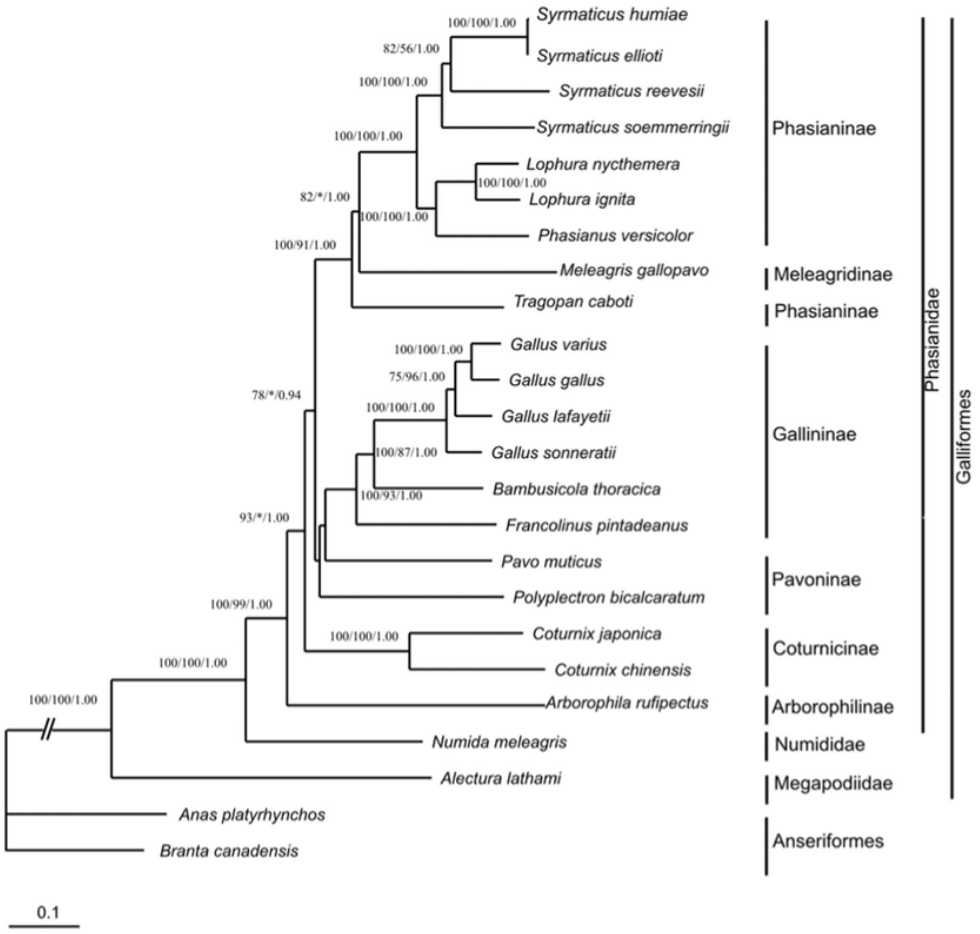


**Figure 1.1. Phylogenetic tree of the relationships between Galliformes**. Galliformes are members of the class *Aves* whose closest relatives are *Crocodilians*. *Gallus gallus domesticus* belong to the family *Phasianidae* and their closest relative is the Red junglefowl, *Gallus gallus*. [Sourced from Kan et al., (2010)]

The supply of poultry, to meet the ever-increasing demand, is often hindered by outbreaks of avian diseases. There are over 140 diseases and conditions that affect the poultry industry, with more than 12 of those being viral diseases (British Poultry Council, 2016). Amongst the most economically detrimental are Newcastle disease, Gumboro, and Avian Influenza (AI). As well as affecting the production of chickens, some viruses, such as Newcastle disease virus, are known to also infect turkeys, pigeons and geese. One avian viral disease of economic importance worldwide is Infectious Bronchitis.

### 1.1.1 Infectious Bronchitis

In 2005 the Department for Environment Food and Rural Affairs (DEFRA) commissioned a report in which Infectious Bronchitis (IB) was identified as being the most economically detrimental disease to the UK poultry industry (DEFRA, 2005). The disease was first described in 1931 in the USA and is currently endemic worldwide (Schalk and Hawn, 1931). Infectious Bronchitis is caused by the virus, infectious bronchitis virus (IBV), which is air-borne, spread by direct chicken to chicken contact or spread indirectly by mechanical means such as contaminated surfaces or drinking water. IBV is only known to naturally infect chickens and pheasants, where the infection establishes itself initially within the respiratory tract (Gough et al., 1977). Infection often leads to secondary bacterial infections, which contribute significantly to the pathology and rate of mortality (Vandekerchove et al., 2004). However, the virus can spread to other organs such as the oviducts, where it interferes with egg production and laying (Cavanagh, 2007, Raj and Jones, 1997). As a result, IB commonly leads to a reduced level of egg laying and a decrease in egg quality (Crinion, 1972). Control of the disease involves the use of both live-attenuated and inactivated vaccines. However, the large number of serotypes, poor cross-protection between the serotypes and the ability of the virus to mutate and recombine resulting in high levels of antigenic shift and drift, make vaccine programmes challenging (Cook et al., 2012).

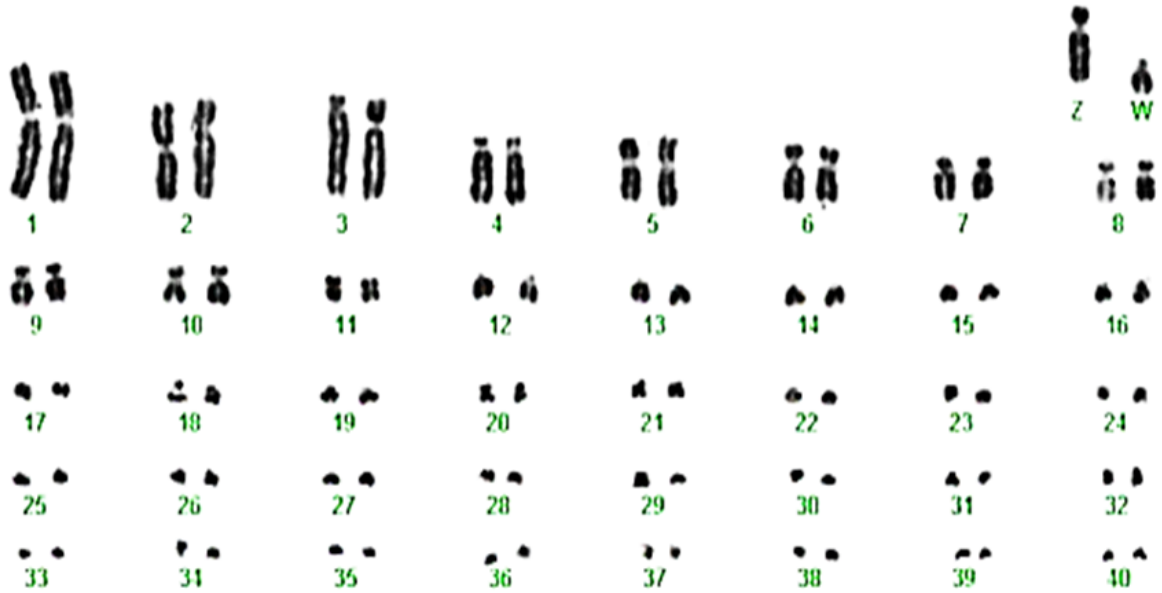


**Figure 1.2. Karyotype of the female chicken** showing 82 macro- and microchromosomes including 40 autosome pairs and two sex chromosomes (Z and W). [Sourced from Romanov et al, (2009)].

## 1.2 Infectious Bronchitis Virus

### 1.2.1 Virus classification – *Coronaviridae*

The *Coronavirinae* sub-family is separated into four genera, the α-, β-, γ- and δ-coronaviruses, devised based on sequence information of the antigenic relationships between the viruses. IBV is classed as a *γ-coronavirus* whereas SARS-CoV, and the recently emerged MERS-CoV are *β-coronaviruses*. The emergence of SARS- and MERS-CoV has attracted much attention to the *Coronavirinae* family. Both viruses are thought to have originated in bats (Li et al., 2005, Wang et al., 2014b), before crossing into the human population through an intermediate host (Alagaili et al., 2014, Haagmans et al., 2014, Hemida et al., 2014, Wang and Eaton, 2007). The ability of coronaviruses to jump between species may be partly attributed to high sequence variation in the spike glycoprotein, a class 1 fusion protein, which is largely responsible for the control of entry (Belouzard et al., 2012).

### 1.2.2 Genome organisation & Viral proteins

IBV is a circular virion with spike-like projections from its membrane caused by the spike proteins. These give the virus, and other coronaviridae, the characteristic 'crown', which can be seen in images taken by transmission electron microscopy (TEM), leading to the term 'corona-virus' (Figure 1.3). The basic structure of IBV can be seen in Figure 1.4A. The virus has three structural membrane proteins, the membrane (M) and envelope (E) and spike (S) proteins are embedded in the viral membrane. IBV S projects out to the exterior of the virion. A schematic of the three transmembrane proteins, S, M and E can be seen in Figure 1.4B. The nucleocapsid protein (N) of IBV encloses a non-segmented, single-stranded, positive sense RNA genome of approximately 27kb (Figure 1.4A). A schematic of the genome is shown in Figure 1.5.

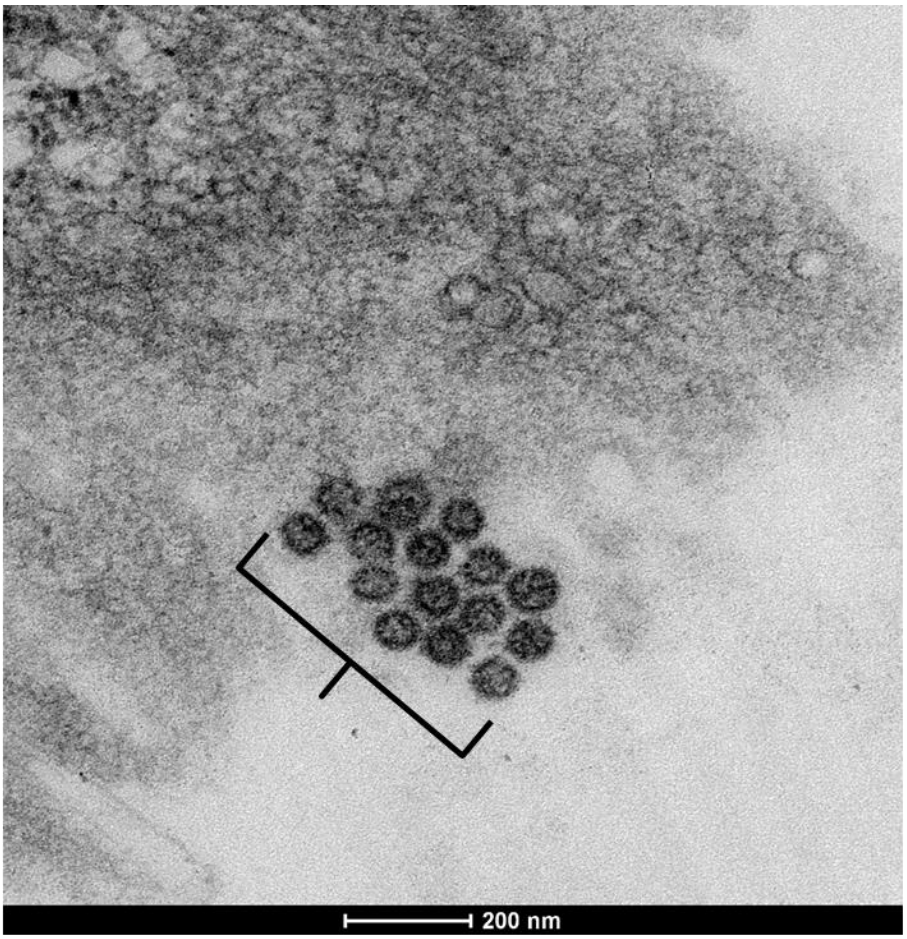


**Figure 1.3 Transmission electron microscopy image of IBV virions in DF1 cells** (highlighted by the black brackets). Projections on the surface of the virions are visible, caused by the viral spike proteins. DF1 cells infected with Beau-R for 24 hpi by Ambalika Batra. TEM performed and image taken by Jennifer Simpson, The Pirbright Institute.

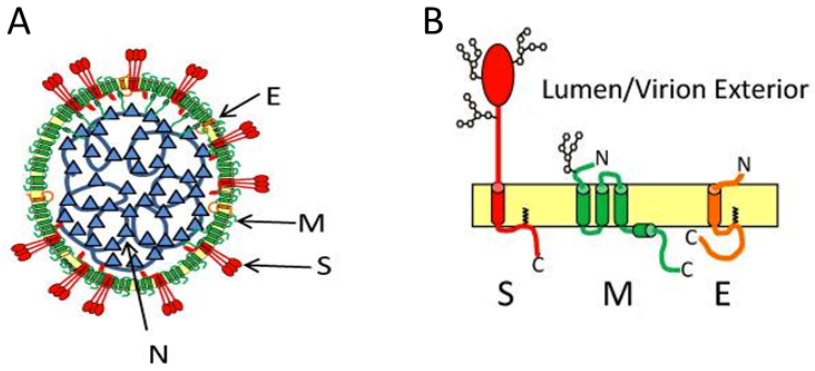


**Figure 1.4. Structure of the coronavirus.** (A) The spike protein (S) is found on the outer membrane of the virus and is involved in attachment to the cell. The membrane proteins (M) along with the envelope proteins (E) are involved in the assembly of the virus. The N protein forms part of the nucleocapsid. (B) The distribution of the S, M and E proteins along viral envelope. The S protein is embedded in the envelope and projects out to the exterior of the virus. [Adapted from Ruch et al, (2012)]

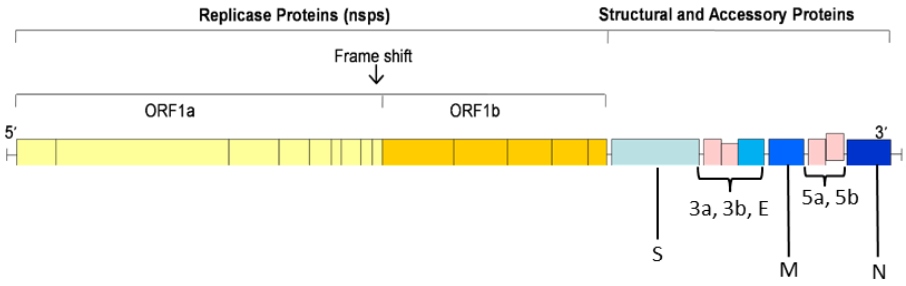


**Figure 1.5. Schematic of the IBV genome and encoded proteins**. The schematic outlines the presence of 4 regions that code for structural proteins. The Nsp (non-structural proteins) coded for by ORF1a and 1b are cleaved post-translationally to form the non-structural proteins numbered 1-15. In γ-coronaviruses such as IBV, the nsp1 is absent. [Maier – unpublished]

*ORF1a and 1b*

Gene 1 occupies approximately two-thirds of the genome and encodes two partially overlapping reading frames (open reading frame (ORF) 1a and 1b) at the 5'-end of the genome. These encode the viral RNA polymerase and the replicase proteins as two large polyproteins. During synthesis the polyproteins are cleaved by virus-encoded proteinases into 15 non-structural proteins (nsps) (Ziebuhr et al., 2000), which assemble at replication complexes. Whilst morphologically similar, *β*- and *γ-coronaviruses* differ in their genome composition. For example, the genome of *β-coronaviruses* such as SARS-CoV encodes 16 non-structural proteins (nsps), whereas *γ-coronaviruses,* such as IBV, lack nsp1 and encode only 15 nps. The SARS-CoV nsp1 has been demonstrated to be involved in (Lokugamage et al., 2012) host-translational shut-off. However, the 5b protein has been implicated in this role during IBV infection (Kint et al., 2016). Other nsps were found to be associated with the activation of cellular processes. For example, the nsp6 of IBV has been shown to induce autophagy during infection (Cottam et al., 2014).

*Spike Protein (S)*

Gene 2 encodes the S protein which is post-translationally cleaved into the N-terminal S1 (92 kDa) and the carboyxl-terminal S2 (84 kDa). S is found in the viral envelope and projects out onto the surface of the virion. It is a type 1 transmembrane protein consisting of a large ectodomain and short endodomain. The large ectodomain of the protein is divided into two subdomains, S1 with receptor binding properties, and S2 which contains the fusion machinery (Knipe and Howley, 2013). The S protein of coronaviruses is responsible for receptor binding and membrane fusion, and is therefore a critical determinant of tissue and cellular tropism (Casais et al., 2003). The first proteolytic cleavage site was found to be a furin cleavage site at the S1/S2 junction and is common amongst all IBV strains. A further site has been identified in S2, S2' (Belouzard et al., 2009). This second cleavage site is differentially cleaved between strains of IBV. The lab adapted strain

of IBV, Beau-R, acquired a mutation at its S2' site which is deemed ideal for furin recognition and cleavage (Casais et al., 2001). The presence of the second S2' cleavage site is thought to be the reason for the extended tissue and cellular tropism, characteristic of the Beau-R strain (Casais et al., 2004).

*Envelope Protein (E)*

The E protein is found embedded in the envelope and is a small 10 kDa protein with a single predicted hydrophobic domain (Ruch and Machamer, 2012). Coronavirus E proteins are generally present in low concentration in virions (Yu et al., 1994, Liao et al., 2006), however are abundant in infected cells where they are targeted to the Golgi and plays a role in assembly of new virions and budding (Liu and Inglis, 1991a, Corse and Machamer, 2000, Corse and Machamer, 2002). IBV E also plays a role in modulating the secretory pathway by altering the luminal environments and re-arranging secretory organelles and host cell membranes such as the Golgi complex. This promotes viral replication and enables efficient trafficking of new virions. (Ruch and Machamer, 2011, Ruch and Machamer, 2012, Lavi et al., 1996).

*Accessory Proteins 3a & 3b*

As well as structural proteins, the IBV genome encodes at least four accessory proteins translated from two polycistronic mRNAs (Liu et al., 1991, Liu and Inglis, 1991b, Liu and Inglis, 1992a, Liu and Inglis, 1992b). ORF 3a and 3b encode accessory proteins (Hodgson et al., 2006). The accessory proteins are small (50-300 aa) proteins that are not essential for virus replication (Hodgson et al., 2006) (Narayanan et al., 2008). During infection with IBV the IFN response of infected cells is suppressed early during infection (Kint et al., 2015b), and the accessory proteins 3a and 3b are involved in this resistance (Kint et al., 2015a).

*Membrane Protein (M)*

The structural membrane protein (M) is a transmembrane protein of between 25 and 33 kDa. The M protein is found embedded within the envelope and has three

domains, a short N-terminal ectodomain, transmembrane domain and a C-terminal endodomain (Armstrong et al., 1984). In infected cells, M is localised primarily in the Golgi and interacts with both E and N proteins to assemble new virions (Neuman et al., 2011, Narayanan et al., 2000, Corse and Machamer, 2003, Siu et al., 2008, Lim and Liu, 2001, de Haan et al., 2000). The M proteins of other coronaviruses such as MHV and SARS-CoV have also been implicated in the process of budding (Tooze et al., 1984), (Siu et al., 2008).

*Accessory Proteins 5a & 5b*

IBV is unique among coronaviruses as it encodes two ORF's, 5a and 5b, the proteins of which are not necessary for replication (Casais et al., 2005). The IBV accessory protein 5b has recently been implicated in host translational shutoff, where the production of host proteins is supressed and a selective increase in the production of viral proteins occurs (Kint et al., 2016).

*Nucleocapsid Protein (N)*

The coronavirus N protein is a soluble phosphoprotein with a molecular weight of ~ 50 kDa, that is involved in many processes during replication (Emmott et al., 2013). These include packaging of viral RNA (Davies et al., 1981, Spencer and Hiscox, 2006), acting as a chaperone for viral RNA, control of transcription, and the modulation of immune responses (Zúñiga et al., 2010).

A final 3'UTR is present downstream of gene 6 which is highly conserved among different strains of IBV (Collisson et al., 1990).

In 2001 a reverse genetics system was developed for IBV that allowed the generation and manipulation of full-length genomic cDNAs of the viral genome (Casais et al., 2001). These full-length cDNAs were cloned into the vaccinia virus genome and recombinant IBV was recovered after *in situ* synthesis of IBV RNA using the bacteriophage T7 RNA polymerase expressed from recombinant fowlpox virus. The development of the reverse genetics system has enabled research into

various aspects of the biology of IBV infections. For example, the system was used to investigate the importance of the S protein in cellular tropism, pathogenicity and immunogenicity (Casais et al., 2003, Hodgson et al., 2004)

## 1.2.2 Viral pathogenesis

Infectious bronchitis virus initially infects the respiratory tract where it can be detected in epithelial cells of the trachea and lung (Hofstad and Yoder, 1966, Ambali and Jones, 1990, Lee et al., 2002, Meir et al., 2004). The highest levels of tissue infection were seen at 2 dpi but were lower by 5 dpi. Accordingly, viral titres were maximal in the nose and trachea within 3 dpi and were high for a further two to five days (Ambali and Jones, 1990). In addition to respiratory organs, several strains of IBV have been isolated from the cecal tonsils, lymphoid organs that elicit protective immunity against pathogens in the intestinal tract, and the kidneys (Benyeda et al., 2009, Lucio and Fabricant, 1990, Terregino et al., 2008, Ganapathy et al., 2012). These include the IBV strain, M41, which is neuropathogenic and causes mortality (Cook et al., 2001). Some strains of IBV has also been detected in the testes (Boltz et al., 2004) and ovaries (Zhong et al., 2016), where infection causes reduced fertility and egg laying.

The host and viral determinants of IBV pathogenicity are still not fully understood. The disease is characterised by increased oculonasal secretion and excess of mucus in the trachea. It supresses weight gain and where the virus also replicates in the oviduct, reduces egg production. The severity of disease has often been measured by investigating levels of ciliostasis in tracheal sections (Donnelly et al., 1974). The cilia and mucociliary apparatus of the respiratory tract allow for protection against pathogens. However, during IBV infection, the cilia of the trachea cease to move and slough off from the trachea. Recently, a study has identified a possible link between levels of apoptosis induced during infection and disease (Chhabra et al., 2016). In particular, the study demonstrated that infection of primary

embryonic kidney cells, with strains of IBV that predominantly cause nephritis (e.g. QX), resulted in higher levels of apoptosis compared to M41, which primarily causes respiratory lesions. This up-regulation of apoptosis was also coordinated with an up-regulation of TLR3, MDA5 and IFN-β in chick kidney cells during infection with QX, compared to M41. These results were reversed in tracheal organ cultures (TOCs) where M41 infection resulted in an up-regulation in the immune-modulatory genes, and QX did not. It was therefore hypothesised that the host innate immune response, and in particular apoptosis, is a key determinant of pathogenicity during IBV infection (Chhabra et al., 2016).

### 1.2.3 Viral Replication

A schematic of generalised coronavirus replication is shown in Figure 1.6.

*Viral Entry*

IBV entry into the host cell is less well characterised than other coronaviruses. To initiate entry, the coronavirus S glycoprotein mediates attachment to the host cell receptors. The cellular receptors vary between different coronaviruses. For example, α-coronaviruses, such as the feline coronavirus and the human coronavirus 229E, bind to aminopeptidase N on the cell surface (Tresnan et al., 1996, Yeager et al., 1992). The cellular receptors for β-coronaviruses are varied, with SARS-CoV binding to angiotensin-converting enzyme 2 (Li et al., 2003), and MHV binding to carcinoembryonic antigen-related cell adhesion molecule 1 (Williams et al., 1991). However, other β-coronaviruses such as bovine coronavirus and porcine hemagglutinating encephalomyelitis virus recognise and bind to sialic acids on the cell surface such as N-acetyl-9-O-acetylneuraminic acid (Vlasak et al., 1988, Schultze and Herrler, 1992, Schultze et al., 1990). The cellular receptors for γ-coronaviruses such as IBV have not been fully characterised. However, IBV is known to bind to α2,3 linked sialic acids on the cell surface, but it is not known if this is the only factor involved (Winter et al., 2006) (Promkuntod et al., 2014).

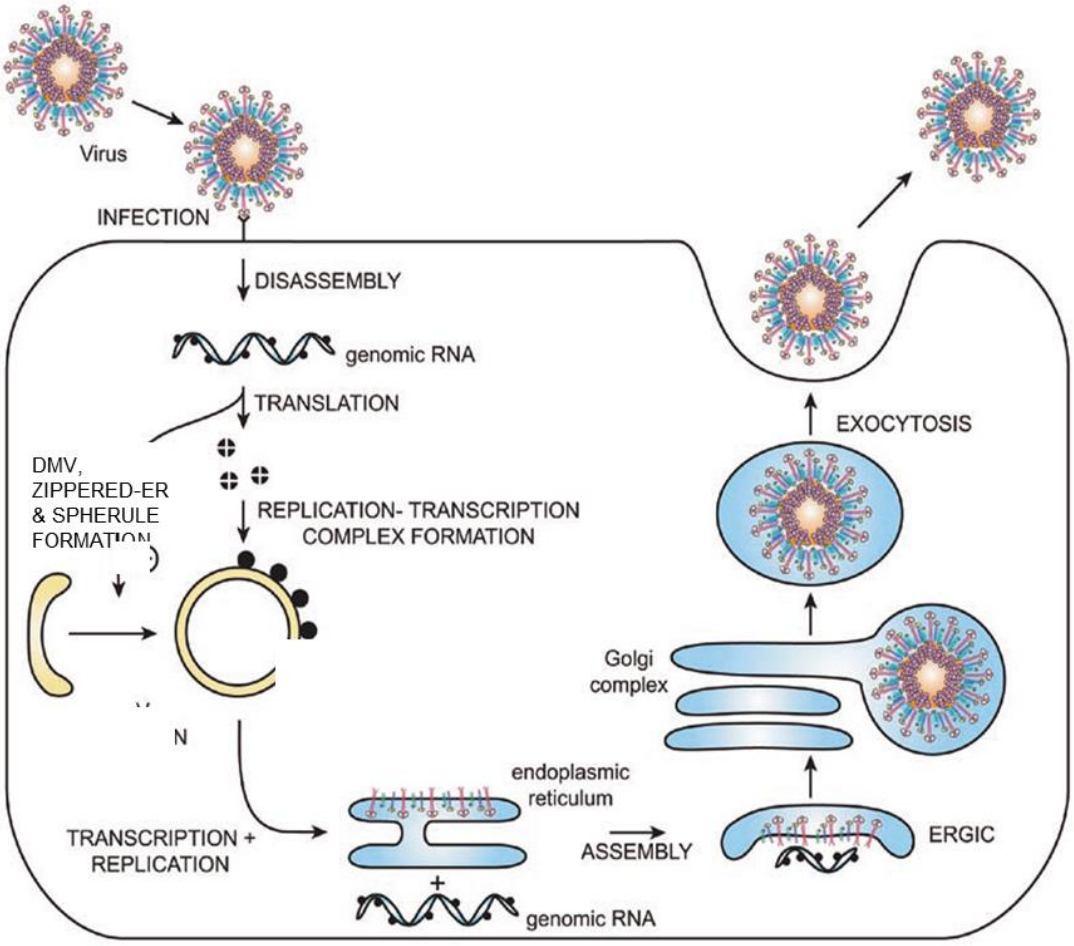


**Figure 1.6. Replication cycle of IBV.** The virus enters the cell through membrane fusion. The virion then disassembles and the genomic viral RNA is released into the cytoplasm. Double-membrane vesicles, along with zippered-ER and spherules that are thought to be the site of replication. Viral mRNA is translated by the host machinery to produce four structural and four accessory proteins. The genome is replicated, bound to the nucleocapsid protein and assembled into a new virus particle at the ERGIC (endoplasmic reticulum/golgi inter-compartment). New virus particles are then released by endocytosis. [Adapted from de Haan and Reggiori, (2008)] .

When S1 binds to the receptor, conformational changes are induced in the spike protein, which lead to viral-cell fusion and release of the nucleocapsid into the cytoplasm (Bonavia et al., 2003). In the case of SARS-CoV and the MHV strain A59, the virus enters the cell via the clathrin-dependent endocytosis pathway, before being transported to early endosomes where entry is pH-dependent (Inoue et al., 2007, Yang et al., 2004a, Eifart et al., 2007). The exact mechanism by which IBV enters the cell is unknown. Patterson et al (1976) observed IBV entry by electron microscopy and determined that entry did not occur by fusion of viral and cellular plasma membranes and instead suggested uptake via an endocytic pathway. Chu et al., (2006) also observed PH-dependent fusion of the viral and cellular membranes and this is now the accepted theory.

*Viral replication and protein synthesis*

The viral mRNA is recognised by host machinery due to the presence of a 5'-cap and 3'-polyA tail on the viral mRNA. Once inside the cytoplasm, viral genomic RNA acts as mRNA for the translation of the replicase polyproteins pp1a and pp1ab in the cytoplasm. The virus encoded proteases, nsp3 and nsp5, proteolytically cleave the replicase polyproteins into 15 non-structural proteins. The expression of viral replicase proteins results in the rearrangement of cellular membranes to assemble viral replication complexes in the majority of positive-strand RNA viruses. The types of membrane rearrangements formed range from single-membrane or double-membrane vesicles to convoluted membranes and small membrane invaginations called spherules (Blanchard and Roingeard, 2015). The replication proteins of positive-strand RNA viruses are often found within these membranes and therefore the replication complexes are likely to be associated with these membrane rearrangements. For example, replication of poliovirus results in the formation of double-membrane vesicles that form from single-membrane vesicles possibly originating from Golgi membranes (Schlegel et al., 1996). The outer membrane of both the single- and double-membrane vesicles is the location of poliovirus replicase

proteins and nascent viral RNA (Belov et al., 2012). The formation of membrane re-arrangements has also been investigated during some coronavirus infections. SARS-CoV and MHV induce double-membrane vesicles derived from the ER (Knoops et al., 2008, Ulasli et al., 2010). Connected to the double-membrane vesicles is a series of convoluted membranes also derived from the ER. The coronavirus replicase proteins are commonly found on both structures. The formation of membrane re-arrangements during IBV infection has recently been investigated by Maier et al. (2013b). In addition to double-membrane vesicles, infection of cells with IBV was found to induce the formation of novel structures termed zippered-ER, which were associated with small spherules. The spherules were connected to the zippered-ER and contained a channel with a diameter large enough to facilitate the movement of nucleotides and RNA structures. These structures had not previously been reported in coronavirus infections and are hypothesised to be the site of IBV replication.

All viruses of the *Nidovirales* order employ sub-genomic mRNA (sgRNA) to mediate expression of structural and accessory proteins. In particular the corona- and arteriviruses employ a discontinuous method of RNA synthesis (Lai & Cavanagh, 1997). Downstream of the replicase gene, the IBV genome encodes for structural and accessory proteins that are expressed from a set of at least five nested mRNAs (Sawicki et al., 2007, van Vliet et al., 2002). Each of these sgRNAs contain a common leader sequence, derived from the 5' terminus of the viral genome (van der Most and Spaan, 1995). The leader and coding sequences are joined by a transcription-regulating sequence (TRS) which is an important factor in sgRNA synthesis (Makino et al., 1991, van der Most et al., 1994, Zhang and Lai, 1994). The N protein of IBV is known to associate with the genomic RNA to form the nucleocapsid that is incorporated into new virions (Klumperman et al., 1994).

*Assembly of new virions and exit from the cell*

The viral structural proteins assemble and bud into the lumen of the ER-Golgi intermediate compartment (ERGIC) to form new virions (Krijnse-Locker et al., 1994). Virus particles then bud off from the Golgi and exit the cell by exocytosis (Tooze et al., 1987). The E, M and S proteins of IBV have all been implicated in the assembly of new virions and exit from the cell. The IBV E protein has been found to direct the release of virus-like particles from the Golgi (Corse and Machamer, 2000). Ruch and Machamer (2011) also demonstrated that when the transmembrane domain (TM) of IBV E was replaced with a non-oligomerizing TM domain of the vesicular stomatitis virus glycoprotein (VSVG), infectious virus particles were not released. Therefore, suggesting a role for IBV E in budding. The interaction of E and M proteins has been found to produce virus-like particles that are similar in size and shape to IBV virions (Corse and Machamer, 2002). The IBV S protein, when expressed alone has recently been found to accumulate near the virus assembly site (Lontok et al., 2004). It was also found to contain trafficking signals such as the ER retrieval signal, and a tyrosine-based endocytosis signal. Studies with IBV S-mutants lacking the endocytosis signal were not able to replicate (Youn et al., 2005). New virions are seen to be released from 6 hpi in cell culture. Whilst the replication cycle of IBV is non-lytic, cytopathic effect (CPE) is observed in IBV infected cells from 24 hpi.

## 1.3 PI3K/AKT signalling

### 1.3.1 AKT Isotypes

AKT, also known as protein kinase B (PKB) is a protein kinase that plays a critical role in the regulation of cell growth and survival. It has most notably been implicated in many forms of cancer such as thyroid cancer (Saji and Ringel, 2010), kidney cancer (Porta and Figlin, 2009) and prostate cancer (Shukla et al., 2007). AKT was first identified as a homolog of the retroviral oncogene viral AKT (v-AKT) (Bellacosa et al., 1991), and has since been categorised as a member of the AGC kinase

family. Members of the AGC kinase family, such as Protein Kinase C (PKC) and Phosphoinositide-dependent Protein Kinase 1 (PDK-1), share a homologous catalytic domain. The family consists of approximately 60 members that are phosphorylated at a serine (S) or threonine (T) residue (Fayard et al., 2005). These phosphorylation sites occur primarily close to lysine or arginine residues.

The PH (Pleckstrin-homology) domain, catalytic domain and the regulatory domain are all well conserved between AKT isotypes. In mammals there are three isotypes of AKT, AKT1, AKT2 and AKT3 (Figure 1.7). The PH domain of AKT is located at the N terminus and is conserved between other signalling molecules that bind phosphoinositides. The catalytic domain or kinase domain is situated in the centre of the protein and is the site of phosphorylation at T308 (in human AKT1). The regulatory domain is at the C-terminus of the protein and contains an amino acid sequence (F-P-Q-F-S-Y) which is conserved among the AGC kinase family in most mammalian isoforms. The regulatory domain of the kinase is also the location of the S473 phosphorylation site (in human AKT1). Whilst the mammalian isoforms have a high level of homology, studies using AKT knockout mice have documented phenotypic differences in their functions. The effect of deletion of the mammalian *AKT1* gene has been investigated in mutant mice (Yang et al., 2004b). Upon examination of the development of embryos in the uterus it was found that deletion of *AKT1* affected both placental development and animal growth (Cho et al., 2001b). Deletion of *AKT2* induced severe diabetes in knockout mice, indicating a role for the isotype in insulin signalling (Cho et al., 2001a). The tissue distribution of AKT2 also illustrates its role in glucose homeostasis, with it being found in high abundance in insulin-responsive organs and tissues such as the liver and skeletal muscle (Yang et al., 2003). The role of the *AKT3* gene in the postnatal development of the brain was identified in *AKT3* knockout mice. AKT3 mutant mice exhibited reduced brain size and weight, suggesting that AKT3 is an important factor in brain development (Yang et al., 2004b).

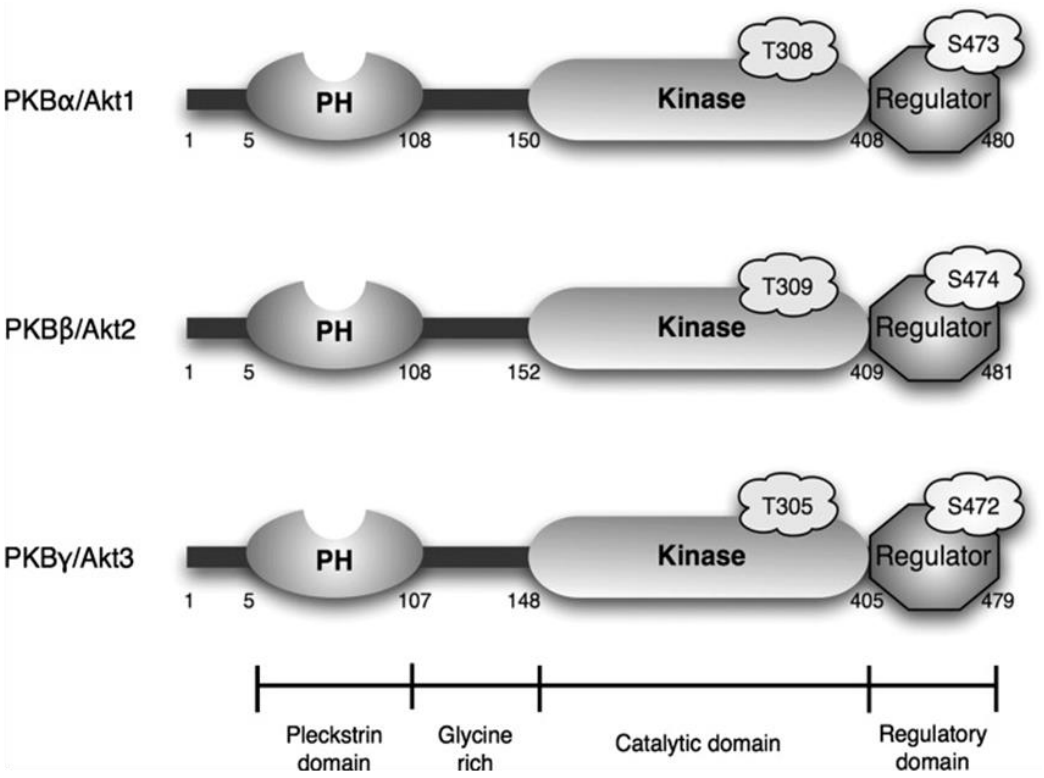


**Figure 1.7. Schematic showing the structure of the mammalian AKT isoforms**. The N-terminus contains a pleckstrin homology (PH) domain that mediates binding to $PIP_3$. The catalytic domain is the site of threonine phosphorylation, which along with phosphorylation of a C-terminus serine, is required for activation. [Adapted from Elghazi et al., 2007].

## 1.3.2 PI3K/AKT mammalian signalling pathway

AKT plays an integral part in many cellular processes including cell growth, cell death and protein synthesis. In most cases AKT works as part of the phosphoinositide-3 kinase (PI3K)/AKT signalling pathway where it is activated indirectly by PI3K, a membrane bound kinase (Figure 1.8). However, AKT can also be activated independently of PI3K, by PKA (cyclic AMP-dependent protein kinase) (Sable et al., 1997, Mahajan and Mahajan, 2012, Yoganathan et al., 2000, Persad et al., 2000, Yano et al., 1998), but will not be described here. Figure 1.8 shows the PI3K signalling pathway upstream of AKT activation.

Growth factors such as the platelet-derived growth factor (PDGF), epidermal growth factor (EGF), fibroblast growth factor (FGF) and the insulin-like growth factor 1 (IGF-1) bind to receptors on the surface of the cell. These receptors are often G-protein coupled receptors which then activate class I PI3Ks (Hawes et al., 1996). Class I PI3Ks are heterodimeric enzymes that contain a regulatory p85 subunit along with an enzymatic p110 subunit (Vanhaesebroeck et al., 1997). The majority are coupled to extracellular receptors and are therefore found at the plasma membrane. However, they are also present at the nuclear membrane along with AKT (Neri et al., 2002). Activation of PI3K leads to the phosphorylation of $PIP_2$ (Phosphatidylinositol 4,5-bisphosphate) into $PIP_3$ (Phosphatidylinositol 3,4,5-trisphosphate) and recruitment of AKT to plasma membrane. PI3K/AKT signalling can be inhibited by inhibition of PI3K activity using the small molecule inhibitor LY294002 (Vlahos et al., 1994). The pathway can also be inhibited at this step by PTEN, which actively dephosphorylate $PIP_3$ (Maehama and Dixon, 1998). The PH-domain of AKT facilitates the interaction between itself and $PIP_3$ (Thomas et al., Bellacosa et al., 1998). Once bound, a conformational change occurs in AKT allowing phosphorylation at T308 by PDK1 (Stephens et al., 1998, Andjelkovic et al., 1997, Alessi and Cohen, 1998). When a PH-domain deletion mutant of AKT was used, $PIP_3$ was not required for phosphorylation at T308 (Biondi et al., 2000).

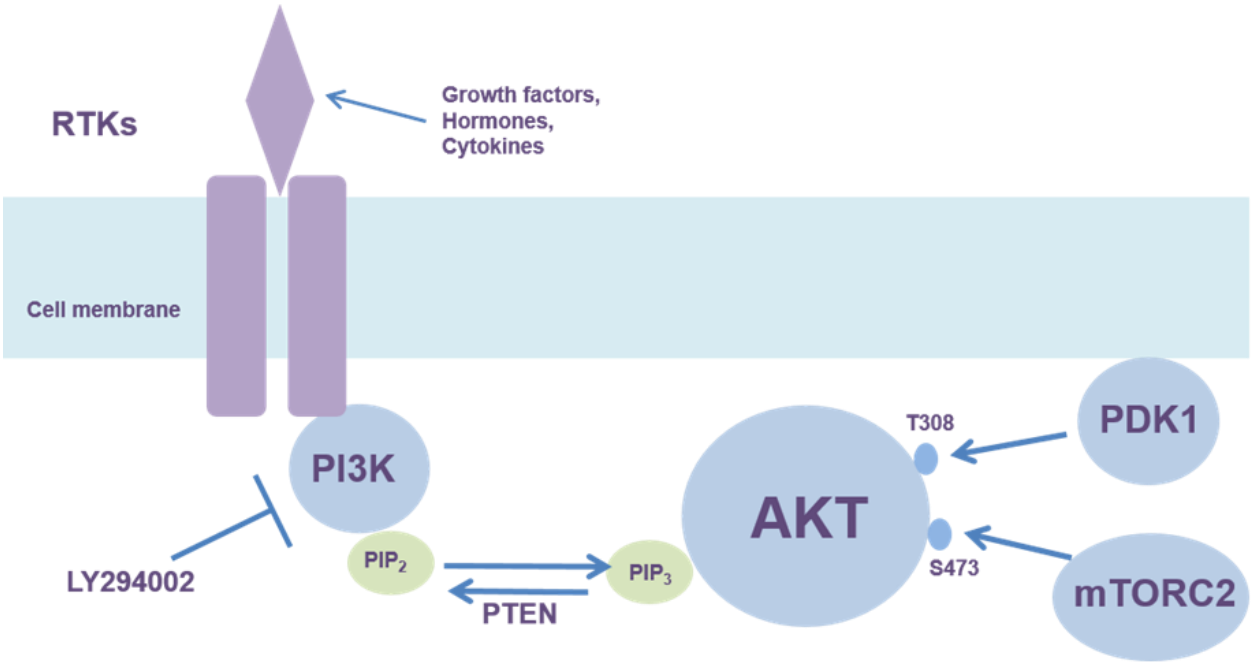


**Figure 1.8. PI3K/AKT signalling pathway**. Receptor tyrosine kinases at the plasma membrane are activated by growth factors, hormones or cytokines. This activation promotes the activity of PI3K which phosphorylates $PIP_2$ into $PIP_3$. Activation of PI3K can be inhibited by LY294002. Accumulation of $PIP_3$ at the plasma membrane induces recruitment of AKT which binds to $PIP_3$ via the PH-domain. PTEN dephosphorylates $PIP_3$. Once at the plasma membrane, AKT is available for activation by phosphorylation at its T308 site by PDK1 and S473 by mTORC2.

For complete activation, phosphorylation at the S473 is also required (Alessi et al., 1996). Phosphorylation at S473 does not occur via the PDK1 pathway (Williams et al, 2010). Instead, it is facilitated by direct interaction with $mTORC_2$ (mammalian target of rapamycin complex 2) (Sarbassov et al., 2005). Activation of AKT at T308, but not S473, allows the kinase to activate some, but not all, of its substrates (Guertin et al., 2006).

After activation at the plasma membrane, the kinase translocates to cellular compartments such as the ER (Boulbes et al., 2011), mitochondria, Golgi (Du et al., 2006) and nucleus (Andjelkovic et al., 1997).

All downstream targets of AKT contain an AKT consensus sequence (R-X-R-X-X-S/T). These include FOX01 and Bad involved in cell survival, GSK3-β, involved in cell cycle and glycogen synthesis and 4E-BP1 involved in cap-dependent translation. Some of the pathways activated downstream of PI3K/AKT signalling are presented in Figure 1.9. The role of the PI3K/AKT signalling pathway in many cellular processes makes it a prime target for control by viruses to aid viral replication and subvert anti-viral responses.

## 1.4 Viral modulation of cellular signalling

As obligate intracellular parasites, all viruses are able to subvert cellular machinery during their life cycle to create an environment that is favourable for virus replication. The earliest point at which the host cellular pathways are activated is during initial attachment and entry of the virus into the cell. The attachment and invasion of the virus into the cell elicits cellular anti-viral responses. Binding of viral proteins to host receptors also initiates signalling cascades that begin to establish a favourable environment for the virus within the cell. For example, within a minute after exposure with HIV-1 more than 200 phosphorylation sites are modified in T-cells, the majority of which are involved in pro-viral processes such as alternative splicing and cell survival (Wojcechowskyj et al., 2013).

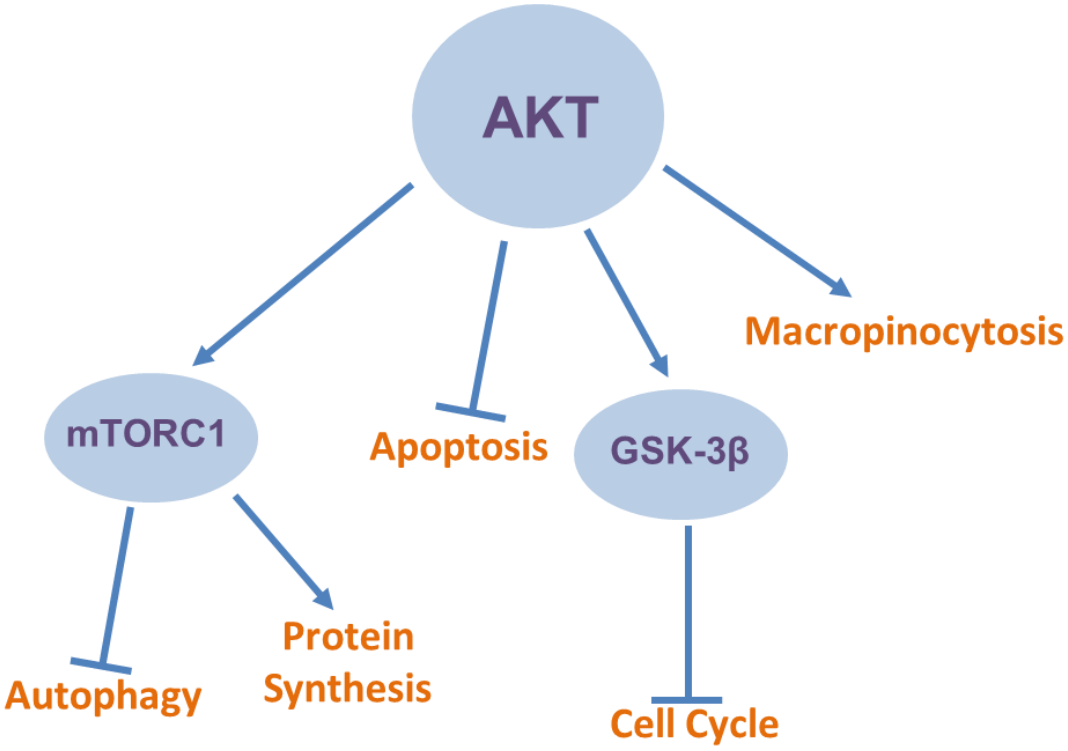


**Figure 1.9. Cellular processes modulated downstream of PI3K/AKT signalling**. The PI3K/AKT/mTOR signalling cascade modulates the activation of both autophagy, through activation of ATG13, and protein synthesis through phosphorylation of 4E-BP1. PI3K/AKT activation also inhibits the apoptotic pathway by indirect inhibition of Bcl-2 and Bax proteins. The activation of AKT inhibits cell cycle progression through the phosphorylation of GSK-3β, as well as other factors. Induction of PI3K/AKT signalling has also been implicated in the control of macropinocytosis.

The binding of influenza A virus (IAV) to the sialic acid receptor of the host cell, results in clustering of plasma membrane lipid rafts that are thought to be involved in signal transduction (Lakadamyali et al., 2004). Attachment of IAV to the cell also leads to the activation of at least two receptor-tyrosine kinases and signalling through the PI3K/AKT signalling pathway to promote viral internalisation (Eierhoff et al., 2010).

### 1.4.1 Viral replication and protein synthesis

Many viruses take advantage of pre-mRNA splicing to produce different transcript isoforms and increase proteomic diversity in the virus. The usage of alternative splice sites is regulated by splicing factors such as serine arginine rich proteins (SR) which bind to cis-regulatory elements near the splice sites. HIV-1 was found to mediate phosphorylation of SR proteins through the PI3K signalling pathway, as inhibition of PI3K results in an altered splicing pattern of HIV-1 mRNAs as well as a significant reduction in viral replication (Hillebrand et al., 2014).

The modulation of AKT activation controls translation of mRNA via the mTOR signalling pathway. During translation of host mRNA the cap-binding protein eIF4E recognises the 7-methyl guanine cap structure at the 5' end (5'-cap) of the mRNA. The eIF4E, together with eIF4G and the eIF4A helicase, form the eIF4F initiation complex. This complex facilitates unwinding of the mRNA and attachment to the 40s ribosomal subunit. The formation of the eIF4F complex can be blocked by the binding of 4E-BP (eIF4E-binding protein) to eIF4E (Figure 1.10). The rate limiting step in the process of mRNA translation is the binding of the mRNA to the ribosomal subunit which is facilitated by the binding of eIF4E to the 5'-cap of mRNA (Khaleghpour et al., 1999). The binding of hypo-phosphorylated eIF4E binding-proteins (4E-BPs) can inhibit this process and therefore control translation (Mader et al., 1995). The phosphorylation of 4E-BPs results in the inability of the proteins to bind to eIF4E, allowing the initiation of translation.

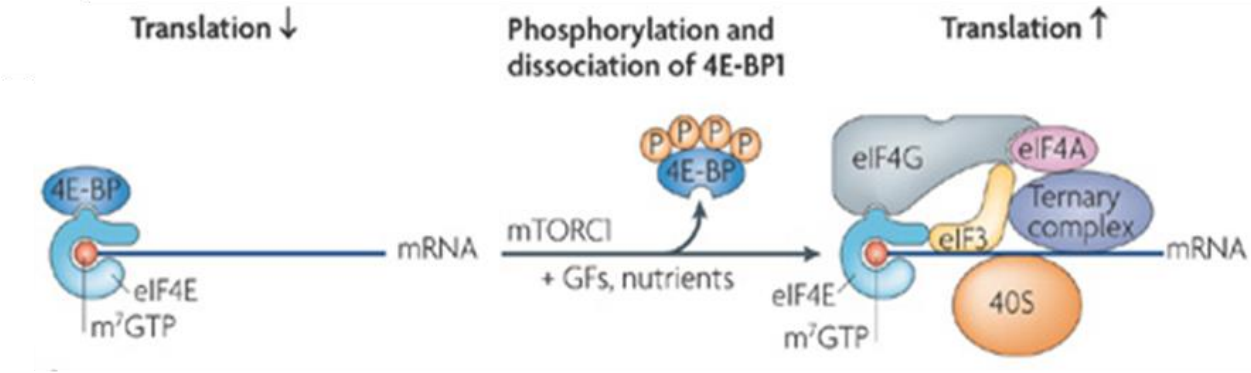


**Figure 1.10. Mechanism and control of cap-dependent translation initiation**. 4E-BP1 bound to eIF4E prevents translation initiation. However, phosphorylation of 4E-BP1 by PI3K/AKT/mTOR releases eIF4E for association with eIF4G and eIF4A to allow the initiation of translation. [Adapted from Ma & Blenis, 2009]

This phosphorylation is modulated by the PI3K/AKT/mTOR signalling pathway (Miron et al., 2003). Some viruses therefore induce dephosphorylation of 4E-BPs to impair cellular translation (Gingras et al., 1996, Connor and Lyles, 2002). The PI3K/AKT/mTOR signalling cascade also modulates translation through activation of the p70-S6 Kinase 1 (S6K1) (Figure 1.11). Several substrates of S6K1 have been identified and are involved in the initiation of translation. Primarily S6K1 induces the phosphorylation and activation of the S6 protein which forms part of the 40s ribosomal subunit. In addition, S6K1 activation also induces phosphorylation of eIF4B and the eEF2 kinase. Phosphorylation of the eEF2 kinase inhibits its activity, which in turn allows the translocation of tRNA from the A site to the P site of the ribosome. As well as modulation of 4E-BP and S6K1, phosphorylation of eIF4E itself can modulate its activity. The mitogen-activated protein kinase interacting kinases (Mnk1/2) phosphorylate eIF4E at S209 (Waskiewicz et al., 1997). Some viruses, for example the murine norovirus 1, have been shown to control translation by modulation of eIF4E phosphorylation directly (Royall et al., 2015).

Many viruses employ the host shutoff mechanism, involving the suppression of host translation and protein synthesis, thereby preventing antiviral host responses. The influenza virus NS1 protein, for example, has been implicated in the suppression of host mRNA translation (Nemeroff et al., 1998, Noah et al., 2003). Host shutoff is often coupled with the selective translation of viral mRNA, as some viruses employ unique strategies to enable translation of viral mRNA. The initiation of viral mRNA translation by most picornaviruses take place at internal ribosome entry sites downstream of the 5'-end, and therefore occurs in a cap-independent manner (Sweeney et al., 2014, Ochs et al., 1999). Other viruses, such as members of the *Caliciviridae* family, employ a viral genome-linked protein (VPg) that is attached to the 5'-end of both genomic and sgRNAs (Herbert et al., 1997, Schaffer et al., 1980).

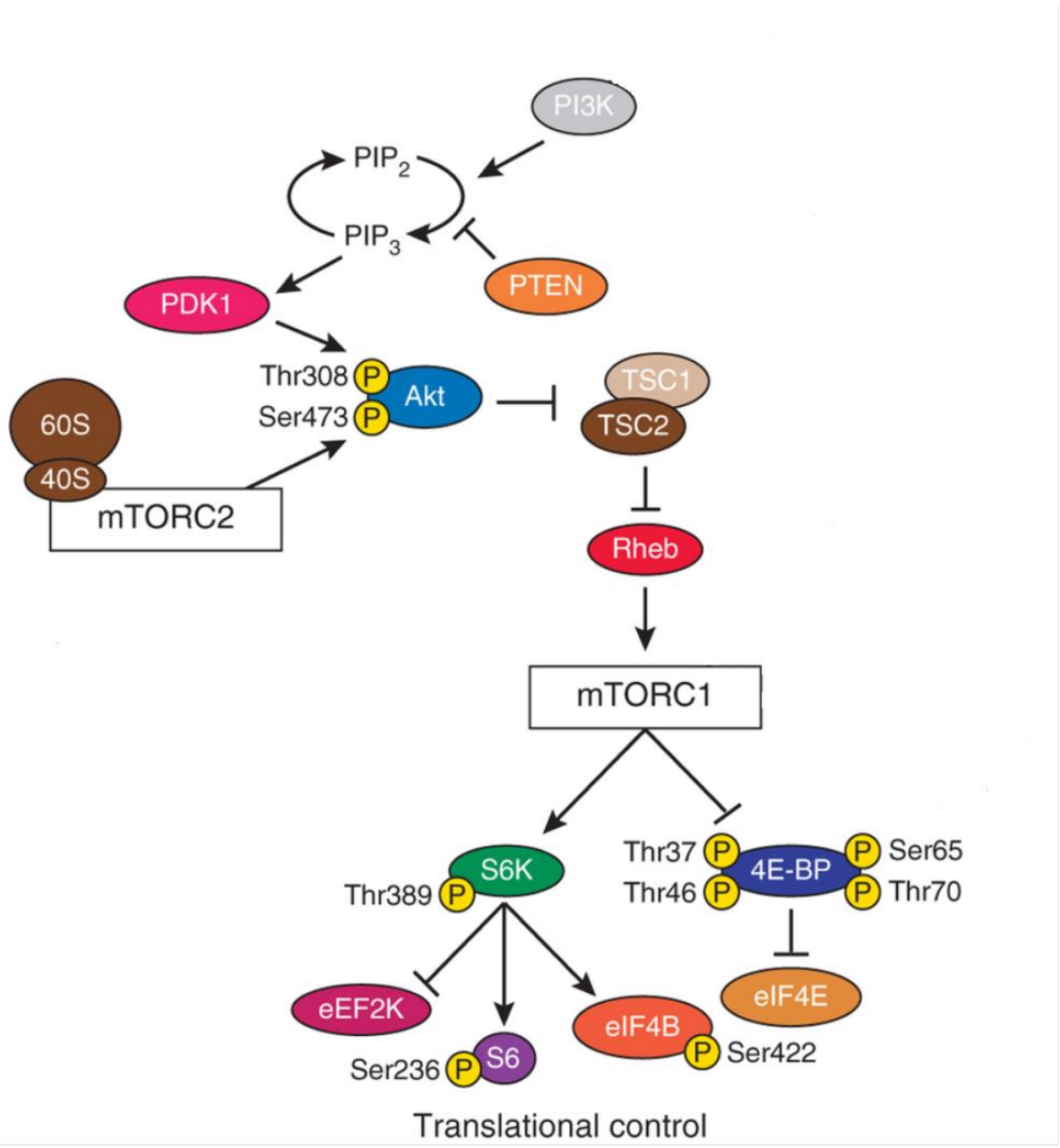


**Figure 1.11 PI3K/AKT/mTOR signalling and translational control.** Activation of the mTORC1 complex by PI3K/AKT initiates downstream signalling involved in the control of translation initiation. Phosphorylation of 4E-BP1 by mTORC1 promotes the formation of the eIF4F initiation complex. Phosphorylation of the p70 S6 kinase (S6K) induces activation of the eEF2 kinase involved in the translocation of tRNA on the ribosome. Phosphorylation of S6K also activates the S6 ribosomal protein and phosphorylation of eIF4B. [Adapted from Costa-Mattioli and Monteggia (2013)]

Binding of the VPg to eIF4E allows for translation of viral mRNA (Daughenbaugh et al., 2003, Goodfellow et al., 2005, Chung et al., 2014).

## 1.4.2 Viral replication and cell survival

Apoptosis was first described in 1972 (Kerr et al., 1972) and an understanding of the mechanisms involved were initially formed from studies of programmed cell death in *Caenorhabditis elegans* (Ellis and Horvitz, 1986). Apoptosis naturally occurs as a homeostatic mechanism allowing cell populations to be maintained in tissues. It is induced in different cell types in different ways. For example, some cells express Fas or TNF receptors that allow ligand binding to induce apoptosis. Whereas, other cells have a constitutively active pro-apoptotic pathway that must be blocked by survival factors such as growth factors or hormones.

There are two known apoptotic pathways, the extrinsic and intrinsic pathway (Figure 1.12). Both pathways are interconnected and it is thought that there is a level of cross-signalling between them (Igney and Krammer, 2002). The extrinsic apoptotic pathway is initiated by activation of death receptors, members of the TNF receptor gene superfamily (Locksley et al., 2001). Death receptors are activated by their ligands at the cell surface and transmit the pro-apoptotic signal into the cell (Ashkenazi and Dixit, 1998, Schulze-Osthoff et al., 1998). This promotes recruitment of cytoplasmic adapter proteins to the cell surface where they bind with the death receptors. For example, the Fas receptor (Nagata and Golstein, 1995) is known to be activated by the Fas ligand (Itoh and Nagata, 1993) which promotes recruitment of the FADD (Fas-associated protein with death domain) adapter proteins to the cellular membrane which contains a FasR binding domain (Yonehara et al., 1989). Once bound to the death receptor, the adapter protein, e.g. FADD, associates with procaspase-8. This forms a death-inducing signalling complex (DISC) resulting in the activation of casapse-8 (Kischkel et al., 1995). Once activated, caspase 8

triggers a pro-apoptotic signalling cascade through caspase 3 (Stennicke et al., 1998).

The intrinsic apoptotic pathway also initiates apoptosis through caspase 3 signalling. This pathway is often modulated by PI3K/AKT signalling and the absence of a pro-survival signal (Bonni et al., 1999). For example, the absence of certain growth factors, cytokines and hormones may prevent activation of the anti-apoptotic PI3K/AKT signalling, therefore failing to supress the apoptotic response (Yao and Cooper, 1995, Kauffmann-Zeh et al., 1997, Kulik et al., 1997). The subsequent pro-apoptotic signal induces changes in the mitochondrial membrane and the release of cytochrome c through Bad and Bax signalling (Kennedy et al., 1999, Yamaguchi and Wang, 2001, Wei et al., 2001). Cytochrome c then binds and activates Apaf-1 and caspase-9 forming an apoptosome (Cain et al., 2002) (Chinnaiyan, 1999, Shiozaki et al., 2002). Activated caspase-9 acts as an initiator caspase to activate caspase-3 (McDonnell et al., 2003). The crucial role of this caspase in both apoptotic pathways means that activation of caspase 3, and also caspase 7, are good markers for measuring apoptotic signalling (Chen et al., 2015). Caspase 3 activates the endonuclease CAD (caspase-activated deoxyribonuclease), which degrades chromosomal DNA in the nuclei and causes the characteristic chromatic condensation (Enari et al., 1998). The activity of caspase 3 also induces cytoskeletal reorganisation and formation of apoptotic bodies (Kothakota et al., 1997). The externalisation of phosphatidylserine (PS) on the surface of apoptotic cells then triggers phagocytic uptake of the cell (Fadok et al., 1992). Like caspase 3 and 7 activation, the externalisation of PS is also an indicator of apoptosis and can be measured by using fluorescently labelled Annexin V that binds specifically to externalised PS (Tait et al., 2004, Andree et al., 1990, Huber et al., 1990).

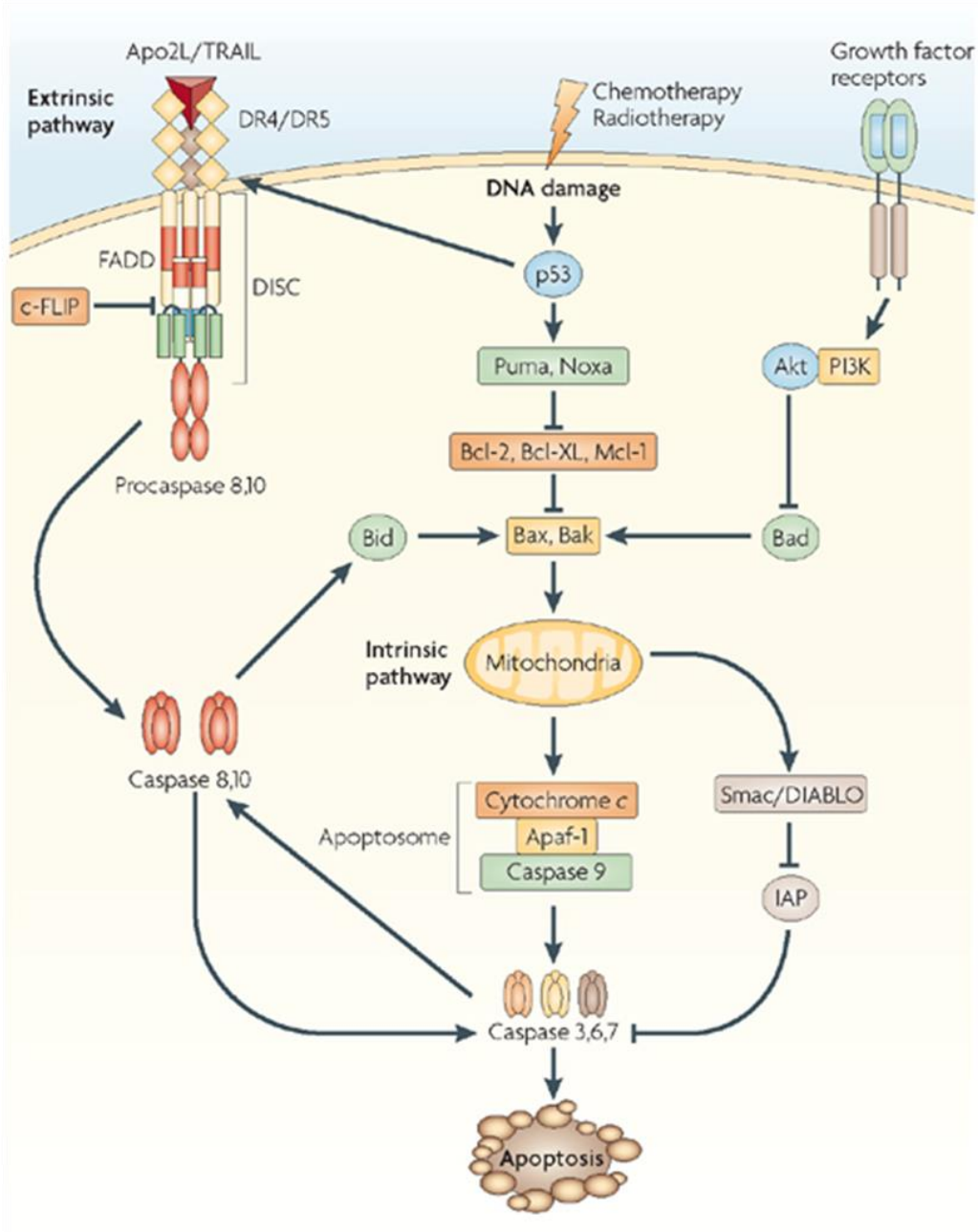


**Figure 1.12. Schematic of the extrinsic and intrinsic apoptosis pathways**. The extrinsic pathway involves the activation of death receptors at the plasma membrane. Adapter proteins bind to activated receptors and associate with procaspase8 and 10 to initiate apoptosis through the caspase 3 pathway. The intrinsic pathway involves activation of pro-apoptotic, or inhibition of anti-apoptotic pathways to induce cytochrome c release from mitochondria. Cytochrome c associates with Apaf-1 and caspase 9 to form an apoptosome and activate the caspase 3 cascade. [Adapted from (Ashkenazi 2008)].

Whilst apoptosis naturally occurs in order to maintain homeostasis, it is also employed as a defence mechanism during immune reactions or cell damage (Norbury and Hickson, 2001). During viral infection regulation of apoptosis can result in pro-viral or anti-viral responses (Koyama et al., 1998). For example, induction of apoptosis by cells early during viral replication may prevent replication and release of new virions, thereby preventing spread of the virus to neighbouring cells. In these cases, the virus may also act to prevent apoptosis by activating anti-apoptotic pathways such as the PI3K/AKT signalling pathway. The SARS-CoV E protein, for example, has been found to have anti-apoptotic effects and its deletion reduces the pathogenicity and mortality in model animals. (DeDiego et al., 2011, DeDiego et al., 2014). Conversely, some viruses require apoptosis to complete replication activation (Tran et al., 2013). Viruses that have a lytic replication cycle may induce apoptosis by inhibiting the anti-apoptotic signalling pathways, thereby allowing the release of new virions during breakdown of the cell or uptake of the virus by phagocytic cells. There is often a delicate interplay between pro-apoptotic and anti-apoptotic signalling. Influenza A virus (IAV) infection triggers apoptosis (Takizawa et al., 1993, Fesq et al., 1994, Mori et al., 1995). During IAV infection the virus uses the apoptotic pathway to promote activation and exportation of the viral RNP complex from the nucleus to the cytoplasm (Wurzer et al., 2003, Chen et al., 2001). However, apoptosis is also known to be involved in the clearance of IAV infected cells and therefore the elimination of infection (Chang et al., 2015). The NS1 protein of IAV also activates NF-kB through the activation of the PI3K/AKT signalling pathway to inhibit apoptosis and increase cell viability (Zhirnov et al., 2002, Zhirnov and Klenk, 2007).

Apoptosis also occurs as a result of ER stress (Liao et al., 2013). The unfolded protein response (UPR) is initiated when the ER is overloaded and proteins are mis-folded and accumulate causing stress to the ER. The UPR is a cellular survival response that is initiated by several sensors (Ron and Walter, 2007). Investigation

into the pathway upstream of UPR has identified three important proteins to date, the protein kinase R-like ER kinase (PERK) (Harding et al., 1999, Harding et al., 2000), activating transcription factor 6 (ATF6) (Haze et al., 1999, Lee et al., 2003) and inositol-requiring enzyme 1 (IRE1) (Calfon et al., 2002, Yoshida et al., 2001). PERK, ATF6 and IRE1 are activated sequentially to induce the UPR which inhibits the synthesis of new proteins and induces degradation of mis-folded proteins therefore relieving ER stress. PERK is instrumental in the inhibition of translation (Harding et al., 1999). Activated by self-phosphorylation, it phosphorylates eIF2α and stabilises the eIF2-Dp-eIF2B complex thereby inhibiting the formation of the 43S initiation complex and subsequent protein synthesis (Bollo et al., 2010). Phosphorylation of eIF2α also results in the enhanced selective translation of the activating transcription factor (ATF4) which activates genes involved in metabolism, oxidative stress and apoptosis (Harding et al., 2000). In this way the UPR is able to re-establish homeostasis and prevent cell death, however, if prolonged ER stress occurs or the ER is damaged, the UPR may be prolonged and induce apoptosis (Lin et al., 2007).

The effect of IBV on ER-stress induced apoptosis has been investigated by Liao et al, (2013). The role of PERK and PKR in the induction of eIF2α activation has been identified during IBV infection. In mammalian Vero cells, eIF2α was found to be activated early during viral replication at between 2 and 8 hpi but to decrease from 8 hpi. Phosphorylation of eIF2α by PKR restricts the activity of eIF2B to form tRNA ternary complexes. This stalls translation and the accumulating tRNA complexes form stress granules in the cytoplasm of infected cells. Phosphorylation of PERK was also seen early during IBV infection, suggesting that ER stress may be induced early during IBV infection and that the UPR response may be triggered to inhibit protein translation but selectively promote translation of ATF4 to induce apoptosis.

## 1.4.3 Viral replication and macropinocytosis

Macropinocytosis, first described in 1931 (Lewis, 1931), can be defined as the bulk uptake of fluid or extracellular components into the cell. It is a clathrin-independent process that is dependent on signals originating as a response to growth factors such as EGF or tumour-promoting factors such as PMA (Phorbol myristate acetate) (Nakase et al., 2015). Macropinocytosis can be identified primarily as it causes ruffling of the plasma membrane (Ridley, 1994) (Figure 1.13). Many lamellipodia fold back in on themselves to fuse with the plasma membrane, creating large macropinosomes (Lim and Gleeson, 2011). Whilst the size of macropinosomes is not consistent, they are generally considered to be more than 0.2 µm in diameter and are considerably larger than micropinosomes and clathrin-coated vesicles (Conner and Schmid, 2003, Kerr and Teasdale, 2009). These macropinosomes allow the intake of large amounts of nutrients into the cell (Lim and Gleeson, 2011). However, the membrane ruffling associated with macropinocytosis has also been implicated in cell motility (Kerr and Teasdale, 2009).

Macropinocytosis is known to be regulated downstream of PI3K as treatment with PI3K inhibitors reduces fluid phase uptake via macropinocytosis (Veithen et al., 1998, Amyere et al., 2000). Recently a model for macropinocytosis signalling has been proposed involving the recruitment of sorting nexins (Kerr et al., 2006, Lim et al., 2008). A direct relationship between the amount of cell surface SNX5 protein and macropinocytic activity has been seen (Lim et al., 2008). It was suggested that the pathway is modulated by the SNX5 (sorting nexin protein 5) which binds preferentially to $PIP_2$. The EGF receptor, and subsequently PI3K, is thought to be activated triggering the production of $PIP_3$. A 5'-phosphatase then generates $PIP_2$ from $PIP_3$.

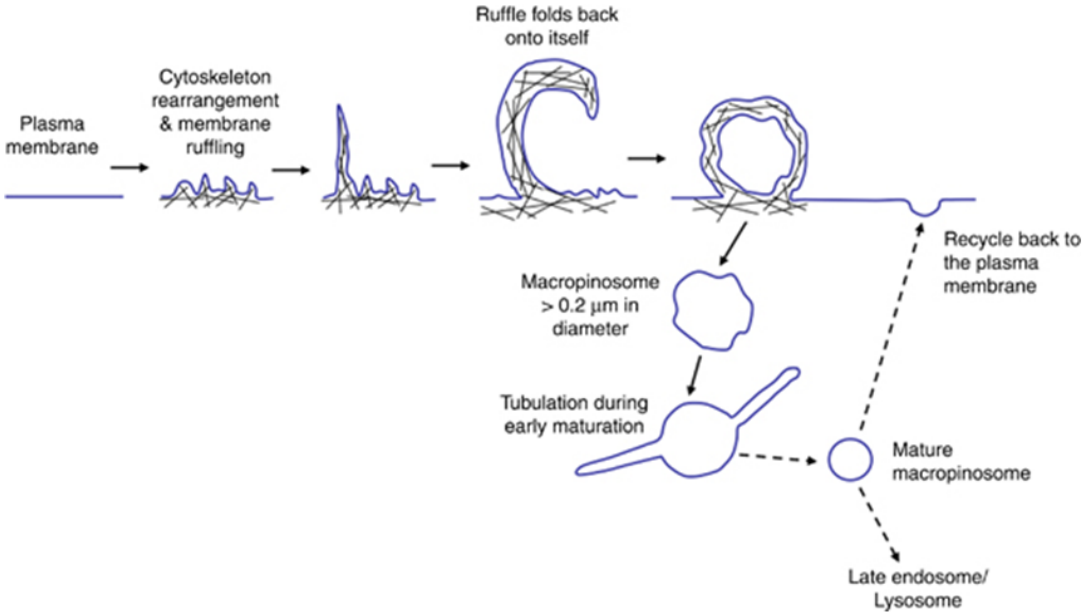


**Figure 1.13 Schematic of macropinosome formation**. Macropinocytosis involves the rearrangement of the actin cytoskeleton at the plasma membrane to form membrane ruffles. The ruffles fold back on themselves and re-fuse with the plasma membrane, trapping large amounts of extracellular matter within them. These macropinosomes then move into the cell where they mature into more spherical vesicles. The content of the macropinosomes are either degraded at the late endosome or recycled back to the plasma membrane. (Lim and Gleeson 2011)

Presence of elevated levels of $PIP_2$ recruits SNX5 to specific areas of the plasma membrane where macropinocytosis is seen to occur. SNX5 may be involved in the deforming of the membrane allowing the formation of macropinocytic pit which then buds off from the cytosolic surface of the plasma membrane (Wang et al., 2010, Carlton et al., 2004, Peter et al., 2004).

Macropinocytosis is often modulated to allow uptake of pathogens into the cell. Amongst these are protozoa such as the parasite *Leishmania* (Wanderley et al., 2006) and bacteria such as *Salmonella* (Garcia-Perez et al., 2003) and *Legionella* (Watarai et al., 2001). The pathway is modulated more frequently however by viruses (Mercer and Helenius, 2012, Mercer and Helenius, 2009, Mercer et al., 2010). Viruses that use macropinocytosis to enter the cell include, vaccinia (Mercer et al., 2010), HIV-1 (Maréchal et al., 2001), adenovirus (Amstutz et al., 2008) and Ebolavirus (Aleksandrowicz et al., 2011, Saeed et al., 2010). The vaccinia virus, for example, envelopes itself in the membrane of a dying infected cell, thereby mimicking a cell undergoing apoptosis (Mercer and Helenius, 2008). When the virus is then presented to a healthy cell, large transient membrane blebs are formed, in which the virus is thought to be taken up. Recently, a role for micropinocytosis in several coronavirus infections has been suggested. Freeman et al., (2014) identified macropinocytic activity in MHV and SARS-CoV infected cells late during infection. They also noted that the coronavirus-induced macropinocytosis occurred independently of virus entry.

## 1.5 Aims and Objectives

The aim of this study was to investigate the role of the PI3K/AKT signalling pathway during infection with avian infectious bronchitis virus. To investigate this role, several objectives were established.

### Objective 1

The first objective was to identify the magnitude and duration of AKT activation in IBV infected cells. Studies of avian viruses are often conducted in mammalian cells due to lack of reagents and established protocols. It was therefore decided that the activation of AKT be investigated in both mammalian and avian cells. This would not only allow the development of protocols in avian cells, but also allow for comparisons in the interaction of the virus with the two cell lines.

### Objective 2

The second objective of this study was to investigate the downstream effects of PI3K/AKT signalling on IBV replication, cellular proteins synthesis, apoptosis and macropinocytosis.

### Objective 3

In addition, the mechanisms by which the virus induces PI3K/AKT signalling and modulation of downstream processes were to be investigated.

### Objective 4

The fourth objective was to determine the localisation and expression levels of avian *AKT* isoforms in avian tissues. This included a bioinformatic investigation into the location of the avian *AKT2* gene.

### Objective 5

Furthermore, the effect of IBV infection on the expression of avian *AKT1* and *AKT3* was to be investigated in avian cells and tissues.

# Chapter 2

## Materials and Methods

# 2.1 Materials

## 2.1.1 General chemicals and enzymes

Unless stated otherwise, all chemical reagents and enzymes were purchased from New England Biolabs (NEB), Roche, GE Healthcare, Invitrogen, Sigma-Aldrich, Stratagene and Promega.

## 2.1.2 Antibodies

Unless stated otherwise all antibodies were purchased from Cell Signalling Technology or Abcam (Table 2.1).

## 2.1.3 Oligonucleotides

Synthetic DNA oligonucleotides were purchased from Sigma-Aldrich. *AKT1* and *AKT3* primers and hydrolysis probes were designed by and purchased from Primer Design UK Ltd.

## 2.1.4 Cell lines

Cell stocks were maintained by The Pirbright Institute Central Services Unit. All cell lines were maintained at 37 °C and 5% $CO_2$.

*Chick Kidney (CK) cells:* Primary chick kidney cells were prepared by trypsonization of the kidneys of 2-3 week old specific pathogen free (SPF) Rhode Island Red chickens (Hennion and Hill, 2015).

*DF1 cells*: Continuous fibroblast cell line originating from the spontaneous transformation of fibroblasts from 10 day old embryos of East Lansing line chickens (Himly et al., 1998).

**Table 2.1 List of antibodies used for Western blot and Immunofluorescence**

| Name | Target | Use | Dilution | Catalogue Number |
|---|---|---|---|---|
| **Phospho-AKT (Ser473) Antibody (Rb)** | AKT phosphorylated at S473 | WB | 1:100 | Cell Signalling Technology #9271 |
| **Phospho-AKT (Thr308) (C31E5E) mAb (Rb)** | AKT phosphorylated at T308 | WB | 1:100 | Cell Signalling Technology #2965 |
| **J2 anti-dsRNA IgG2a (Ms)** | double stranded RNA | IF | 1:25 | Scicons #10010200 |
| **β-actin (D6A8) mAb (Rb)** | β-actin | WB | 1:1000 | Cell Signalling Technology #8457 |
| **Phospho-GSK-3β (Ser9) (D85E12) XP mAb (Rb)** | GSK-3β phosphorylated at S9 | WB | 1:100 | Cell Signalling Technology #5558 |
| **Phospho-4E-BP1 (Thr37/46) (236B4) mAb (Rb)** | 4E-BP1 phosphorylated at T37/46 | WB | 1:100 | Cell Signalling Technology #2855 |
| **Anti-alpha Tubulin antibody (DM1A) – Loading Control (Ms)** | α-tubulin | WB | 1:1000 | Abcam #ab7291 |
| **Anti-PDI antibody (RL90) (Ms)** | Endoplasmic Reticulum | IF | 1:100 | Abcam #ab2792 |
| **Anti-Golgi Complex antibody (Ms)** | Golgi apparatus | IF | 1:100 | Abcam #ab103439 |
| **Phospho-4E-BP1 (Thr70) Antibody (Rb)** | 4E-BP1 phosphorylated at T70 | WB | 1:100 | Cell Signalling Technology #9455 |
| **Phospho-4E-BP1 (Ser65) Antibody (Rb)** | 4E-BP1 phosphorylated at S65 | WB | 1:100 | Cell Signalling Technology #9451 |
| **Anti-Infectious Bronchitis (Massachusetts) antibody (Ck)** | Infectious Bronchitis virus | WB | 1:100 | Abcam #ab31671 |
| **Monoclonal Anti-FLAG M2 antibody (Ms)** | FLAG tag | WB | 1:100 | Sigma-Aldrich #F1804 |
| **Anti-E IE7 (Ms)** | IBV envelope protein | WB | 1:100 | |
| **PrioMab Chicken IBV Monoclonal 26.1 (Ms)** | IBV spike protein, S2 subunit | WB | 1:100 | ThermoFisher Scientific |

*Vero cells:* Continuous kidney epithelial cell line originating from the African Green monkey.

## 2.1.5 Cell culture media

Minimum Essential Medium (MEM), Dulbeccos Minimum Essential Medium (DMEM) and Foetal Calf Serum (FCS) were all purchased from Sigma-Aldrich. Phosphate Buffered Saline A (PBSa) was provided in-house by The Pirbright Institute Central Services Unit.

CK cells were grown in CK growth media (Table 2.2) CK cells were maintained in 1x BES media (Table 2.3). DF1 cells were maintained in DMEM growth media (Table 2.4). Vero cells were maintained in EMEM growth media (Table 2.5).

## 2.1.6 Virus

*M41-CK:* Pathogenic strain of IBV adapted to grow in CK cells (Darbyshire et al., 1979).

*IBV Beau-R:* Beau-R is a molecular clone of the Beaudette-CK (Beau-CK) strain of IBV (Casais et al., 2001). It was adapted to grow in CK cells by multiple passages in embryonated eggs. Wider host range than M41-CK with the ability to replicate in mammalian Vero cells.

*IBDV:* Infectious bursal disease virus was kindly donated by Dr Andrew Broadbent, The Pirbright Institute.

## 2.1.7 Plasmids

The pcDNA 3.1- S protein expression plasmid was provided by Phoebe Stevenson-Leggett, Avian Endemic Viruses, The Pirbright Institute.

**Table 2.2 Components of CK cell growth media**

| Reagent | Final concentration in 1x BES | Final concentration in 2x BES |
|---|---|---|
| **10x EMEM (Sigma)** | 1x | 2x |
| **Tryptose Phosphate Broth** | 10% | 20% |
| **10% BSA (Sigma)** | 0.2% | 0.4% |
| **1M N,N bis(2-hydroxethyl)-2-aminoethanesulfonic acids (BES) (Sigma)** | 20 mM | 40 mM |
| **7.5% sodium bicarbonate** | 0.4% | 0.8% |
| **L-glutamine (200 mM) (Life technologies)** | 2 mM | 4 mM |
| **Nystatin (100,000 U/ml) (Sigma)** | 250 U | 500 U |
| **Penicillin/Streptomycin (100,000 U/ml) (Sigma)** | 100 U | 200 U |

**Table 2.3 Components of 1x and 2x BES media**

| Reagent | Final concentration in 1x BES | Final concentration in 2x BES |
|---|---|---|
| 10x EMEM (Sigma) | 1x | 2x |
| Tryptose Phsophate Broth | 10% | 20% |
| 10% BSA (Sigma) | 0.2% | 0.4% |
| 1M N,N bis(2-hydroxethyl)-2-aminoethanesulfonic acids (BES) (Sigma) | 20 mM | 40 mM |
| 7.5% sodium bicarbonate | 0.4% | 0.8% |
| L-glutamine (200 mM) (Life technologies) | 2 mM | 4 mM |
| Nystatin (100,000 U/ml) (Sigma) | 250 U | 500 U |
| Penicillin/Streptomycin (100,000 U/ml) (Sigma) | 100 U | 200 U |

The pCI-neo-N protein expression plasmid was provided by Julian Hiscox (University of Liverpool) (Hiscox et al., 2001). It contains the Beau-CK N gene inserted into pCi-Neo. Expression is under the control of both the cytomegalovirus RNA polymerase II promoter and the T7 RNA polymerase promoter.

Construction of plasmids for the expression of IBV-Envelope (pcDNA3.1-E) and IBV-Membrane (pcDNA3.1-E-FLAG) is described in section 2.8.

## 2.2 Virological methods

### 2.2.1 Infection of avian and mammalian cells with IBV

Cells were seeded to 70-80% confluency and infected with an appropriate volume of neat virus for the well size. The cells were incubated for 1 hr at 37 °C and 5% $CO_2$. The virus inoculum was then removed and replaced with 1x BES media.

### 2.2.2 Infection with IBDV

DF1 cells were seeded to 70-80% confluency and infected with an appropriate volume of virus for the well size. The cells were incubated for 1 hr on a rocker at room temperature. The virus inoculum was then removed and replaced with DMEM growth media.

### 2.2.3 Viral growth kinetics

DF1 cells were seeded onto 12-well plates. The PI3K inhibitor LY294002 was diluted in DMEM growth media. Half of the wells were treated with 10 µM LY294002 for 1 hr prior to, and for the duration of infection. Cells were infected with neat virus or mock infected and left to incubate at 37 °C for 1 hr. After 1 hr the inoculum was removed and 2 ml DMEM growth media was added to each well. At 1, 2, 6, 8, 12, 18, 20 and 24 hours post infection (hpi) the supernatant was collected for titration by tissue culture infectious dose ($TCID_{50}$). The cells were washed twice in PBSa and

lysed in 500 µl Qiagen RNeasy RLT buffer containing β-mecaptoethanol on ice for 20 mins. The lysates were collected and 250 µl was stored at -80 °C for RNA

**Table 2.4 Components of 1x DMEM growth media**

| Reagent | Final concentration in 1x DMEM growth media |
|---|---|
| 10x DMEM (Sigma) | 1x |
| 10% FBS (Gibco) | 0.2% |
| Penicillin/Streptomycin (100,000 U/ml) (Sigma) | 100 U |

**Table 2.5 Components of 1x EMEM growth media**

| Reagent | Final concentration in 1x EMEM growth media |
|---|---|
| 10x EMEM (Sigma) | 1x |
| 10% FBS (Gibco) | 0.2% |
| Penicillin/Streptomycin (100,000 U/ml) (Sigma) | 100 U |

extraction. The other 250 µl was centrifuged at 12,000 rpm for 20 mins at 4 °C. The supernatant was collected and 1x Laemmli sample buffer (BIO-RAD) was added for subsequent protein analysis.

## 2.2.4 Titration of IBV by $TCID_{50}$

DF1 cells were seeded onto 96-well plates. Supernatant from DF1 cells infected with IBV in the presence or absence of LY294002 were collected at 8, 12, 18, 20 and 24 hpi (Section 2.2.3). The supernatants were serially diluted 10 fold to $10^{-8}$ in DMEM growth media. Cells were inoculated with 200 µl of each virus dilution in five replicates. Infected cells were left to incubate at 37 °C for 5 days. The number of wells containing cells exhibiting cytopathogenic effect (CPE) was counted by visualisation under a microscope and comparison to control wells. CPE was identified as a rounding of cells and disturbance of the monolayer. The $TCID_{50}$ was calculated using the $TCID_{50}$ calculator developed by Marco Binder, Dept. Infectious Diseases, Molecular Virology, Heidelberg University. $TCID_{50}$ was calculated by the Spearman & Kärber algorithm (Heierholzer and Killington, 1996).

## 2.2.5 Titration of IBV by plaque assay

To measure the titre of new batches of IBV grown on CK cells, plaque assays were used as standard. CK cells were seeded into 12-well plates. Virus was serially diluted 10-fold in 1x BES medium and CK cells inoculated with 250 µl of virus. After 1 hr the inoculum was removed and cells were overlaid with 2 ml 1x BES in 1% agar. Cells were incubated for 72 hrs at 37 °C, 5% $CO_2$ then fixed by addition of 10% formaldehyde in PBSa for 30 mins. Agar was removed and cells stained with 0.1% crystal violet for 20 mins to visualise the plaques.

## 2.2.6 Inactivation of IBV with BEI

IBV was inactivated using Binary ethylenimine (BEI). A neat stock of virus was incubated in 0.1 M BEI for 48 hrs at 37 °C. After 48 hrs BEI was inactivated by the

addition of 1 M sodium thiosulfate. The inhibition of viral replication was confirmed by qPCR (Section 2.5.1) and the virus stored at -80 °C.

## 2.3 Protein based methods

### 2.3.1 Cell lysis for protein collection

Cells were treated as per experimental design. At the time points indicated cells were washed twice with cold PBSa on ice. Cells were then lysed in 1x Cell Lysis Buffer (NEB) containing a phosphatase inhibitor. For 12-well plates cells were lysed in 350 µl cell lysis buffer. Immediately prior to lysis, 1x Protease Inhibitor Cocktail (NEB) was added to the lysis buffer. Cells were incubated on ice for 20 minutes and the lysate collected. Lysates were centrifuged at 13,000 rpm at 4 °C for 10 mins and the supernatants collected and stored at -20 °C.

### 2.3.2 SDS-PAGE

Cell lysates were denatured in 1x Laemmli Sample Buffer (BIO-RAD) containing β-mecaptoethanol and heated to 100 °C for 10 minutes. Protein samples were loaded into a Mini-PROTEAN TGX$^{TM}$ Precast Gel (BIO-RAD) and electrophoresed in Tris/Glycine SDS running buffer (BIO-RAD) at 80 V for the first 10 mins then 110 V.

### 2.3.3 Coomassie staining

SDS-PAGE gels were incubated in Coomassie Brilliant Blue R-250 Staining Solution (BioRad) and de-stained using Coomassie Brilliant Blue R-250 Destaining Solution (BioRad) according to manufacturer's protocol.

### 2.3.4 Western blotting

For western blotting, proteins separated by SDS-PAGE were transferred onto nitrocellulose membrane in Trans-Blot Turbo transfer buffer (BIO-RAD) using a Trans-Blot Turbo Transfer System (BIO-RAD). Membranes were submerged in Ponceau S solution (Sigma-Aldrich) for 5 mins to stain for total protein. This was to

ensure equal loading and check for bubbles on the membrane. The stain was removed by washing in sterile water. Membranes were then incubated for 1 hr or overnight in 2.5% Marvel/2.5% BSA and 0.1% Tween 20 in PBSa (PBST). The membrane was then washed once in PBST and incubated in primary antibody (see Table 2.1) for 1 hr or overnight. Following this, the membrane was washed at least 3 times in PBST and incubated with a fluorescent IRDye secondary antibody (LI-COR) diluted 1:1000 in 1% BSA in PBST for 1 hr in the dark. The membrane was washed a further 3 times in PBST and the protein bands detected and quantified on an Odyssey CLx Imaging System (LI-COR).

### 2.3.5 Fixing, labelling and staining for immunofluorescence

Cells were seeded onto glass coverslips in 24-well plates and infected or treated as in previous sections. Cells were fixed either in the original 24-well plate, or coverslips were carefully moved into another 24-well plates for fixation during time courses. Plates were incubated on ice and cells were washed twice with cold PBSa then fixed in 250 µl 4% paraformaldehyde for 20 minutes on a rocker. Cells were then washed once in cold PBSa and stored at 4 °C for up to 72 hours after fixation, further processing was not done on ice.

For staining of filamentous actin with Alexa Fluor Phalloidin 568 (ThermoFisher Scientific), cells were incubated in the dye diluted in PBSa at 1:500.

For incubation in antibodies, cells were permeabilised with 0.1% Triton X-100 in PBSa for 10 minutes. After permeabilisation the cells were washed once with PBSa and blocked in 0.5% BSA in PBSa for 1 hr on a rocker. Cells were then incubated in primary antibody (Table 2.1) for 1 hour on a rocker. After incubation cells were washed five times in PBSa prior to incubation in fluorescent secondary antibodies at a concentration of 1:250 for 1 hr in the dark on a rocker. After 1 hr the cells were washed five times in PBSa.

After incubation in stain or antibodies, the nuclei of the cells were stained with DAPI (1:20,000) and mounted onto microscope slides with Vectashield Antifade Mounting Media (Vector Laboratories).

Cells were imaged using a Leica TCS SP5 confocal Microscope

## 2.3.6 Fixing for electron microscopy

Electron Microscopy was performed by Jennifer Simpson, The Pirbright Institute. DF1 cells were seeded onto round plastic coverslips in 24-well plates to 90% confluency. Cells were mock infected or infected with IBV in the presence or absence of LY294002. At 24 hpi media was removed from cells and 1 ml fixative was added to the cell.

EM fixative was made as follows, stored at -20 °C until use and thawed overnight at 4 °C before use.

Initially a 0.02 M buffer solution was using 50 ml Solution A and 32 ml Solution B (Table 2.6). The pH of the solution was checked and adjusted to 7.2 if needed.

Table 2.6 Components of Solution A and B for fixative buffer preparation

| Solution A | Solution B |
|---|---|
| 2.722g sodium dihydrogen orthophosphate in 100 ml distilled water | 0.8 g sodium hydroxide in 100 ml distilled water |

Subsequently, a 0.05 M buffer was made by diluting 1 part 0.2 M buffer in 3 parts distilled water and the pH re-confirmed as 7.2.

The fixative was then made by adding 8 ml of 25% glutaraldehyde and 1.71 g sucrose to 92 ml of the 0.05 M buffer and mixed well.

## 2.4 Stimulation and Inhibition of PI3K/AKT pathway

### 2.4.1 Cytotoxicity assays

Cells were seeded onto 96-well plates to 90% confluency. Inhibitors (Section 2.4.2 & 2.4.3) were diluted in growth media to various dilutions. Media was removed from the cells and replaced with 100 µl of the diluted inhibitors. Cells were incubated at 37 °C for 24 hrs with the inhibitors. After 24 hrs the viability of the cells was assessed using the CellTiter-Glo Assay (Promega) according to manufacturer's protocol. In short 50 µl of media was removed from the cells and discarded. Then 50 µl CellTiter-Glo Reagent was added to the cells inducing lysis. Cells were mixed for 2 mins on an orbital shaker and the plate incubated for a further 10 mins without shaking. The luminescence was measured using a GloMax Luminometer (Promega).

### 2.4.2 Inhibition of PI3K by LY294002

PI3K activity was inhibited by incubating the cells in a final concentration of 10 µM LY294002 for 1 hr prior to and for the duration of infection or treatment.

### 2.4.3 Stimulation of PI3K/AKT by EGF

The PI3K/AKT pathway was activated by incubating the cells in 5 ng/ml EGF for 15 mins.

## 2.5 RNA and DNA based methods

### 2.5.1 Real-time qPCR for IBV detection

TaqMan qPCR was performed using TaqMan® Fast Universal PCR 2x Master Mix (ThermoFisher Scientific). Primers and probes were designed by Helena Maier (The Pirbright Institute) (Maier et al., 2013b). Primers were used at 500 nM and hydrolysis probes at 125 mM final concentrations.

Copies of IBV genome were detected by amplifying the 5′-UTR of the viral genome.

Table 2.7 Oligonucleotide sequences for 5′UTR primer/probe set

| Oligonucleotide | Sequence |
|---|---|
| IBV 5′ UTR (forward) | 5′-GCTTTTGAGCCTAGCGTT-3′ |
| IBV 5′ UTR (reverse) | 5′-GCCATGTTGTCACTGTCTATTG-3′ |
| IBV 5′ UTR probe | 5′-(FAM)-CACCACCAGAACCTGTCACCTC-(TAMRA)-3′ |

Copies of viral mRNA were detected by amplifying the N-message mRNA produced during replication.

Table 2.8 Oligonucleotide sequences for N-message primer/probe set

| Oligonucleotide | Sequence |
|---|---|
| N-message (forward) | 5′-GCTTTTGAGCCTAGCGTT-3′ |
| N-message (reverse | 5′-TTGTCCCGCGTGTACCTCTC-3′ |
| N-message probe | 5′-(FAM)-ACAAAGCAGGACAAGCA-(TAMRA)-3′ |

The qPCR was run on a 7500 Fast Real Time System (Applied Biosystems) with the following cycle profile: 95 °C for 1 mins and then 40 cycles at 95 °C for 10 secs and 60 °C for 30 sec.

Copy number was calculated from a standard curve created from amplification of target sequences from plasmids containing the target sequences (Maier et al., 2013b).

## 2.5.1 Real-time PCR primer design

Candidates for reference gene primers were identified using the GenScript Real-time PCR (TaqMan) Primer Design tool (https://www.genscript.com/ssl-

bin/app/primer). The candidate sets were then modified and final sets selected using the Primer Express Software (ThermoFisher Scientific). The primers were then ordered from Sigma at a stock concentration of 100 µM. Hydrolysis probes were ordered after the probes were tested for specificity and gDNA amplification by endpoint PCR. Primer and probe sets were designed in collaboration with Karen Staines (Lincoln University) and William Mwangi (The Pirbright Institute). Full primer sequences in Chapter 5, Table 5.3.

## 2.5.2 Total RNA extraction from tissue

Tissues were removed from Rhode Island Red chickens, aged between 8 days and 3 weeks, and immediately stored in TRIzol (Thermofisher) at -80 °C. No more than 100 mg of each tissue sample was placed into 500 µl TRIzol in a safelock tube containing a sterile metal bead. Tissues were disrupted in a bead beater until fully homogenised. Tissue debris was left to settle at room temperature for 5 mins before the addition of 100 µl chloroform. The tubes were shaken vigorously for 15 secs and left to settle again for 5 mins at room temperature. The samples were then centrifuged at 12,000 xg for 15 mins at 4 °C to separate RNA from DNA. The upper aqueous RNA phase was collected into a new tube and purified through an RNeasy Mini column (Qiagen) according to manufacturer's protocol. The RNA was eluted in 30 µl RNase-free water and quantified on a NanoDrop (Thermo Fisher Scientific).

## 2.5.3 Total RNA extraction from cells

Cells were lysed in RLT buffer containing β-mecaptoethanol on ice. RNA was extracted using the RNeasy Mini Kit (Qiagen) according to the manufacturer's protocol. The RNA was eluted in 30 µl RNase-free water and quantified on a NanoDrop (ThermoFisher Scientific).

## 2.5.4 Reverse transcription

RNA was reverse transcribed using SuperScript III Reverse Transcriptase (Invitrogen). RNA samples were diluted to 100 ng/µl. Between 500 ng and 1 µg of RNA was reverse transcribed using 50 ng of random primers according to the manufacturer's protocol.

## 2.5.5 End-point PCR

End-point PCR reactions were performed using GoTaq DNA polymerase (Promega). Briefly 250 ng cDNA was added to, 1x Green GoTaq Reaction Buffer, 0.5 µM forward and reverse primers, 1.25 U GoTaq DNA Polymerase and 0.2 mM dNTPs to a final volume of 50 µl in nuclease-free water. The PCR was run using the following cycling method: 95 °C for 5 mins, 30 cycles of 95 °C for 1 min, 54 °C for 1 min, 72 °C for 1 min then 75 °C for 15 minutes. PCR product was stored at -20 °C.

## 2.5.6 Agarose gel electrophoresis

The PCR products produced in 2.5.5 were run on a 1% TBE agarose gel containing ethidium bromide at 50 V. Gels were then imaged using a Gel Doc EZ Gel Documentation System (BioRad).

## 2.5.7 Real-time quantitative PCR with SYBRgreen

The SYBRgreen qPCR was performed using the Power SYBR Green Master Mix (ThermoFisher Scientific) and a final concentration of 0.3 µM each primer. Amplification and detection was performed with a 7500 Fast Real Time System (Applied Biosystems) using the following cycle profile: 50 °C for 20 sec, 95 °C for 10 min and then 40 cycles of 95 °C for 15 sec, 60 °C for 1 min. On completion of cycling, a dissociation stage was run.

## 2.5.8 Real-time quantitative PCR with TaqMan hydrolysis probe

Quantitative PCR was performed using 1x TaqMan Universal PCR Master Mix and a final concentration of 0.5 µM each primer and 50 nM hydrolysis probe in a 20 µl reaction. Amplification and detection of the specific products was performed with the 7500 Fast Real Time System (Applied Biosystems) with the following cycle profile: 50 °C for 5 min, 95 °C for 2 min and then 40 cycles of 95 °C for 3 sec and 60 °C for 30 sec. A total of 500 ng of reverse transcribed RNA was used for each reaction.

## 2.5.9 Reference gene stability analysis by geNorm

The $C_q$ values of each candidate reference gene across the subset of samples were calculated using the 7500 Fast Real-Time PCR Software version 2.3. (Life Technologies). Raw $C_q$ values were then exported as .csv files and imported into the qbase+ real-time qPCR software version 3.0 (Biogazelle). The software employs the geNorm algorithm (Vandesompele et al., 2002) to calculate the geNorm M value representing the stability of each reference genes and the geNorm V values which suggest the optimal reference gene number.

## 2.5.10 Real-time quantitative PCR data analysis

The quantification cycle ($C_q$) values for each sample were calculated on the 7500 Fast Real-Time PCR Software version 2.3 (Life Technologies). Raw $C_q$ values were then exported as .csv files and imported into Qbase+ Real-time qPCR Software version 3.0 (Biogazelle) where $C_q$ values were normalised to those of reference genes and the relative expression of each gene was calculated in each sample. The software also allowed quality control where by the consistency of technical replicates could be confirmed.

## 2.6 Analysis of Macropinocytosis

### 2.6.1 Stimulation of macropinocytosis

DF1 or Vero cells were seeded onto glass coverslips in 24-well plates to 80% confluency. Cells were treated with 400 nM Porbol-12-myristate-13-acetate (PMA) or DMSO control for 1 hr.

### 2.6.2 Inhibition of macropinocytosis

DF1 or Vero cells were seeded onto glass coverslips in 24-well plates to 80% confluency. Cells were inhibited with 1 mM Amiloride or DMSO control for 1 hr prior to infection.

### 2.6.2 Fluorescent Nanoparticle Uptake

DF1 or Vero cells were stimulated with PMA, mock infected or infected with IBV on glass coverslips in a 24-well plate in triplicate. The nanoparticles used were blue-green 1.0 µm fluorescent (430/465) Fluospheres Polystyrene Microspheres for tracer studies (Life Technologies). A concentration of 100 nanoparticles (np) per cell was calculated and added to each well for 20 mins prior to and for the duration of the infection/treatment. At the indicated time points the cells were washed 3x in PBSa and fixed in 4% paraformaldehyde in PBSa for 20 minutes on ice. Coverslips were then stained with DAPI (4',6-diamino-2-phenylindole) at 1:10,000 in water and mounted onto glass slides. The number of cells containing at least one nanoparticle were counted in three random fields of view on each replicate. If more than 25 cells were visible in a given field of view only the first 25 cells were counted. Cells containing the nanoparticles were identified by scanning through the z-axis of the cell to identify particles present within the cell rather than on the surface or below. Cells were imaged on Leica TCS SP5 Confocal Microscope.

## 2.7 Analysis of Apoptosis

### 2.7.1 Stimulation of apoptosis

Cells were seeded onto 96-well plates to 80% confluency. Apoptosis was stimulated by treatment with 10 µM Staurosporine from point of infection at 0hpi.

### 2.7.2 Caspase 3/7 Cleavage Assay

Cells were seeded into 96-well plates to 80% confluency. Cells were then either stimulated with staurosporine, mock infected or infected with IBV in the presence or absence of LY294002 (see 2.4.2). Cells were incubated in the inoculum for 1 hr at 37 °C and 5% CO2. After 1 hr the inoculum was removed and replaced with 100 µl growth media per well (also containing LY294002). Measurement of caspase 3/7 cleavage was performed using the Caspase-Glo 3/7 Assay (Promega). At various time points post infection 50 µl of the media was removed and replaced with 50 µl of the luminescent caspase substrate. The cells were shaken for 2 mins to lyse the cells and then incubated for 1 hr at room temperature in the dark. After 1 hr, 80 µl of the substrate was removed and placed into a white opaque 96–well plate for reading on a GloMax Luminometer (Promega).

### 2.7.3 Annexin-V-FITC FACS Assay

Cells were seeded into 12-well plates to 80% confluency. Cells were then either stimulated with staurosporine, mock infected or infected with IBV. Cells were then detached from the plates with Accutase Cell Detachment Solution in PBS. The FITC Annexin V Apoptosis Detection Kit II (BD Biosciences) was used to determine the number of cells undergoing apoptosis by flow cytometry. The assay was run according to the manufacturers protocol. Detached cells were washed in cold PBSa and resuspended in 1 ml 1x Binding Buffer. 100 µl of the suspension was transferred to a 5 ml FACS tube and 5 µl FITC Annexin V was added. The cells were gently vortexed and incubated for 10 mins at room temperature in the dark. 5

µl of PI was then added and incubated for a further 5 mins in the dark. 400 µl 1x Binding Buffer was then added to the suspension and fluorescence was immediately analysed on a MACS QUANT flow cytometer.

The flow cytometry analysis is illustrated in Appendix 1-3 and was performed as follows. A population of DF1 cells was selected for by gating, removing cellular debris. Single cells were subsequently selected for on an SSC area vs height plot. The population of single cells was then plotted on an Annexin V-FITC vs PI plot and quadrant gates added.

## 2.8 Cloning of IBV structural proteins

### 2.8.1 Primer design

Primers were designed to amplify the region of the IBV genome encoding either the envelope (E) or membrane (M) protein.

Table 2.9 Oligonucleotide sequences for IBV_E and IBV_M expression plasmids

| Oligonucleotide | Sequence |
|---|---|
| Beau-R_ E_Fwd | 5'-TATAGCGGCCGCATGAATTTATTGAATAAGTCGC-3' |
| Beau-R_E_Rev | 5'-ATATAAGCTTTCAAGAGTACAATTTGTCTCGTTGG-3' |
| Beau-R_M_Fwd | 5'- TATAGCGGCCGCATGCCCAACGAGACAAATTG-3' |
| Beau-R_M_Rev | 5'-ATATAAGCTTCTAAGCGTAATCTGGAACATCGTATGGGTATGTGTAAAGACTACTTCC-3' |

Restriction sites for *NotI* and *Hind III* were included in both designs (yellow and blue respectively). The M primers were designed including an HA tag on the reverse primer as no anti-M antibody was available (pink).

## 2.8.2 Amplification of insert and PCR purification

An endpoint PCR was run to amplify the Beau-R_E or Beau-R_M inserts. The amplification was performed using Platinum Taq DNA Polymerase High Fidelity (ThermoFisher Scientific). One unit (U) of Taq was added to a final concentration of 1x High Fidelity PCR Buffer, 2.0 mM $MgSO_4$, 0.2 mM dNTPs (each), 0.2 µM each primer and 500 ng Beau-R virus stock cDNA in a 50 µl reaction. The following cycle profile was used: 94 °C for 30 sec then 35 cycles of 94 °C for 15 sec, 65 °C for 30 sec and 68 °C for 1 min. PCR products were then visualised by running on a 1% TBE agarose gel containing ethidium bromide. The products were then extracted from the gel using a Qiaquick Gel Extraction Kit (Qiagen) according to the manufacturer's protocol. DNA was eluted in 30 µl elution buffer.

## 2.8.3 Restriction Digests

Both PCR products were digested alongside the pcDNA 3.1 (-) vector using *Not1-HIFI* (High Fidelity) and *HindIII* in buffer 2.1 (NEB). Fifteen µl of the purified PCR product was digested with 2.5 µl of the buffer, NotI, HindIII and nuclease-free water. 3 µg of the vector was digested with 2 µl of buffer, 2 µl *Not1*, 2 µl *HindIII* and 1 µl alkaline phosphatase in 9 µl nuclease-free water. Both samples were digested for 2 hrs at 37 °C and stored at -20 °C.

## 2.8.4 Ligation

The Beau-R_E and Beau-R_M inserts were inserted into the pcDNA 3.1 (-) vector using T4 Ligase (NEB) according to the manufacture's protocol. Ligation was performed overnight at 15 °C.

## 2.8.5 Transformation into competent cells

The samples were transformed in NEB 5-alpha Competent *E. coli* (High Efficiency) cells (NEB). Three µl of the ligation mix made in 2.8.4 was added to 50 µl competent cells and incubated on ice for 20 mins. After 20 mins the cells were heat-shocked at

42 °C for 45 secs before being returned to ice for 2 mins. 250 µl SOC media was added and the transformation mix incubated at 37 °C for 1 hr in a shaking incubator. 100 µl of the mix was then plated onto ampicillin plate and incubated overnight at 37 °C.

## 2.8.6 Plasmid Miniprep

From the colonies grown on the ampicillin plates in 2.8.5, 6 colonies were picked and grown in LB containing ampicillin resistant bacteria overnight at 37 °C in a shaking incubator. A glycerol stock was made by mixing 600 µl overnight culture with 400 µl glycerol and stored at -80 °C. Plasmids from the remaining culture was purified using a Plasmid Miniprep Kit (Qiagen) according to manufacturer's protocol. The plasmids were then digested according to the protocol in 2.8.3 and visualised on a 1% TBE gel to ensure that the insert was present. Plasmids were also sequenced by sanger sequencing.

## 2.8.7 Plasmid DNA Maxiprep

From the glycerol stocks prepared in 2.8.6 a new 100 ml culture of plasmid was grown and the plasmid DNA purified using a Plasmid DNA Maxiprep Kit (Qiagen) according to the manufacturer's instructions.

## 2.8.8 Transfection of plasmids into DF1 cells

DF1 cells were seeded onto 12-well plates or on glass coverslips in 24-well plates for immunofluorescence to 80% confluency. Cells were transfected with expression plasmids using Lipofectamine 2000 (ThermoFisher Scientific) according to the manufacturer's protocol. A ratio of 2 µl:1 µg of lipofectamine 2000 to plasmid was used. Transfection was performed in Optimem media for 24 hrs.

## 2.9 Statistical Analysis

All graphs were created and statistical analysis performed using GraphPad Prism 7 (GraphPad Software, Inc.). For each data set the type of statistical analysis used is noted in the figure legend.

# Chapter 3

## PI3K/AKT activation during IBV infection

## 3.1 Introduction

All viruses, as intracellular parasites, require control over cellular machinery to replicate within the cell. Signalling pathways of host cells are often modulated during viral infection. One of the most commonly used pathways is PI3K/AKT, which controls processes such as translation, protein synthesis, actin re-arrangement, glycogen synthesis, cell cycle progression and cell death. The earliest point at which the host cellular pathways are modulated by a virus is during initial attachment and entry into the cell. However, pathways are also modulated to induce pre-mRNA splicing (Hillebrand et al. (2014), cell survival (Bagchi et al. (2010) and protein synthesis (Johnson et al. (2001). Molecular interactions between cellular signalling pathways and IBV are examined in this chapter. The effect of IBV infection on the activation state of AKT, in the context of PI3K/AKT signalling, has been investigated. PI3K specific inhibitors were utilised to understand the importance of signalling pathways in viral replication. The structural proteins of other coronaviruses have been implicated in the activation of cellular signalling pathways (Tsoi et al., 2014). We therefore investigated the effect of over expression of the IBV structural proteins on PI3K/AKT modulation.

## 3.2 Cellular tropism of IBV strains M41 and Beau-R

The phenotypes and cellular tropism of different coronaviruses are often determined by variations in the spike protein, which is involved in receptor binding and membrane fusion with the host cell. Two laboratory strains of IBV were used in this study. The first is the pathogenic M41 strain that has been adapted to grow in chick kidney cells (CK cells) (Darbyshire et al., 1979). The second is the apathogenic molecular clone of Beaudette CK (Beau-R) (Casais et al., 2001). Beau-R, in comparison to M41, has an extended cellular tropism.

In order to confirm these reports, the tropism of both viruses was investigated in a variety of cell types by immunofluorescence (Figure 3.1).

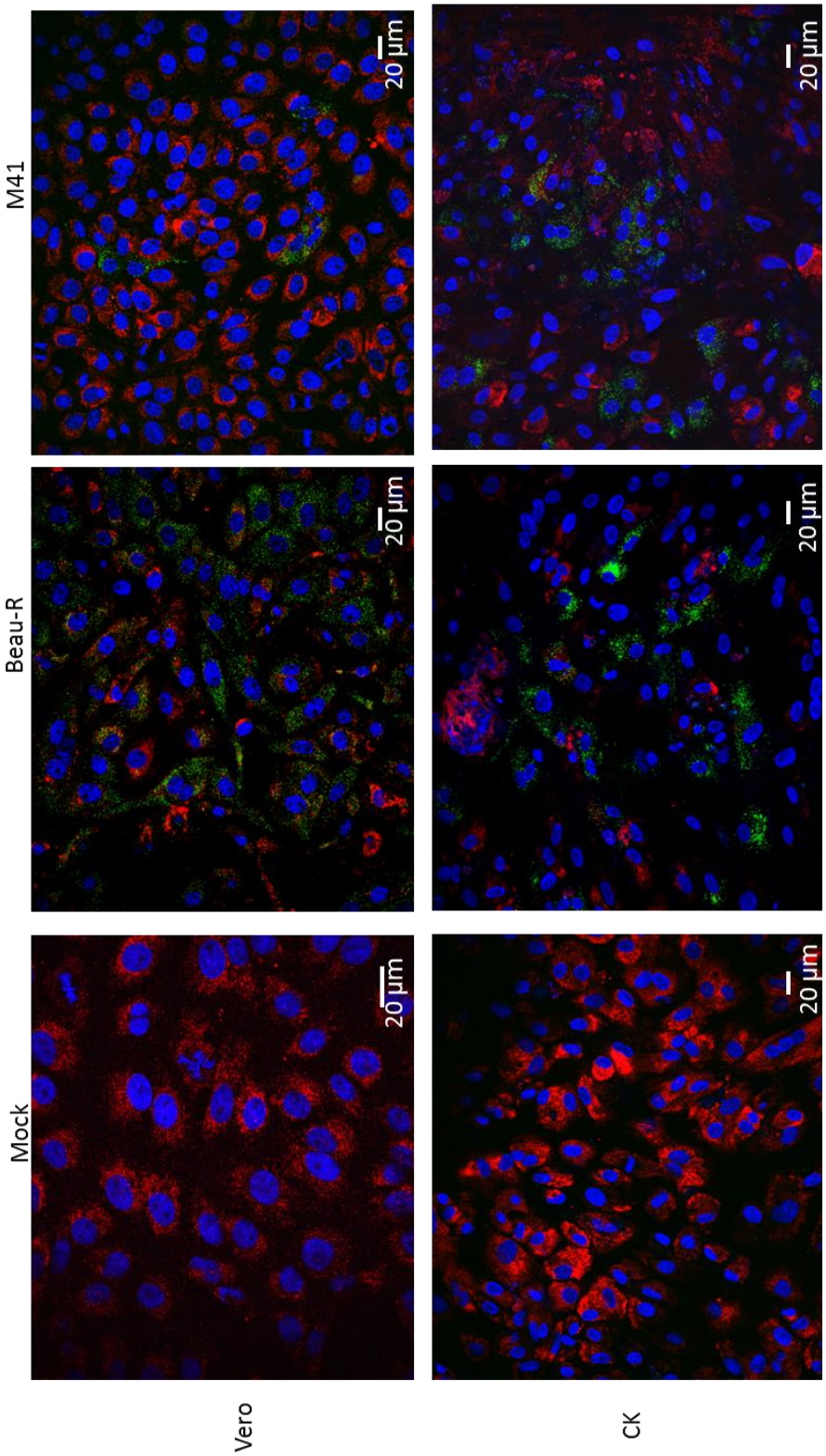
Vero
CK
Mock
Beau-R
M41
20 µm

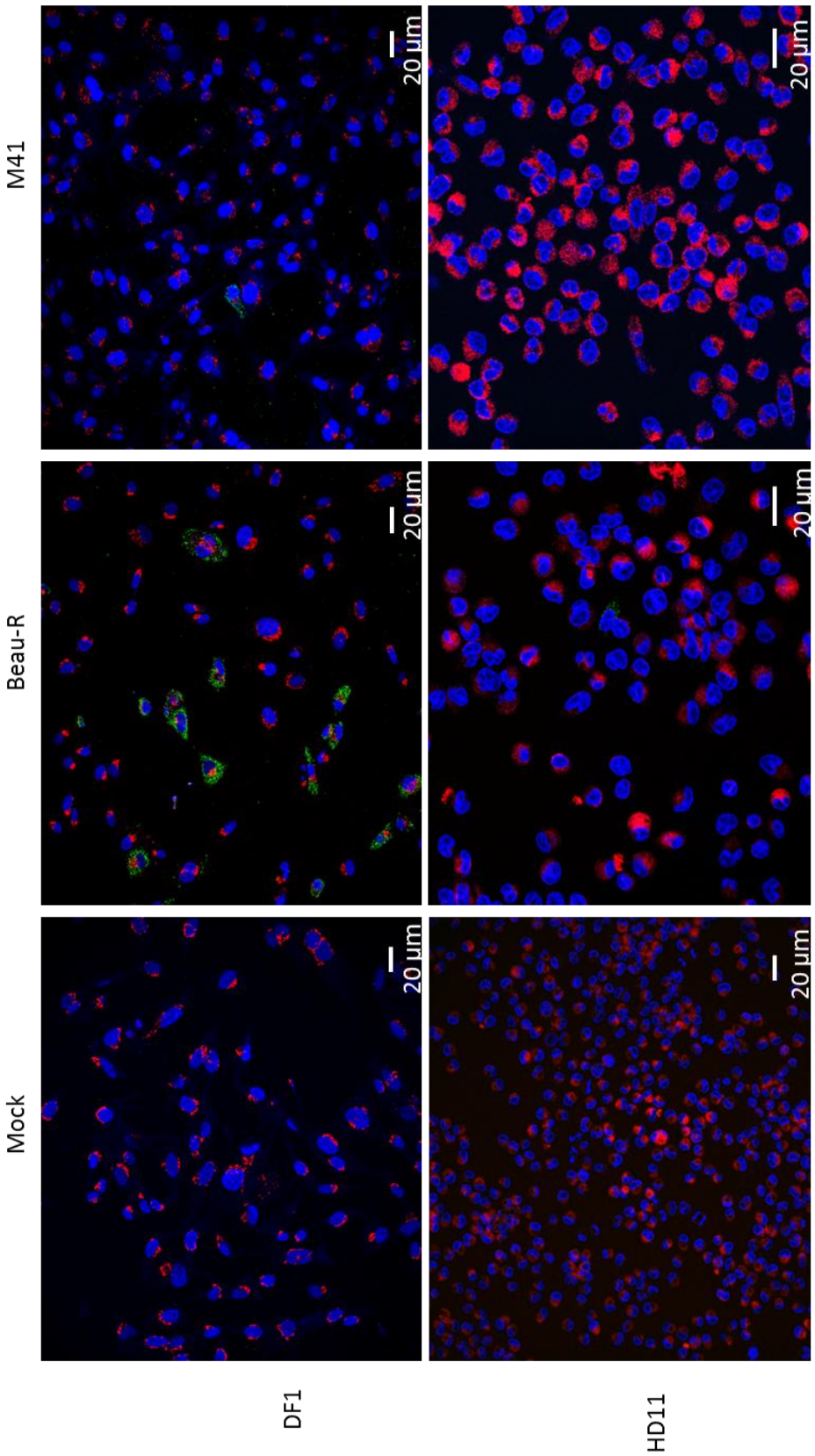


**Figure 3.1 Immunofluorescence of avian and mammalian cells demonstrating susceptibility to IBV Beau-R and M41 infection.** Vero, DF1, HD11 and CK cells treated were mock infected, infected with Beau-R or M41 and fixed at 24 hpi. Cells were permeabilised and labelled with anti-dsRNA (green), anti-ER (red) in Vero cells and anti-Golgi (red) in DF1, CK and HD11 cells. Nuclei were stained with DAPI.

**Table 3.1 Qualitative description of IBV infection of different cell types.**

| | Vero | CK | DF1 | HD11 |
|---|---|---|---|---|
| Beau-R | +++ | +++ | ++ | + |
| M41 | + | +++ | + | -- |

-- = 0 cells infected, + < 10 cells infected, 10 < ++ < 20 cells infected , +++ > 20

The susceptibility of the mammalian kidney cell line, Vero, was compared to that of various avian cell types. The avian dendritic fibroblast line of DF1 cells, the HD11 macrophage cell line and primary chick kidney (CK) cells were also tested. All cells were infected with M41 for 24 hrs. The cells were fixed and labelled with antibodies against the golgi apparatus (anti-golgi), the endoplasmic reticulum (anti-ER) and anti-dsRNA to identify viral infection. Nuclei were stained with DAPI. Some dsRNA labelling was observed in the mammalian Vero cell line. However, the extent of labelling was lower than that in the avian CK cells, in which the virus is regularly grown and titrated. Infection of the avian DF1 cell line was also very low, with only one or two cells showing dsRNA labelling per field of view. No dsRNA was observed in HD11 cells infected with M41. The same cell lines were also infected with Beau-R. In contrast to M41 infected cells, high levels of dsRNA labelling was observed in the Vero, CK and DF1 cells infected with Beau-R. The Beau-R infected HD11 cells exhibited a very low level of dsRNA labelling with only one or two cells infected per field of view. The ability of the virus to infect both mammalian and avian cells was essential for this project to allow the comparison of signalling modulation during infection of different cell types. Therefore, for the purpose of this study, Beau-R was used as a model for IBV infection in mammalian and avian cells, unless otherwise stated.

## 3.3 AKT activation during IBV infection

### 3.3.1 IBV infection induces AKT activation in mammalian cells in a PI3K-dependent manner

The immunofluorescence study shown in Figure 3.1 demonstrated the ability of the IBV strain Beau-R to infect and replicate within mammalian Vero cells. The PI3K/AKT signalling pathway is well characterised in mammalian cells and has been shown to be activated by receptor tyrosine kinases (RTK) at the cellular membrane. One known activator of RTKs is epidermal growth factor (EGF). To assess AKT

activation by EGF, Vero cells were mock treated with DMSO or EGF for 15 minutes (Figure 3.2). The cells were lysed, proteins separated by SDS-PAGE and transferred onto nitrocellulose membranes. Western blots were performed using an AKT antibody specific to the S473 phosphorylated form of the protein (anti-pAKT S473) and anti-β-actin (Figure 3.2A).

Densitometric analysis of the western blot demonstrated elevated levels of pAKT S473 in the EGF stimulated cells relative to control, and normalised to levels of β-actin (Figure 3.2B). The AKT signalling pathway is involved at various points during viral replication. To determine whether IBV infection activated AKT, and to identify at which time points this occurred, Vero cells were infected with IBV and lysed at 2, 6 12 and 24 hpi. Western blots were ran as previously described and probed with anti-pAKT S473 and anti-β-actin (Figure 3.3A). Densitometric analysis showed that pAKT S473 levels began to increase at 6 hpi with large increases in activation seen at 12 and 24 hpi (Figure 3.3B).

Activation of AKT can occur in a PI3K-dependent or independent manner. To determine whether IBV-induced activation of mammalian AKT was PI3K dependent, PI3K was inhibited using a specific inhibitor, LY294002.

Initially, the cytotoxicity of LY294002 in Vero cells was assessed using the CellTitre –Glo assay (Promega) that measures the quantity of metabolically active cells (Figure 3.4A). The viability of the cells was not significantly affected by the addition of LY294002 at final concentrations of either 10 or 20 µM. However, at 50 µM cellular activity decreased significantly ($p<0.02$). The efficacy of LY294002 at 10 µM was assessed by western blot (Figures 3.4B & 3.4C). Vero cells were mock stimulated with DMSO or stimulated with EGF in the presence or absence of LY294002. After 15 minutes the cells were lysed and separated by SDS-PAGE.

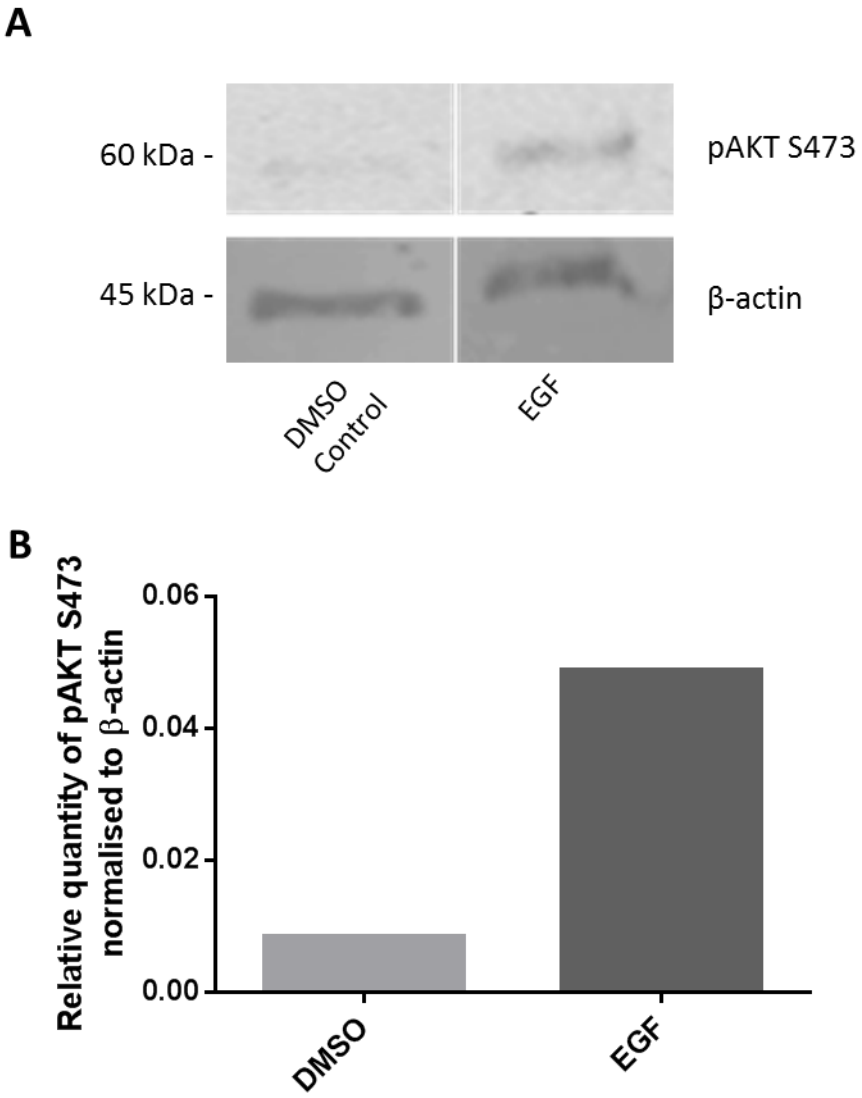


**Figure 3.2 Phosphorylation of AKT at S473 in mammalian cells stimulated with EGF.** (A) Vero cells were treated with a DMSO control or stimulated with EGF for 15 minutes and lysed. Lysates were separated by SDS-PAGE and western blot performed with anti-β-actin or anti-pAKT S473. Molecular weights indicated. Blots are representative of 3 separate experiments. (B) Densitometry of western blot bands, normalized to levels of anti-β-actin.

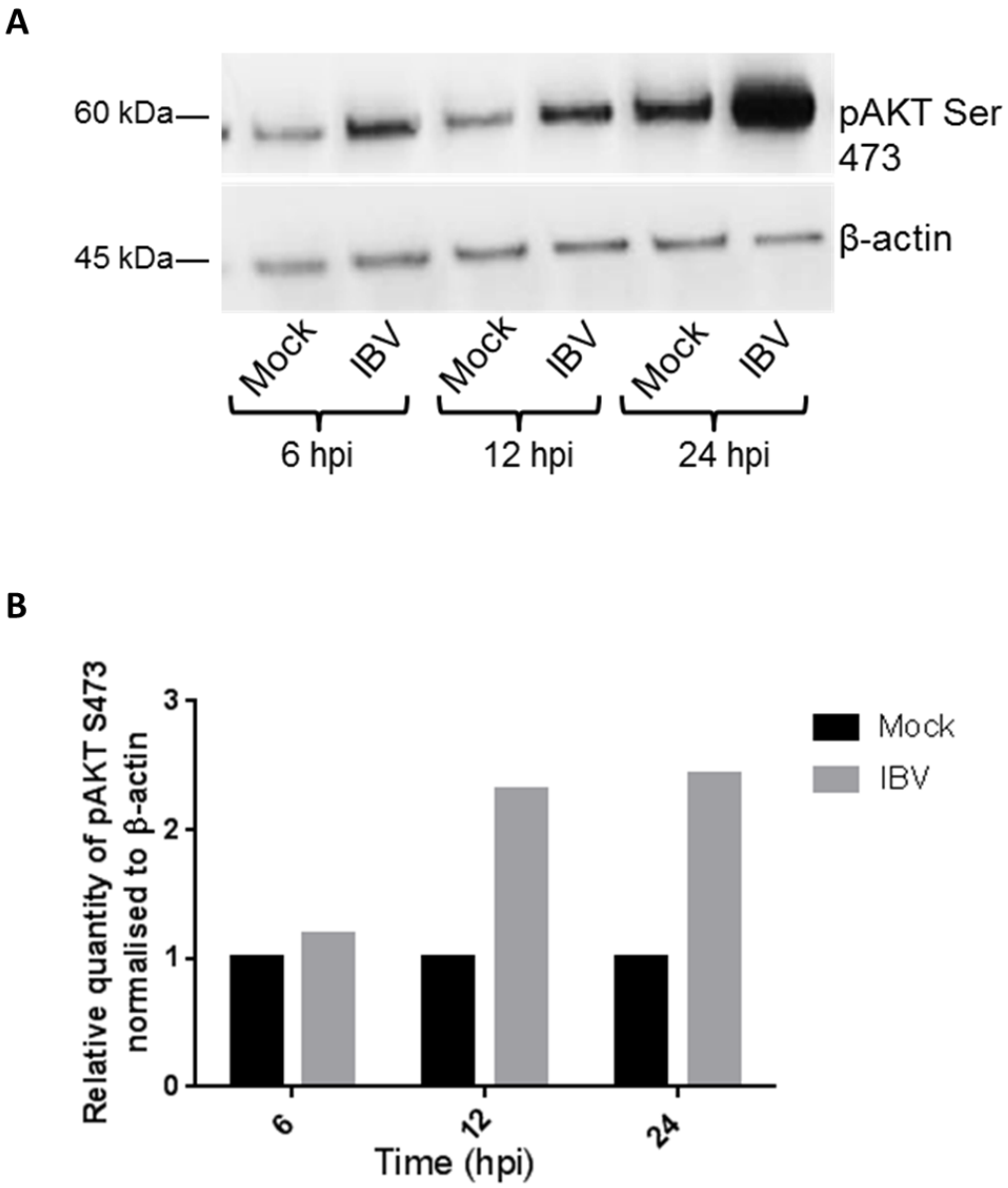


**Figure 3.3 Phosphorylation of AKT at S473 in mammalian cells late during infection.** (A) Vero cells were mock infected or infected with IBV and lysed at the indicated time points. Lysates were separated by SDS-PAGE and western blot performed with anti-β-actin or anti-pAKT. Molecular weights indicated. Blots are representative of 3 separate experiments. (B) Densitometry of western blot bands, normalized to levels of anti-β-actin.

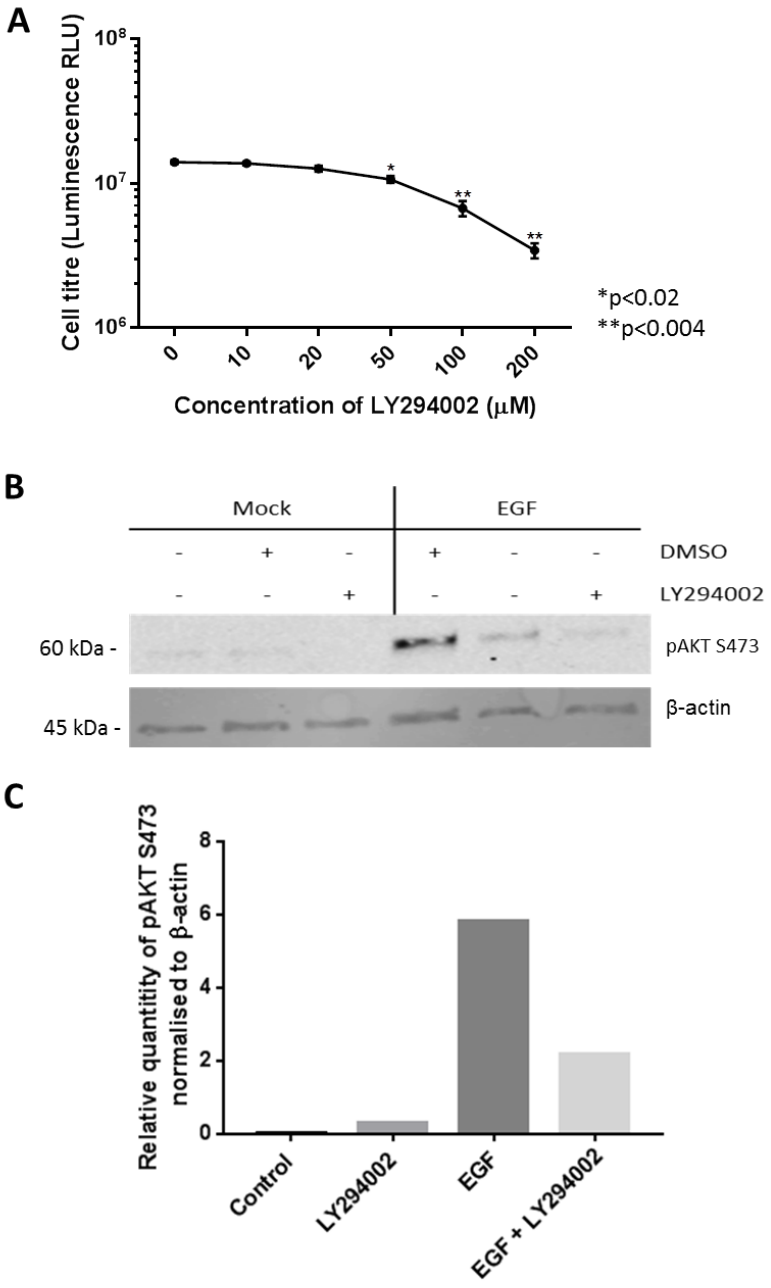


**Figure 3.4 Optimisation of LY294002 concentration on Vero cells.** (A) Vero cells were treated with different concentrations of LY294002 and the cytotoxicity of the inhibitor measured by chemiluminescent cell viability assay. P values calculated by unpaired t-test. (B) Vero cells were mock treated or stimulated with EGF in the presence or absence of LY294002. After 15 minutes the cells were lysed and proteins were separated by SDS-PAGE and western blot performed with anti-β-actin or anti-pAKT. Molecular weights indicated. Blots are representative of 3 separate experiments. (C) Densitometry of western blot bands, normalized to DMSO controls and levels of anti-β-actin.

Proteins were then subjected to western blotting and probed with anti-pAKT S473 and anti-β-actin (Figure 3.4B). Analysis of the western blots showed an increase in pAKT S473 in cells stimulated with EGF. However, this activation was inhibited by LY294002 at 10 µM (Figure 3.4C).

Vero cells were subsequently infected with IBV in the presence or absence of the LY294002. At 12 and 24 hpi the cells were lysed, proteins separated by SDS-PAGE and transferred onto membrane for western blotting. The membranes were probed with anti-pAKT and anti-β-actin (Figure 3.5A). Whilst IBV infection induced activation of AKT at 24 hpi, analysis of the blots showed that treatment of cells with LY294002 prevented this, indicating that IBV induced activation of AKT occurs in a PI3K-dependent manner in mammalian cells (Figure 3.5B).

### 3.3.2 IBV infection of avian cells induces AKT activation in a biphasic manner

Recombinant mammalian EGF was previously shown to activate AKT in mammalian cells (Section 3.3.1). Its effect on avian cells was subsequently investigated. DF1 cells were treated with either 5 ng/µl or 10 ng/µl of EGF and lysed at different time points. Western blots were prepared and probed with anti-pAKT S473 and anti-β-actin (Figure 3.6). Treatment of DF1 cells with EGF did not induce AKT activation at any time point or concentration tested. Stimulation of PI3K/AKT signalling with lipopolysaccharides (LPS) was also tested (data not shown). However, LPS stimulation also did not induce AKT activation. Therefore, infectious bursal disease virus (IBDV) was used as a positive control as it is known to activate AKT (Wei et al., 2011). DF1 cells were mock infected or infected with IBDV at a MOI of 10. Cells were lysed at 8, 12, 18 and 24 hpi and proteins separated by SDS-PAGE. Western blots were incubated in anti-pAKT S473 or anti-β-actin (Figure 3.7). The western blot confirms the findings of Wei et al. (2011).

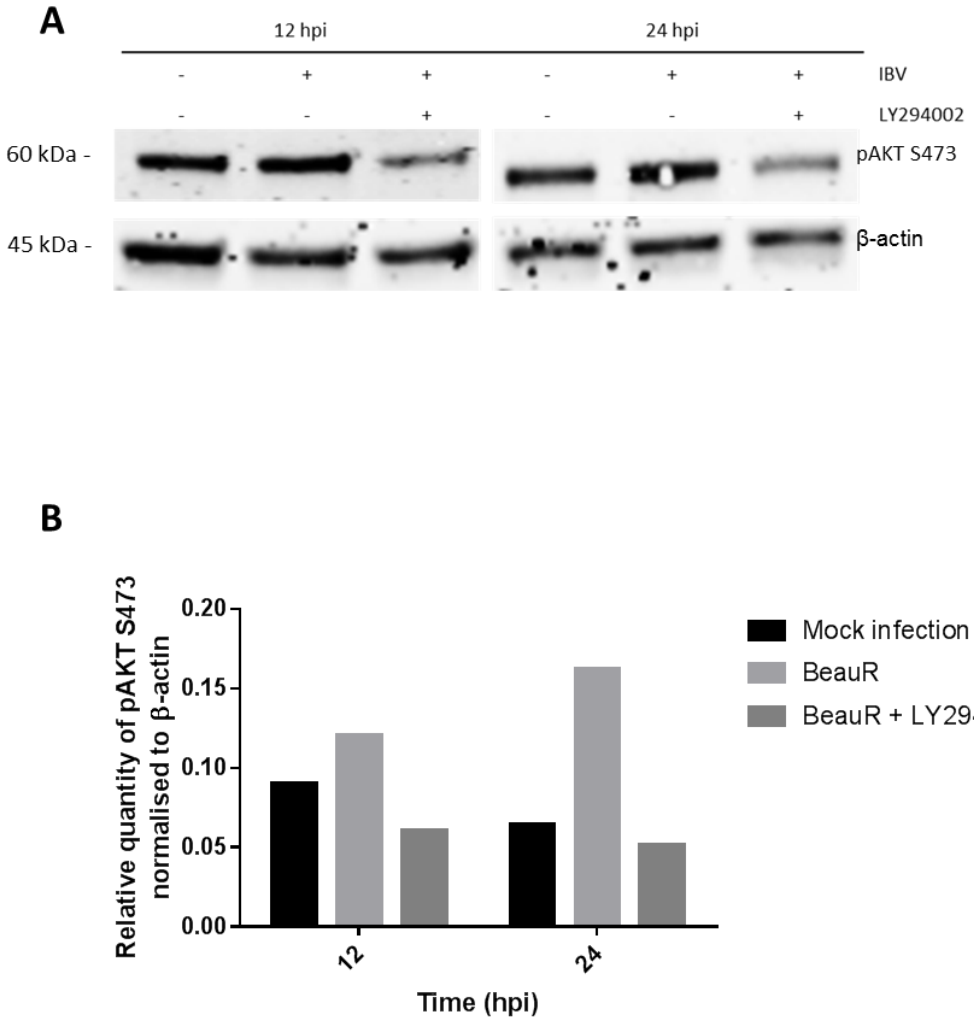


**Figure 3.5 Phosphorylation of AKT during IBV infection in the presence and absence of PI3K inhibitor.** (A) Vero cells were mock infected or infected with IBV in the presence or absence of LY294002. Cells were lysed at 12 and 24 hpi and lysates separated by SDS-PAGE. Proteins were transferred to membranes and a western blot performed using anti-pAKT and anti-β-actin. Blot is representative of 3 experiments. Molecular weights indicated. (B) Densitometry of western blot bands, normalized to levels of anti-β-actin.

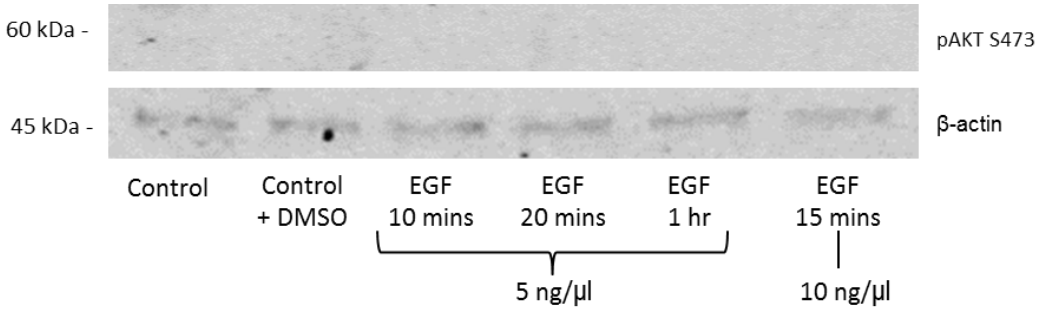


**Figure 3.6 EGF stimulation of AKT in DF1 cells.** DF1 cells were control treated or stimulated with EGF at 5 ng/ml or 10 ng/ml. Cells were lysed at 10 mins, 15 mins, 20 mins or 1 hour. Proteins were separated by SDS-PAGE and transferred onto a membrane. Blots were incubated in anti-pAKT S473 and anti-β-actin. Representative of 3 experiments. Molecular weight indicated.

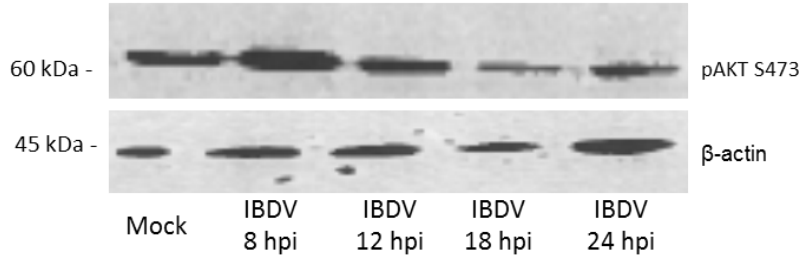


**Figure 3.7 Infection of DF1 cells with IBDV.** DF1 cells were mock infected or infected with IBDV and cells lysed at 8, 12, 18 and 24 hpi. Proteins were separated by SDS-PAGE and transferred onto a membrane. Two separate blots were probed with anti-pAKT S473 or anti-β-actin. Blots were imaged using ECL reagent. Representative of 3 experiments. Molecular weight indicated.

IBDV infection of DF1 cells induces phosphorylation of AKT at S473 over time with a peak at 8 hpi. In the absence of another positive control, IBDV infection was used.

The effect of LY294002 on AKT activation in avian cells was consequently investigated using IBDV as a positive control. Initially the cytotoxicity of LY294002 in DF1 cells was established using a cell titre assay (Figure 3.8A). The viability of DF1 cells was not significantly affected by addition of LY294002 at 10 μM, however at 100 μM the cellular activity decreases significantly ($p<0.0001$). DF1 cells were more sensitive to the effects of LY294002 than Vero cells, with a decrease of 7.4 RLU in Vero cells and 11.4 RLU in DF1 cells from 0 μM to 100 μM. Subsequently DF1 cells were mock infected or infected with IBDV in the presence or absence of 10 μM LY294002. Cells were lysed at 8 hpi and western blots probed with anti-pAKT S473 and anti-β-actin (Figure 3.8B). Analysis of the western blot showed pAKT S473 activation in IBDV infected cells which was inhibited by the presence of LY294002 (Figure 3.8C).

The effect of LY294002 on IBV-induced activation of AKT was investigated. Avian DF1 cells were infected with IBV in the presence or absence of LY294002 and at 2, 8, 12, 16 and 24 hpi, the cells lysed, proteins separated by SDS-PAGE and western blots incubated with anti-pAKT S473 and anti-β-actin (Figure 3.9A). Densitometric analysis of the western blot showed that, in the absence of LY294002, IBV induced a biphasic activation of AKT that increased at 2 hpi, was supressed by 8 hpi and then increased again from 16 to 24 hpi (Figure 3.9B).

In all replicates in the presence of LY294002, AKT activation was suppressed at 16 and 24 hpi. However, there was variation in pAKT S473 levels during PI3K inhibition at earlier time points. This suggests that that the modulation of AKT at these early time points may be dependent on several factors which result in large variation between samples.

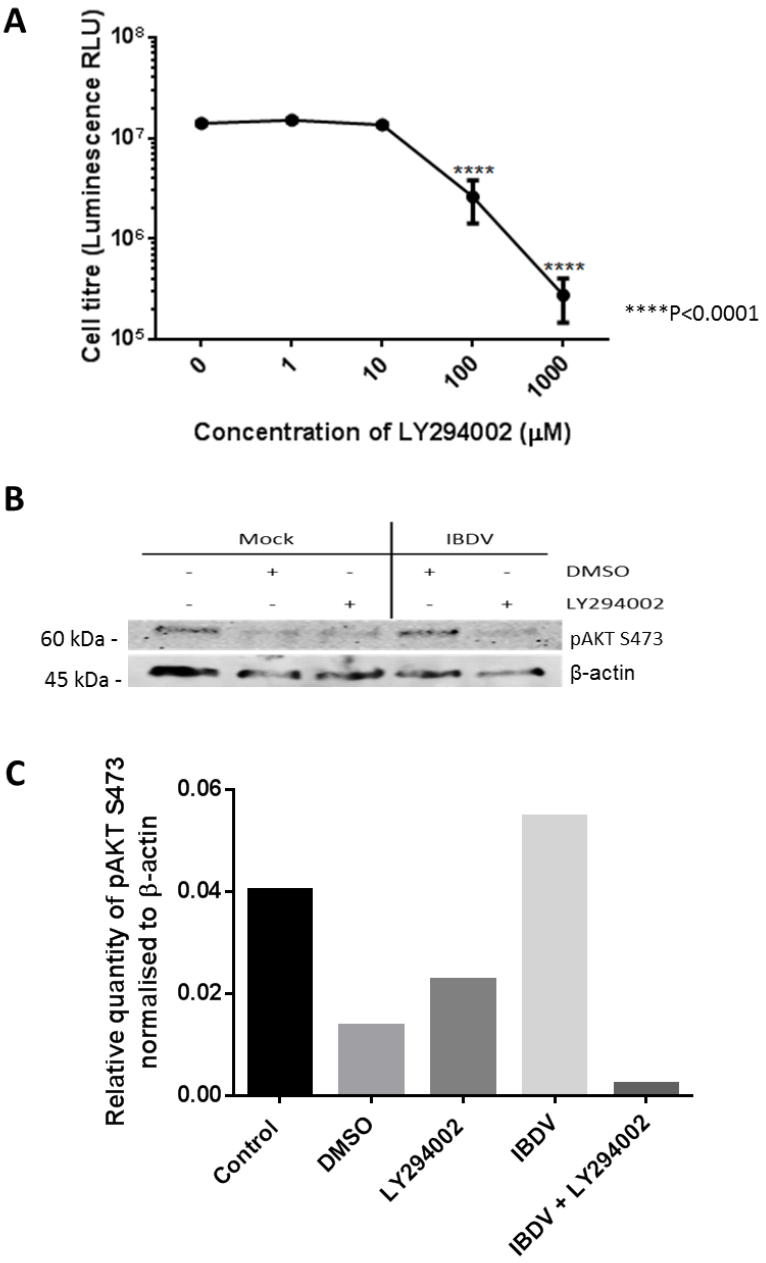


**Figure 3.8 Optimisation of LY294002 concentration on DF1 cells.** (A) DF1 cells were treated with different concentrations of LY294002 and the cytotoxicity of the inhibitor measured by chemiluminescent cell viability assay. P values calculated by unpaired t-test. (B) DF1 cells were mock infected or infected with IBDV in the presence or absence of 10 µM LY294002. Lysates were separated by SDS-PAGE, transferred onto membrane and incubated with anti-β-actin and anti-pAKT. Molecular weights indicated. (C) Densitometry of western blot bands, normalized to levels of anti-β-actin.

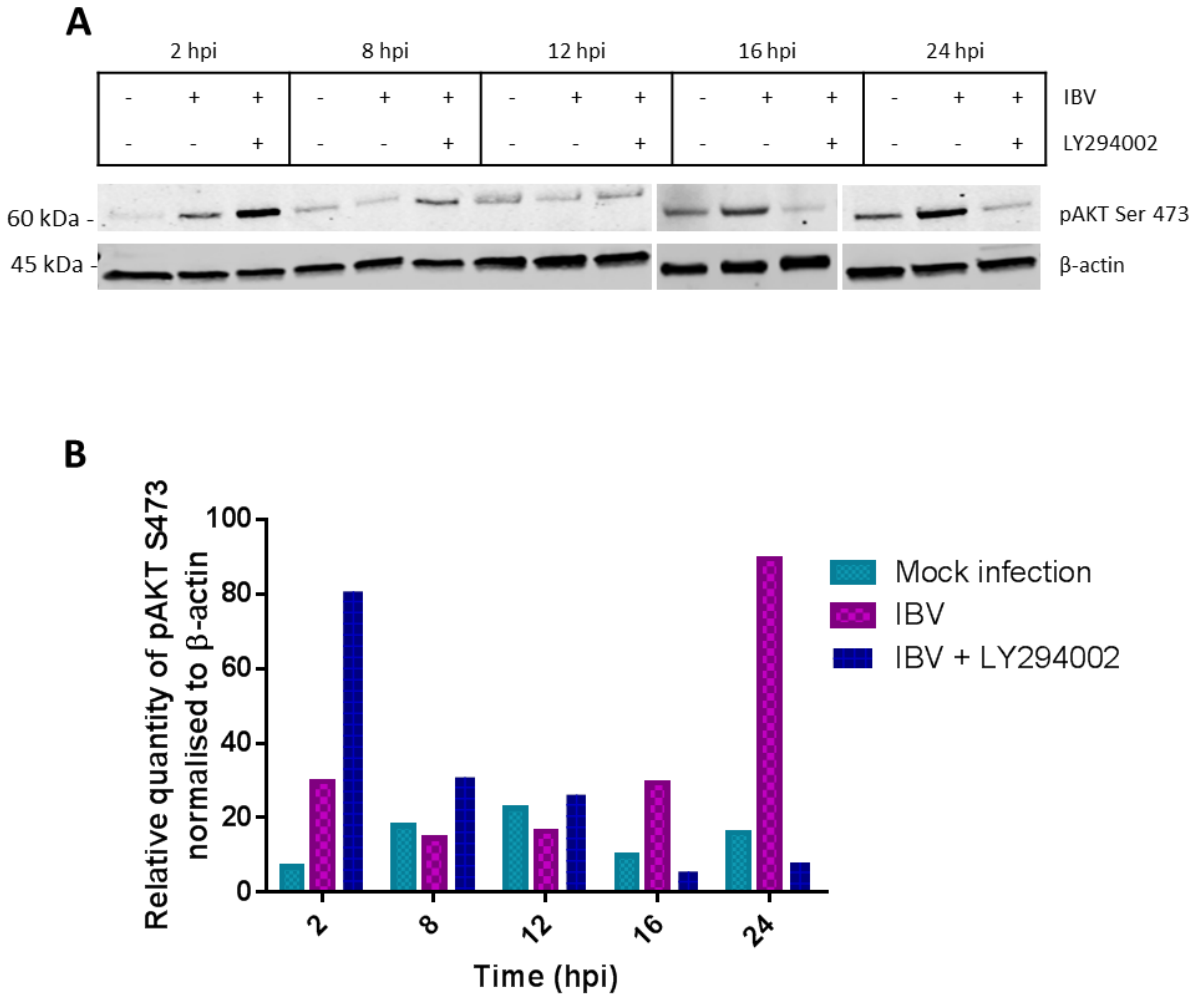


**Figure 3.9 Phosphorylation of pAKT S473 in DF1 cells infected with IBV in the presence or absence of LY294002**. (A) DF1 cells were mock infected or infected with IBV in the presence or absence of LY294002. Cells were lysed at 2, 8, 12, 16 and 24 hpi, lysates separated by SDS-PAGE and a western blot performed with anti-pAKT S473 and anti-β-actin. Blot representative of 3 experiments. Molecular weights indicated. (B) Densitometry of western blot bands, normalized to levels of anti-β-actin.

Complete activation of AKT in mammals requires phosphorylation at two sites, S473 and T308. Therefore, it could be hypothesised that variations in avian pAKT T308 would be consistent with those of pAKT S473 during IBV infection.

To establish this, lysates from mock or IBV infected DF1 cells in the presence or absence of LY294002 were subjected to western blot. Blots were probed with anti-pAKT T308 and anti-β-actin (Figure 3.10A). Analysis of the western blots show a similar pattern of T308 phosphorylation as S473 (Figure 3.10B). A biphasic phosphorylation of AKT at T308 was seen and activation at 24 hpi was found to be dependent on PI3K activity.

### 3.3.3 Initial phase of AKT phosphorylation is dependent on viral entry

Several viruses have been found to modulate the PI3K/AKT signalling pathway to aid cell entry. Interestingly, HIV has been found to activate signalling pathways as early as a minute post infection (Wojcechowskyj et al., 2013). AKT activation occurs early during infection in avian cells (Section 3.3.2). In order to assess whether the activation of AKT was a result of receptor biding and viral entry, an inactivated form of IBV was prepared (methods section 2.2.6). The viral RNA of Beau-R was inactivated with 0.1M binaryethylemine (BEI) without affecting viral proteins, allowing the virion to bind to cellular receptors and enter the cell but not replicate.

In order to ensure that replication was inhibited, qPCR was used to quantify copies of viral genome alongside wild-type (wt-IBV) infected cells (Figure 3.11A). A four log increase in genome copy number in wt-IBV infected cells was seen at 24 hpi. However, no significant increase in viral genome copy number was observed with the inactivated virus.

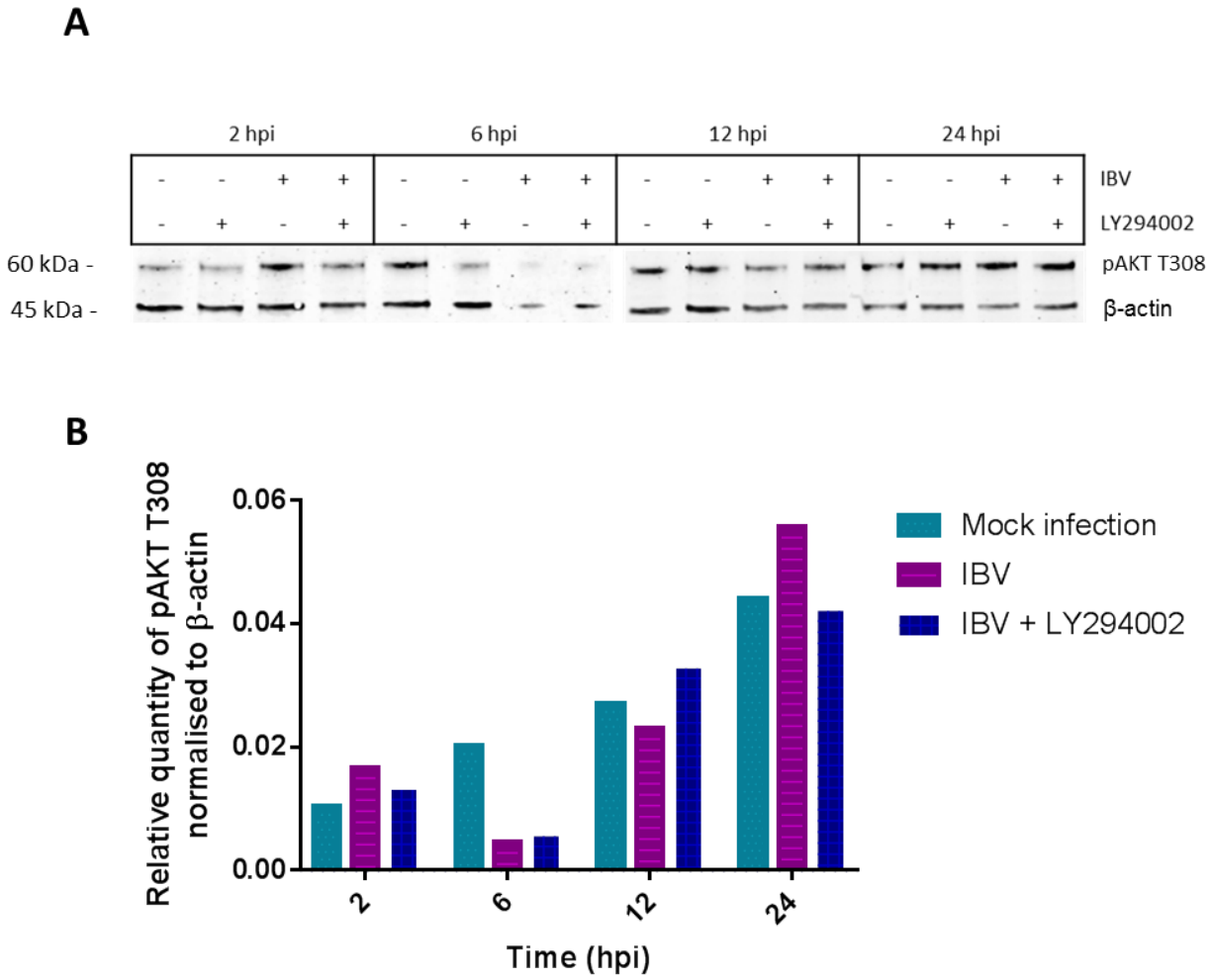


**Figure 3.10 Phosphorylation of pAKT at T308 in DF1 cells infected with IBV in the presence or absence of LY294002**. DF1 cells were mock infected or infected with IBV in the presence or absence of LY294002. Cells were lysed at 2, 8, 12, 16 and 24 hpi, lysates separated by SDS-PAGE and western blotted with anti-pAKT T308 and anti-β-actin. Blot representative of 3 experiments. Molecular weights indicated. (B) Densitometry of western blot bands show in graph, normalized to levels of anti-B-actin.

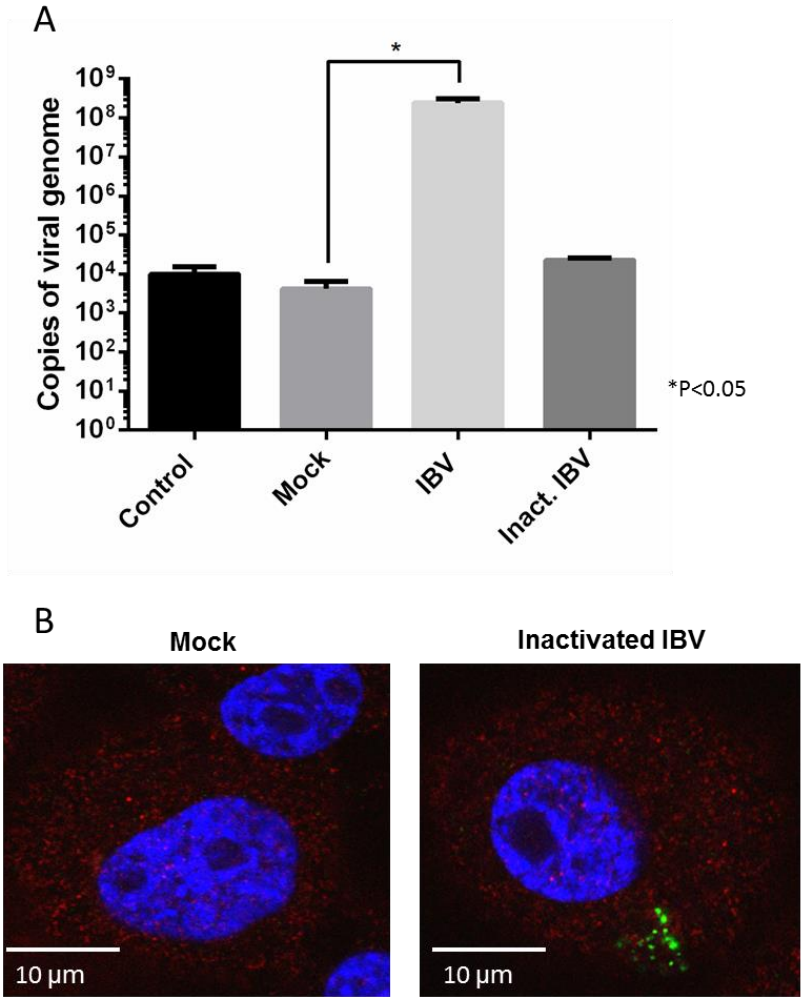


**Figure 3.11 Inactivation of IBV with binaryethylemine (BEI).** (A) DF1 cells were mock infected or infected with inactivated IBV or wt-IBV. At 24 hpi cells were lysed and RNA extracted. Quantitative real-time PCR (qPCR) amplifying the 5'UTR section of the IBV genome was run. Copy number was calculated from Cq values on a standard curve. P values calculated by multiple t-tests. (B) DF1 cells were mock infected or infected with inactivated IBV and fixed at 1 hpi. Cells were stained with anti-S2 (green) and DAPI and imaged by confocal microscopy.

To ensure entry of the virus into the cells, DF1 cells were mock infected or infected with the inactivated IBV. At 30 mins post infection, cells were fixed and labelled with anti-IBV S2, to indicate virions, and anti-tubulin (Figure 3.11B). Nuclei were stained with DAPI. IBV S2 labelling is localised within the cytoplasm as indicated by tubulin, suggesting that the virus was capable of binding and entry. Taken together, these data demonstrate that the inactivated virus binds and enters the cell, however is not able to replicate.

Having successfully created an inactivated form of IBV, DF1 cells were infected with the wild-type or inactivated virus and lysed at 30 mins, 1 and 24 hpi. The proteins were separated by SDS-PAGE, transferred to a membrane and probed with anti-pAKT S473 and anti-β-actin (Figure 3.12A). Levels of pAKT S473 were normalised to levels of β-actin. Densitometry results for both wt-IBV and inactivated IBV samples were normalised to mock. Analysis of the western blots demonstrated an increase in the activation of AKT as early as 30 mins post infection in cells infected with the wild type as well as the inactivated IBV (Figure 3.12B). This suggests that binding of viral proteins to cellular receptors, fusion of viral membrane or presence of viral genome in the cell is sufficient to activate AKT.

## 3.4 Replication of IBV requires an active PI3K/AKT signalling pathway

The role of the PI3K/AKT signalling pathway in the replication of other viruses has been well documented. Many viruses require an active PI3K/AKT pathway to replicate efficiently within a cell, and activation of the pathway is often induced by the virus. It is therefore possible that IBV induces AKT activation to promote viral replication. If correct, inhibition of the pathway may affect replication of the virus. This was investigated and the effect of PI3K inhibition was determined at various points during the viral replication cycle.

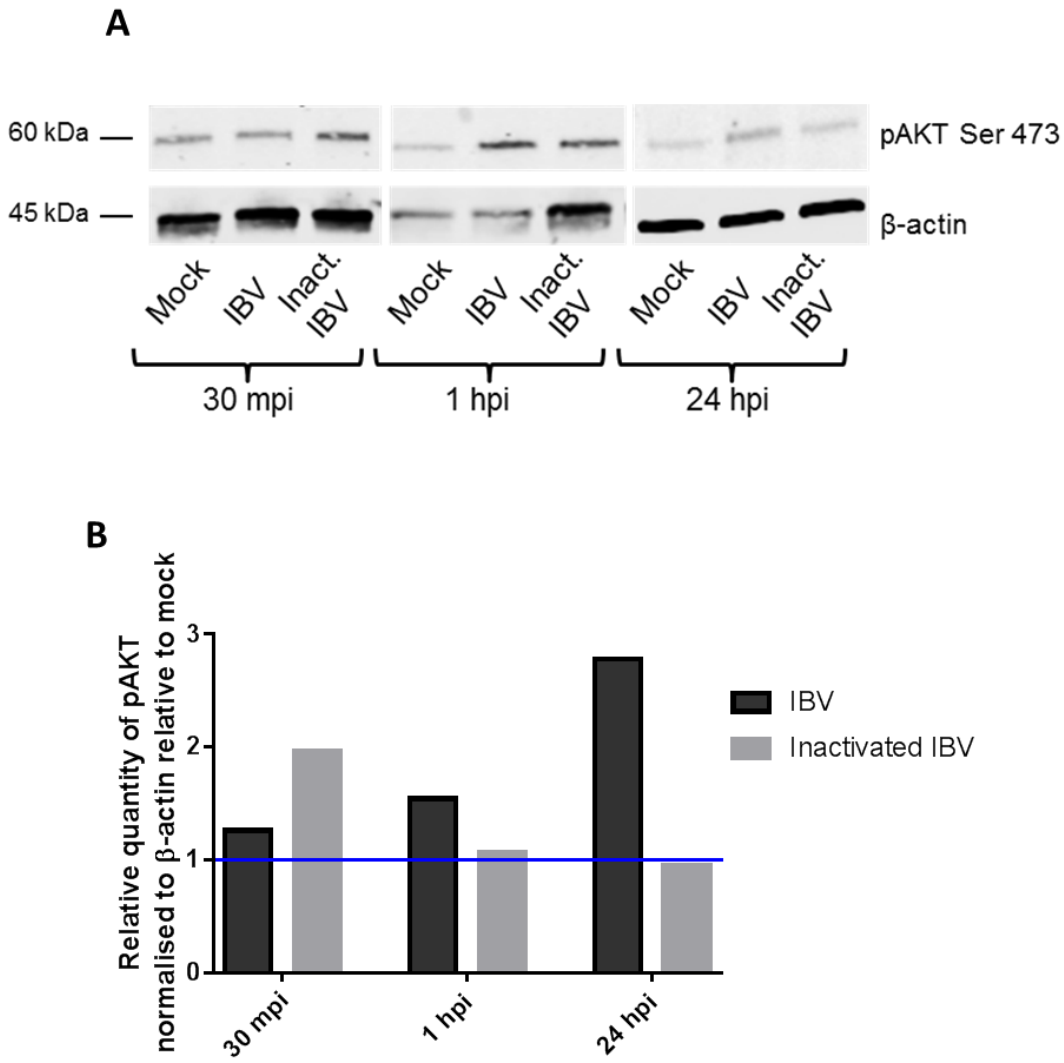


**Figure 3.12 DF1 infection with inactivated IBV.** (A) DF1 cells were mock infected, infected with wt-IBV or with inactivated IBV and lysed at 30 mins, 1 and 24 hpi. Lysates were separated by SDS-PAGE and a western blot performed with anti-β-actin and anti-pAKT S473. Molecular weights indicated. (B) Densitometry of western blot bands, normalized to levels of anti-β-actin. Blue bar represents mock level.

### 3.4.1 Viral genomic and sub-genomic RNA

DF1 cells were infected with IBV in the presence or absence of the PI3K inhibitor LY294002, and RNA extracted from the cells at 1, 2, 6, 12 and 24 hpi. The replication of viral genome was measured by amplification of the 5' untranslated region (5' UTR) of the genome by qPCR and genome copy number was calculated by interpolating of $C_q$ values from a standard curve (Figure 3.13A). Production of viral genome is significantly delayed during PI3K inhibition from 6 hpi to 24 hpi ($p<0.01$) (Figure 3.13B). The levels of viral mRNA synthesis was measured by amplification of mRNA encoding the nucleocapsid protein (N-message). Copy number was again calculated by interpolating the data on a standard curve (Figure 3.14A). In contrast to levels of viral gRNA, viral mRNA transcription was not significantly affected by inhibition of the AKT pathway with similar levels of transcription in both sample sets (Figure 3.14B).

### 3.4.2 Translation of viral proteins

The effect of PI3K inhibition on levels of intracellular viral protein was also investigated. DF1 cells were infected with IBV in the presence or absence of LY294002 and lysed at 2, 8, 12 and 24 hpi for western blot analysis. The membranes were probed with anti-S2 and anti-β-actin as a loading control (Figure 3.15A). Levels of anti-S2 were normalised to β-actin. Densitometric analysis of the western blot suggests a decrease in viral protein production by 24 hours post infection during inhibition of PI3K (Figure 3.15B).

### 3.4.3 Infectious virus particle release

The delay in viral genome replication and protein synthesis was examined in the context of production and release of new infectious virions. The supernatant from infected DF1 cells was collected and the released virus titrated by TCID50 in DF1 cells (Figure 3.16).

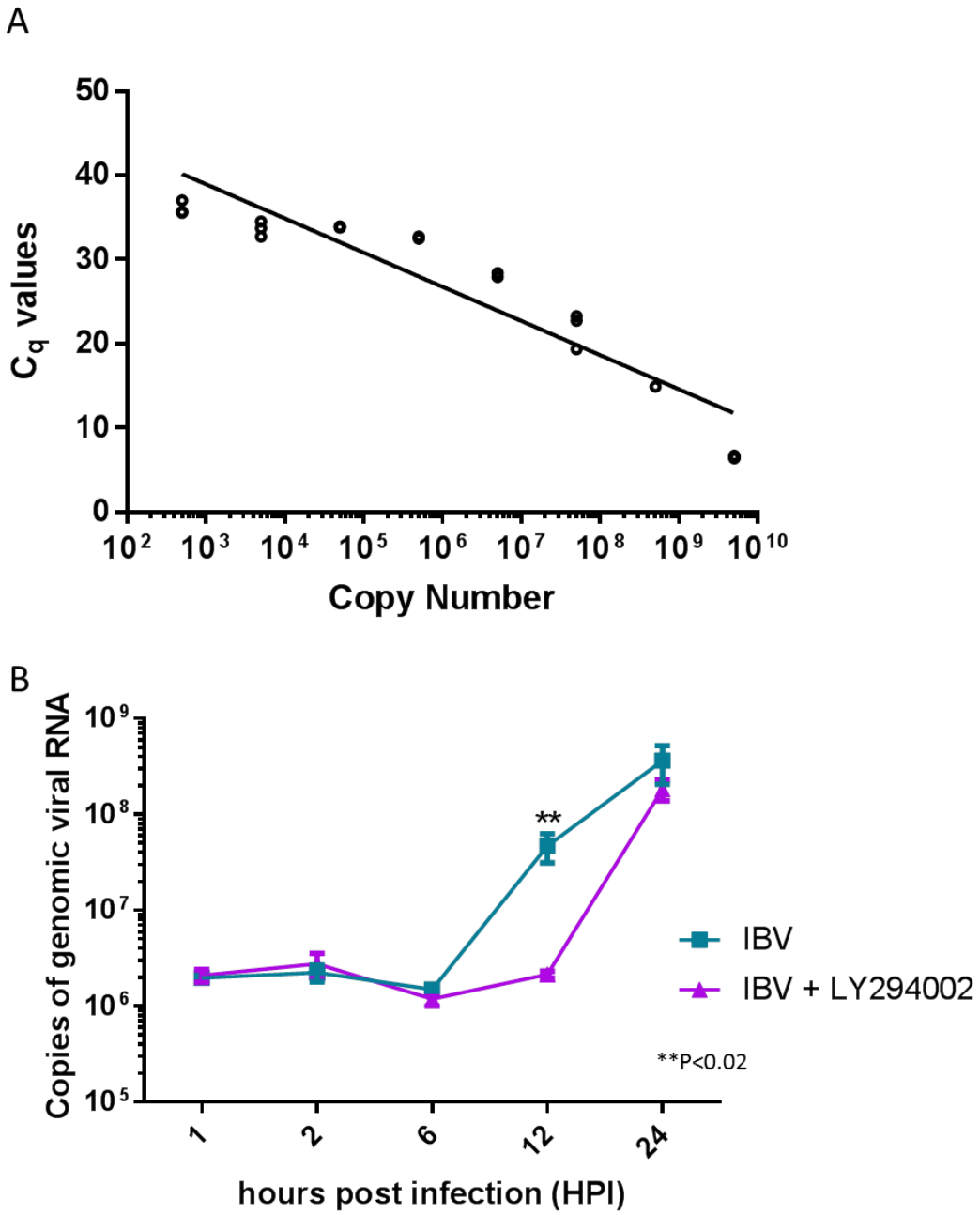


**Figure 3.13 Replication of viral genome mRNA in presence and absence of PI3K inhibitor.** DF1 cells were infected with IBV in the presence and absence of LY294002. Cells were lysed and RNA extracted for qPCR. (A) Standard curve of 5'UTR standards. (B) Replication of viral genome is quantified by measuring expression of 5'UTR region of genome. P values calculated by multiple t-tests.

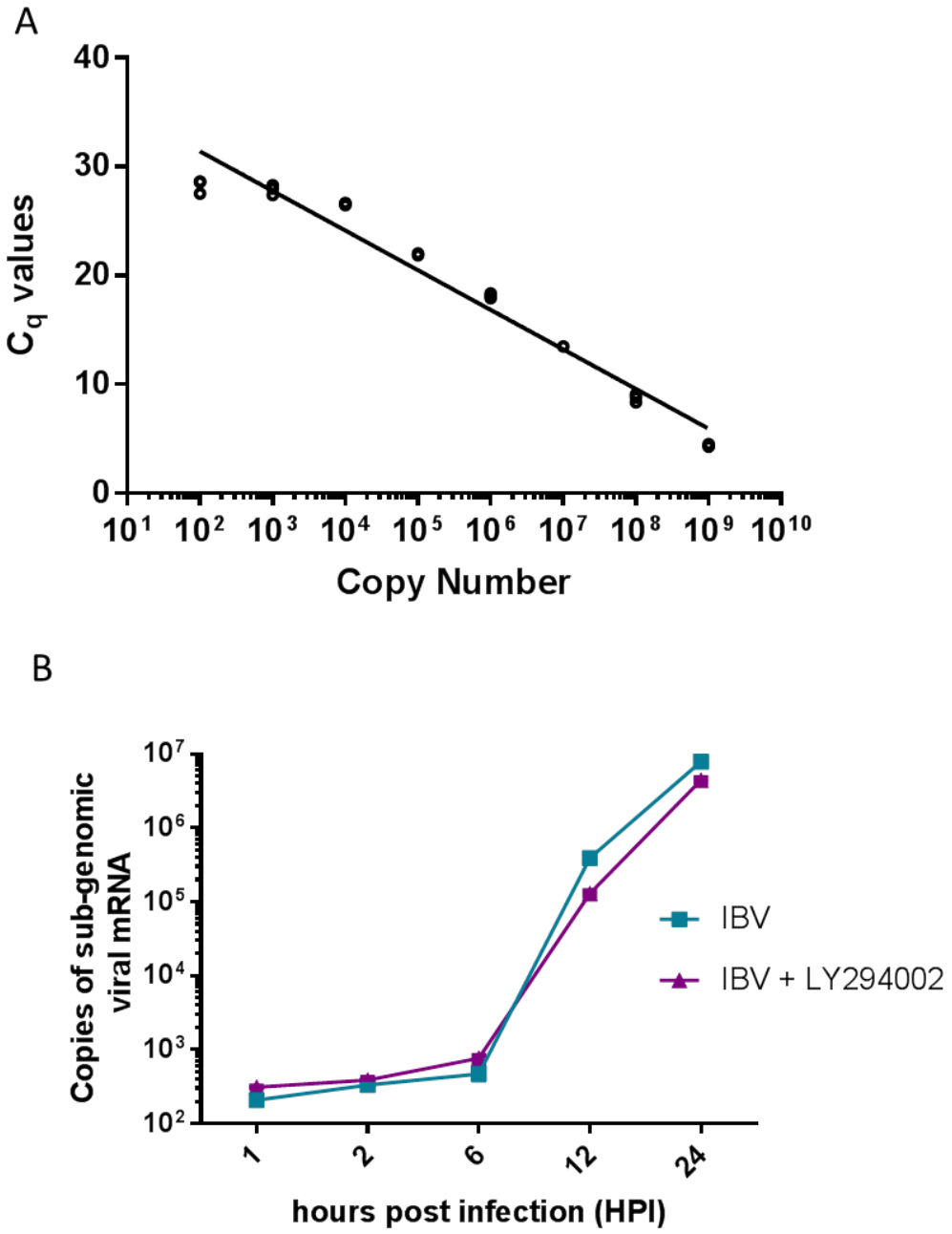


**Figure 3.14 Transcription of viral N-message sgRNA in the presence or absence of PI3K inhibitor.** DF1 cells were infected with IBV in the presence and absence of LY294002. Cells were lysed and RNA extracted for qPCR. (A) Standard curve of N-message standards. (B) Transcription of viral mRNA is quantified by measuring expression of N-message.

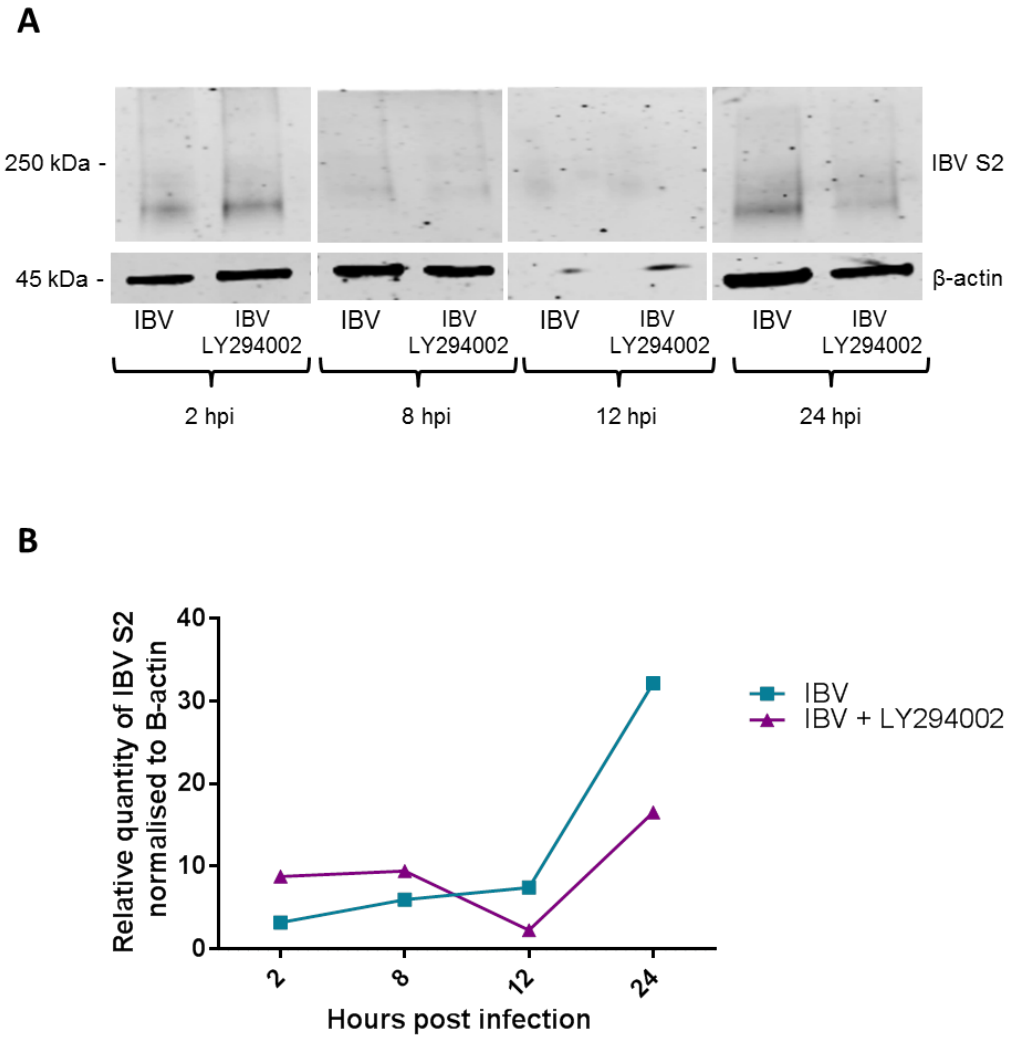


**Figure 3.15 Expression of the spike protein subunit 2 (S2) in IBV infected cells in the presence and absence of PI3K inhibitor.** (A) DF1 cells were infected with IBV in the presence or absence of LY294002. At 2, 8, 12, 16 and 24 hpi cells were lysed and subjected to Western blot. Membranes were probed with anti-S2 and anti-β-actin. Molecular weights indicated. (B) Densitometry of western blot bands normalised to β-actin.

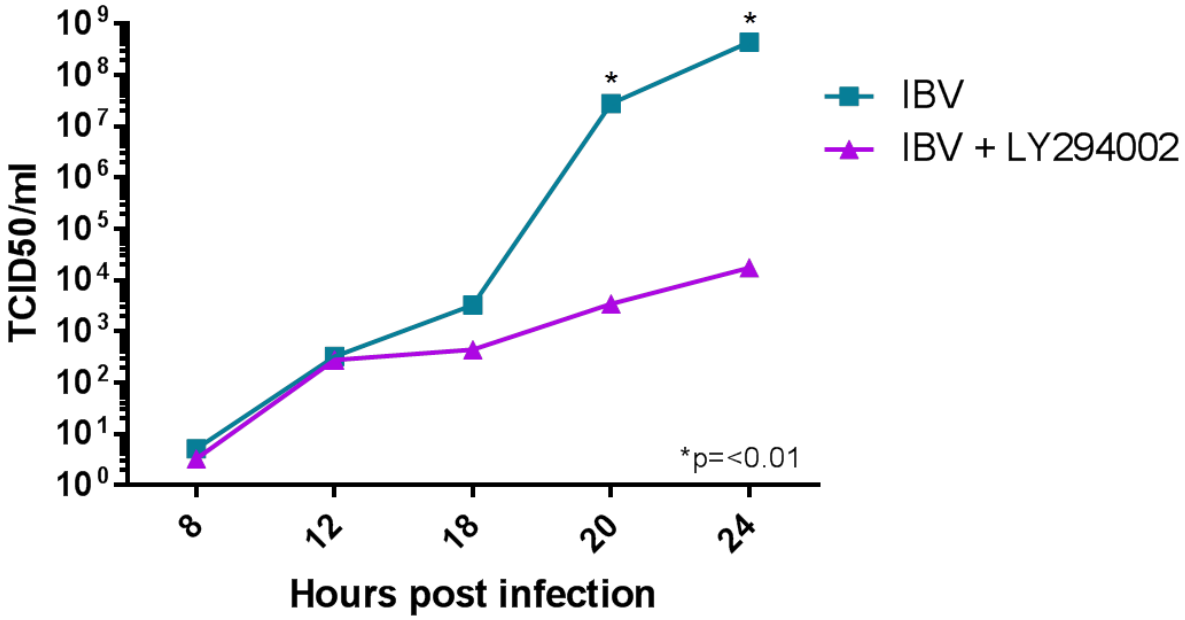


**Figure 3.16 Titre of released virus from cells infected with IBV in the presence or absence of PI3K inhibitor.** DF1 cells were infected with IBV in the presence or absence of LY294002. At the indicated time points the supernatant was removed and virus titre was measured by TCID50 in DF1 cells. P values calculated by 2-way ANOVA.

Inhibition of PI3K led to a significant decrease in release of virus from 20 hpi in the presence of LY294002 ($p<0.001$). By 24 hpi, there was a 4 log difference in titre. This correlated with levels of viral protein that were also lower during PI3K inhibition by 24 hpi (Figure 3.14).

### 3.4.4 Possible replication sites and membrane structures

One feature of all positive-strand RNA viruses is rearrangement of cellular membranes during infection. These membrane rearrangements occur to facilitate viral RNA synthesis through the formation of replication-transcription complexes. The type of membrane structures formed differs between families of virus. Membrane rearrangements observed vary from single- to double-membrane vesicles, to convoluted membranes and spherules. The origin of the membranes also changes between viruses, with membrane rearrangements found to be derived from intracellular vesicles, ER, Golgi, mitochondrial and plasma membrane.

Recently, studies into membrane rearrangements during IBV infection have identified double-membrane vesicles, but also novel structures that have not been seen in coronaviruses before (Maier et al., 2013b). Maier et al. (2013b) observed spherules connected to regions of ER that had become zippered together. The spherules contain a channel connecting the interior of the spherule to the cytoplasm. The channel has a large enough diameter to allow the exchange of nucleotides and RNA products (Kopek et al., 2007). It is therefore possible that these spherules are the site of viral RNA synthesis.

Inhibition of PI3K by LY294002 results in a decrease in viral replication and in particular a suppression of viral RNA synthesis. It was therefore hypothesised that PI3K/AKT signalling may be involved in the formation of viral RNA replication complexes. DF1 cells were therefore infected with IBV in the presence or absence of LY294002 and at 24 hpi were chemically fixed for transmission electron microscopy (TEM) analysis (Figure 3.17). The TEM analysis was kindly performed

by Jennifer Simpson (The Pirbright Institute). IBV infected DF1 cells exhibited double-membrane vesicles as well as spherules attached to zippered-ER. These membrane re-arrangements were not observed in the mock infected cells. Inhibition of PI3K with LY294002 induced no visible change in membrane re-arrangements in IBV infected cells, and the cells exhibited both double membrane vesicles and spherules attached to zippered-ER. Together this data suggests that the delay in viral RNA synthesis, observed in the presence of LY294002, is not a result of modifications to membrane re-arrangements.

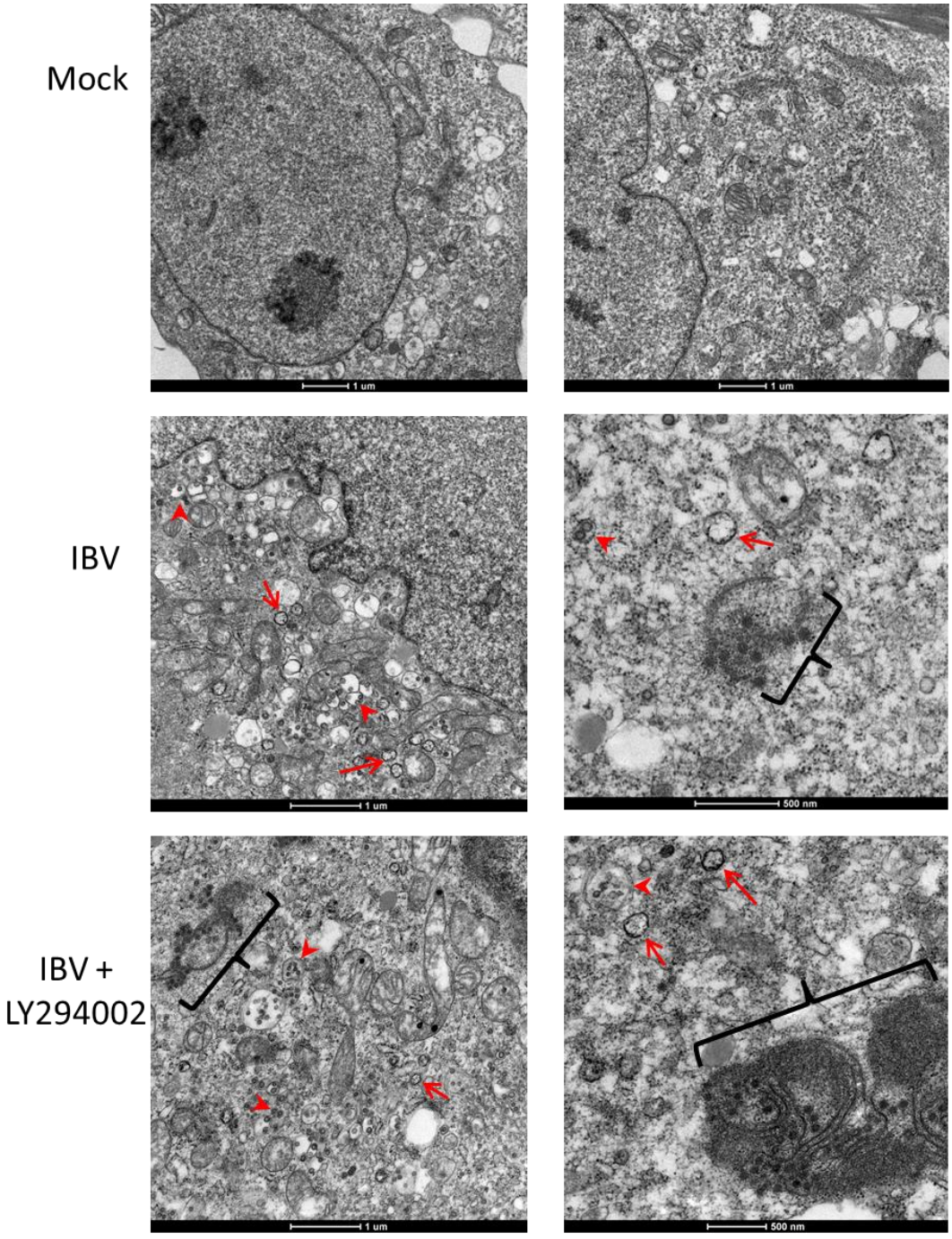


**Figure 3.17 Transmission electron microscopy images of IBV infection in the presence and absence of LY294002.** DF1 cells were mock infected or infected with IBV in the presence or absence of the PI3K inhibitor, LY294002. At 24 hpi cells were fixed by chemical fixation. Red arrows indicate double-membrane vesicles, red arrow heads indicate virus particles present within vesicles and black brackets highlight regions of zippered-ER with spherules.

## 3.5 Role of IBV structural proteins in PI3K/AKT modulation

The viral proteins responsible for modulating PI3K/AKT pathway in other nidoviruses have been identified. For example, the M protein of SARS-CoV is known to interact with the PI3K/AKT signalling pathway (Chan et al., 2007). In order to identify which viral proteins are involved in the induction of the biphasic activation of AKT during IBV infection, several expression plasmids were produced (Methods section 2.8)

Plasmids expressing the IBV membrane (M) and envelope (E) proteins were transfected into DF1 cells. After 24 hours cells were fixed, permeabilised and labelled with anti-E or anti-FLAG (for overexpression of M protein) (green), anti-tubulin (red) and DAPI (Figure 3.18A). Transfection of the expression plasmids resulted in overexpression of the respective viral proteins in DF1 cells. DF1 cells were then transfected and lysed after 24 hours for western blot analysis. The blots were probed with anti-pAKT S473 and anti-β-actin (Figure 3.18B). Analysis of the western blot suggested that an overexpression of IBV M but not E protein may result in activation of AKT, albeit marginal (Figure 3.18C).

The effect of overexpression on the spike (S) and nucleocapsid (N) proteins was also investigated. Expression of N and S were confirmed by immunofluorescence. DF1 cells were transfected, fixed, permeabilised and labelled with anit-S2, anti-N and anti-tubulin (Figure 3.19A). Nuclei were stained with DAPI. A duplicate set of transfected cells were lysed, proteins separated by SDS-PAGE and transferred onto a membrane. The membranes were then probed with anti-pAKT S473 and anti-β-actin (Figure 3.19B). Analysis of the western blot identified little change in pAKT levels during overexpression of IBV S. Overexpression of the N protein resulted in decreased levels of pAKT S473 in 4 out of 5 replicates however this was not conclusive due inconsistencies between replicates (Figure 3.19C).

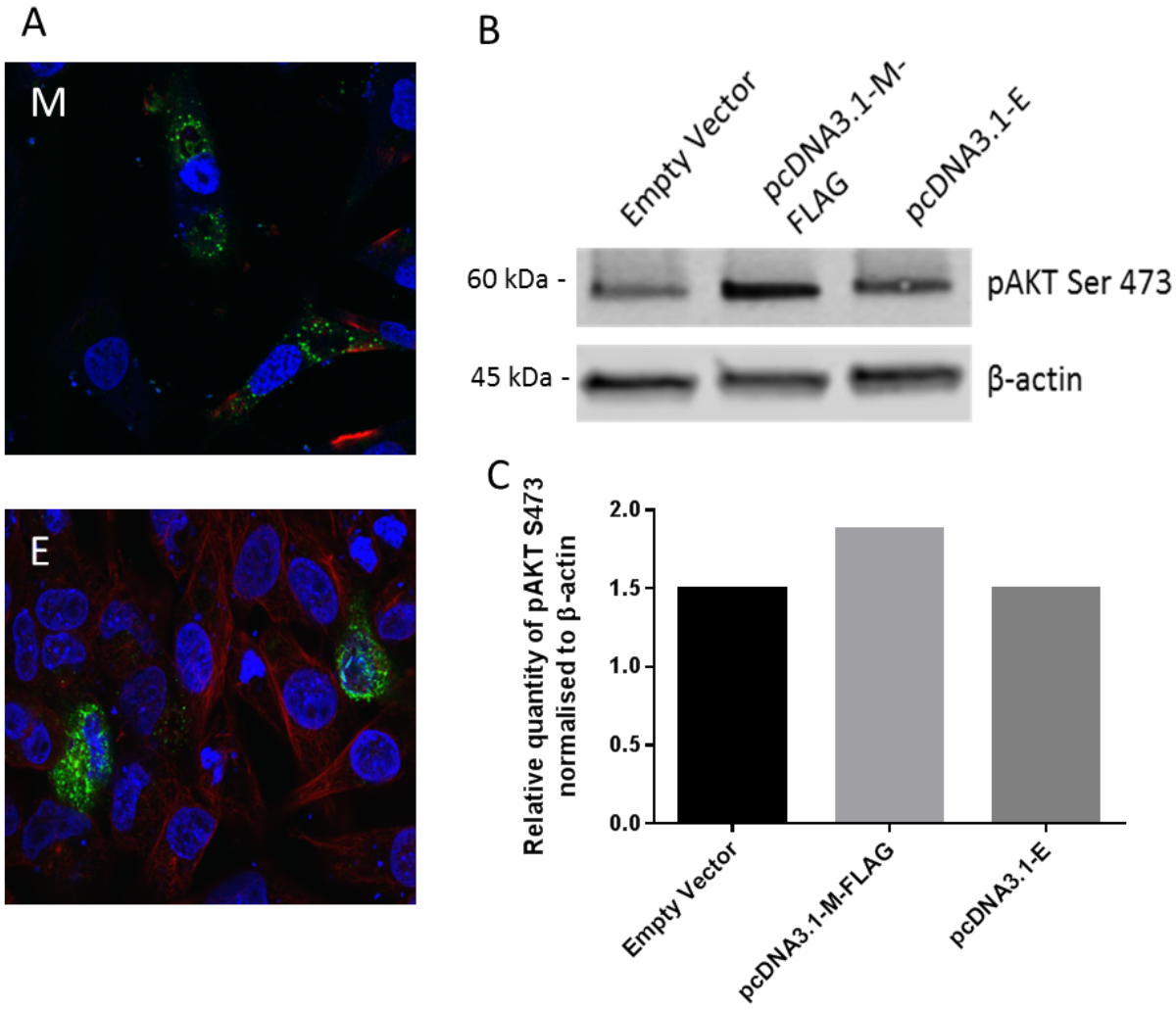


**Figure 3.18 Phosphorylation of AKT in DF1 cells overexpressing IBV membrane (M) and envelope (E) proteins.** DF1 cells were transfected with pcDNA3.1 expressing the IBV membrane (M) protein and a C-terminal FLAG tag or the envelope (E) protein. (A) At 24 hours post transfection the cells were fixed and labelled with anti-Flag or anti-E (green), anti-tubulin (Red) and DAPI. Images were taken by confocal microscopy. (B) After 24 hours cells were lysed and proteins subjected to western blot. Membranes were probed with anti-pAKT S473 and anti-β-actin. Molecular weights indicated. (C) Densitometry data of western blot normalised to levels of β-actin. Data representative of three experiments.

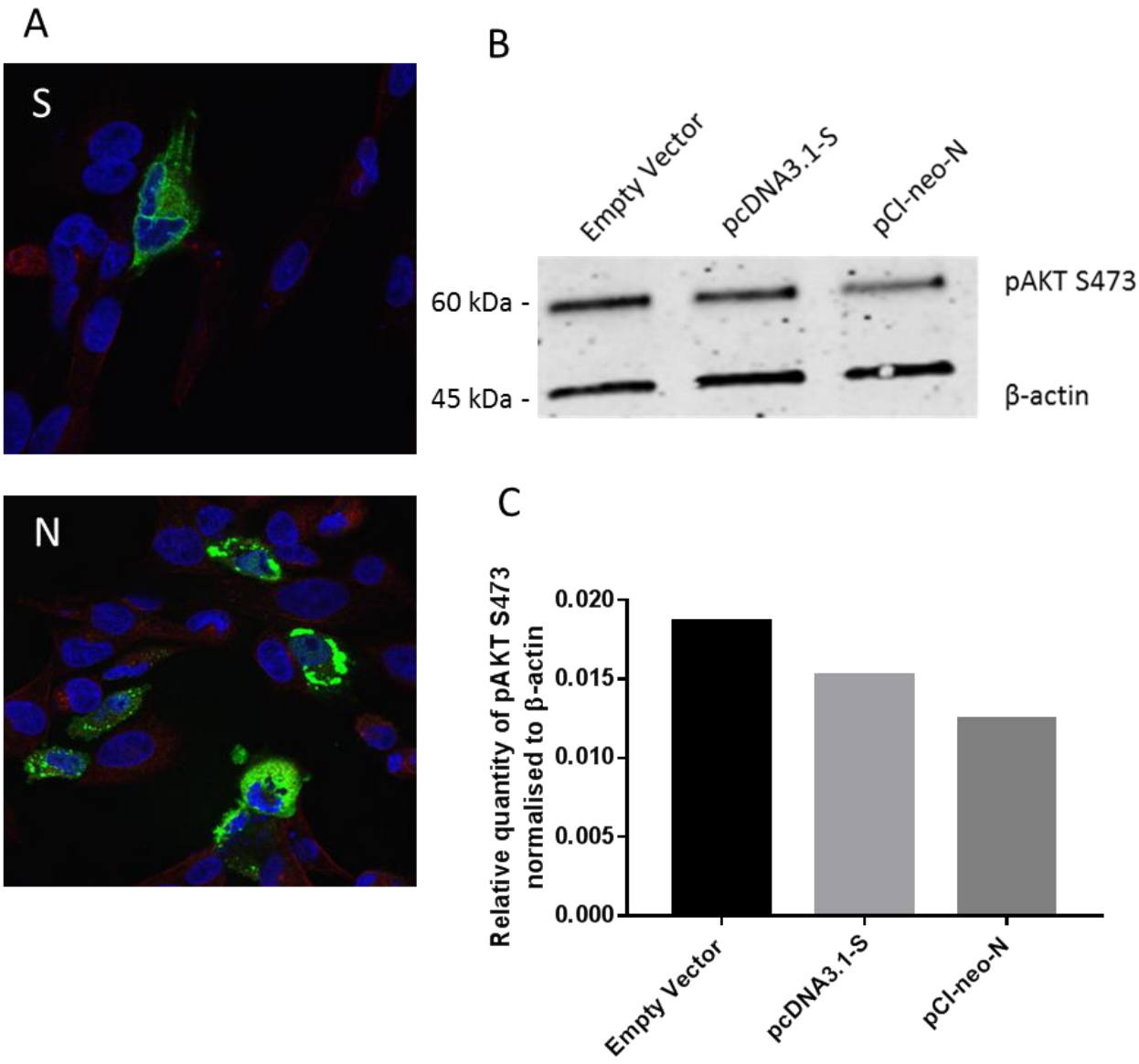


**Figure 3.19 Phosphorylation of AKT in DF1 cells overexpressing IBV spike (S) and nucelocapsid (N) proteins.** DF1 cells were transfected with plasmids encoding the S or N proteins of IBV BeauR. (A) At 24 hours post transfection the cells were fixed and labelled with anti-S2 or anti-N (green), anti-tubulin (Red) and DAPI. Images were taken by confocal microscopy. (B) After 24 hours cells were lysed and proteins subjected to western blot. Membranes were probed with anti-pAKT S473 and anti-β-actin. Molecular weights indicated. (C) Densitometry data of western blot normalised to levels of β-actin. Data representative of three experiments.

## 3.6 Discussion

The results presented in this chapter detail studies of the interaction between IBV and the PI3K/AKT signalling pathway. Initially the cellular tropism of the pathogenic strain of IBV (M41), and the apathogenic recombinant Beaudette strain (Beau-R) were assessed. IBV is the aetiological cause of the respiratory disease Infectious Bronchitis and therefore initially infects cells of the respiratory tract of chickens. However, pathogenic strains of IBV have also been found to infect other organs such as the kidney, where infection is known to cause nephropathology (Winterfield and Albassam, 1984, Abdel-Moneim et al., 2009). The receptors for IBV in its native host cells remain unknown, however it is thought that aminopeptidase N (APN) and sialic acid may be important for primary attachment (Miguel et al., 2002, Winter et al., 2006). Among other factors, the furin content of the cell is thought to have an effect on the ability of the virus to infect and replicate within a cell (Yamada et al., 2009). Our immunofluorescence studies in Section 3.2 confirm the findings of others, that the Beau-R strain of IBV has a wider cellular tropism than the pathogenic M41 strain. Both strains of IBV were able to replicate in primary CK cells as expected. Beau-R, but not M41, was also able to replicate in the avian DF1 and mammalian Vero cell lines.

The low levels of dsRNA labelling seen in some cell lines do not necessarily correspond with low levels of infection. It was previously thought that dsRNA was a replicative intermediate that occurs as a result of viral RNA synthesis. However, recent immunofluorescence studies in our laboratory have demonstrated that dsRNA does not co-localise with the RNA-dependent RNA polymerase (RdRP) suggesting that it occurs independently of RNA synthesis sites (Maier et al. 2016). Whilst the function and origin of dsRNA is unknown during IBV infection, it remains a reliable marker for viral infection in the absence of adequate IBV specific antibodies.

The activation of AKT was assessed with antibodies specific to the active form of the kinase, when phosphorylated at S473. Levels of phosphorylated AKT were normalised to cellular levels of β-actin, a protein commonly used for western blot analysis (Soares et al., 2009). Several studies have previously normalised AKT phosphorylation to the amount of total AKT being expressed in the cell (Sharma et al., 2010, Liu et al., 2012). This method of normalisation was attempted, however the antibodies used did not produce consistent results when tested on the avian samples. Therefore, there is the potential that any change in AKT phosphorylation seen may be a result of the differential expression of the AKT protein. However, other studies have demonstrated that levels of AKT protein expression remain constant throughout viral infection, and it is widely accepted that control of AKT signalling occurs via phosphorylation of AKT.

The mammalian PI3K/AKT signalling pathway is modulated upstream by receptor tyrosine kinase receptors which can be activated by cytokines and growth factors such as epidermal growth factor (EGF). The ability of EGF stimulation to activate AKT was demonstrated by western blot (Figure 3.2). Subsequently the effect of IBV infection on the mammalian AKT signalling pathway was investigated. An increase in pAKT S473 was seen from 6 to 24 hpi. The most widely studied activation pathway of AKT involves PI3K. Activation of PI3K induces the accumulation of $PIP_3$ which prompts recruitment of AKT to the cellular membrane. Downstream processes of this pathway include mTOR signalling, apoptosis, protein synthesis, translation and cell growth. PI3K-independent activation of AKT has also been documented in mammalian cells. Whilst activation of AKT can occur independently of PI3K, many mammalian viruses have been found to modulate AKT through PI3K (Wang et al., 2014c, Diehl and Schaal, 2013). Alongside others, the human coronavirus MERS-CoV is known to modulate mTOR signalling via PI3K/AKT (Kindrachuk et al., 2015). The effect of IBV infection on the PI3K/AKT signalling pathway was therefore examined using a specific PI3K inhibitor, LY294002. In Vero cells, treatment with

LY294002 supressed EGF induced AKT activation (Figure 3.4). They were then infected with IBV at 12 and 24 hpi and the phosphorylation of AKT was also supressed by the inhibitor at 24 hpi (Figure 3.5). It can therefore be concluded that in mammalian cells IBV induces activation of AKT late during infection and that the activation is dependent on active PI3K.

Studies of avian viruses are often performed in mammalian cells due to an abundance of reagents and a lack thereof in the avian field. Whilst not the perfect model for avian viral replication, many insights can be drawn from these studies. The mammalian AKT signalling pathway has been well characterised however few studies have investigated its avian counterpart. In this chapter the effect of IBV replication on the mammalian PI3K/AKT signalling pathway was compared to that of the avian pathway. Understanding how viruses interact with different cell types may give us insights into the basic cellular biology of the different cells. The effect of IBV infection on the avian AKT signalling pathway was investigated by western blot (Section 3.3.2). EGF was evaluated for use as a positive control in avian cells. However, it did not induce AKT activation at any concentration or time tested (Figure 3.6). The EGF used was a recombinant mammalian protein, suggesting that EGF or the EGF receptor (EGFR) in avian cells may be different to that of mammalian cells. Another known stimulator of PI3K/AKT signalling, LPS was also tested (data not shown), however this was also unable to stimulate AKT phosphorylation in avian cells. Therefore IBDV was used as a known activator of PI3K/AKT signalling (Wei et al., 2011) and the activation confirmed by western blot of infected DF1 cells (Figure 3.7). At 8 hpi IBDV infection induced high levels of AKT activation compared to mock. The PI3K inhibitor was able to supress the IBDV induced activation of AKT as expected, confirming the efficacy of the inhibitor and antibody in avian cells (Figure 3.8C).

The effect of IBV infection on the PI3K/AKT signalling pathway in avian cells was then investigated. In contrast to mammalian cells where activation occurred after 6 hpi, IBV was found to induce AKT activation in a biphasic manner in avian cells (Figure 3.9). An increase in pAKT S473 was seen at 2 hpi which was supressed by 6 hpi. A second peak in AKT activation was then observed from 16 to 24 hpi. A similar pattern was seen in phosphorylation of AKT at its T308 site (Figure 3.10). This biphasic activation has been previously reported for several mammalian viruses (Zhu et al., 2011a, Ehrhardt et al., 2006). In these studies, it is suggested that the early activation of AKT is a result of an antiviral response that is subsequently supressed by the virus. It is not clear however, whether the second phase of activation is a cellular response to the replication of the virus or a viral response to ensure cell survival. The second phase of activation during influenza infection is an anti-apoptotic signal induced by the virus (Ehrhardt et al., 2007). It may therefore be the case for IBV and this is investigated in Chapter 4. It is also not clear if the initial phase of activation and subsequent suppression is a result of viral activity or a cellular response to infection.

The attachment of the virus to the cell is the earliest point at which cellular signalling pathways can be activated by a virion. It is the binding of the viral attachment protein to the cellular receptor embedded in the membrane that initiates signalling cascades within the cell. For example, HIV-1 is known to activate signalling pathways as early as 1 minute post infection (Wojcechowskyj et al., 2013). The avian reovirus is also known to activate AKT early during infection, from 15 mins to 4 hpi (Lin et al., 2010). The presence of PI3K/AKT signalling at the cellular membrane and early activation of AKT suggested that binding and entry of IBV may result in activation of the pathway. This was investigated using an inactivated form of the virus that was able to bind and enter the cell but not replicate (Figure 3.11). Activation of AKT was found to occur as a result of viral receptor binding and entry, but found to be independent of active replication (Figure 3.12). Activation of AKT by the inactivated

virus occurred from 30 mins to 1 hpi. Interestingly, AKT activation decreased again by 1 hpi suggesting that either the stimulus was no longer present or that this activation was suppressed. Due to the fact that levels of AKT activation during IBV-WT infection continued to increase, it is more likely that the proteins in the BEI inactivated virus were degraded quickly and the stimulus lost. The binding of the virus to the cellular receptor may therefore be the initial activator of AKT. The treatment of virus with BEI may have affected the ability of the virus to attach and enter the cell and therefore there was less virus present to induce a prolonged activation of AKT as seen in the WT infections. Interestingly the early activation with the wild-type virus was not seen in mammalian cells. This suggests that avian cellular pathways are activated differently from mammalian cells during IBV infection. This may be due to different viral attachment receptors between the species. Alternatively, the entry mechanism of the virus in avian cells may be different to that in mammalian cells. Unfortunately, comparatively little is known about IBV entry compared to other coronaviruses. The initial phase of AKT activation may be induced by the virus as a pro-viral response and the virus may not be able to produce this effect in mammalian cells. Interestingly IBV infection has been found to induce interferon-gamma production as early as 1 hpi in avian cells but not mammalian cells, suggesting that different pathways are activated in the two species (Ariaans et al., 2009).

Specific inhibitors of cellular signalling pathways have been investigated as antiviral treatments against viruses such as Influenza (Planz, 2013). More specifically inhibition of PI3K/AKT signalling has previously been reported as a potential antiviral strategy for treatment of MERS-CoV (Kindrachuk et al., 2015, Josset et al., 2013). In this study the effect of PI3K/AKT inhibition on replication of IBV in avian cells was investigated (Figures 3.13-3.16). The inhibition of PI3K/AKT with LY294002 inhibited viral replication by suppression of viral genome replication and protein synthesis. Inhibition of PI3K resulted in a significant decrease in the amount of infectious virus

particles released. Interestingly levels of N-message mRNA did not change when the pathway was inhibited. However, the delay in spike protein production suggests that the results seen here are not representative of all mRNAs and may be specific to the N-message. Coronavirus proteins are synthesised from a set of nested sub-genomic mRNA that are transcribed in a discontinuous manner (Sawicki et al., 2007). As N is involved in the formation of the nucleocapsid and protection of the viral genome, it may be translated in higher amounts than other messages. There has been evidence for the requirement of sustained replication of the nucleocapsid protein for optimal replication of coronaviruses (Almazan et al., 2004).

The site of IBV RNA synthesis is yet to be identified. However, the viral replicase proteins of other coronaviruses, such as SARS-CoV, have been found to associate with cellular membranes such as the ER and the formation of double-membrane vesicles (Snijder et al., 2006). A previous study identified IBV-induced membrane rearrangements similar to those seen in other positive strand virus infections but not in other coronaviruses (Maier et al., 2013b). These include double-membrane vesicles and zippered-ER with attached spherules. These novel membrane re-arrangements were identified during IBV infection of Vero and primary CK cells as well as ex-vivo tracheal organ cultures. However, in this study both double-membrane vesicles and spherules connected to zippered-ER were observed (Figure 3.17). The novel membrane structures were hypothesised to be the site of viral RNA synthesis. The suppression of viral replication by PI3K/AKT inhibition, and the role of the PI3K/AKT in many cellular processes, may implicate the pathway in the formation of these novel membrane structures. The effect of PI3K activation on the formation of the membrane structures during IBV infection was therefore investigated. No qualitative change was observed in the structure or number of vesicles over three separate samples in the presence of LY294002. This suggests that either PI3K/AKT signalling has no role in the formation of the membrane

structures during IBV replication, or that the novel structures identified by Maier et al (2013) are not the site of viral RNA synthesis.

The effect of various IBV structural proteins on PI3K/AKT signalling has been investigated. Overexpression of the IBV M protein was observed to stimulate the activation of AKT consistently in each replicate. However, overexpression of the E and S proteins did not consistently alter levels of AKT expression. The overexpression of IBV N protein reduced levels of AKT activation in 4 out of 5 replicates. The effect of various coronavirus proteins on PI3K/AKT signalling has previously been studied. For example, the SARS-CoV M protein has been found to modulate the PI3K/AKT signalling pathway to induce apoptosis (Tsoi et al., 2014). Whilst this may be the case for IBV, the SARS-CoV M protein was found to down-regulate AKT phosphorylation to induce apoptosis. The expression of SARS-CoV N protein has also been found to down-regulate AKT and induce apoptosis (Surjit et al., 2004). None of the structural proteins produced a large increase in AKT phosphorylation, compared to whole virus, indicating that there may be several viral proteins acting in concert to modulate the PI3K/AKT signalling.

Together, this data indicates an important role of PI3K/AKT signalling in IBV replication and suggests a complicated interplay between the modulation of signalling pathways by the virus and the host cell.

## 3.8 Chapter Summary

IBV infection of mammalian cells:

- Induces AKT activation from 12 to 24 hpi
- AKT activation at 24 hpi is dependent on PI3K activity

IBV infection of avian cells:

- Induces a biphasic activation of AKT at 2 hpi and then from 16 to 24 hpi
- The later phase of AKT activation, from 16 to 24 hpi, occurs in a PI3K-dependent manner
- Viral binding and entry is sufficient to induce the initial phase of AKT activation
- Virus replication requires an active PI3K/AKT signalling pathway

Overexpression of IBV membrane protein may stimulate AKT activation

## 3.7 Future work

The cellular furin content of different cell lines is thought to be a factor in the susceptibility of avian and mammalian cells to IBV infection (Tay et al., 2012). It would therefore be interesting to study this interaction by measuring levels of furin in different cell lines and correlating this to their susceptibility to IBV infection. By overexpressing furin in HD11 cells which are known to not be susceptible to IBV, we could elucidate the importance of furin in establishing infection. Whilst dsRNA is a good indicator of viral infection, qPCR assays are more sensitive and efficient. It would therefore be beneficial to repeat the cellular tropism study using qPCR of genomic and sub-genomic RNA.

The biphasic activation of AKT has been previously reported for Influenza where it was suggested that the first phase of AKT activation was a cellular response to initial infection (Ehrhardt et al., 2006). The suppression of AKT activity was thought to be a pro-viral response to ensure cell survival. This may be the case for IBV however further studies need to be conducted to assess the basis of the AKT modulation during infection. The effect of PI3K inhibition on the early phases of AKT activation was not consistent. It would therefore be beneficial to look at levels of PI3K activation during the initial stages of infection using a PI3K specific antibody. This would elucidate the relationship between PI3K and AKT at these early stages of the viral life cycle. Likewise, it would be interesting to look at levels of PI3K activation in mammalian cells during infection to see whether at the earlier time points PI3K was activated.

An inactivated form of the virus was able to activate AKT up to 1 hpi. It is therefore possible that this initial phase of AKT activation is a result of binding of the virus to avian cellular receptors. The cellular receptors for IBV are unknown, however it would be interesting see if binding of the virus to the cell was sufficient to induce AKT activation. This could be done by incubating the cells with virus on ice to prevent entry. As BEI inactivation involves diluting the virus stock, a UV inactivated virus could be produced which would allow us to incubate the cells in the same number of virus particles as wt-IBV.

The finding that inhibition of PI3K, by LY294002, significantly reduced the ability of IBV to replicate in avian cells was interesting. This could be further investigated by siRNA knockdown of key PI3K/AKT regulators such as PDK1 and $PIP_3$, although this may be lethal to the cell. This finding also provides us with potential candidates for antivirals against IBV. Other AKT inhibitors such as MK2206 have been recommended for use as antiviral treatments (Denisova et al., 2014).

The overexpression of IBV M and N proteins were found to modulate AKT activation (Figure 3.18/19). The IBV M protein was found to increase AKT phosphorylation, and the N protein to down regulate it. This needs to be investigated further by examining the interactions of the viral proteins with cellular factors. For example, the C-terminus of the SARS-CoV membrane protein is known to interact with the PH domain of PDK1. Therefore, the effect of M and N overexpression of PDK1 and PI3K could initially be investigated by western blot. Protein pull downs or immunofluorescence co-localisation studies could then be performed to identify if there is an interaction between the avian PDK1 and the IBV membrane or nucleocapsid proteins. It is possible that several of the viral proteins are involved in modulation of PI3K/AKT signalling. For example, several of the coronavirus non-structural proteins (nsps) have been found to modulate cellular pathways. Therefore, the effect of nsp deletion mutants on AKT activation could be assessed. Mass spectrometry could also be employed to identify the interaction partners of key pathway proteins such as PI3K.

# Chapter 4

## PI3K/AKT signalling during IBV infection

## 4.1 Introduction

The effect of IBV infection on the PI3K/AKT signalling pathway was investigated in Chapter 3. IBV was found to induce AKT activation in a biphasic manner in avian cells, and replication of the virus was found to be reliant on an active PI3K/AKT signalling pathway. In this chapter the downstream effects of PI3K/AKT activation during IBV infection are investigated. Many viruses modulate the pathway to aid viral replication. For example, several structural proteins of the SARS-CoV are known to induce apoptosis in Vero cells through the down-regulation of AKT phosphorylation (Surjit et al., 2004, Chan et al., 2007). Some avian viruses have been found to modulate apoptosis via PI3K/AKT, including Newcastle disease virus (Ravindra et al., 2008a, Ravindra et al., 2008b) and avian reovirus (Lin et al., 2010). IBV also modulates caspase-dependent apoptosis in Vero cells (Liu et al., 2001), however the pathway by which this occurs is still not fully elucidated and few studies have been performed in avian cells.

As well as apoptosis, other downstream pathways are known to be modulated through PI3K. For example, the mTOR pathway involved in cell growth, autophagy and mRNA translation is also involved in viral replication. Porcine Respiratory and Reproductive Syndrome Virus (PRRSV) targets the PI3K/AKT signalling pathway to induce autophagy through mTOR signalling (Pujhari et al., 2014). Lentiviruses also modulate mTOR signalling by down regulating PI3K, AKT and 4E-BP1 (Du et al., 2014). Few studies examining the interaction between avian viruses and the mTOR pathway have been performed. Although recent studies in Vero cells have identified activation of autophagy during IBV replication, the same did not occur in avian DF1 cells. Interestingly, however, when expressed alone, nsp6 was able to induce autophagy in both Vero and DF1 cells (Cottam et al., 2011). Again, whilst various signalling pathways are activated during IBV infection, the exact mechanism by which they occur is still unknown.

Another downstream pathway, often regulated by PI3K/AKT signalling, is macropinocytosis. Many viruses utilise the macropinocytosis pathway to enter the cell. For example the filamentous form of Influenza virus enters the cell via macropinocytosis (Rossman et al., 2012). African Swine Fever and Nipah Viruses have also been found to use the same mechanism (Pernet et al., 2009, Sanchez et al., 2012). Recently, a role for the pathway that is independent of entry has been suggested as a result of CoV replication (Freeman et al., 2014). In the case of MHV, macropinocytosis signalling has been implicated as a tool for the recruitment of membranes and nutrients into infected cells and syncytia formation. No studies to date have investigated the involvement of macropinocytosis in IBV infection.

In this chapter the effect of IBV infection on downstream processes controlled by the PI3K/AKT signalling pathway including, apoptosis, mRNA translation and macropinocytosis are investigated.

## 4.2 Apoptosis

Previous studies have investigated the effect of IBV infection on the apoptotic signalling pathway in Vero cells (Liu et al., 2001, Li et al., 2007). To confirm their findings, the cleavage of caspase 3 and 7 was measured by a luciferase luminescent assay (Methods section 2.7.2). Vero cells were mock infected or infected with IBV and at 1, 6, 12 and 24 hpi and the amount of caspase cleavage was measured by luciferase assay (Figure 4.1). Caspase cleavage was seen at 1 hpi however, levels in mock samples increased at 6 hpi. From 12 to 24 hours levels of caspase cleavage were higher in the infected cells ($p<0.002$ & 0.005 respectively).

The effect of IBV infection on apoptotic signalling was subsequently investigated in avian DF1 cells. The efficacy of the caspase cleavage luminescent assay in avian

cells was initially determined by treatment of DF1 cells with a known activator of apoptosis, staurosporine. DF1 cells were treated with 0.01 mM staurosporine and the amount of caspase cleavage measured by luciferase assay at 2, 6, 12, 18 and 24 hours post stimulation (Figure 4.2). Staurosporine induced caspase cleavage in DF1 cells from 6 hpi with a sharp increase from 12 to 18 hpi. Subsequently, the effect of IBV infection on the apoptotic pathway was investigated. DF1 cells were mock infected or infected with IBV and levels of caspase cleavage measured at 2, 6, 12, 18, 24 and 36 hpi (Figure 4.3). An initial period of caspase cleavage was observed at 2 hpi which was suppressed again by 6 hpi to 24 hpi. From 24 hpi to 36 hpi a significant increase in caspase cleavage was seen in IBV infected cells ($p<0.005$).

The apoptotic signalling pathway can be regulated upstream by the anti-apoptotic PI3K/AKT signalling pathway. To determine whether PI3K/AKT signalling was involved in the modulation of apoptosis during IBV infection, DF1 cells were infected with IBV in the presence or absence of LY294002, a specific PI3K inhibitor. At 2, 6, 12, 18, 24 and 36 hpi levels of caspase 3/7 cleavage were measured (Figure 4.4). Inhibition of PI3K with LY294002 resulted in no significant change in caspase 3/7 cleavage at any time point during IBV infection.

Whilst caspase 3/7 cleavage is a good indicator of apoptosis, it occurs early in the pathway and several factors may be employed further downstream to inhibit or induce apoptosis. Therefore, the effect of IBV infection on the apoptotic pathway was also measured by labelling with Annexin V that binds to phosphatidyl-serine (PS). PS translocates to the outside of the plasma membrane during apoptosis and so, with propidium iodide (PI) labelling, flow cytometry can be used to measure the amount of early and late apoptosis occurring in a population of cells.

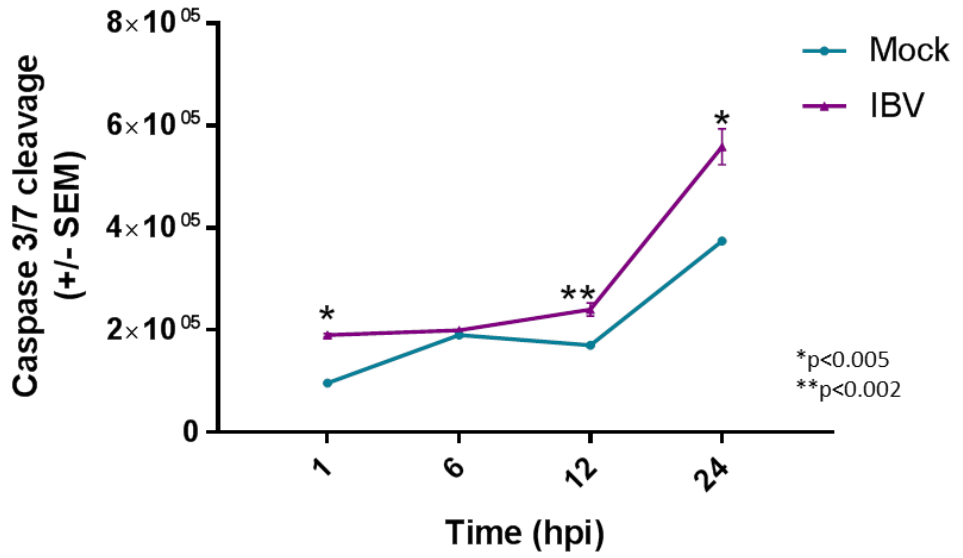


**Figure 4.1 Caspase 3/7 cleavage in Vero cells infected with IBV.** Vero cells were mock infected or infected with IBV and caspase 3/7 cleavage measured at 1, 6, 12 and 24 hpi by luminescent assay. Significance calculated by multiple un-paired t tests.

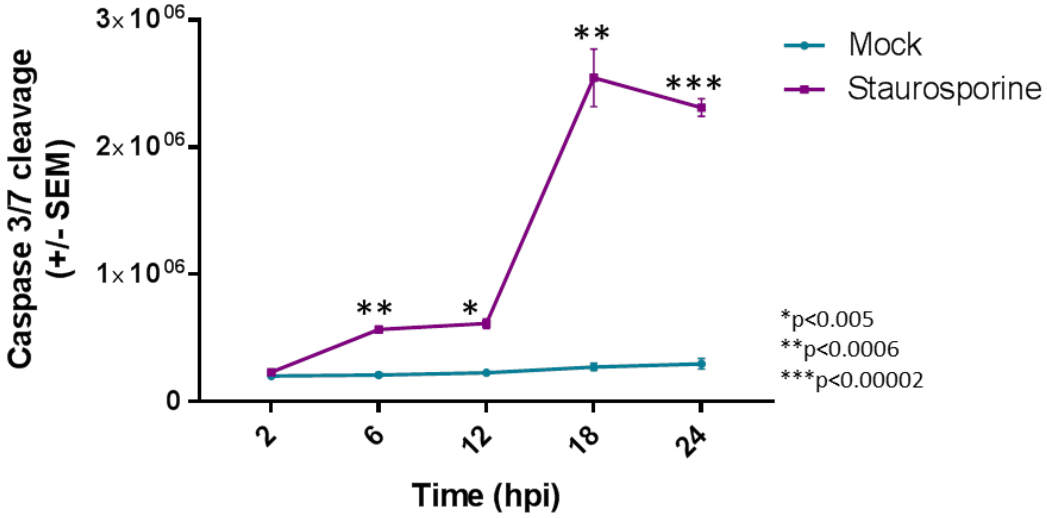


**Figure 4.2 Caspase 3/7 cleavage in DF1 treated with staurosporine.** DF1 cells were treated with 0.01 mM staurosporine or the equivalent volume of DMSO and caspase 3/7 cleavage measured at 2, 6, 12,18 and 24 hpi by luminescent assay. Significance calculated by multiple un-paired t tests.

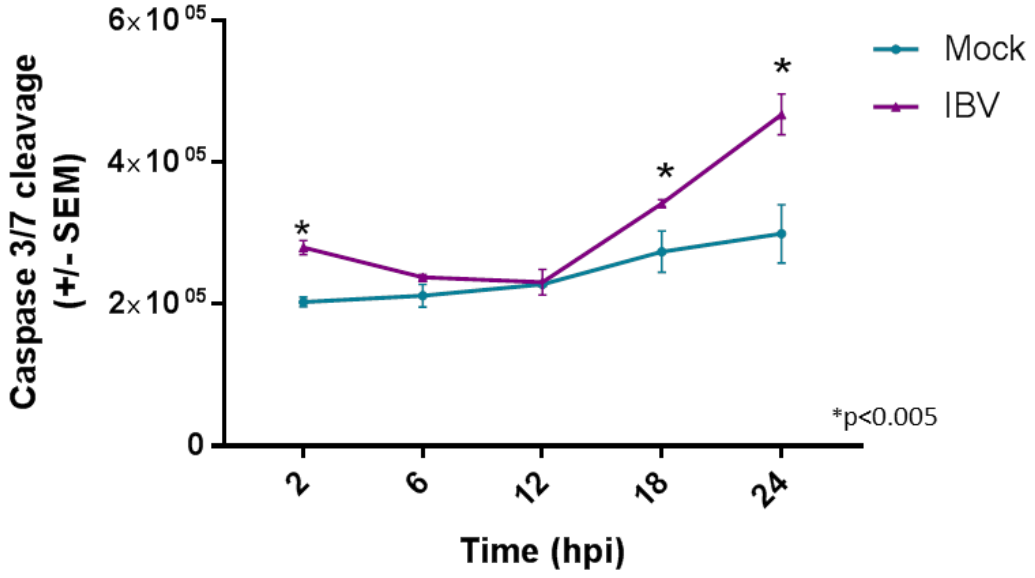


**Figure 4.3 Caspase 3/7 cleavage in DF1 infected with IBV.** DF1 cells were mock infected or infected with IBV and caspase 3/7 cleavage measured at 2, 6, 12,18, 24 and 36 hpi by luminescent assay. *Significance calculated by multiple un-paired t tests.

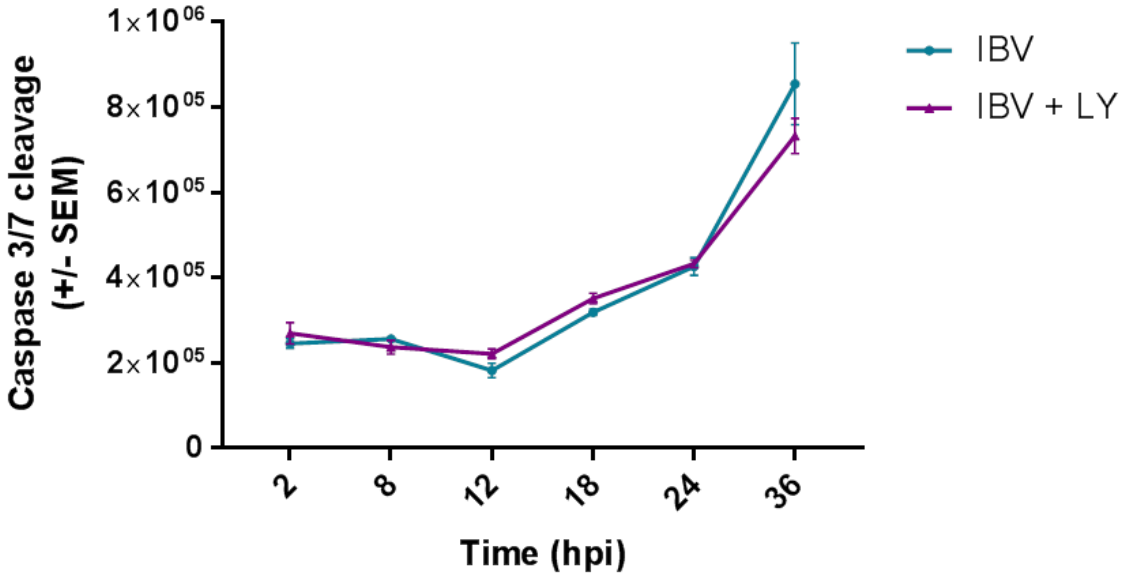


**Figure 4.4 Caspase 3/7 cleavage in DF1 cells infected with IBV in the presence or absence of LY294002.** DF1 cells infected in the presence or absence of LY294002 and caspase 3/7 cleavage measured at 2, 6, 12, 18, 24 and 36 hpi by luminescent assay.

DF1 cells were either mock infected, infected with IBV or treated with staurosporine and labelled with Annexin V-FITC and PI at 24 hpi. The flow cytometry data for the mock infected, staurosporine treated and IBV infected samples are attached in appendix 1, 2 and 3 respectively. For ease of analysis the percentage of live cells (FITC negative, PI negative), cells in early apoptosis (FITC positive, PI negative), late apoptosis (FITC positive, PI positive) and necrotic cells (FITC negative, PI positive) are plotted for each treatment (Figure 4.5). The percentage of cells in early apoptosis increases significantly from 6% in mock to 24% in staurosporine treated cells ($p<0.0001$) (Figure 4.5A). The percentage of cells undergoing early apoptosis in IBV infected cells does not change significantly from mock levels. The percentage of cells in late apoptosis or undergoing necrosis was also measured (Annexin V-FITC positive, PI positive) (Figure 4.5B). A smaller increase in the percentage of cells in late apoptosis/necrosis was observed in DF1 cells treated with staurosporine compared to early apoptosis. However, no change was seen in IBV infected cells at 24 hpi.

## 4.3 GSK-3β

The role of glycogen synthase kinase-3β (GSK-3β) in cellular pathways is widespread. It is involved in a variety of functions such as differentiation, growth, motility, cell cycle progression, apoptosis and the insulin response. Phosphorylation at the S9 site by kinases, including AKT, results in inactivation. The effect of IBV infection on phosphorylation of GSK-3β at S9 was determined by western blot.

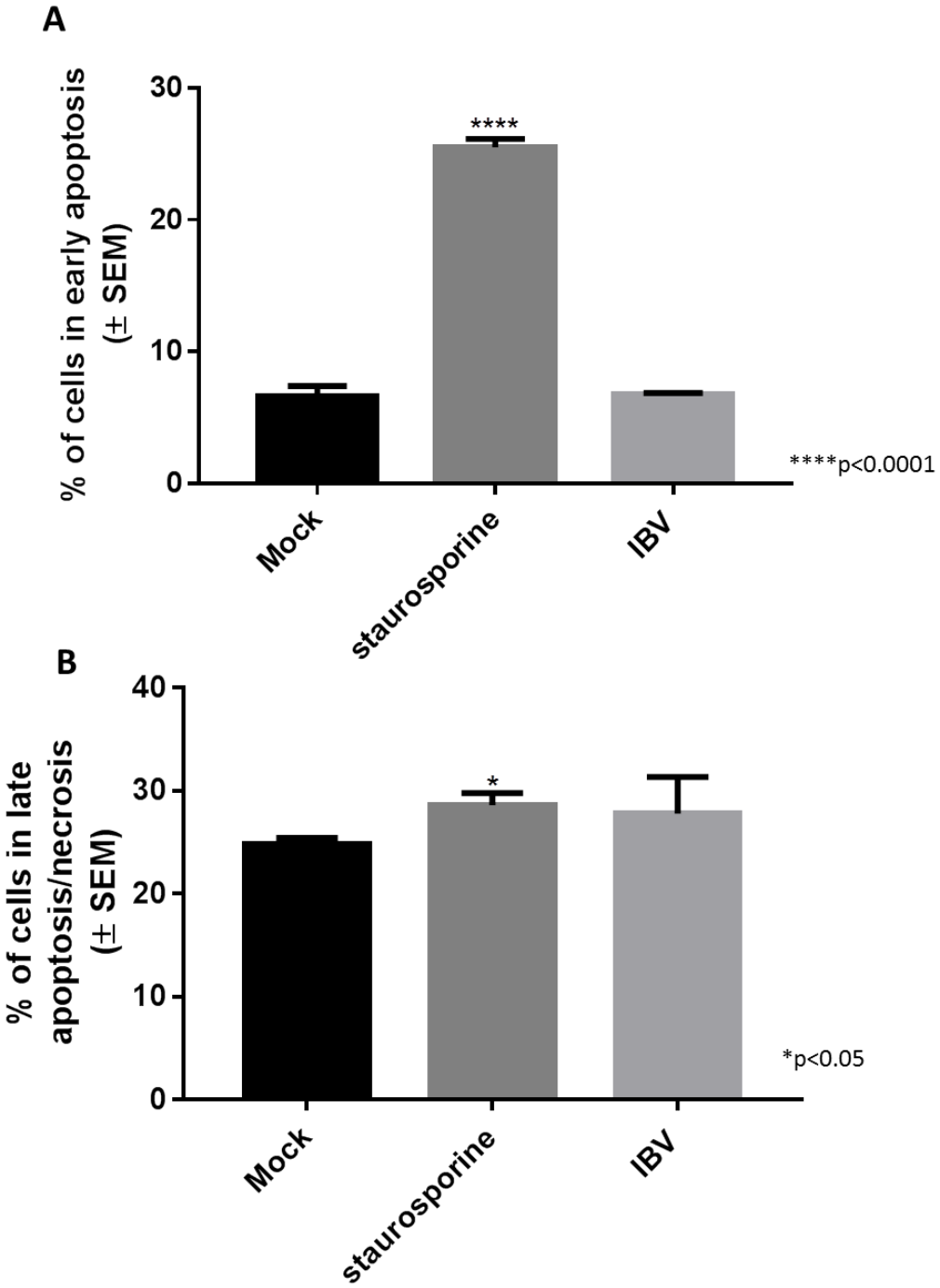


**Figure 4.5 Percentage of DF1 cells in early and late apoptosis during IBV infection and stimulation.** DF1 cells were mock infected, infected with IBV or treated with staurosporine for 24 hpi. Cells were then labelled with Annexin V FITC or PI and fluorescence measured by flow cytometry. (A) Average percentage of cells in early apoptosis calculated from % of cells in LR quadrant in Appendix 1-3. (B) Average percentage of cells in late apoptosis or undergoing necrosis calculated from % of cell in UR quadrant in figures 4.4 – 4.6. Significance calculated by un-paired t test.

DF1 cells were mock infected or infected with IBV in the presence or absence of the PI3K inhibitor LY294002. At 2, 6, 12 and 24 hpi cells were lysed and proteins separated by SDS-PAGE. Proteins were transferred onto a membrane and probed with anti-pGSK-3β S9 and anti-β-actin (Figure 4.6A). Analysis of the western blot suggests an increase in GSK-3β S9 phosphorylation during infection compared to mock at 2 hpi (Figure 4.6B). At 24 hpi there is an increase in GSK-3β phosphorylation in mock infected cells that was unexpected. At 2, 6 and 12 hpi inhibition of LY294002 results in a decrease in GSK-3β S9 phosphorylation suggesting a dependency on an active PI3K/AKT signalling pathway. At 24 hpi the results from the three replicates were inconsistent with two out of three replicates having higher levels of GSK-3β phosphorylation in the mock sample.

## 4.4 Cap-dependent translation

The activation of the PI3K/AKT/mTOR signalling cascade by growth factors, cytokines and hormones is known to induce cap-dependent translation (Gingras et al., 1998). The 4E-BPs, in their hypo-phosphorylated state, bind to and inhibit the interaction of eIF4E and the eIF4F complex (Pause et al., 1994). Activated PI3K/AKT/mTOR signalling facilitates phosphorylation of the 4E-BPs to inhibit its interaction with eIF4E and therefore allows cap-dependent translation to occur.

DF1 cells were mock infected or infected with IBV in the presence or absence of the PI3K inhibitor LY294002. At 2, 12 and 24 hpi cells were lysed and proteins separated by SDS-PAGE. Proteins were transferred onto a nitrocellulose membrane and labelled with anti-p4E-BP1 T37/46 and anti-β-actin (Figure 4.7A). Analysis of shows suppression of 4E-BP1 phosphorylation in mock infected cells when PI3K is inhibited at 2 hpi (Figure 4.7B). Densitometry also suggests that IBV infection may induce 4E-BP1 phosphorylation in DF1 cells at 2, 12 and 24 hpi. The phosphorylation appeared to be dependent on active PI3K with levels of p4E-BP1 T37/46 supressed when the cells were treated with LY294002.

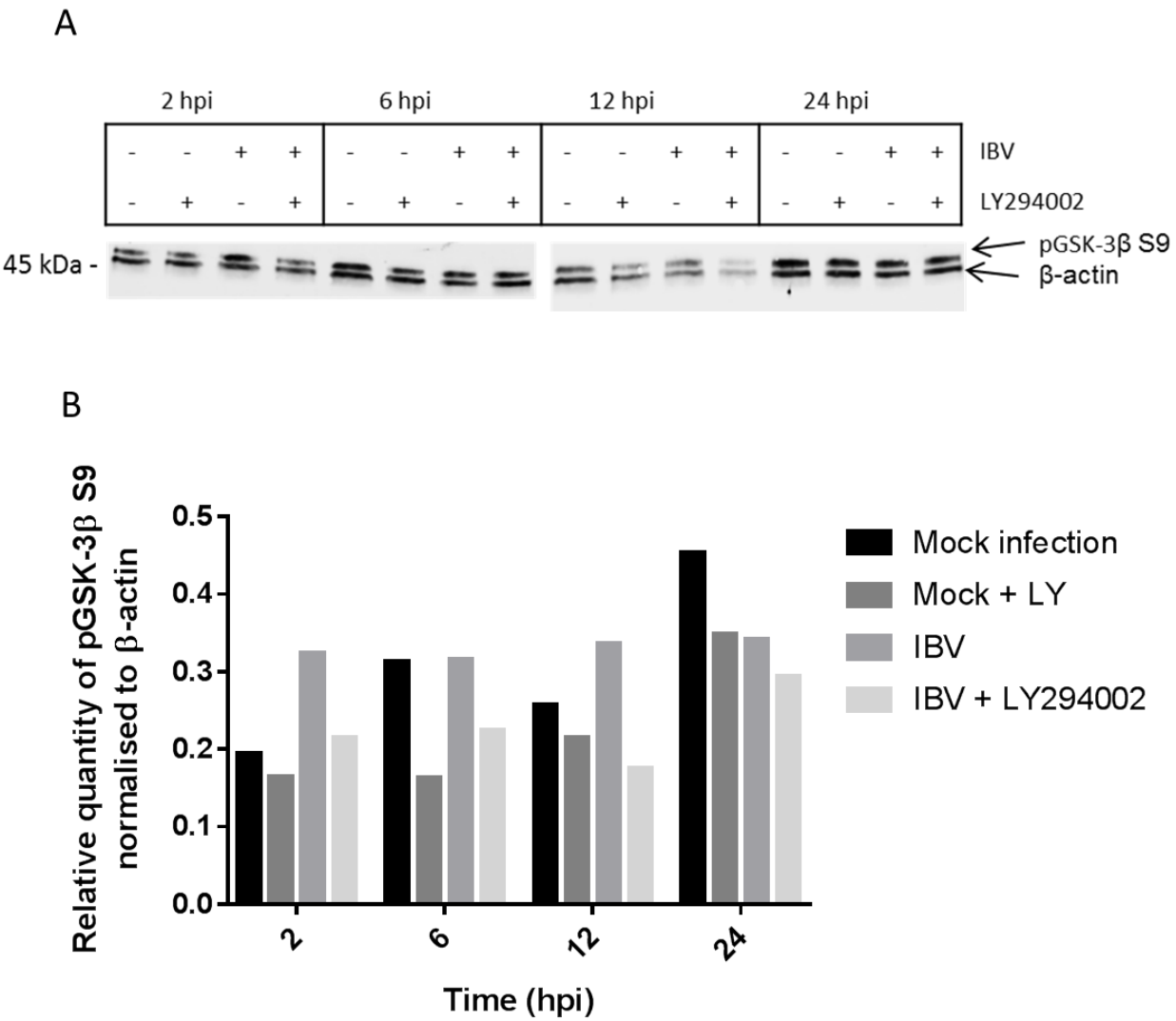


**Figure 4.6 Western blot of pGSK-3β S9 infected with IBV in the presence or absence of LY294002.** (A) DF1 cells were mock infected or infected with IBV in the presence or absence of LY294002. Cells were lysed at 2, 6, 12, and 24 hpi, lysates separated by SDS-PAGE and a western blot performed with anti-pGSK-3β S9 and anti-β-actin. Blot representative of 3 experiments. Molecular weights indicated. (B) Densitometry of western blot bands, normalized to levels of anti-β-actin.

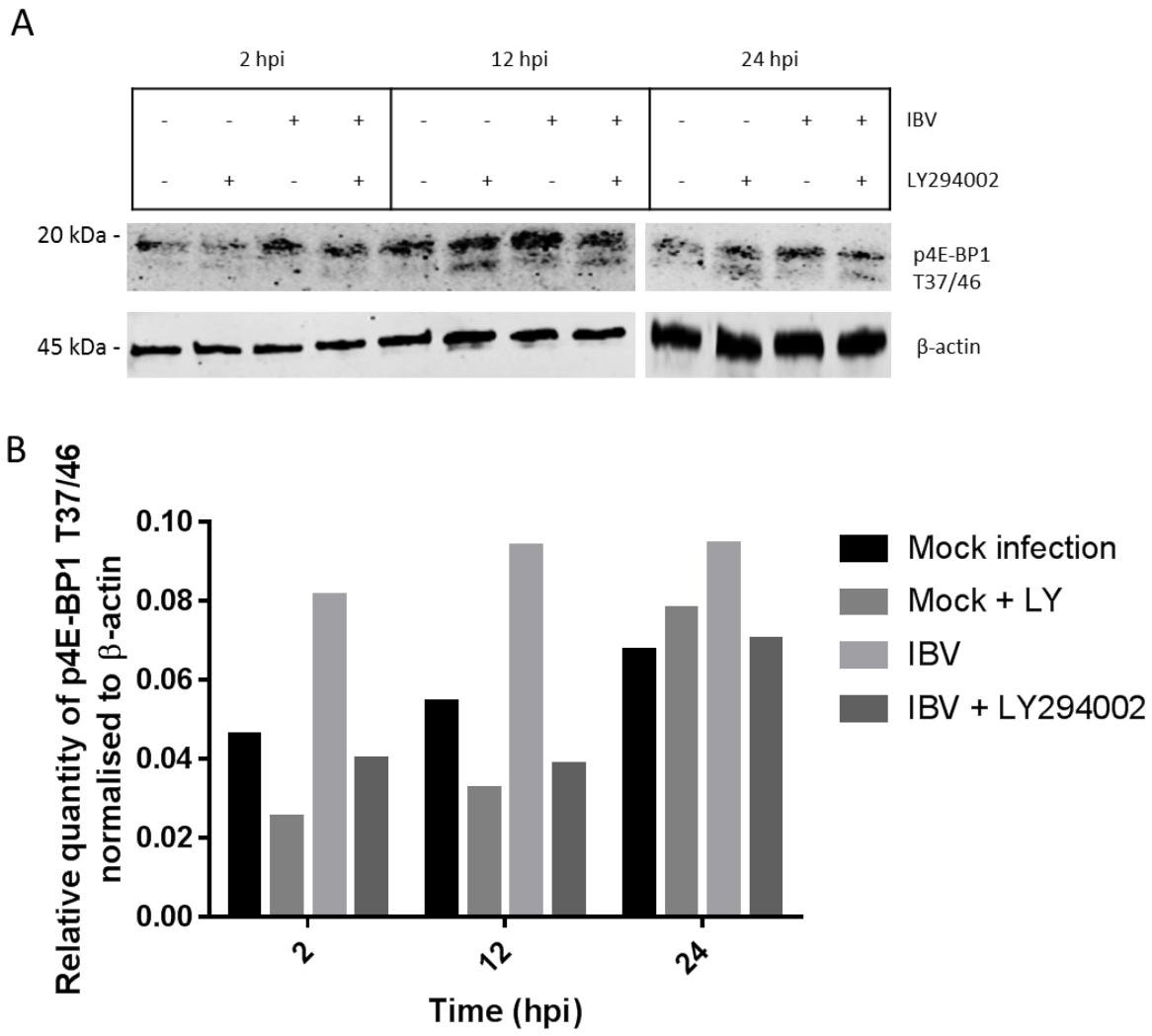


**Figure 4.7 Western blot of p4E-BP1 T37/46 infected with IBV in the presence or absence of LY294002.** (A) DF1 cells were mock infected or infected with IBV in the presence or absence of LY294002. Cells were lysed at 2, 12, and 24 hpi, lysates separated by SDS-PAGE and a western blot performed with anti-p4E-BP1 T37/46 and anti-β-actin. Blot representative of 3 experiments. Molecular weights indicated. (B) Densitometry of western blot bands, normalized to levels of anti-β-actin.

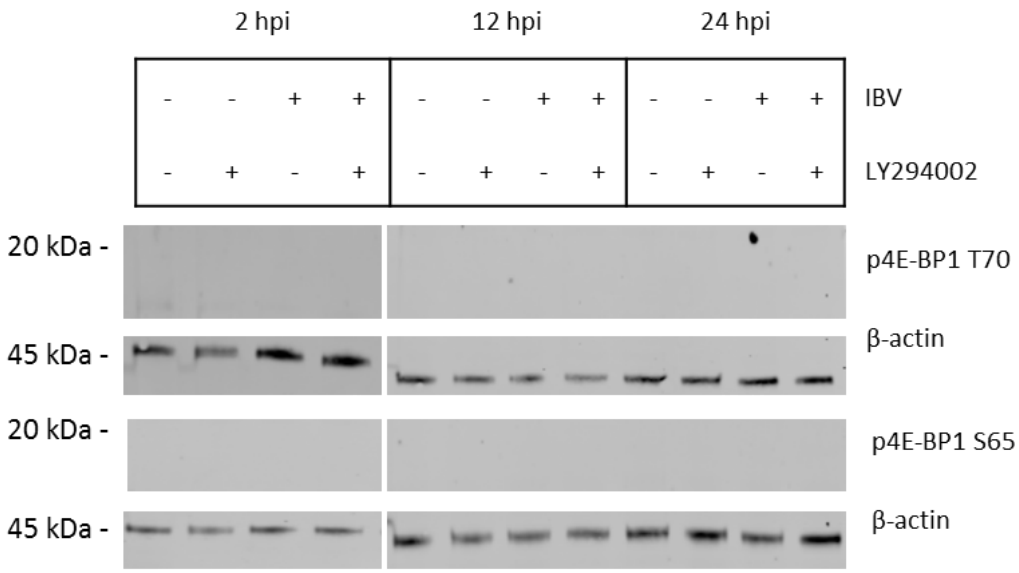


**Figure 4.8 Western blot of p4E-BP1 T70 & S65 infected with IBV in the presence or absence of LY294002.** DF1 cells were mock infected or infected with IBV in the presence or absence of LY294002. Cells were lysed at 2, 12, and 24 hpi, lysates separated by SDS-PAGE and a western blot performed with anti-p4E-BP1 T70 and anti-β-actin or anti-p4E-BP1 S65 and anti-β-actin. Blot representative of 3 experiments. Molecular weights indicated.

The phosphorylation of 4E-BP1 at T37/46 is known to prime the protein for phosphorylation at the T70 and S65 sites (Gingras et al., 1999). Therefore, the same lysates were probed with anti-p4E-BP1 T70 and S65, along with anti-β-actin (Figure 4.8). The antibodies were used at a 1:1000 however neither of the phosphorylated versions of the protein were bound by the antibodies.

## 4.5 Macropinocytosis

MHV is known to activate macropinocytosis in an entry-independent manner. The ability of IBV infection to induce macropinocytosis was therefore investigated. Macropinocytosis involves actin re-arrangement and is characterised by bulk fluid uptake. Phorbol esters such as phorbol myristate acetate (PMA) increase the rate of bulk fluid uptake and the abundance of macropinosomes in a PI3K dependent manner (Araki et al., 1996, Yoshida et al., 2015). Several methods are available for studying the macropinocytosis in cells, however none of the methods had been tested in avian cells. A method for establishing levels of macropinocytosis in avian cells was therefore investigated. Initially the ability of PMA to induce actin re-arrangement, as a measure of macropinocytosis, was measured in Vero cells. Vero cells were treated with 400 nM PMA or the equivalent volume of DMSO diluted in media as a control. After 30 minutes the cells were washed and fixed. Actin was then stained with Phalloidin 568 and the nuclei with DAPI (Figure 4.9). The arrangement of actin within the control cells is defined along the plasma membrane (Figure 4.9A). However, when treated with PMA, the plasma membrane became less defined as cell wide actin re-arrangement occurred (Figure 4.9B). This demonstrates the efficacy of PMA in inducing actin re-arrangement in Vero cells. Whilst actin re-arrangement was identified during PMA stimulation, infection of cells with IBV did not results in any obvious membrane re-arrangement or membrane ruffling (Figure 4.10). This suggests that either IBV does not induce macropinocytosis in Vero cells or that membrane ruffling is not a good indication of the macropinocytic activity in these cells.

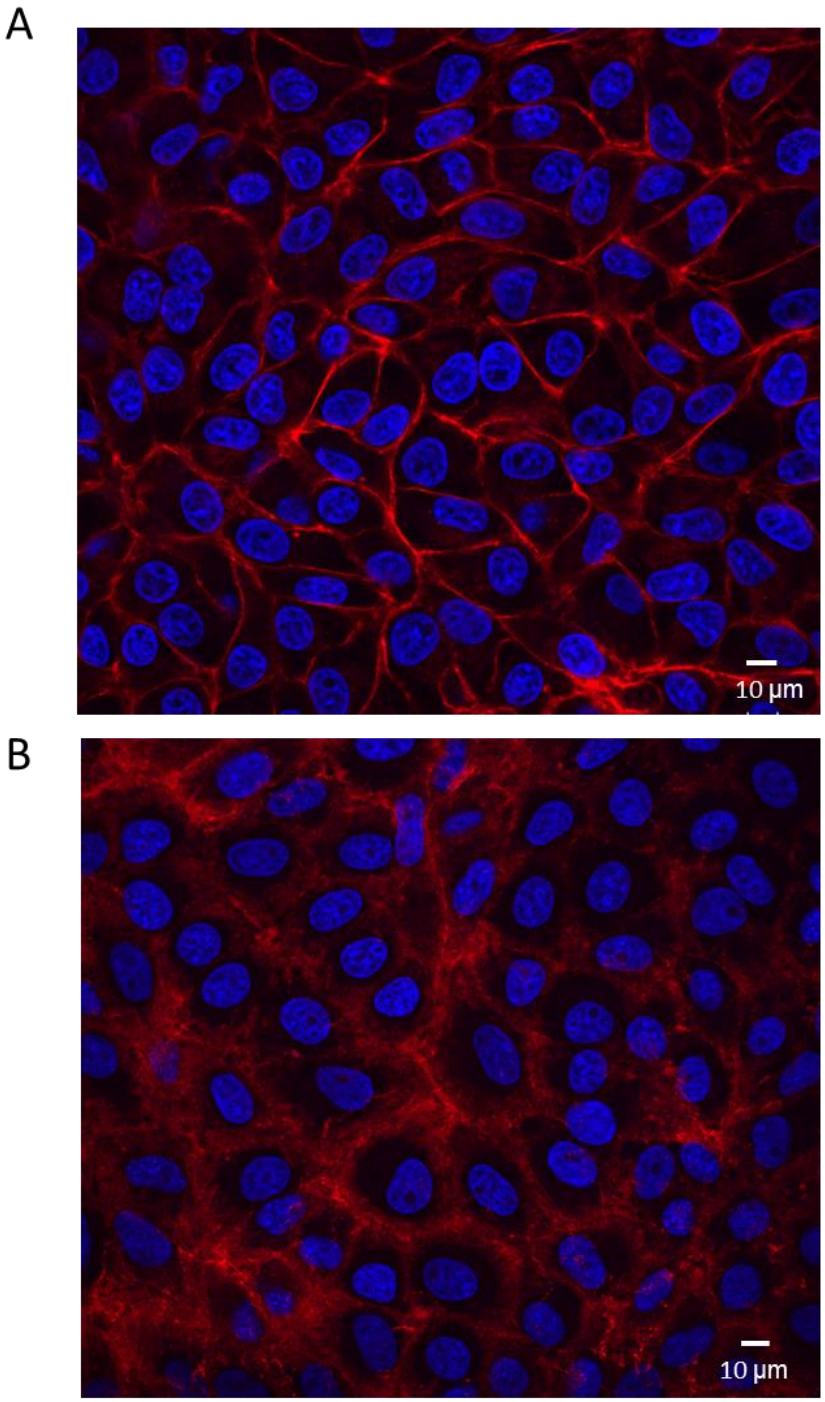


**Figure 4.9 Vero cells treated with DMSO or PMA to stimulate macropinocytosis.** Vero cells were treated with (A) DMSO diluted in growth media or (B) 400 nM PMA for 30 minutes. Cells were then fixed, permeabilised and actin stained with Phalloidin 568 and nuclei stained with DAPI.

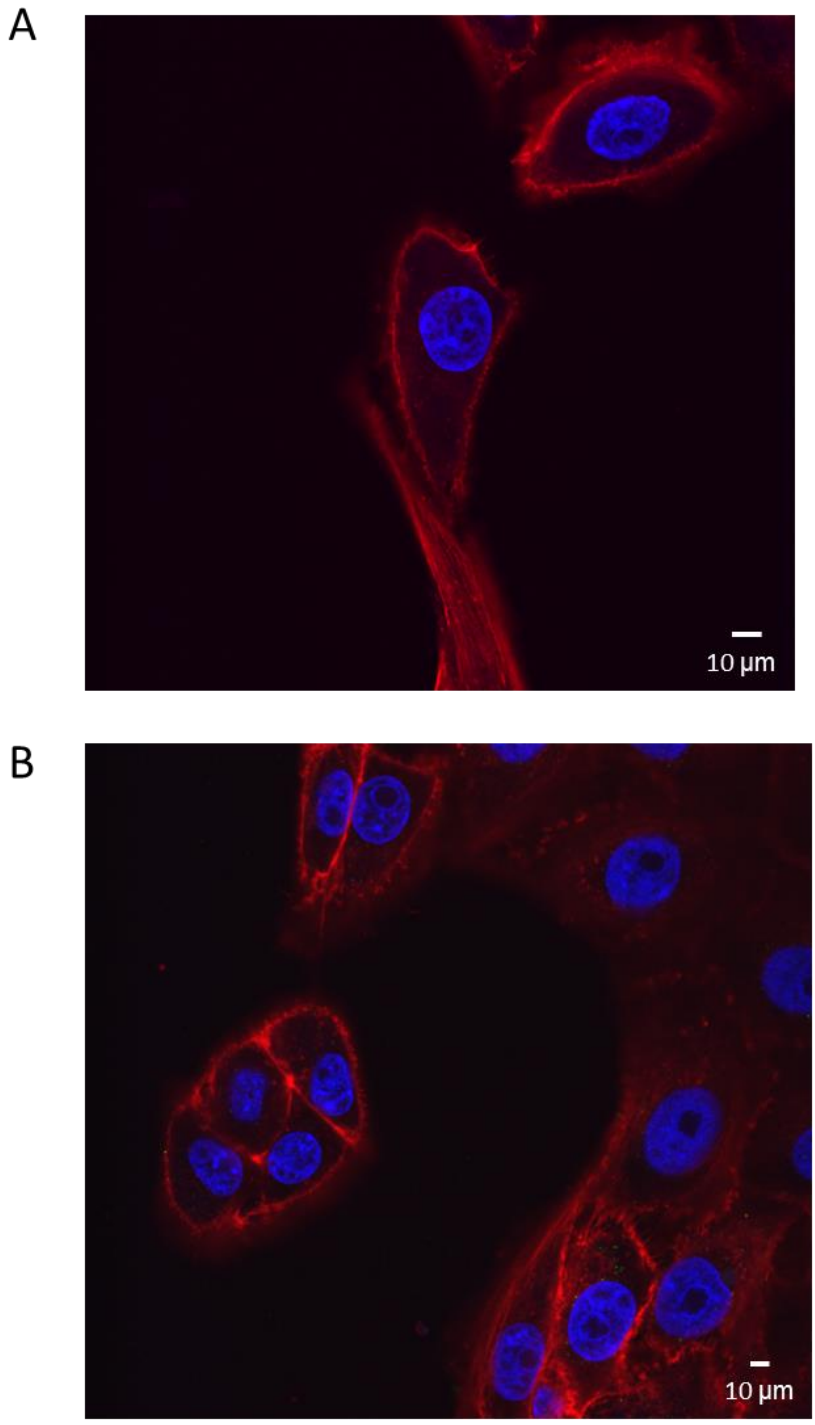


**Figure 4.10 Vero cells mock infected or infected with IBV.** Vero cells were (A) mock infected or (B) infected with IBV and fixed at 24 hpi. Cells were permeabilised and probed with anti-dsRNA for viral infection (green), actin stained with Phalloidin 568, nuclei stained with DAPI and .

Therefore, another assay, to measure levels of micropinocytosis, was tested on Vero cells. Along with actin re-arrangement, bulk-fluid uptake is another indicator of macropinocytosis. To measure levels of bulk fluid uptake in DF1 cells, 800 nm fluorescently labelled polystyrene nanoparticles were added to the cell culture media. The particles were too large to be taken up by endocytosis but small enough to be engulfed in a macropinosome (Lim and Gleeson, 2011). Cells were incubated in 1 µg/ml fluorescently labelled nanoparticles for 24 hours. After 24 hrs, cells were washed in PBSa and fixed. Actin was labelled with Phalloidin 568 and nuclei with DAPI (Figure 4.11). Several cells had nanoparticles present on the plasma membrane (indicated with * Figure 4.11). Others had internalised nanoparticles (indicated with + Figure 4.11). The location of the nanoparticles within the cell was confirmed by scanning through the z-axis of each cell. The effectiveness of PMA to induce bulk fluid uptake in Vero cells was then investigated using the fluorescently labelled nanoparticles. Cells were incubated with the nanoparticles for 1 hour prior to treatment with various concentrations of PMA. The cells were incubated with PMA for 1 hour and then fixed and stained with Phalloidin 568 and DAPI. At 200 nM an increase in the percent of cells containing internalised nanoparticles was seen from 41% to 79% ($p<0.02$). At 400 nM, PMA induces actin re-arrangement (Figure 4.12) and an increase in the percentage of nanoparticle internalisation was observed from 41% to 91% of cells at that concentration. The large amount of variation and inconsistency throughout the replicates suggested that further controls needed to be employed in order to for this protocol to be used.

The effect of the macropinocytosis inhibitor Amiloride was then investigated. Vero cells were incubated in different concentrations of Amiloride for 24 hours. After 24 hours the cytotoxicity of the inhibitor was determined by luminescent cell titre assay (Figure 4.13). The addition of Amiloride at 0.5 µM was found to cause no significant drop in cell titre however increasing the concentration to 1 µM decreased the luminescence output from $2x10^7$ to $8.3x10^6$ RLU.

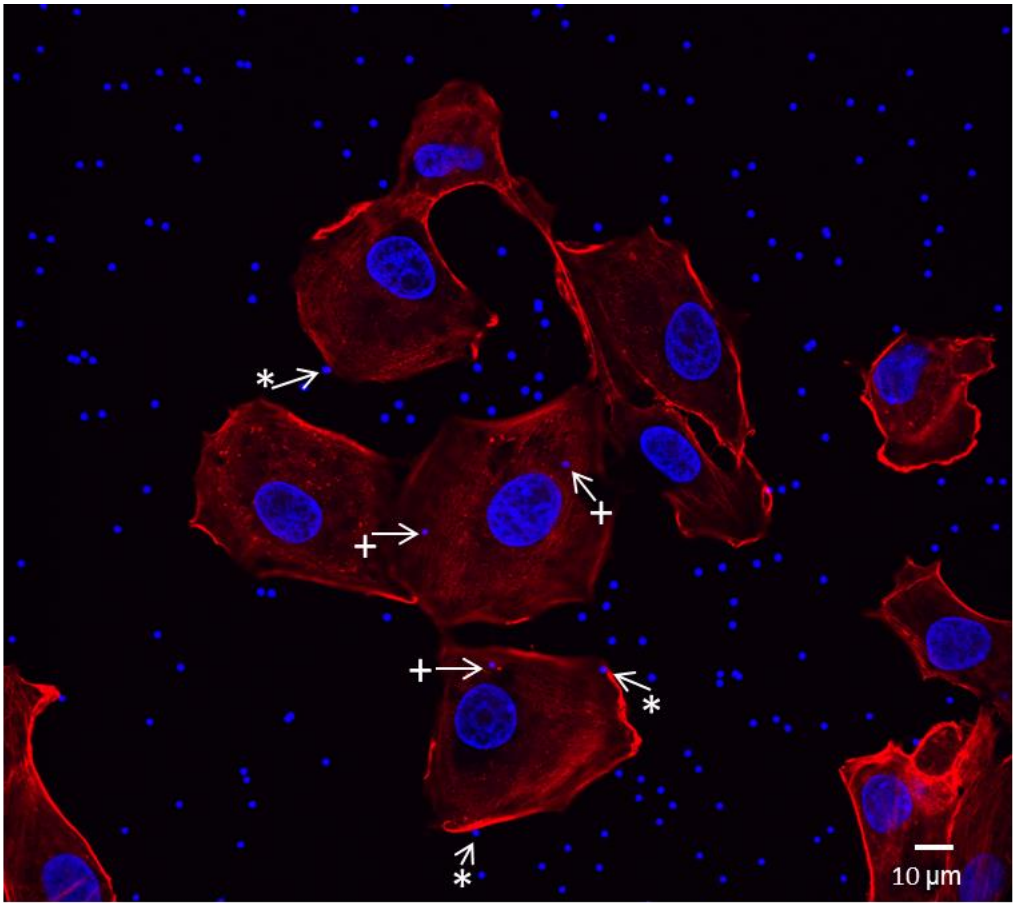


**Figure 4.11 Vero cells incubated in 1 µg/ml fluorescent nanoparticles.** Vero cells were incubated in 1 µg/ml 800 nm fluorescent polystyrene nanoparticles for 24 hrs then washed. Cells were fixed and actin stained with Phalloidin 568 and nuclei with DAPI. *Nanoparticles on or within cellular membrane. ⁺Internalised nanoparticles

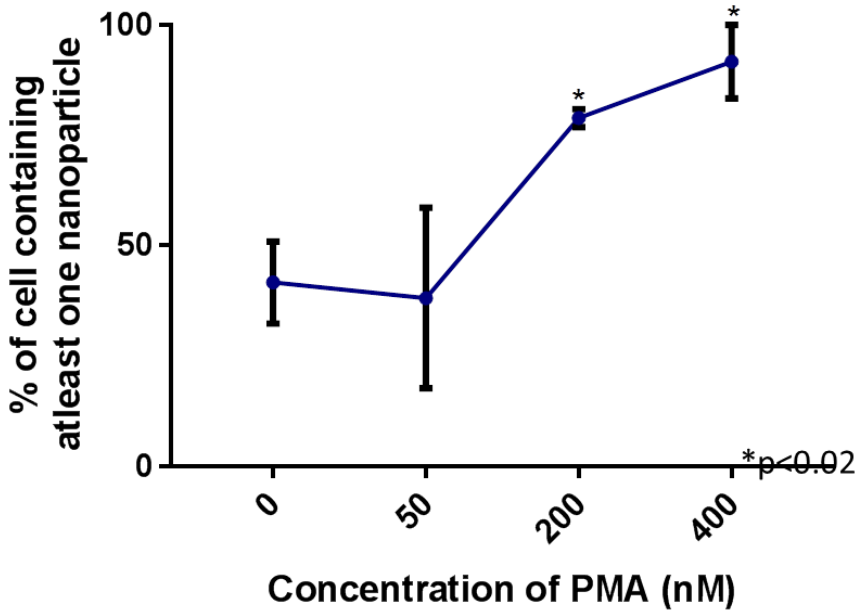


**Figure 4.12 Vero cells incubated in nanoparticles and treated with different dilution of PMA.** Vero cells were incubated in 1 µg/ml fluorescent nanoparticles and macropinocytosis stimulated with different concentrations of PMA for 1 hour. Cells were washed and fixed. Actin was stained with Phalloidin 568, nuclei with DAPI and the % of cells containing at least one nanoparticle was determined for each concentration of PMA. Average of 3 fields on three different coverslips. *Significance calculated by un-paired t test.

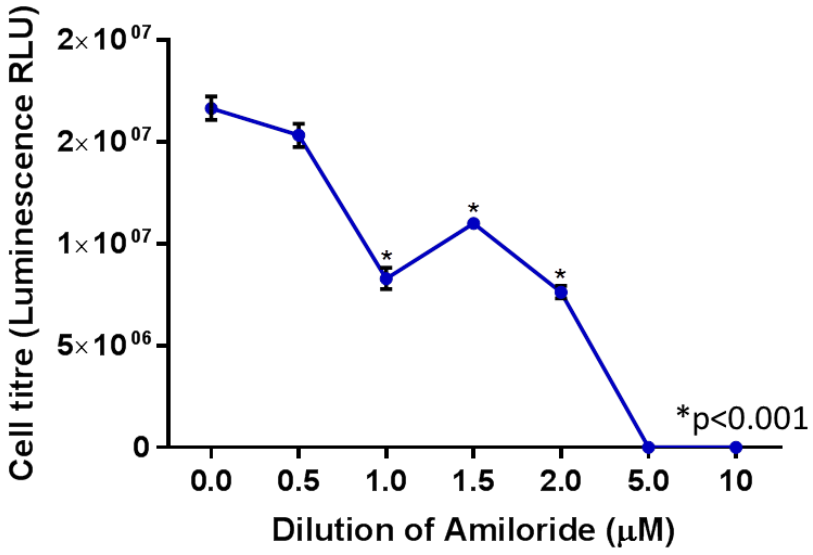


**Figure 4.13 Cytotoxicity assay of Vero cells incubated in Amiloride.** Vero cells were incubated in a serial dilution of the macropinocytosis inhibitor, Amiloride for 24 hrs. The cytotoxicity of the inhibitor was measured by cell titre luminescent assay. *Significance calculated by un-paired t test.

To establish the efficacy of Amiloride as a macropinocytosis inhibitor at 0.5 μM, Vero cells were incubated in nanoparticles and pre-treated with Amiloride or an equivalent volume of DMSO for 1 hour. Cells were also incubated in LY294002 to determine if PI3K was involved in this signalling pathway. After 1 hour, cells were stimulated with PMA or the equivalent volume of DMSO for another hour. Cells were then washed, fixed and actin stained with Phalloidin 568 and the nuclei with DAPI. The percentage of cells containing at least one internalised nanoparticle was determined for each condition (Figure 4.14). Whist a decrease in the percentage of cells with internalised nanoparticles was seen during both PI3K and macropinocytosis inhibition, neither of these results were statistically significant. The stimulation of control cells with PMA was not seen to induce a significant increase in nanoparticle internalisation in this experiment either.

The effect of IBV infection on the internalisation of nanoparticles was also investigated. Cells were incubated in the fluorescent nanoparticles for an hour and then either mock infected or infected with IBV. At 2, 6, 12 and 24 hpi cells were fixed and actin stained with Phalloidin 568, and the nuclei with DAPI. The percentage of cells containing at least one nanoparticle was calculated (Figure 4.15). At 2 hpi there was a significant increase in nanoparticle uptake between the mock infected and infected cells, from 8% to 34% ($p=0.03$). There was no significant change in nanoparticle uptake at any other time point. However, due to the lack of an appropriate positive and negative control, this data could not be confirmed.

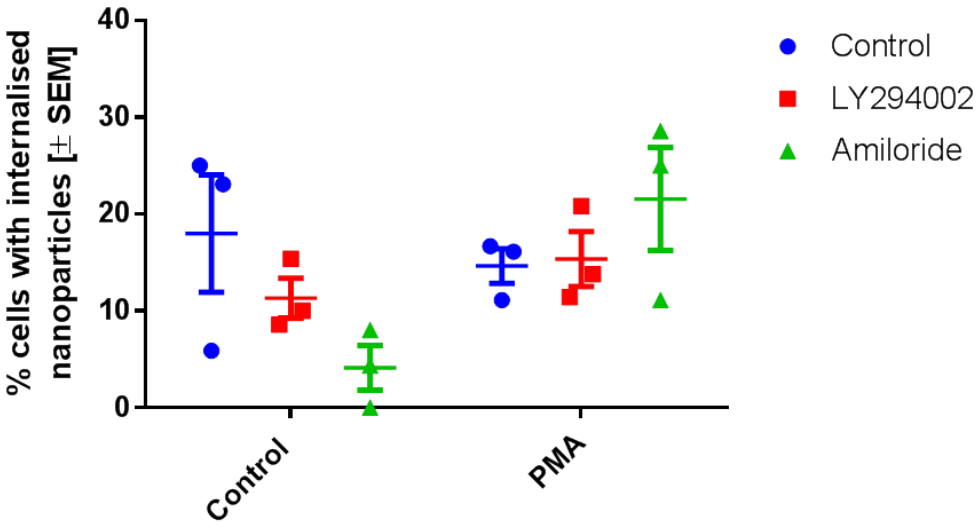


**Figure 4.14 Vero cells incubated in nanoparticles and treated with PMA and Amiloride.** Vero cells were incubated in 1 µg/ml fluorescent nanoparticles. Macropinocytosis was stimulated with PMA and inhibited with Amiloride. Cells were washed and fixed. Actin was stained with Phalloidin 568, nuclei with DAPI and the % of cells containing at least one nanoparticle was determined for each treatment. Average of 3 fields on three different coverslips. *Significance calculated by 2way ANOVA with multiple comparisons.

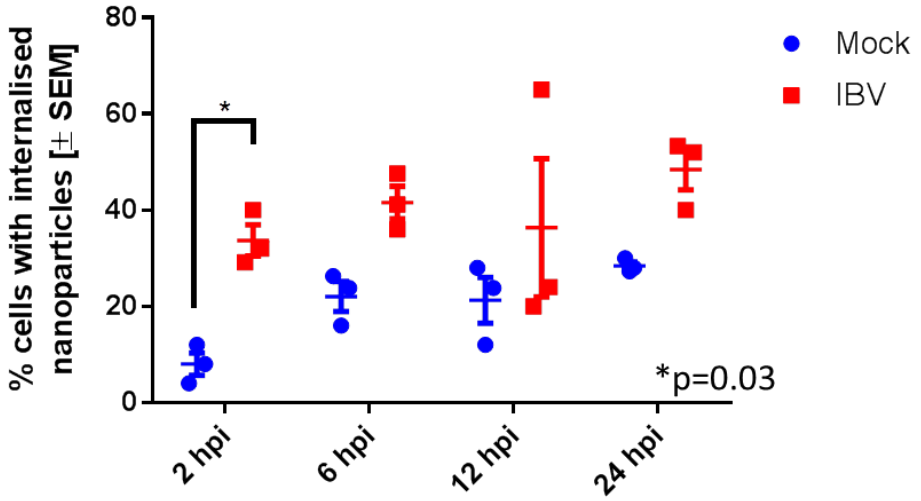


**Figure 4.15 Vero cells incubated in nanoparticles and mock infected or infected with IBV.** Vero cells were incubated in 1 µg/ml fluorescent nanoparticles and mock infected or infected with IBV. At 2, 6, 12 and 24 hpi cells were washed and fixed. Actin was stained with Phalloidin 568, nuclei with DAPI and the % of cells containing at least one nanoparticle was determine. Average of 3 fields on three different coverslips. *Significance calculated by 2way ANOVA with multiple comparisons.

## 4.6 Discussion

Apoptosis has been reported to occur in IBV infected Vero cells by using terminal deoxynucelotidyl transferase dUTP nick end labelling (TUNEL) assay (Liu et al., 2001, Li et al., 2007). Whilst the TUNEL assay is often used for reporting levels of apoptotic activity, it may not allow for the differentiation between necrotic and apoptotic cells. Liu et al (2001) then went on to confirm the involvement of caspase in IBV induced apoptosis of mammalian cells using a specific caspase inhibitor z-VAD-FMK. This study provides results that suggest a similar response in avian cells. Interestingly, an early activation of caspase 3/7 in Vero cells was observed, suggesting that activation of apoptosis also occurs in a biphasic manner.

The effect of IBV infection on the apoptotic pathway was then investigated in avian cells. Staurosporine, a known activator of apoptosis, induced caspase 3/7 cleavage in DF1 cells from 6 to 24 hpi (Figure 4.2). IBV infection was also found to induce caspase 3/7 cleavage above mock levels at 2 hpi and then subsequently from 24 to 36 hpi (Figure 4.3). A similar pattern of caspase cleavage was seen in IBV infected Vero cells, however in DF1 cells activation of caspase cleavage is delayed until 24 hpi. Interestingly IBV infection of both Vero and DF1 cells results in an increase in caspase cleavage at 2 hpi that is subsequently supressed by 6 hpi. This is potentially an antiviral response that is subsequently supressed by viral factors. The rotavirus for example, supresses viral-induced cellular apoptosis to facilitate viral growth (Bagchi et al., 2010). The increase in caspase cleavage correlates with an increase in AKT activation seen in Chapter 3 (Figure 3.10) suggesting a role of the PI3K/AKT signalling pathway in pro-apoptotic responses.

The effect of PI3K inhibition by LY294002 on caspase 3/7 cleavage was investigated. Levels of caspase 3/7 cleavage induced by IBV infection were not altered by inhibition of PI3K (Figure 4.4). This suggests that the PI3K/AKT signalling pathway is not involved in IBV induced apoptosis in DF1 cells. A previous study

presented evidence of ER stress during IBV infection of mammalian cells (Fung et al., 2014). ER stress is known to induce apoptosis through cleavage of caspase 9 and then subsequently signalling through the caspase 3,6 and 7 complex. It is therefore possible that the cleavage of caspase 3/7 seen in Figure 4.3 is a result of an ER stress response. The independence of this activation from PI3K/AKT activity supports this hypothesis, as the ER stress/apoptosis pathway does not involve PI3K/AKT activation. Fung et al (2014) also suggest that the IBV-induced ER stress response triggers the anti-apoptotic IRE1α, which in turn modulates pro-survival responses via JNK and AKT. This may be an explanation for the activation of the PI3K/AKT signalling pathway. Replication of viral proteins may induce ER stress, resulting in the activation of the pro-apoptotic pathway and cleavage of caspase 3/7. The virus may then modulate pro-survival pathways such as AKT through IRE1α, preventing apoptosis.

Whilst IBV infection of DF1 cells was found to induce caspase cleavage, it was not found to induce the translocation of PS to the outside of the plasma membrane, another marker of apoptosis. The signals underlying the externalisation of PS during apoptosis are unknown, however it is generally assumed that it occurs as a consequence of caspase cleavage (Huigsloot et al., 2001). In the case of IBV infection of avian DF1 cells, caspase 3/7 cleavage may occur in the absence of PS externalisation. Since PS externalisation occurs as a result of a pro-apoptotic pathway, a factor downstream of the caspase complexes may be inhibiting apoptosis during IBV infection. Alternatively, due to the fact that PI3K inhibition does not alter caspase 3/7 cleavage, the anti-apoptotic PI3K/AKT signalling pathway may be acting downstream of the caspase complex to supress apoptosis. Many viruses are known to induce apoptosis through caspase activation. For example, the Influenza virus induced caspase-dependent apoptosis, however no viruses have been noted to induce caspase activation without the triggering of PS externalisation (Takizawa et al., 1999).

The role of GSK-3β in many cellular processes, and its position downstream of AKT, suggested that it may be modulated during IBV infection. Among other pathways, GSK-3β is known to have a pro-apoptotic function where it indirectly activates p53 and Bax to induce the caspase cascade. An increase in caspase 3/7 cleavage during IBV infection was previously shown to be independent of PI3K activity (Figure 4.4). The PI3K dependent inhibition of GSK-3β during infection, suggests that the cleavage of caspase 3/7 also be GSK-3β independent and a cellular anti-viral response occurring independently of PI3K/AKT signalling (Figure 4.6). The de-activation of GSK-3β by phosphorylation at S9 may therefore be a pro-viral response elicited by the virus in an attempt to counteract the cellular pro-apoptotic response.

GSK-3β has also recently been found to be involved in the modulation of antiviral activity by the zinc-finger antiviral protein (ZAP) (Sun et al., 2012). The antiviral ZAP is a host factor that is known to inhibit the replication of HIV-1 (Zhu et al., 2011b) and alphaviruses such as Sindbus virus (Zhang et al., 2007). GSK-3β was found to enhance the activity of ZAP by phosphorylation at specific sites (Sun et al., 2012). It is therefore possible that the PI3K-dependent inactivation of GSK-3β is a pro-viral response to prevent ZAP from targeting viral mRNA and therefore inhibiting viral replication. This may also suggest why inhibition of PI3K was found to reduce genome replication, viral protein production and infectious virus particle release.

Cellular mRNA is recognised by the cap-binding protein eIF-4E which exists as part of the eIF-4F complex. The binding of the cap-binding protein facilitates unwinding of the mRNA 5' secondary structure and allows attachment of the 40s ribosomal subunit. The 4E-BPs are translational repressors that act by attaching to the eIF-4E complex. Growth factors and hormones activate protein translation by phosphorylation and inactivation of the eIF4E-binding proteins. The 4E-BPs are phosphorylated and therefore inactivated by the PI3K/AKT/mTOR signalling

cascade allowing translation to occur (Gingras et al., 1998). The deactivation of 4E-BPs occurs initially by phosphorylation at T37/46 which primes the protein for subsequent phosphorylation at T70 and S65. Unfortunately, the antibodies for p4E-BP1 T70 and S65, raised against mammalian proteins, did not cross-react with the avian DF1 cells. Due to a lack of time, the assay was not repeated on mammalian cells. However, p4E-BP1 at T37/46 was detected by western blot. An increase in the phosphorylation of 4E-BP1 at T37/46 was observed at some time points during IBV infection, which appeared to be dependent on PI3K activity. The protocol however requires further adjustments as the data is inconsistent.

In Chapter 3, IBV infection was seen to induce AKT activation at 2 hpi and then subsequently from 16 hpi to 24 hpi (Figure 4.7). The PI3K dependency of the 4E-BP1 phosphorylation and the activation of AKT seen at these time points suggests that phosphorylation of 4E-BP1 may be induced via the PI3K/AKT signalling pathway. The effect of LY294002 on the growth of the virus was investigated in Chapter 3 and it was found that inhibition of PI3K reduced viral genome replication, protein synthesis and release of infectious virus particles. This suggests that by inhibiting PI3K, the IBV induced phosphorylation of 4E-BP1 could be hindered, therefore inhibiting cap-dependent translation. That, in turn, may have a knock-on effect on protein synthesis and release of infectious virus particles. The role of the modulation of translation during viral replication is often multi-faceted. For example, the respiratory syncytial virus was found to modulate translation via de-phosphorylation of 4E-BP1 (Pérez-Gil et al., 2015). However, it was recently found that stress granules were formed in cells infected with RSV and that the presence of the granules did not alter viral replication (Lindquist et al., 2010). This suggests that the virus is able to control processes that allow the replication of viral proteins despite the cell being under stress. The PI3K dependent activation of AKT, subsequent phosphorylation of 4E-BP1 T37/46, and activation of cap-dependent translation during IBV infection, is therefore hypothesised to be a pro-viral response

induced by the virus. Interestingly, the replication of other coronaviruses has been found to be dependent on eIF4E-eIF4G interactions (Cencic et al., 2011).

Macropinocytosis is an actin-dependent process that involves the non-selective uptake of molecules, nutrients and antigens. The large size of macropinosomes allows the uptake of viruses such as the nipha virus (Pernet et al., 2009), influenza virus (Rossman et al., 2012), African swine fever virus (Sanchez et al., 2012) and foot-and-mouth disease virus (Han et al., 2016). MHV was found to induce macropinocytosis in an entry-independent manner (Freeman et al., 2014). There is increasing evidence that the PI3K/AKT signalling pathway is involved in the regulation of macropinosome formation through Ras and $PIP_3$. Ras is known to induce $PIP_3$ through binding to PI3K, and the attenuation of $PIP_3$ results in the inhibition of macropinocytosis (Rodriguez-Viciana and Downward, 2001, Araki et al., 1996). AKT is then subsequently recruited to macropinosomes by $PIP_3$ along with other effector molecules containing PH-domains (Rupper et al., 2001). The role of the PI3K/AKT signalling pathway in IBV infection seen in Chapter 3 suggested that the macropinocytosis pathway may be involved. However, methods employed to measure macropinocytosis have not been extensively tested in avian cells. Initially the ability of PMA to stimulate actin re-arrangement in Vero cells was assessed in order to optimise the assays prior to testing in DF1 cells. PMA was found to induce actin re-arrangement (Figure 4.9) however no visible change actin arrangement was seen in IBV infected cells at 24 hpi (Figure 4.10). The assessment of actin re-arrangement was deemed too subjective and therefore a more quantitative assay was tested. The level of bulk fluid uptake was assessed by the addition of fluorescent nanoparticles to the media (Figure 4.11). The fluorescently labelled 800 nm polystyrene nanoparticles were previously used by Freeman et al (2014) in the study of macropinocytosis during MHV infection. An average of 42% of the mock infected cells were found to contain at least one internalised nanoparticle. This was a lot higher than expected as levels of particle uptake in the mock infected DBT cells

from the Freeman et al (2014) paper were below 10%, increasing to 40% during infection with MHV and SARS-CoV. At a concentration of 400 nM PMA, increased nanoparticle uptake into cells was observed (Figure 4.12). However, the replicates were highly variable. A known inhibitor of macropinocytosis, Amiloride was then assessed for its efficacy in Vero cells. It was found to not be cytotoxic at 0.5 μM (Figure 4.13) but did not significantly reduce nanoparticle uptake in control or PMA stimulated cells (Figure 4.14). As the macropinocytosis pathway is known to be dependent on PI3K/AKT signalling, the same experiment was performed using the PI3K inhibitor LY294002. As with Amiloride, LY294002 did not significantly inhibit nanoparticle uptake in either the control or PMA stimulated cells (Figure 4.14). However in the experiments performed in the presence of Amiloride and LY294003, PMA did not significantly induce nanoparticle uptake and again the individual replicates were highly variable. The fact that PMA was not able to induce nanoparticle uptake in these experiments but was able to in earlier experiments suggested that the assay was highly susceptible to slight variations in cell confluency and passage number. Whilst every attempt was made to ensure that the confluency of the cells was the same in each replicate, the density of the cells in different areas of the coverslip may also have resulted in these errors. Despite this there is a general trend in each replicate suggesting a suppression of nanoparticle internalisation in the presence of LY294002 compared to control and even more so with Amiloride.

The protocol was also tested on IBV infected mammalian cells (Figure 4.15). A 4 fold increase in the number of cells containing nanoparticles was seen at 2 hpi but not at 6, 12 or 24 hpi. These results were again the average of three fields of view from three different coverslips. However only cells displaying infection (as determined by dsRNA staining), or those immediately adjacent to the infected cells were counted. This may have resulted in less variability in the data. A general trend of an increase in nanoparticle uptake during IBV infection was seen at each time

point except 12 hpi. The increase in macropinocytosis seen at 2 hpi does not coincide with increases in PI3K activation that are only observed from 6 hpi in Vero cells. Due to the lack of nanoparticle internalisation at the later infection time points, the involvement of PI3K/AKT activation in macropinocytosis in Vero cells was not thought to be likely. The experiment was not repeated in DF1 cells due to time restraints. However, the highly variable nature of the assay in these cells suggested that it would be unlikely to be successful in the less consistent DF1 cell line.

## 4.7 Summary

Apoptosis

- IBV infection results in caspase 3/7 cleavage at early and late phases of infection in avian and mammalian cells
- IBV-induced caspase 3/7 cleavage is not dependent of active PI3K
- Externalisation of PS does not occur during IBV infection of DF1 cells at 24 hpi

GSK-3β

- GSK-3β is phosphorylated at S9 early during IBV infection and in a PI3K-dependent manner

Cap-dependent translation

- 4E-BP1 is phosphorylated at T37/46 late during IBV infection in a PI3K-dependent manner

Macropinocytosis

- Bulk fluid uptake is induced in Vero cells at 2 hpi with IBV

## 4.8 Future Work

The effect of PI3K inhibition on caspase 3/7 cleavage was investigated however, its effect was not determined on levels of PS externalisation. It would be interesting to investigate if inhibition of PI3K or AKT lead to an increase in PS externalisation, therefore implicating the pathway in suppression of apoptosis downstream of caspase 3/7 cleavage. Apoptosis has been previously identified to occur as a result of ER stress during IBV infection. It would be of interest to investigate whether the inhibition of IRE1α altered the activation of the PI3K/AKT signalling pathway. Also, by measuring caspase-12 cleavage, the origin of the pro-apoptotic response could be distinguished.

The activity of the mTOR pathways was not investigated in this chapter. However, it would be interesting to measure levels of mTOR activity and to investigate its susceptibility to PI3K and AKT inhibitors to confirm the presence of the PI3K/AKT/mTOR signalling cascade in chickens. Should the activity of the signalling cascade be confirmed, it would be interesting to investigate the hypothesis that the phosphorylation of 4E-BP1 is a pro-viral response elicited by the virus. This could be done by specifically inhibiting various elements of the pathway, such as AKT activation, mTOR activation and the formation of the eIF4F translation initiation complex. During inhibition the amount of viral genome, mRNA and protein production as well as the release of infectious virus particles could be measured.

Possible methods for determining levels of macropinocytosis during IBV infection were investigated in this chapter. The experiments were originally tested in Vero cells. However due to the high workload involved and a lack of time, the experiments were not repeated in DF1 cells. It would be interesting to do so. The nanoparticle assay was time consuming and involved the processing of large amounts of data. The apparent sensitivity of the assay lead to large variations in

replicates. Therefore, another method for measuring macropinocytosis could be investigated. By incubating the cells in a fluorescently labelled hydrophilic dye such as Dextran the amount of bulk fluid uptake can be measured by flow cytometry (Wang et al., 2014a). Using a marker for IBV infection it would be possible to selectively measure bulk fluid uptake in infected and uninfected cell populations by flow cytometry. This would allow large amounts of data to be processed easily and cells infected with IBV could be selected from the population for analysis.

The interaction between GSK-3β and the apoptosis pathway during IBV infection was interesting and something that could be followed up. GSK-3β is known to not only be pro-apoptotic but also anti-apoptotic in the right conditions (Jacobs et al., 2012). The effect of GSK-3β inhibition on caspase cleavage and apoptosis could therefore be investigated. This could be done using GSK-3β inhibitors such as Anilino maleimides that are known to specifically inhibit GSK-3β.

Further studies should also be conducted to look at the role of ZAP in IBV infection. To date there have been no studies examining the effect of ZAP on coronaviruses. It may be interesting to measure levels of ZAP phosphorylation during infection and see if it alters with inhibition of GSK-3β.

The downstream effects of AKT activation during IBV infection are varied and most likely extensive. Whilst apoptosis, cap-dependent translation and macropinocytosis have been investigated and discussed, there are numerous pathways that may be involved in IBV infection. For example, the NFκB pathway is known to be activated by AKT signalling and is involved in the antiviral response. Investigation into the activity of the pathway during IBV infection may elucidate the cause for the biphasic activation of AKT seen in Chapter 3. It is possible that the early phase of activation is an anti-viral response to infection and may involve the NFκB pathway.

Whilst this project focused mainly on the role of the PI3K/AKT signalling pathway during IBV infection. The involvement of many cellular signalling pathways during

IBV infection could be established by performing a phosphoproteomic study. This would allow us to map the activated pathways in both uninfected and infected cells to identify which are being modulated by the virus

# Chapter 5

## Expression of ch*AKT1* & ch*AKT3* in avian tissues

## 5.1 Introduction

The protein kinase, AKT plays a critical role in the regulation of cell growth and survival. It is a member of the AGC kinase family that consists of approximately 60 members that are phosphorylated at serine or threonine residues (Fayard et al., 2005). There are three isoforms of mammalian AKT, AKT1, AKT2, and AKT3 which exhibit strong homology in their catalytic domains. However, the functions of each isoform differ. The human AKT genes have been well characterised and their location on the human genome identified (Table 5.1). *AKT1* is present on chromosome 14, *AKT2* on chromosome 19 and *AKT3* on chromosome 1.

The expression profile of the AKT genes in human tissues has been well investigated (Figure 5.1). *AKT1* is the most widely expressed of the three genes and is found in most tissues at high levels (Stambolic and Woodgett, 2006). *AKT2* is expressed at lower levels than *AKT1* and at lower levels in the brain and liver compared to other tissues. The third isoform, *AKT3,* is expressed in high levels in the brain and muscle but in low levels in other tissues. The expression patterns of the genes can provide an insight into the function of the encoded proteins. There is strong homology in their catalytic domains with between 87% and 90% identical amino acids. However, despite this homology, the expression and function of each isoform is different. For example, *AKT2* is known to be an important factor in insulin signalling (Cho et al., 2001a) and *AKT1* is involved in anti-apoptotic signalling and promotes cell survival (Dummler et al., 2006, Chen et al., 2001). The function of *AKT3* is less well characterised, however, mice lacking the protein develop smaller brains, suggesting that it is involved in neural development (Easton et al., 2005).

**Table 5.1 *Homo sapien AKT1, AKT2* and *AKT3* identifiers**

| Gene Name | Accession number | Location |
|---|---|---|
| **AKT1** (AKT serine/threonine kinase 1) | Ensembl: ENSG00000142208 | Chromosome 14: 104.769.349-104.795.751 |
| **AKT2** (AKT serine/threonine kinase 2) | Ensembl: ENSG00000105221 | Chromosome 19: 40.230.317-40.285.536 |
| **AKT3** (AKT serine/threonine kinase 3) | Ensembl: ENSG00000117020 | Chromosome 1: 243.488.233-243.851.079 |

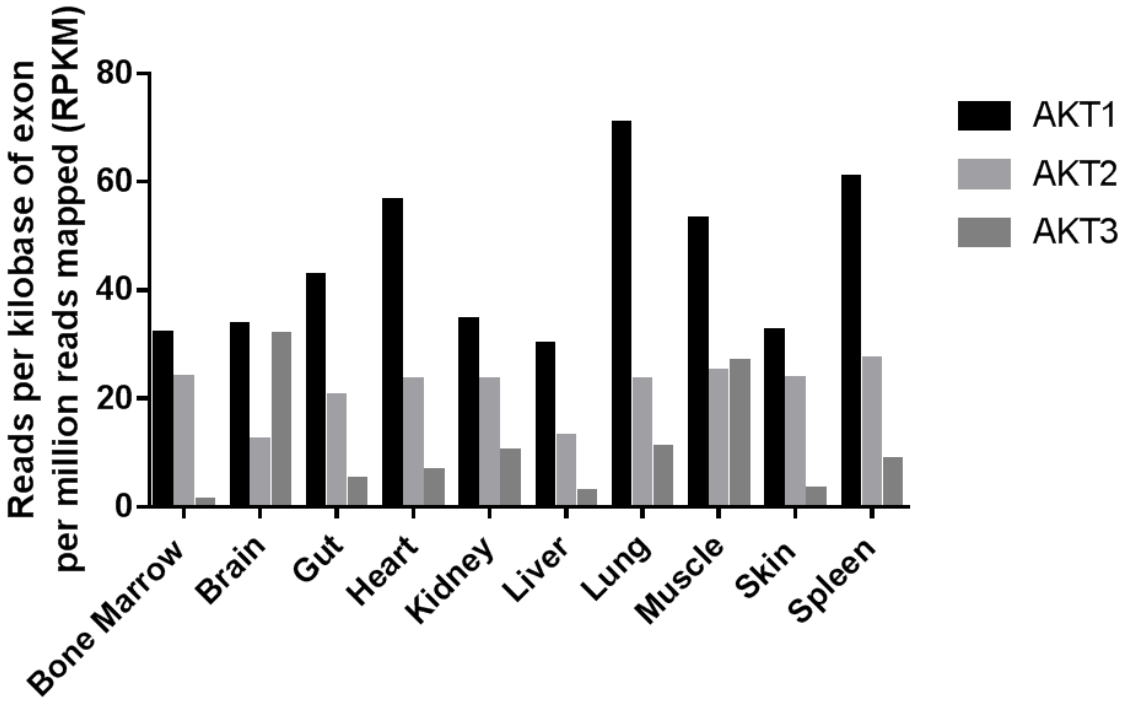


**Figure 5.1 Relative expression of AKT1, AKT2 and AKT3 mRNA in human tissues.** [Adapted from The Human Protein Atlas (http://www.proteinatlas.org)]

## 5.2 Avian isoforms of AKT

There is little known about the avian AKT genes with only two of the three predicted isoforms mapped in the chicken genome. In this chapter the avian AKT isoforms are discussed, the tissue distribution determined and expression in the context of IBV infection investigated.

### 5.2.1 Location of AKT genes

A search of the *Gallus gallus* genome revealed that only chicken *AKT1* (*chAKT1*) and chicken *AKT3* (*chAKT3)* had been identified and mapped (Table 5.2). *chAKT1* is present on chromosome 5 and *chAKT3* on chromosome 3 of the chicken genome. The third isoform remains unmapped on the chicken genome.

### 5.2.2 The search for chAKT2

Initially, a search of the chicken genome (Galgal4) resulted in the identification of a partial cds of the *Gallus gallus* protein serine/threonine kinase (*AKT2*) mRNA (gi|5853304|gb|AF181260.1). A BLAT nucleotide search of the chicken genome, using the partial *chAKT2* sequence, indicated that the gene had not been mapped in the genome. Two partial cds were highlighted with high identity to the original sequence. One sequence was within *chAKT1* on chromosome 5 with 85% identity. The second was located on a scaffold (AADN03011991.1:177-301) with 99.2% identity. One of the closely related species to have a fully sequenced genome is the Duck. A search of the BGI_duck_1.0 genome resulted in the identification of all three AKT genes. The duck *AKT2* gene was found to be positioned on a scaffold that had not been mapped to a chromosome, therefore it could not be used to check for synteny between the species. A BLAT nucleotide search using the duck *AKT2* sequence (ENSAPLG00000016235) was performed on the chicken genome. Two scaffolds were identified with high identity to the duck *AKT2* sequence. One of the scaffolds had been identified previously, AADN03011991.1:175-301.

**Table 5.2 *Gallus gallus* *AKT1* and *AKT3* identifiers**

| Gene Name | Accession number | Location |
|---|---|---|
| **AKT1** v-akt murine thymoma viral oncogene homolog 1 [ **Gallus gallus** (chicken) ] | Ensembl: ENSGALG00000011620 | Chromosome 5 - NC_006092.3 |
| **AKT3** v-akt murine thymoma viral oncogene homolog 3 [ **Gallus gallus** (chicken) ] | Ensembl: **ENSGALG00000010709** | Chromosome 3 - NC_006090.3 |

The other, AADN03013585.1:434-570 was found to have 88.32% identity to the duck sequence. This suggests that the gene exists in the chicken genome, and has been sequenced over several scaffolds. Unfortunately, these scaffolds have not been mapped to chromosomes as yet. An attempt to align the scaffolds and look for any overlap in the sequence was unsuccessful.

## 5.3 Method development

The expression of both *chAKT* isoforms was measured in a panel of tissues from uninfected and IBV infected chickens by quantitative real-time PCR (qPCR).

The qPCR assay is widely used in many research contexts. Diagnostic techniques often rely on efficient, specific and reliable qPCR assays that are normalised to the expression of stable reference genes. Other studies that investigate differential expression of genes across experimental conditions, such as viral infection, also require normalisation. In these cases, it is important that target gene expression is normalised to reference genes that are known to be stable across the experimental conditions. The MIQE (Minimum Information for Publication of Quantitative Real-Time PCR Experiments) guidelines published in 2009 (Bustin et al., 2009) provide a comprehensive list of requirements for the publication of qPCR research. In addition to discussion of publication requirements and nomenclature, it also discusses the selection of stable reference genes. The guidelines describe how reference genes, that are known to be stably expressed across all experimental conditions, should be initially selected. The primer/probe sets for the reference genes should be designed to amplify efficiently and not amplify DNA. The stability of the reference genes should then be assessed by use of algorithms such as geNorm (Vandesompele J., 2002), BestKeeper (Pfaffl et al., 2004) or NormFinder (Andersen et al., 2004).

Initially, to identify a panel of stable genes, an assortment of candidate reference genes were selected, primer/probe sets designed and stability assessed in a variety of experimental conditions. The oligonucleotide sequences were designed, tested

and optimised in collaboration with Karen Staines and William Mwangi and published (Staines et al., 2016). The effect of inappropriate normalisation on the analysis of qPCR assays has been investigated using IBV infection as a model and published (Appendix 4) (Batra et al., 2016).

The schematic in Figure 5.2 describes the process by which reference genes can be selected, designed and included in an experimental set up. Genes that are expected to be stable across all experimental conditions are selected. Primers are designed and tested to ensure that they amplify efficiently and do not amplify genomic DNA. The qPCR can then be run using SYBR Green, or hydrolysis probes can be designed. It is recommended that each gene is tested on all samples, however in some cases a cross-representative subset is sufficient. The individual Cq (quantification cycle) values from each candidate reference gene can then be analysed using the geNorm, NormFinder or BestKeeper algorithm. This allows identification of the most stable reference genes for the experimental samples tested. The stable genes may subsequently be run alongside the target genes and used for normalisation. Also included is a description of experimental sample processing which aims to ensure minimal contamination of DNA.

### 5.3.1 Selection of reference gene panel

Initially a panel of candidate reference genes were selected based on a review of literature relating to mammalian and avian qPCR studies. All of the genes selected are known to be highly conserved in mammalian species and have orthologs in avian species. A description of the genes and the function of the encoded proteins is presented in Table 5.3.

Table 5.3 Reference gene panel selected for this study

| Gene | Protein description[1] | Accession number[2] |
|---|---|---|
| **ACTB** (β-Actin) | Involved in cell motility, structure and integrity | NM_205518 |
| **GAPDH** (Glyceraldehyde 3-phosphate dehydrogenase) | Plays a role in glycolysis and activity in the nucleus. | NM_204305 |
| **HMBS** (Hydroxymethlybilane Synthase) | Hydroxymethylbilane synthase – enzyme involved in the production of heme | XM_417846 |
| **HPRT1** (Hypoxanthine phosphoribosyltransferase 1) | Plays a central role in the purine salvage pathway | NM_204848 |
| **PGK1** (Phosphoglycerate Kinase 1) | Glycolytic enzyme | NM_204985 |
| **28s rRNA** (28s ribosomal RNA) | Ribosomal RNA | JN639848.1 |
| **RPL13** (Ribosomal Protein L13) | Ribosomal protein | NM_204999 |
| **RPLP0** (Ribosomal Protein, Large, P0) | Ribsomal protein, functional equivalent of E.coli protein L10 | NM_204987 |
| **TBP** (TATA Box Binding Protein) | Transcription factor that forms part of the DNA-binding multiprotein factor TFIID | NM_205103 |

[1]Protein information obtained from GeneCard Human Gene Database
[2]NCBI accession numbers

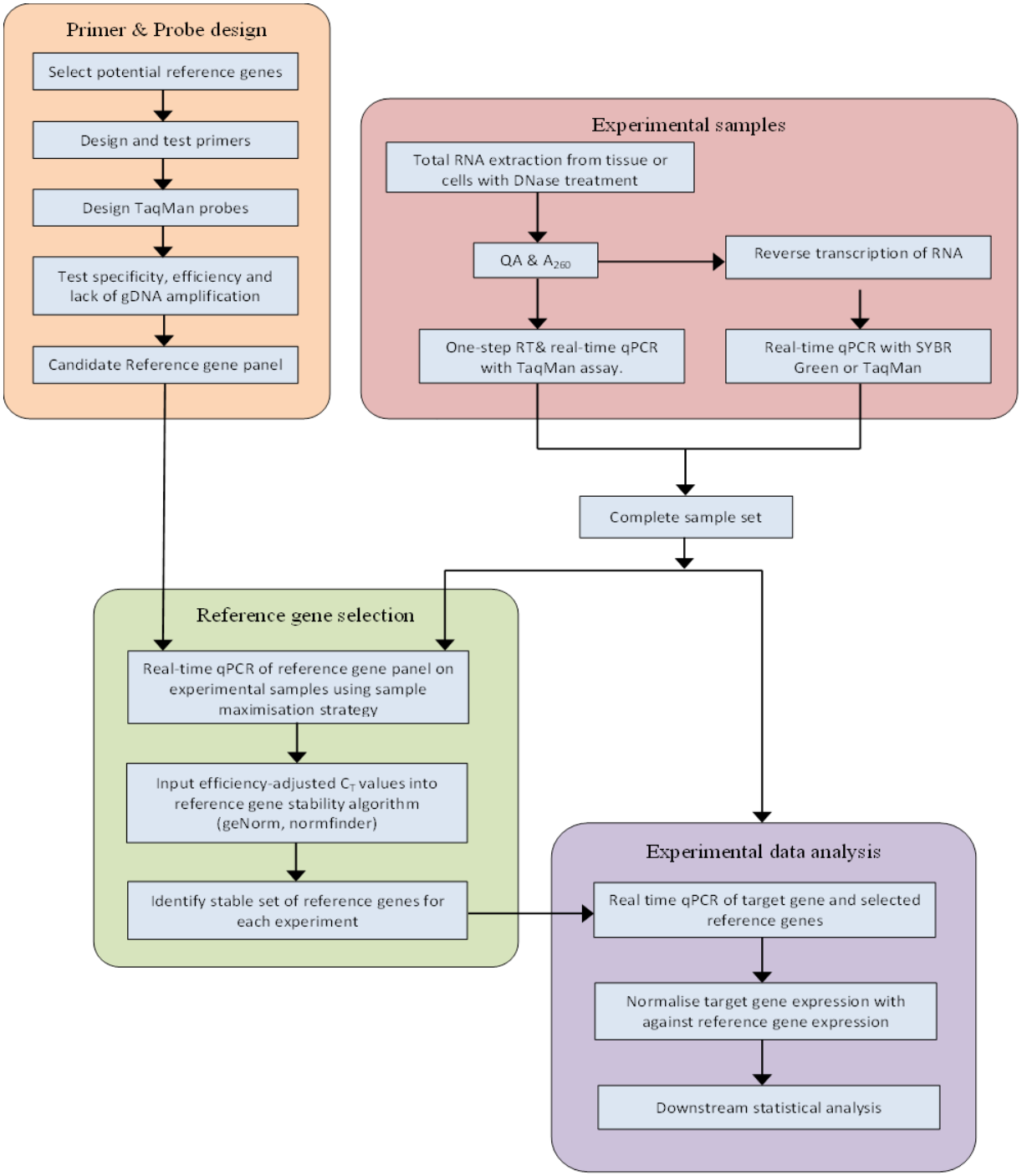


**Figure 5.2 Flow chart of reference gene design and selection.** Primer and probe sets for each gene were designed and tested before use as reference genes. The stability of reference genes is then measured using algorithms such as geNorm and Normfinder. The optimal number of reference genes is determined and reference genes for that assay are identified. Appropriate processing of experimental samples is important to ensure minimal contamination of DNA and efficient amplification.

## 5.3.2 Design of primer/probe sets for panel of reference genes

The design of efficient and specific primer/probe sets for reference genes is important to ensure accurate normalisation of data. Several requirements for primer/probe design have been identified (Rodriguez et al., 2015) (Table 5.4). The guanine (G) and cytosine (C) content of both primer and hydrolysis probes must be between 30 – 80% with more G than C bases in the probes. The $T_m$ of the primers should be between 55 – 60 °C and should not differ by more than 2 °C between the two. If the $T_m$ of the forward and reverse primers differ by more than 2 °C hairpins may form. The probes should have a $T_m$ of between 60 -70 °C and should be between 8 – 10 °C higher than that of the primer. Additionally, the primer and probes should both be between 15 – 30 base pairs (bp) in length and the products between 50 – 150 bp. To ensure stability, the last 5 bp of the primers should not contain more than two G or C bases and there should be a maximum of 3 runs of identical nucleotides, none of which should be Gs. The primers and probes were designed to amplify over an intron, with either one of the primers or the probe sequence spanning an intron. This ensured no amplification of gDNA.

Primer and probe sets were designed for this study ensuring that the above requirements were taken into consideration. However, it was not always possible to fulfil the requirements due to the high GC content of avian genes. Initial selection of primer pairs was undertaken using GenScript (https://www.genscript.com/ssl-bin/app/primer) which allowed identification of a number of candidate oligonucleotide sequences. GenScript was preferred for initial assessment, as it provided a selection of oligo sequences at various positions across the gene. Candidates that spanned introns were selected for further optimisation. Primer Express (Applied Biosystems, Foster City, California, USA) was then used to choose the most appropriate oligonucleotide pairs from the candidates identified by GenScript as it allowed more stringent design and the implementation of more detailed criteria.

Table 5.4 Design of qRT-PCR primer and probes (adapted from Rodriguez et al. (2015))

| Requisites | Primers | Probes |
|---|---|---|
| GC content | 30–80% | |
| Calculated $T_m$ | 55-60 °C<br>($T_m$ of primers should not differ >2 °C) | 68-70 °C<br>(8-10°C above $T_m$ primer) |
| Runs of identical nucleotides | Maximum 3 runs (No G bases) | |
| Primer/probe length | 15-30bp | |
| PCR product length | 50 – 150 bp (optimum <80 bp) | |
| 3' instability | Maximum two G or C in the last 5 bp | - |
| GC ratio | - | C>G |
| Position in gene | Either primer or probe must span intron | |

Table 5.5 Primer and probe sequences for candidate reference genes

| Gene | | Sequence | Accession Number |
|---|---|---|---|
| *ACTB* | Forward | 5'-CAGGTCATCACCATTGGCAAT-3' | NM_205518 |
| | Reverse | 5'-GCATACAGATCCTTACGGATATCCA-3' | |
| | Probe | 5′ -(FAM)-CACAGGACTCCATACCCAAGAAAGATGGC-(TAMRA)-3′ | |
| *HMBS* | Forward | 5'-GGTTGAGATGCTCCGTGAGTTT-3' | XM_417846 |
| | Reverse | 5'-GGCTCTTCTCCCCAATCTTAGAA-3' | |
| | Probe | 5'-(FAM)-CCTGACCTCTGCTTTGAGATTGTTGCCA-(TAMRA)-3' | |
| *HPRT1* | Forward | 5'-TGGTCAAAAGAACTCCTCGAAGT-3' | NM_204848 |
| | Reverse | 5'-TGTAATCGAGGGCGTATCCAA-3' | |
| *PGK1* | Forward | 5'-GTTTATGTCAATGATGCTTTTGGAA-3' | NM_204985 |
| | Reverse | 5'-GCCTTTGCAAAATAATCCAGTTCT-3' | |
| *RPL13* | Forward | 5'-TCGTGCTGGCAGAGGATTC-3' | NM_204999 |
| | Reverse | 5'-TCGTCCGAGCAAACCTTTTG-3' | |
| | Probe | 5'-(FAM)-TAATGCCCGCCAGTTTAAGCTCTTCTAGGC-(TAMRA)-3' | |
| *RPLP0* | Forward | 5'-TTGTTCATCACCACAAAGATT-3' | NM_204987 |
| | Reverse | 5'-CCCACTTTGTCTCCGGTCTTAA-3' | |
| *TBP* | Forward | 5'-CTTCGTGCCCGAAATGCT-3' | NM_205103 |
| | Reverse | 5'-GCGCAGTAGTACGTGGTTCTCTT-3' | |
| *28s rRNA* | Forward | 5′-GGCGAAGCCAGACCAAACT-3′ | X59733 |
| | Reverse | 5′-GACGACCGATTTGCACGTC-3′ | |
| | Probe | 5′-(FAM)-AGGACCGCTACGGACCTCCACCA-(TAMRA)-3′ | |
| *GAPDH* | Forward | 5′-GGTGGTGCTAAGCGTGTTA-3′ | X01578 |
| | Reverse | 5′-CCCTCCACAATGCCAA-3′ | |

The selected primer pairs were tested experimentally by end-point PCR and agarose gel electrophoresis with RNA and DNA templates by Karen Staines (Staines et al., 2016). Only the primer pairs that produced a single product band of the expected size from the RNA template were chosen.

### 5.3.3 Experimental testing of primer sets

The primer sets in Table 5.5 were selected as they had produced only one band on an agarose gel from end-point PCR, and fulfilled the requirements for proper design as far as possible. In order to further confirm that the primers would efficiently amplify the respective genes, a SYBR Green qPCR was performed for each set. In all assays, the primer sets amplified cDNA at least 10 cycles below the no-reverse transcriptase (no-RT) and no template control (NTC) (Figure 5.3A). A dissociation stage was included and melt curves produced for each set of primers (Figure 5.3B). Only the amplification and melt curves for *ACTB* are shown as a representative sample. Each melt curve showed a single peak suggesting the amplification of only one product.

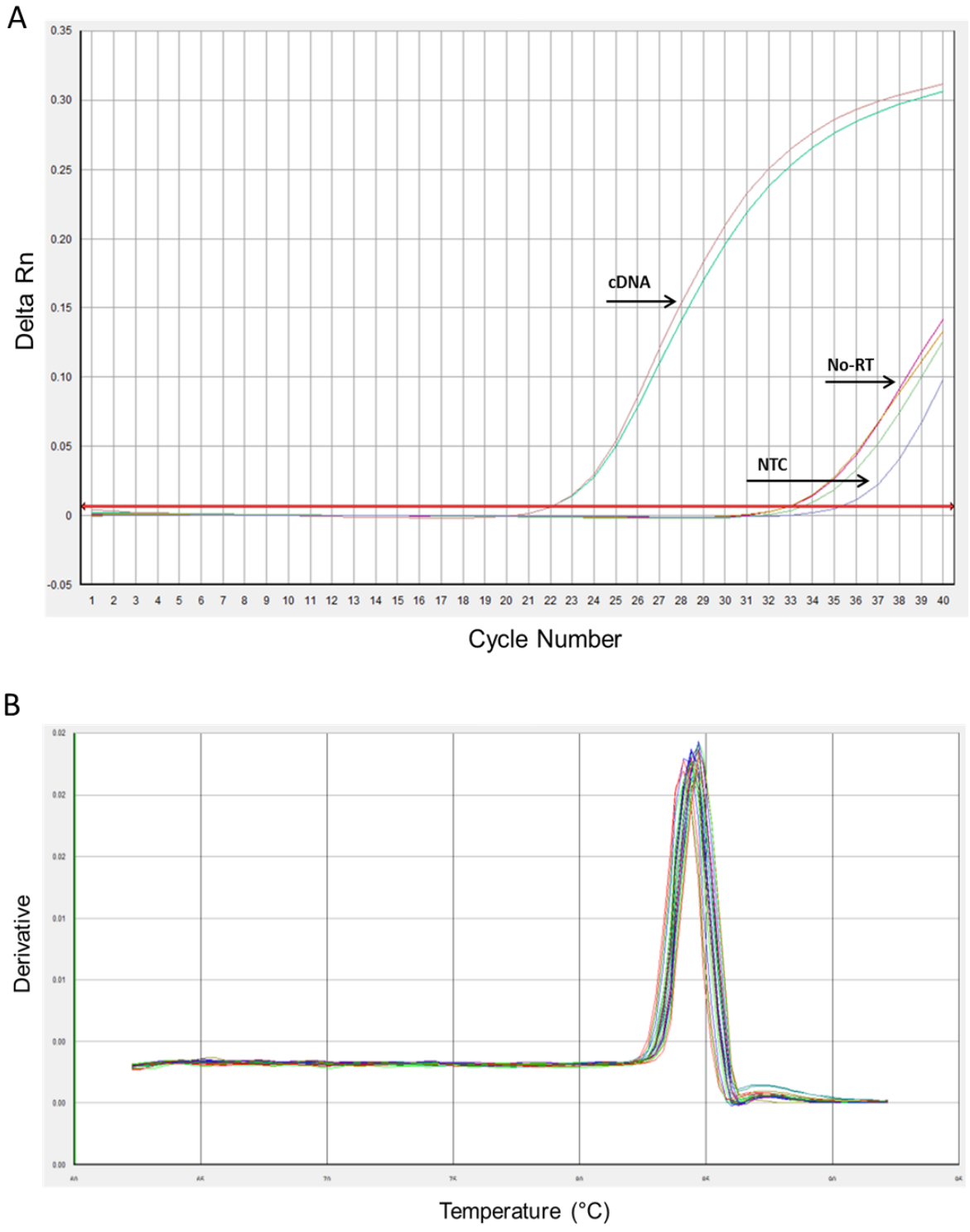


**Figure 5.3 qPCR data from reference gene amplification in chicken tissue.** RNA was extracted from chicken tissues and reverse transcribed with random primers. Quantitative PCR was performed using *ACTB* primers on cDNA, no-RT and NTC. (A) Amplification plots with amplification curves for cDNA, no-RT and NTC are shown. (B) A dissociation stage was run and the dissociation curves shown.

## 5.4 Differential expression of *chAKT1* and *chAKT3* in avian tissues

Using the gene sequences available for *chAKT1* and *chAKT3*, primer and probes were designed for expression analysis. The primer and probe sets were designed by PrimerDesign Ltd (Methods section 2.1.3). Using the panel of reference genes designed and tested in section 5.3.1 (Table 5.5), expression of *chAKT1* and *chAKT3* was normalised to optimised stable reference genes.

Tissues were collected from 2 week old Rhode Island Red birds, lysed and RNA collected by TRIzol® extraction and subsequently purified on a Qiagen RNeasy column (Methods section 2.5.2). The tissues collected are listed below.

Blood
Brain
Cecal Tonsil
Heart
Liver
Bone Marrow
Bursa
Gut
Kidney
Lung
Thymus
Muscle
Trachea
Skin

Several of the tissues collected were specific to birds. For example, the bursa of fabricius is a highly specialised lymphoid organ that is the site of hematopoiesis (Ratcliffe, 2006).

To investigate the effects of viral infection on AKT expression, tissues that are known to be involved in viral replication or the host response were also selected. The avian cecal tonsils are also lymphoid organs that elicit protective immune responses against pathogens in the intestinal tract (Heidari et al., 2014). The trachea was selected as it is the primary site of replication for many avian viral

respiratory diseases, including IBV. The M41 strain of IBV is also known to infect the kidneys and cause nephropathogenisis.

The stability of six candidate reference genes across the tissue panel was assessed by geNorm. *TBP*, *PLA2*, *RPLPO*, *RPL13*, *HMBS* and *ACTB* were chosen as a reference panel based on previous assays run by Staines et al, 2016. The qPCR was run using SYBR Green and employing the sample maximisation run layout that negates the need for inter-run calibration. The sample maximisation run layout involves analysing amplification of one gene across all samples on one plate. It is therefore not necessary to run the reference genes on the same plate as the target gene. This is useful when the number of samples does not allow every gene to be analysed on a single plate. The Cq values for each run were imported into the qbase+ [Biogazelle] software for geNorm analysis (Figure 5.4). The y-axis indicates the geNorm M value for each reference gene. The M value is a measure of the stability of the reference genes where, the lower the M value the more stable the genes. *PLA2*, with the lowest M value, represents the most stable gene across the samples. The next gene, *TBP* is the gene that produces the least change in the stability of the reaction. In this way the genes are ranked from least to most stable as, *ACTB*, *HMBS*, *RPL13*, *RPLP0*, *TBP* and *PLA2*. The geNorm algorithm also recommends a suitable number of reference genes to use. In this case the software recommended the use of the first three most stable genes, *PLA2*, *TBP* and *RPLP0*.

The expression profiles of *chAKT1* and *chAKT3* were therefore assessed in the panel of chicken tissues and normalised to *PLA2*, *TBP* and *RPLP0* expression (Figure 5.5).

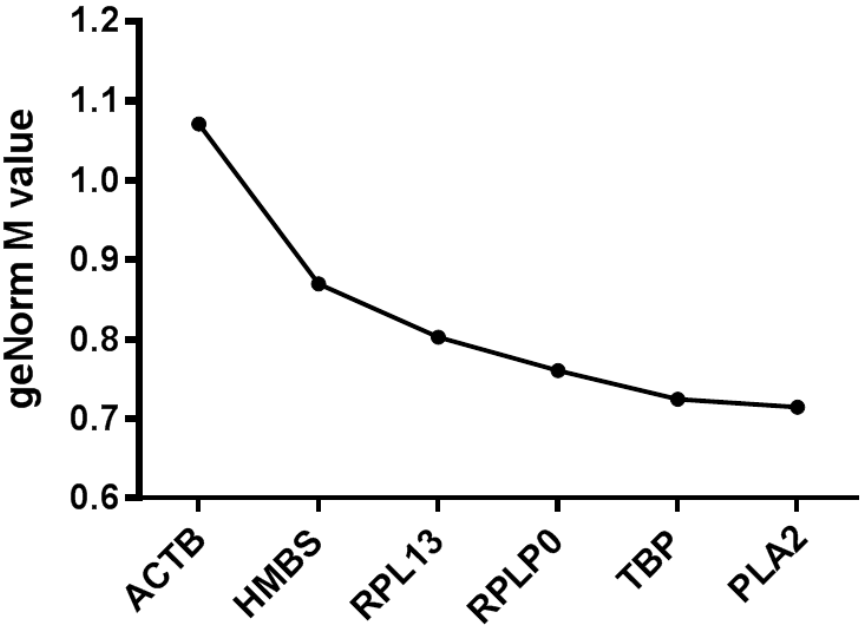


**5.4 GeNorm analysis of candidate reference genes.** Candidate reference genes were amplified in a panel of tissues collected from a three two week old Rhode Island Red chickens. Cq values were imported into qbase+ software for geNorm analysis. Left axis (blue) indicated the geNorm M values for each gene, representing the stability of the gene across the tissue panel.

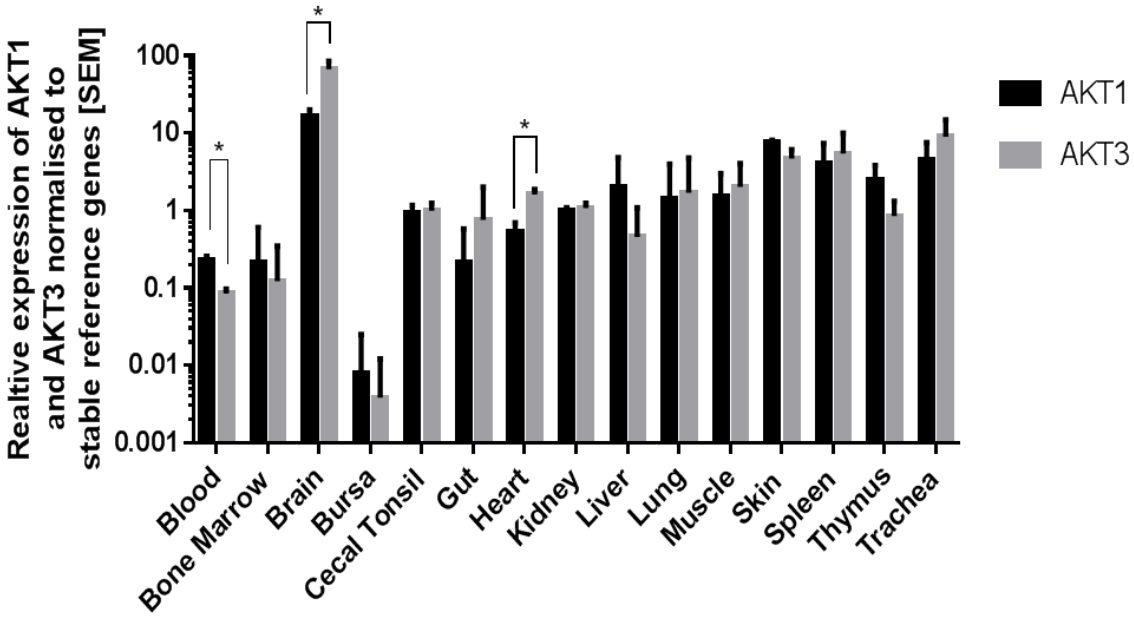


**5.5 Expression of AKT1 and AKT3 in a panel of chicken tissues.** The expression of AKT1 and AKT3 in tissues from 2 week old Rhode Island Red birds. Cq values were normalised to those of stable reference genes, PLA2, TBP, RPLP0 and RPL13. Average of 3 biological replicates ($p<0.05$).

TaqMan qPCR assays were run for *chAKT1*, *chAKT3*, *PLA2*, *TBP* and *RPLP0*. The Cq values for each gene were analysed using the qbase+ software and the relative expression of each gene across the tissue panel was determined (Figure 5.5). The expression of *chAKT1* and *chAKT3* was consistent in most tissues. However, expression of both genes was lower in the bursa than the other tissues. Expression of *chAKT3* was significantly higher in the brain at 66.60 Rq (relative quantities) compared to 16.70 Rq of *chAKT1*. Chicken *AKT3* expression was also significantly higher in the heart (1.61 Rq in *chAKT3* expression compared to 0.54 Rq for *chAKT1*). In contrast, expression of *chAKT3* in the blood is significantly lower than that of *chAKT1*.

## 5.5 Differential expression of *chAKT1* & *chAKT3* in tissues during infection with IBV

Infection of avian cells with IBV has been found to induce activation of the AKT protein (Chapter 3). It is not known however whether AKT activity is also modulated by gene expression. Therefore, the expression of *chAKT1* and *chAKT3* was measured in tissues collected from IBV infected birds.

Eight-day old Rhode Island Red SPF birds were mock infected or infected with the M41 strain of IBV. At day 4, 6 and 7 post infection, tissues were collected and stored in RNAlater. The tissues were collected as part of an IBV challenge experiment and the type of tissue available for analysis was limited. RNA from samples of spleen, brain, kidney, lung and trachea was TRIzol extracted and subsequently purified on an RNeasy column. The RNA was then reverse transcribed into cDNA for the qPCR analysis.

Initially, the level of IBV infection in each tissue, at all time-points, was assessed by qPCR. The number of copies of IBV genome was measured using primers that amplified the 5′ UTR of the genome (Figure 5.6).

Copy number was calculated from a standard curve and normalised to mock levels. Genome copy number was calculated as an indication of the presence of IBV virions within the tissue. Copies of viral genome were found in all tissues except the brain. Levels of IBV genome were significantly higher in the trachea at day 4 compared to other tissues, but decreased at day 6 and 7. Genome copy number increased in several birds at day 6 in the kidney however levels then dropped by day 7 post infection.

The level of IBV infection was also investigated by qPCR using primers specific to the N-message region of the genome (Figure 5.7). This assay allowed the identification of replicating virus within the tissues, as viral mRNA is synthesised during active viral replication. Copy number was again inferred from a standard curve and normalised to mock levels. High levels of replicating virus was present in the trachea at day 4 which then decreased at day 6 and day 7. At day 6 several of the birds had more copies of viral mRNA in the kidney and lung than at day 4. By day 7 however, levels of replicating virus in the tissues decreased, suggesting that the virus was being cleared in those birds by day 7. Although replication virus levels were higher in the brain and spleen at day 4, and day 7, the copy number was extremely low and not thought to be biologically relevant.

The stability of candidate reference genes in the mock infected and infected tissues was established by geNorm analysis (Figure 5.8). Reference genes were amplified in each tissues sample across each time point. The Cq values were imported into qbase+ and the stability of the reference genes ranked by geNorm M value. The reference genes were ranked from least to most stable as *PLA2, ACTB, TBP, HMBS*, *RPL13* and *RPLP0*. The geNorm algorithm was again not able to recommend a suitable number of reference genes for this assay, therefore the three most stable reference genes, *RPLP0*, *RPL13* and *HMBS* were used to normalise gene expression levels.

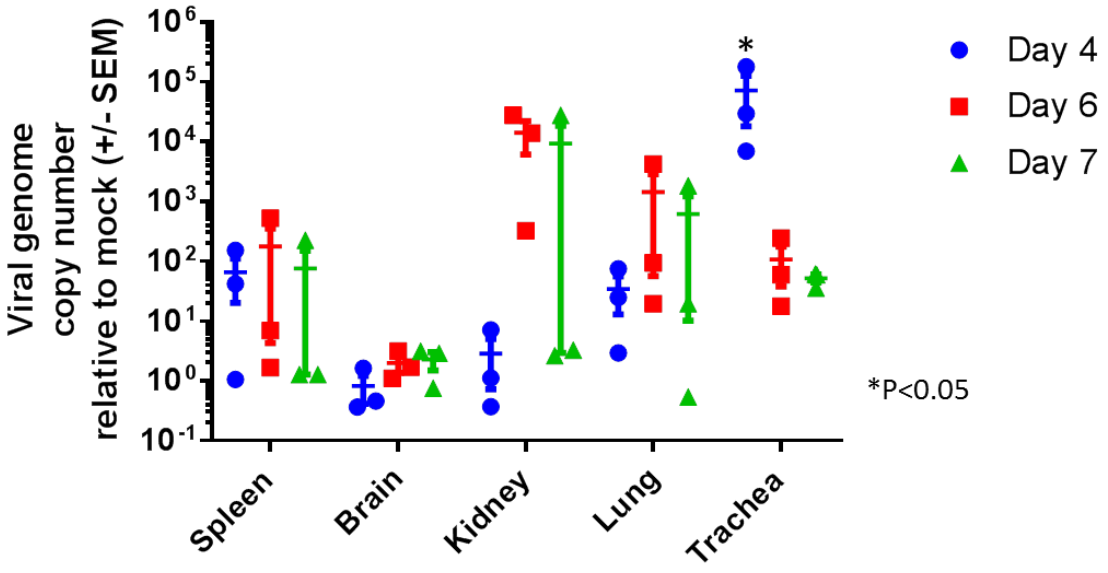


**5.6 Expression of viral genome in the tissues of birds infected with IBV.** Tissue samples from three birds infected with M41 were collected at 4, 6 and 7 days post infection. The RNA was extracted and reverse transcribed. The 5' UTR of the IBV genome was amplified and copy number was calculated from a standard curve and values normalised to mock levels.

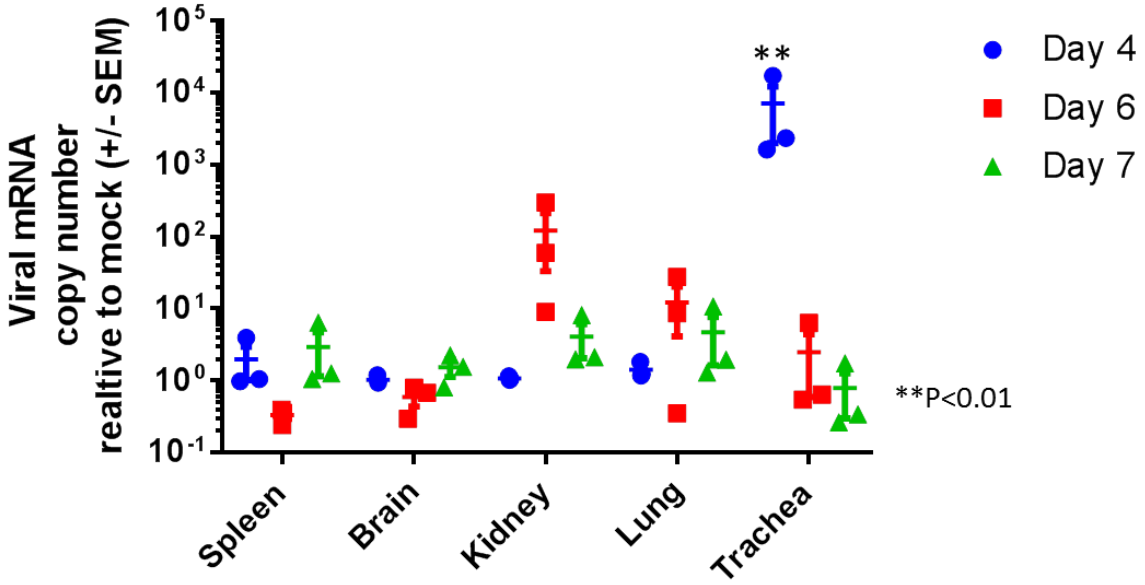


**5.7 Expression of viral N-message mRNA in the tissues of birds infected with IBV.** Tissue samples from three birds infected with M41 were collected at 4, 6 and 7 days post infection. The RNA was extracted and reverse transcribed. The 5' UTR of the IBV genome was amplified and copy number was calculated from a standard curve and values normalised to mock levels.

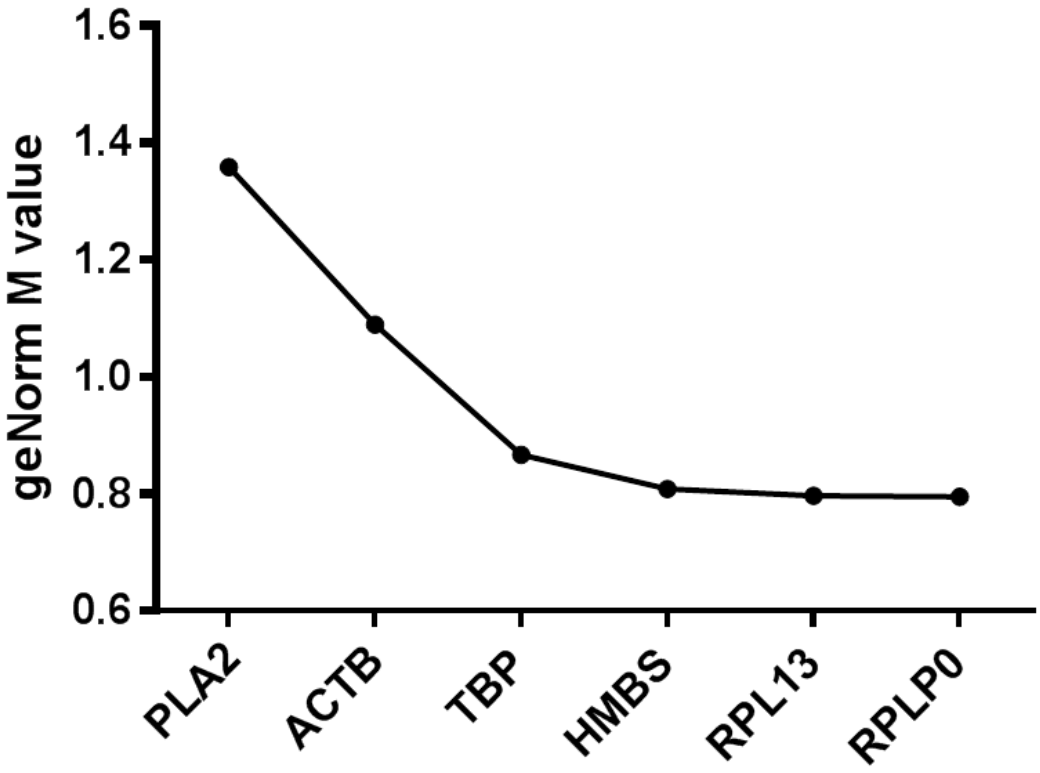


**5.8 GeNorm analysis of candidate reference genes in IBV infected tissues.** Candidate reference genes were amplified in a panel of tissues collected from 10 day old mock infected or IBV infected birds. Cq values were imported into qbase+ software for geNorm analysis. GeNorm M values represent the stability of each gene across the tissue panel.

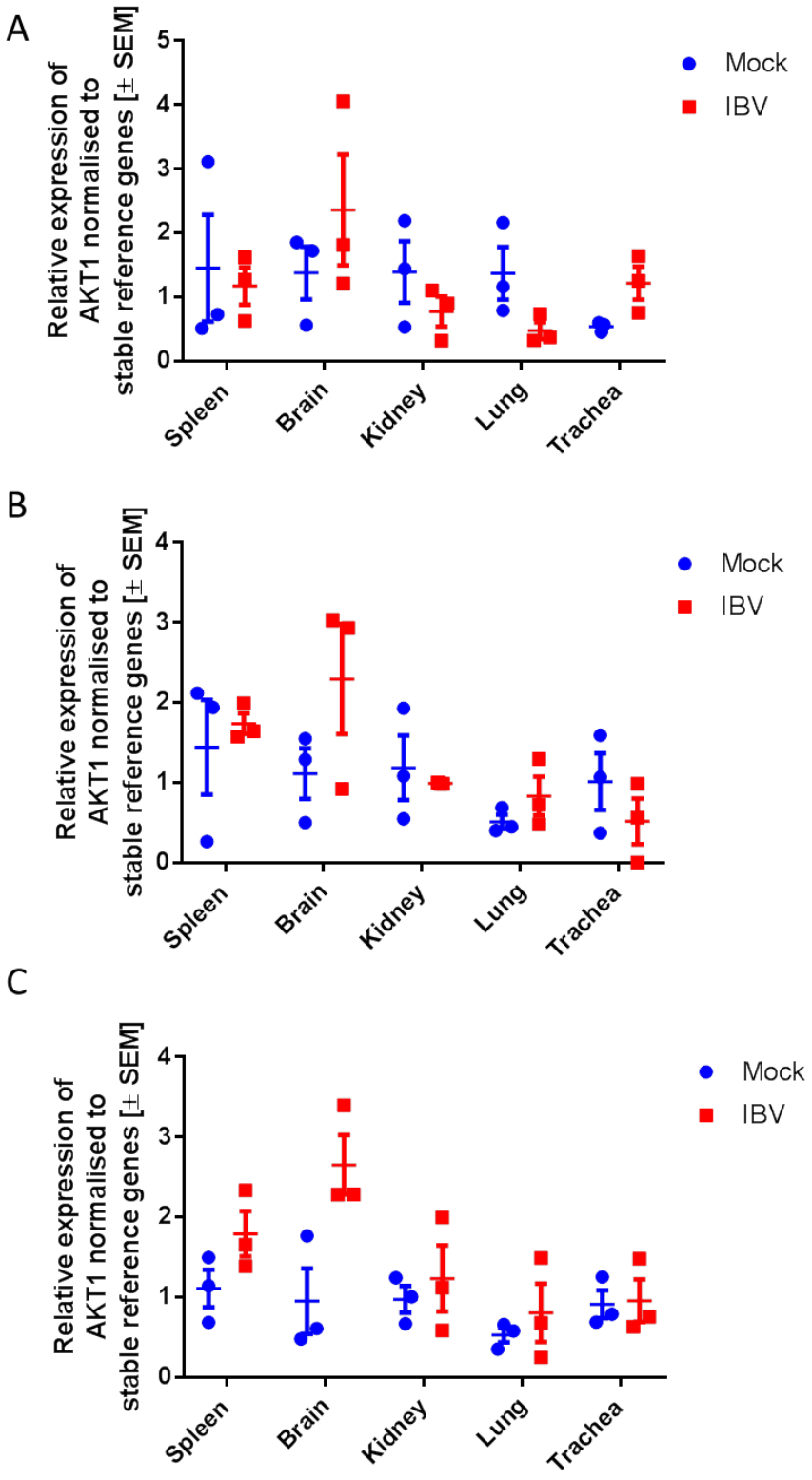


**5.9 Expression of AKT1 in the tissues of birds infected with IBV.** Tissue samples from three birds mock infected or infected with M41 were collected at (A) 4, (B) 6 and (C) 7 days post infection. The RNA was extracted and reverse transcribed. AKT1 expression was normalised to expression of stable reference genes chosen by geNorm.

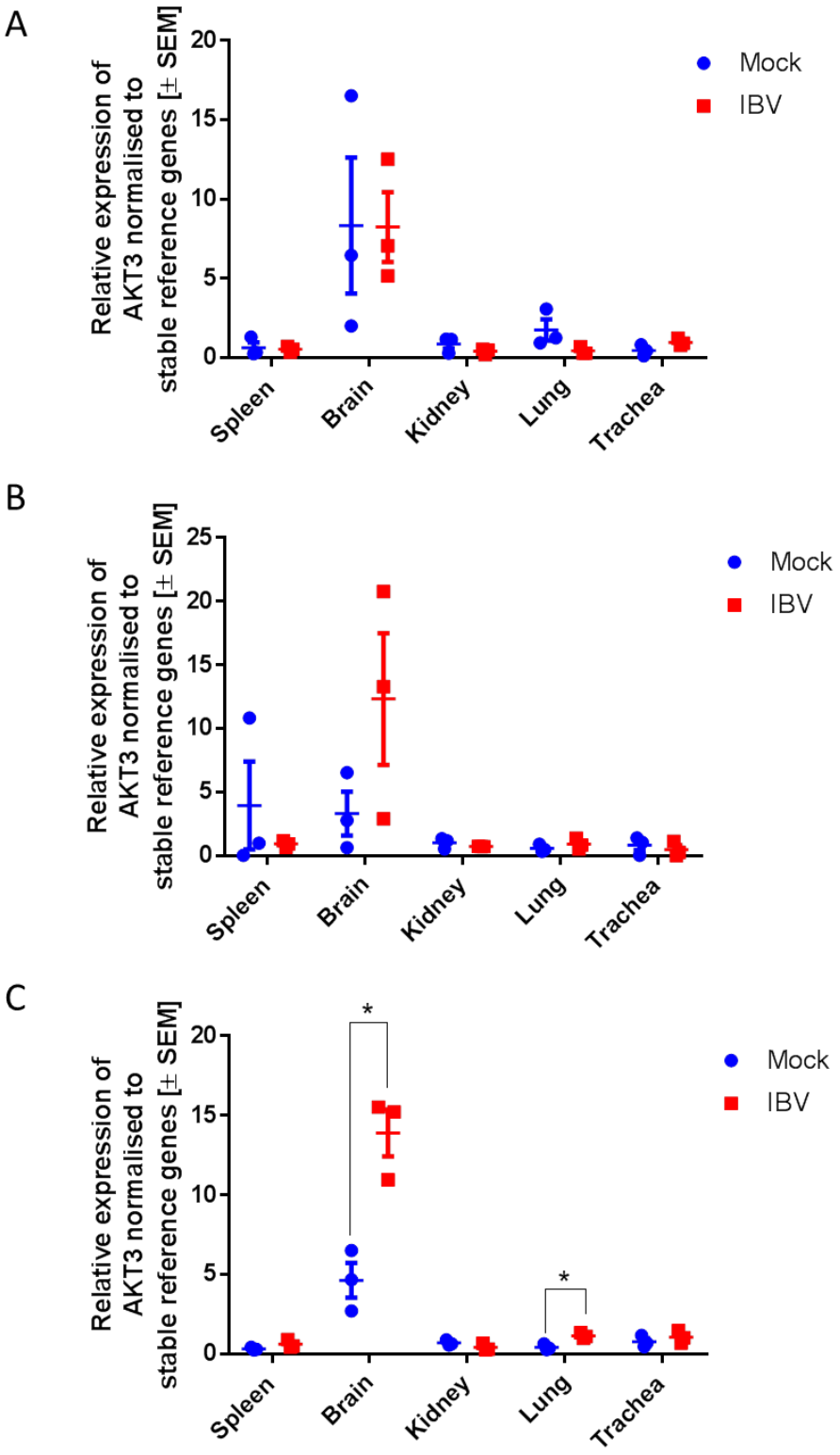


**5.10 Expression of AKT3 in the tissues of birds infected with IBV.** Tissue samples from three birds mock infected or infected with M41 were collected at (A) 4, (B) 6 and (C) 7 days post infection. The RNA was extracted and reverse transcribed. AKT3 expression was normalised to expression of stable reference genes chosen by geNorm. * $p<0.05$ calculated by t-test

The expression of *chAKT1* and *chAKT3* were then measured in the tissues collected from mock infected and IBV infected birds at day 4, 6 and 7 post infection. The analysis of relative expression was performed using the qbase+ software. Levels of *chAKT1* expression were normalised to expression of stable reference genes chosen by geNorm (Figure 5.9). There was no significant change in the expression of *chAKT1* in any of the tissues at any day post infection between mock and infected tissues. However, there were large amounts of variation between birds, with several birds having high levels of expression in the spleen, brain and kidney compared to others.

The expression of *chAKT3* was normalised to levels of reference gene expression (Figure 5.10). Relative to *chAKT1*, expression of *chAKT3* was lower in all samples except the brain. Expression of *chAKT3* was significantly higher in the brain of IBV infected birds at day 7 compared to mock infected birds. Levels of *chAKT3* expression was also found to be statistically higher in the lung at day 7 in infected birds, however this was not expected to be biologically relevant.

## 5.6 Discussion

The design of primers and probes is one of the most important factors that affect the quality of qPCR experiments. In this chapter requirements for the design of primers and probes for qPCR studies are presented that have been established in mammalian systems (Table 5.4). Included in the requirements is the GC content of the primer and probes. It is suggested that both primer and probes should contain between 30-80% GC content. The high GC content of the avian genes often means that it is difficult to find areas of the target sequence that are not GC rich. GC rich sequences result in a reduction in amplification efficiency as they do not denature easily.

The GC content of the sequences will also have a direct effect on the melting temperature of the primers and probe (Rodriguez et al., 2015, Mitsuhashi, 1996b, Mitsuhashi, 1996a).

The GC content was often more than 80% of the selected region of the target gene. As other constraints, such as the need for a long intron and missing sequence had to be accommodated, not all of the requirements for design were achieved. For example, some primers contained more than two GC bases at the 3' end. Priority was initially given to the design of primer and probes that would not amplify gDNA. Sequences identified using GenScript that spanned introns were selected and subsequently modified using Primer Express. It would be useful to re-evaluate and re-design a list of prerequisites for the design of avian primer/probes. These requirements could take into account the GC rich avian genes and establish a set of guidelines by which avian primer and probe sequences could be designed. These may be less stringent than the mammalian requirements and focus more on preventing the formation of secondary and tertiary structures, such as the tetra-plex structures formed from poly-C and G regions.

Whilst the *Gallus gallus* genome has been fully sequenced, there remain many gaps where certain areas of the genome have not been mapped. From the available data, it seems likely that the *chAKT2* gene resides within one of these gaps. Partial sequences of the gene appear to be spread across multiple scaffolds, including AADN03011991.1:175-301. However, the scaffolds do not align. Analysis of RNA sequencing data also suggests that the *chAKT1* gene has been mis-annotated and is missing an exon (Paolo Ribeca, The Pirbright Institute, unpublished). It is expected that this will be rectified in the next annotation/assembly update.

The stability of reference genes across the tissue panels was assessed using the geNorm algorithm (Vandesompele J., 2002). Other algorithms such as Normfinder are available, however our previous study has shown that both algorithms provide

similar results (Staines et al., 2016). The geNorm analysis of reference genes was performed using candidate sequences previously designed in Staines et al. (2016). In the current study, the algorithm was unable to select a suitable number of reference genes based on the calculated geNorm V values for the IBV infected sample set. This is potentially a result of small amounts of variation in the expression of the reference genes between the samples. Vandesompele J. (2002) suggest the use of the three most stable reference genes in situations where the optimal number could not be calculated.

The expression of *chAKT1* and *chAKT3* mRNA across a panel of avian tissues was examined (Figure 5.5). In human tissues, *AKT1* was the most abundant isotype and was expressed at higher levels in all tissues than *AKT2* and *AKT3*. The same was not found for *chAKT1,* where levels of expression were not significantly different to *chAKT3* in the majority of tissues. The similar expression levels of both *chAKT1* and *chAKT3* in the avian tissues suggests alternative roles for *chAKT3* compared to those of human *AKT3*. However, it is also possible that human *AKT3* is turned over faster than *chAKT3*. Like human *AKT3*, *chAKT3* was expressed at significantly higher levels in the brain (66.6 Rq) than *chAKT1* (16.7 Rq). Expression of *chAKT3* was also higher in the heart than *chAKT1*. This pattern of expression is not seen in human tissues and again suggests an alternative role for *chAKT3* that has not yet been identified. The expression of both *chAKT1* and *chAKT3* was lower in the bursa than other tissues. The bursa of fabricious is the primary site of B cell development in the chicken. Interestingly, AKT is known to be involved in the complicated B-cell development signalling cascade (Limon and Fruman, 2012). Therefore, we would expect *chAKTs* to be expressed in higher levels in the bursal tissue. However, this is not the case and warrants further investigation.

Tissues from IBV infected birds were collected at days 4, 6 and 7 post infection. The level of IBV infection in each tissue was measured by qPCR. Two qPCR assays were performed that measured genome copy number, representing the presence of virus in the tissues, and viral mRNA copy number, to represent replicating virus in the tissues. The birds were inoculated via the ocular/nasal route, and therefore one of the primary sites of infection is the trachea. At day 4 both viral genome and mRNA was found at higher levels in the trachea than any other tissue (Figure 5.6 & 5.7). Viral copy number then drops in the trachea at days 6 and 7 post infection as the infection is cleared. This is consistent with other studies that have shown the highest levels of infection between 2-5 dpi, and also noted an absence of clinical signs by day 7 post infection (Armesto et al., 2011, Hodgson et al., 2004). There are large amounts of variation in the viral infection of tissues between the different birds. However, it is interesting to note that whilst viral genome and mRNA copy number drops in the trachea it increases in other tissues at day 6 post infection in certain birds. For example, genome copy number is 4 log higher in the kidney at day 6 than at day 4 and infection is confirmed by viral mRNA copy number increasing by 2 log (Figure 5.6 and 5.7). The spleen and lung also have higher genome copy numbers at day 6 compared to day 4, however no N-message was detected. The brain, in contrast had very low copy number of both genome and viral mRNA at all days post infection.

At day 7 post infection the amount of virus present in the tissues, as measured by genome copy number, does not seem to alter from day 6. There are high levels in the kidney and lung with lower levels in the spleen, trachea, and negligible levels in the brain. Viral mRNA copy number however, representing the amount of replicating virus present, decreases by 2 log in the kidney from day 6 to day 7. This data suggests that there is an initial established infection of the trachea at day 4 post infection, by day 6 there is virus present in the kidney and lung however

replicating virus is cleared by day 7 in the kidney. No previous studies have investigated the tissue distribution of IBV during infection. The M41 strain of IBV is known to be nephropathogenic, however it is not known how the virus is transported to the kidneys (Cavanagh, 2007). The results presented here suggest that the virus is transported to other organs, such as the spleen, but is not able to establish an infection. This may be due to the specificity of the spike protein and the absence of the cellular receptor in splenocytes.

The expression of *chAKT1* in tissues collected from mock infected or IBV infected birds was measured by qPCR (Figure 5.8). Levels of *chAKT1* expression did not change significantly in any of the tissues during infection at any day post infection. However, expression of *chAKT1* was found to be higher in the brain than other tissues in the uninfected tissue panel (Figure 5.5). This was not reflected in the mock infected data in Figure 5.9 and expression of *chAKT1* in the brain of infected birds was higher in several replicates.

Levels of *chAKT3* expression in infected birds were significantly higher in the brain and lung at 7 days post infection compared to mock. Although statistically significant, the increase in *chAKT3* expression in the lung was minimal. The viral genome and mRNA copy number were very low in the lung at day 7, suggesting that the infection had been cleared. No viral infection was detected in the brain at any time point. This suggests that the increase in *chAKT3* expression was an indirect response to an overall viral infection in the bird. Expression of *chAKT3* may have been triggered as a response to stress or immune reaction stimulated by IBV infection.

Whilst every effort was taken to ensure that tissue samples were collected from the same area of the tissue, and as quickly as possible to minimise degradation,

there remains a large spread in the expression of *chAKT1* and *chAKT3* in the different birds. The levels of viral infection in the trachea of each bird also vary, likely due to phenotypic differences between the birds and efficacy of infection. The spread in the expression data of *chAKT1* and *chAKT3* suggests that there is no significant change in expression during IBV infection. However, this is not conclusive due to the natural high variation in the biological systems used.

The data from this study suggests that IBV infection does not induce modulation of *chAKT* gene expression in the tissues examined. However, IBV infection does induce an increase in *chAKT3,* and potentially *chAKT1,* expression in the brain by day 7 post infection, independently of tissue infection.

## 5.7 Summary

*chAKT2*

- Has not been mapped in the chicken genome
- Partial sequences have been identified over several scaffolds of the sequenced genomes

*chAKT1*

- Is expressed in all of the avian tissues tested
- Is expressed in blood at higher levels than chAKT3
- Expression is not significantly affected by infection of the bird or tissues with IBV

*chAKT3*

- Is expressed in all of the avian tissues tested
- Is expressed in the brain and heart at higher levels than chAKT1
- Expression is not significantly affected by tissue specific infection
- Expression is significantly higher in the brain during IBV infection of the bird, but independently of tissue infection

## 5.8 Future Work

An initial nucleotide search of the chicken genome suggested that *chAKT2* exists, however is yet to be mapped to a chromosomal location. Data from The Human Protein Atlas is invaluable for studies of not only pathogen-host interactions, but also development and cancer. There is comparatively very little known about the proteome of *Gallus gallus* which often hinders complete and efficient research. This project is a good example of where this has happened. It would be beneficial to be able to compare the expression of *chAKT2*, in addition to *chAKT1* and *chAKT3* across a panel of avian tissues.

The expression of *chAKT1* and *chAKT3* was normalised to reference genes selected by geNorm. As the optimal number of reference genes could not be calculated from the geNorm V values, the three most stable reference genes were used for normalisation of target mRNA levels. Whilst this is suitable in most cases, it would be beneficial to investigate the stability of further reference genes across these tissue panels.

The differential pattern of *chAKT1* and *chAKT3* expression seen in chicken tissues, as compared to human tissues, suggests an alternative role for *chAKT3* in chickens. Human *AKT3* is documented to be expressed in high quantities in the brain but not in other tissues. *AKT3* knockout mice were found to develop smaller brains compared to wild type (Easton et al., 2005). Therefore, it would be interesting to look at the protein level and investigate the functions of AKT1 and AKT3 in avian tissues. In particular, the role of AKT3 in the heart and brain.

The lower expression of *chAKT1* and *chAKT3* in the Bursa, compared to other tissues, merits further investigation. The bursa of chickens is at its largest within a few weeks of hatch, after which it gets smaller and its function changes. The expression of *chAKT1* and *chAKT3* in the bursas of birds of different ages could

be investigated to understand more about the genes function. As the bursa is the primary site of B-cell development, it may be beneficial to investigate the role of AKT1 and AKT3 proteins in the development of B-cells. This could be done initially by investigating the pathways involved using specific antibodies to AKT1 and AKT3 in B-cells. Subsequently, the proteins could be overexpressed in the cells and the effect of overexpression investigated.

Copies of IBV genome were detected in the spleen at day 6 and 7 post infection in several birds, however no viral mRNA was detected. This suggests that the virus is able to enter splenocytes but not replicate and establish an infection, as was seen in the kidney. The presence of virus in the spleen, kidney and lungs, but not the brain suggests that the virus may be transported to these sites in the blood. Little is known about how the virus establishes infections in organs outside the respiratory system. It would be interesting to investigate this further by measuring viral genome and mRNA levels in a further panel of tissues, including the blood and primary cells.

The National Avian Research Facility (NARF) at The Roslin Institute, Edinburgh houses eight inbred lines of chicken, some of which are known to have varying susceptibility to avian viruses. It would also be interesting to examine the expression profile of the *AKT* isoforms in the different lines to establish whether *AKT* gene expression plays a role in viral pathogenesis.

# Chapter 6

## Discussion

## 6.1 Significance of this work

The coronaviridae family of viruses infects many species of birds and mammals including humans. Over recent years' coronaviruses have attracted much attention due to their ability to transmit between species. This was exemplified most recently by the emergence of Middle East respiratory syndrome coronavirus (MERS-CoV) and also severe acute respiratory syndrome coronavirus (SARS-CoV). Both of these novel viruses were thought to originate in bats before crossing into the human population. Such zoonotic potential is concerning especially since global trade, deforestation, urbanization and high density farming practices increase the risk of severe zoonotic outbreaks. Of particular note are zoonotic avian diseases. In the UK alone there are around 875 million chickens produced in over 2,500 poultry farms each year (BPC, 2016). Over recent years the consumption of poultry has risen from 77 to 86 million metric tons compared with consumption of beef and veal at only 55 million metric tons (FAS, 2012). The vast quantities of poultry farmed for meat and egg production, as well as the quantity of domestic poultry kept for small scale farming, provides a perfect environment for the spread of a zoonotic avian virus. A recent example of this was the avian influenza H5N1 and H7N9, both of which have been found to cause disease in humans (Kandun et al., 2006, Li et al., 2014). There is presently no reason to expect the tropism of avian coronaviruses to extend to humans. However, further research into the pathogenicity and basic biology of the virus will be beneficial to economies and poultry industries worldwide and will inform study of related coronaviruses with potential significance to human health.

The aim of this project was to identify the role of the PI3K/AKT signalling pathway during avian infectious bronchitis virus infection in the natural host. The study of the interactions between viruses and cellular pathways can often provide insights into viral replication that lead to the development of the next generation of vaccines or therapeutics. A key example of this occurred in the development of PI3K inhibitors for the treatment of IAV infections (Hsu et al., 2015). At the same time,

understanding the replication cycle and basic biology of viral infections often leads to the discovery of novel aspects of cell biology. In research fields such as avian virology, where knowledge about both avian viral replication and cell biology is often limited, these studies are vital for the progress of the field.

## 6.2 Summary of results

The main aim of this project was to investigate the role of the PI3K/AKT signalling pathway during IBV infection. The first objective was to identify the magnitude and duration of AKT activation in IBV infected cells. The results in this study suggest a biphasic activation in PI3K/AKT signalling during infection of avian cells. The initial phase of activation was found to be dependent on viral attachment and entry into the cell, however, early activation was not seen to be dependent on viral replication. During the later phase of AKT activation, an active PI3K/AKT signalling pathway was identified as being necessary for viral replication. Interestingly, activation of PI3K/AKT signalling during IBV infection in mammalian cells was not found to be biphasic, with an increase in AKT activation seen only from 6 hpi.

Subsequently, the effect of IBV-induced PI3K/AKT activation on protein synthesis, apoptosis and micropinocytosis was investigated. IBV infection of avian cells was found to induce phosphorylation of 4E-BP1 in a PI3K-dependent manner at 2 and 12 hpi, suggesting activation of cap-dependent translation. The cleavage of caspase 3/7 was seen to increase in a biphasic manner in IBV infected avian and mammalian cells. However, it was not found to be dependent on active PI3K in avian cells. Two methods were employed to investigate levels of macropinocytic activity during IBV infection. Unfortunately, due to a lack of functioning controls and variability in the growth of the cell lines, no conclusions could be drawn from these results.

In addition to investigating the effects of IBV infection on the phosphorylation state of AKT, levels of *chAKT* mRNA expression were also measured. Initially, the location of the *chAKT2* gene was investigated as it has not been mapped to the chicken genome. The partial cds available for *chAKT2* was mapped to two scaffolds, suggesting that it is present in the chicken genome but has not yet been mapped to a chromosome.

In order to measure the expression of *chAKT1* and *chAKT3* in avian cells and tissues, reference genes were selected and primer and probe sets designed. The most stable reference genes, in each sample set, were then chosen by geNorm analysis. The stable reference genes were then used to normalise the expression of *chAKT1* and *chAKT3*.

The expression of *chAKT1* and *chAKT3* was investigated by qPCR in cell culture and *in vivo* following IBV infection. IBV infected DF1 cells demonstrated increased levels of *chAKT1* expression during infection. However, this increase was minimal and not believed to be biologically relevant. The expression of both *chAKT1* and *chAKT3* was determined in tissue collected from chickens infected with IBV. No significant increase in gene expression was seen in IBV infected tissues. However, an increase in *chAKT3* expression was noted in the brain of IBV infected cells, despite the absence of virus in the tissue.

## 6.3 The role of PI3K/AKT signalling during infection of avian cells

In this study the PI3K/AKT signalling pathway was found to be activated during IBV infection of both mammalian and avian cells. The characteristics of AKT activation differed between IBV infected avian and mammalian cells. Activation of mammalian AKT occurred from 6 hpi continuing to 24 hpi, however activation of avian AKT occurred in a biphasic manner. The difference in the patterns of AKT activation between the species suggest differences in the interaction between the virus and avian or mammalian cells. Other studies have also noted differences in the

interaction between IBV and avian or mammalian cells. For example, autophagy has been found to occur in Vero cells, but not avian CK or DF1 cells during IBV infection (Maier et al., 2013a). These differences in virus-host interactions may be a result of the inability of the avian virus to stimulate mammalian signalling pathways. Alternatively, the early phase of AKT activation in avian cells may be an anti-viral response elicited by the cell. Mammalian cells may be slower to, or not able to elicit such a response during IBV infection.

The role of AKT activation during IBV infection of avian cells can be summarised as follows (Figure 7.1).

(i) The binding of the virus to cell surface sugars, and potentially other receptors, induces activation of AKT as early as 30 mins post infection.

(ii) The virus enters the cell and the viral genome is released into the cytoplasm. Viral mRNA and genome is replicated, possibly in spherules attached to zippered-ER (Maier et al., 2013b). This process is dependent on an active PI3K/AKT signalling pathway and is supressed by treatment with the PI3K inhibitor LY294002. In CK cells viral mRNA, and in particular N-message, is replicated from 2-3 hpi. Viral genome however is only seen from 4-5 hpi (Maier et al., 2013b).

(iii) Viral RNA is translated by the host machinery to synthesise viral proteins. Synthesis of viral proteins was also dependent on an active PI3K/AKT signalling pathway. However, this may be a result of suppression of viral RNA replication. The overexpression of IBV E may be involved in the activation of AKT, suggesting that activation of AKT during this stage of IBV infection could be a result of the expression of E.

(iv) Viral proteins assemble at the ERGIC along with viral genome to form new virions.

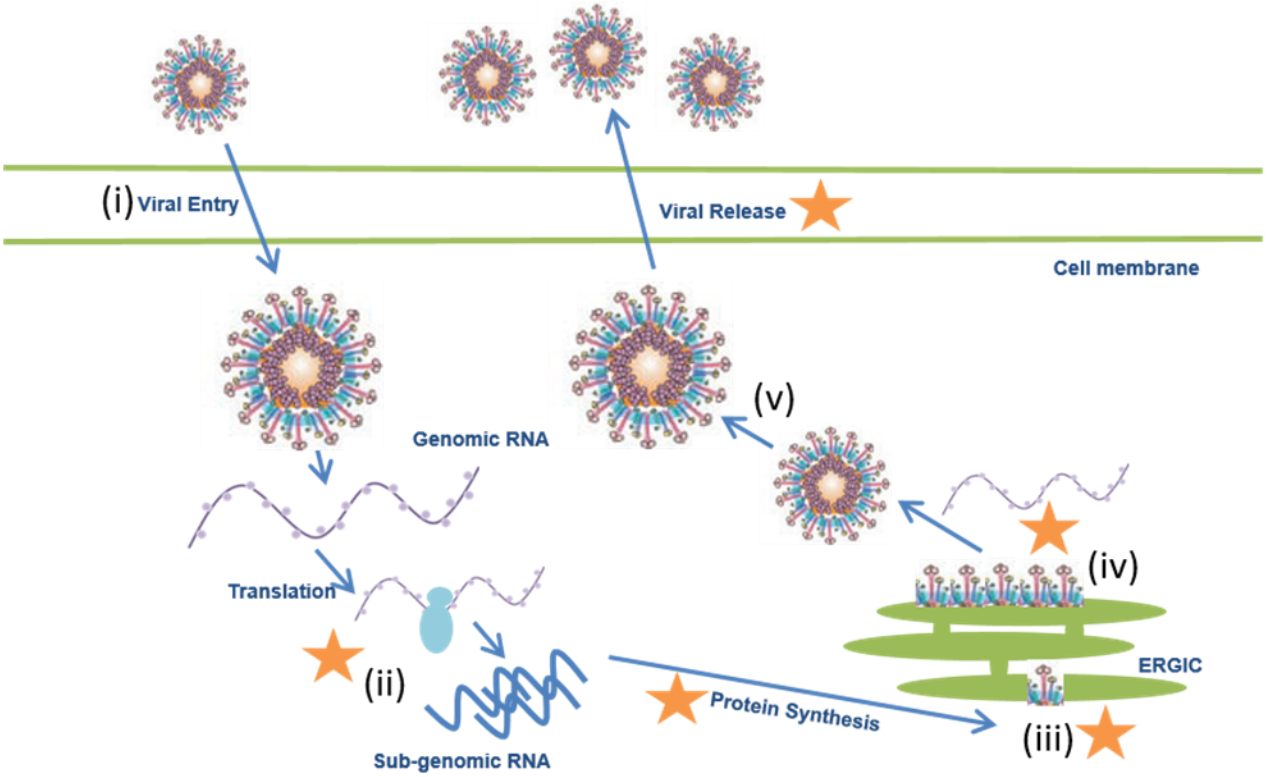


Figure 6.1 Schematic depicting the replication of IBV in avian cells. (i) IBV attaches to cellular receptors and enters the cell. (ii) Viral RNA is released into the cytoplasm and viral mRNA and genome is replicated. (iii) Viral proteins are synthesised from mRNA by host machinery and processed in the ER. (iv) Viral proteins assemble with viral gRNA to form new virions. (v) New virions bud off from the ERGIC and are trafficked to the plasma membrane where they exit the cell by exocytosis. Yellow stars identify process during IBV replication that are dependent on an active PI3KAKT pathway.

(v) The new virions are then trafficked to the plasma membrane where they are released by exocytosis. Release of infectious particles was supressed by inhibition of PI3K, potentially as a result of a reduction in viral RNA replication and protein synthesis.

The activation of avian AKT during IBV infection occurs in a biphasic manner. A model for the proposed role of PI3K/AKT signalling during IBV infection is depicted in Figure 7.2. In summary, it is hypothesised that avian cell infection with IBV induces cellular signalling modulation that occurs in three distinct phases. These were characterised initially by activation of AKT signalling.

(A) The 1st phase of infection results in activation of AKT at 2 hpi, which is then supressed by 8hpi. This period of pAKT suppression is represented as the 2nd phase. By 16 hpi AKT activation is again restored and occurs until 24 hpi which represents the 3rd phase of IBV infection and is PI3K dependent (Figure 7.2 - Line A).

This study investigated the modulation of several pathways downstream of PI3K/AKT signalling and together with other published data, models for their role in IBV infection of avian cells is summarized (Figure 7.2 lines B-D). (B) The cleavage of caspase 3/7 was found to coincide with all phases of IBV infection, however activation of the caspase cascade was found to be PI3K-independent. As with AKT, caspase cleavage is supressed during the second phase of infection. The UPR is known to be induced early during infection, before 8hpi (Fung et al., 2014). The activation of the caspase cascade may therefore be supressed by the UPR by 8 hpi (as seen in the 2nd phase of infection). This process has previously been suggested to occur via AKT and JNK. However, in this study the level of caspase cleavage was not found to be dependent on PI3K (Fung et al., 2014). During the 3rd phase of infection there is again an increase in caspase cleavage which was not dependent on PI3K. This increase in pro-apoptotic signalling is possibly induced by ER-stress.

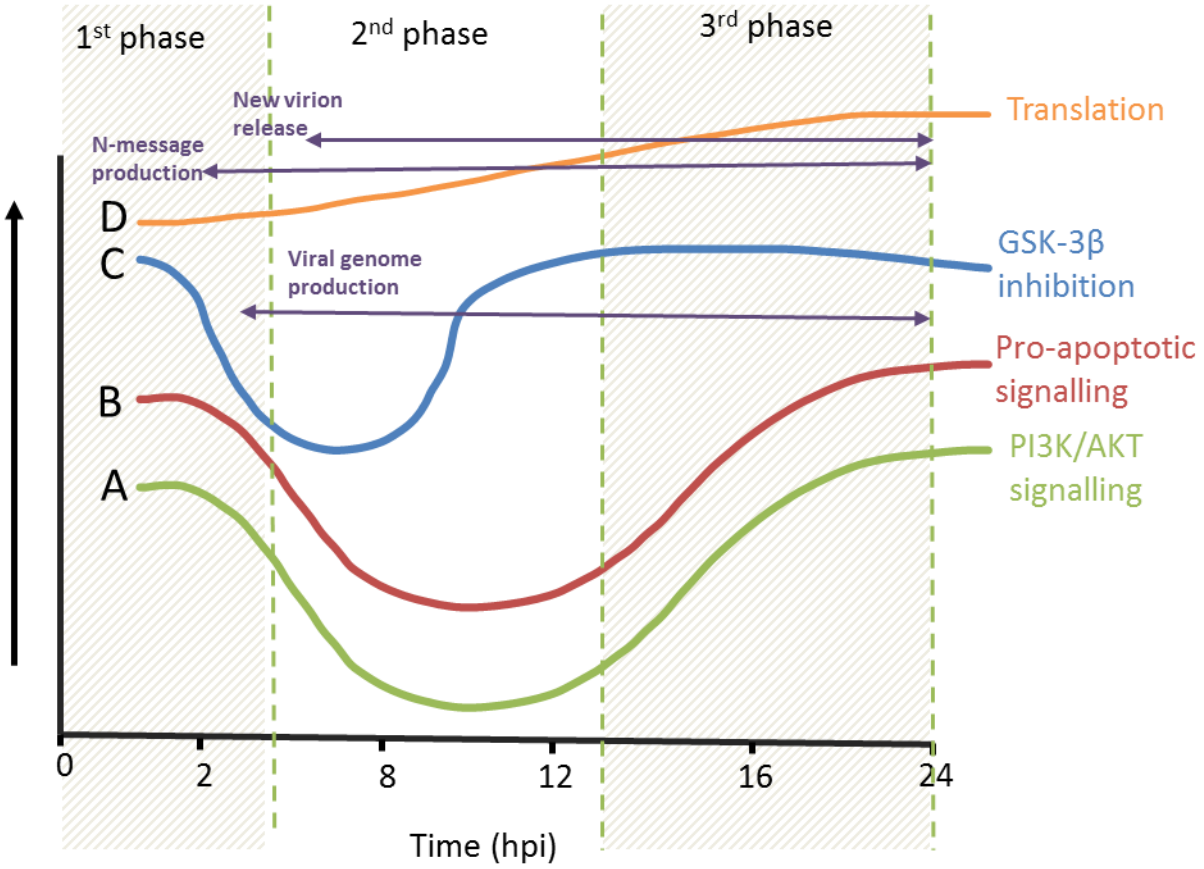


Figure 6.2 Schematic describing the proposed model of the role of PI3K/AKT signalling during IBV infection. (A) The initial phase of IBV infection induces AKT activation between 0 and 2 hpi. This activation is suppressed by 8 hpi but increases again by 16 hpi to 24 hpi (green line). (B) Activation of caspase cleavage also follows a biphasic pattern suggesting the activation of apoptosis. (C) GSK-3β inhibition may occur early during infection in order to supress pro-apoptotic responses. (D) Phosphorylation of 4E-BP1 was higher in IBV infected cells from 2 – 24 hpi suggesting and increase in levels of cap-dependent translation during IBV infection.

Whilst this would normally be controlled by the UPR, infection with IBV imposes a heavy burden on the ER which may overload the UPR and induce apoptosis.

(C) Inhibition of GSK3-β by phosphorylation at S9 was found to occur at 2 hpi however data suggests a similar biphasic pattern of phosphorylation as seen with AKT. The pro-apoptotic nature of GSK3-β suggests that it's inhibition by PI3K/AKT may be a survival mechanism to prevent apoptosis and cell death. Viral sgRNA is made from as early as 2 hpi therefore, a build-up of viral protein will have occurred by 8 hpi and stress put on cellular machinery.

(D) PI3K/AKT signalling is also involved in the phosphorylation of 4E-BP1 at T37/46 which primes the protein for phosphorylation at T70 and S65, resulting in its dissociation eIF4E. The phosphorylation 4E-BP1 occurred during the initial phase of infection and continued to 12 hpi. This phosphorylation of the 4E-BP1 is hypothesised to result in an increase in translation. Previous studies of IBV infection have demonstrated host translational shutoff during infection of CK, Vero and DF1 cells (Kint et al., 2016). The accessory protein 5b was found to be involved in suppression of host translation, and infection with a 5b deletion mutant induced higher concentration of type 1 interferon. This suggests a role for 5b in the suppression of host innate immune responses to infection. Our data on 4E-BP1 does not correlate with the findings of host shut-off as it suggests an increase in translation. However, viral translation may be specifically modulated through the phosphorylation of 4E-BP1. The mechanism for host shut-off during IBV infection is not fully understood. However, the activation of the UPR response involves the activation of PERK which directly phosphorylated eIF2α to decrease protein synthesis (Rajesh et al., 2015). It is therefore possible that IBV induces host shut-off through activation of the UPR response. The phosphorylation of 4E-BP1 seen in this study may be a by-product of the activation of AKT to stimulate another pathway.

Alternatively, the phosphorylation of 4E-BP1 during the 1st phase of infection may be a response elicited by the cell to promote an innate immune response.

In addition to the activation of PI3K/AKT signalling, IBV infection has been found to induce autophagy during the 3rd phase of replication in mammalian cells (Cottam et al., 2011, Maier et al., 2013a). Whilst the role of PI3K/AKT signalling during IBV induced autophagy was not investigated in this project, it is likely to be involved, at least in mammalian cells. Activation of autophagy can be a pro- or anti-viral response. For example, replication of the Herpes Simplex virus 1 (HSV-1) and Sindbis viruses is inhibited by autophagy and inhibition of the pathway leads to increased replication and virulence (English et al., 2009, Orvedahl et al., 2010). The membranes required for autophagosome formation often originate from the endoplasmic reticulum. This initial step is controlled downstream of the PI3K/AKT signalling cascade, by mTOR. The mTOR signalling cascade inhibits autophagy when nutrients are available and conditions are favourable to promote growth. The activation of the PI3K/AKT/mTOR pathway would therefore be expected to prevent autophagy, however during the 3rd phase of infection the opposite occurs. MHV has been shown previously to induce autophagy in infected cells and along with other CoVs (Prentice et al., 2004). However, again the exact mechanism behind this activation is unknown.

In conclusion, the initial phase of PI3K/AKT signalling is hypothesised to be a preliminary anti-viral response elicited by the cell as a result of virus infection. This anti-viral response is subsequently supressed by viral factors that work on the host pathways to prevent cell shut-down and death. These may include the accessory protein 5b which is involved in translational control and the suppression of the interferon response (Kint et al., 2016). By the 3rd phase of infection, viral factors activate PI3K/AKT signalling and other pathways to modulate processes that are beneficial to replication, for example apoptotic signalling.

This study highlights the importance of the PI3K/AKT signalling pathway in viral infection and also points to differences in viral modulation of cellular pathways in avian and mammalian cells.

# References


Abdel-Moneim, A. S., Zlotowski, P., Veits, J., Keil, G. M. & Teifke, J. P. 2009. Immunohistochemistry for detection of avian infectious bronchitis virus strain M41 in the proventriculus and nervous system of experimentally infected chicken embryos. *Virol J,* 6**,** 15.

Alagaili, A. N., Briese, T., Mishra, N., Kapoor, V., Sameroff, S. C., Burbelo, P. D., De Wit, E., Munster, V. J., Hensley, L. E., Zalmout, I. S., Kapoor, A., Epstein, J. H., Karesh, W. B., Daszak, P., Mohammed, O. B. & Lipkin, W. I. 2014. Middle East respiratory syndrome coronavirus infection in dromedary camels in Saudi Arabia. *MBio,* 5**,** e00884-14.

Aleksandrowicz, P., Marzi, A., Biedenkopf, N., Beimforde, N., Becker, S., Hoenen, T., Feldmann, H. & Schnittler, H.-J. 2011. Ebola Virus Enters Host Cells by Macropinocytosis and Clathrin-Mediated Endocytosis. *Journal of Infectious Diseases,* 204**,** S957-S967.

Alessi, D. R., Andjelkovic, M., Caudwell, B., Cron, P., Morrice, N., Cohen, P. & Hemmings, B. A. 1996. Mechanism of activation of protein kinase B by insulin and IGF-1. *EMBO J,* 15**,** 6541-51.

Alessi, D. R. & Cohen, P. 1998. Mechanism of activation and function of protein kinase B. *Current Opinion in Genetics & Development,* 8**,** 55-62.

Almazan, F., Galan, C. & Enjuanes, L. 2004. The nucleoprotein is required for efficient coronavirus genome replication. *J Virol,* 78**,** 12683-8.

Ambali, A. G. & Jones, R. C. 1990. Early pathogenesis in chicks of infection with an enterotropic strain of infectious bronchitis virus. *Avian Dis,* 34**,** 809-17.

Amstutz, B., Gastaldelli, M., Kälin, S., Imelli, N., Boucke, K., Wandeler, E., Mercer, J., Hemmi, S. & Greber, U. F. 2008. Subversion of CtBP1-controlled macropinocytosis by human adenovirus serotype 3. *The EMBO Journal,* 27**,** 956-969.

Amyere, M., Payrastre, B., Krause, U., Smissen, P. V. D., Veithen, A. & Courtoy, P. J. 2000. Constitutive Macropinocytosis in Oncogene-transformed Fibroblasts Depends on Sequential Permanent Activation of Phosphoinositide 3-Kinase and Phospholipase C. *Molecular Biology of the Cell,* 11**,** 3453-3467.

Andersen, C. L., Jensen, J. L. & Orntoft, T. F. 2004. Normalization of real-time quantitative reverse transcription-PCR data: a model-based variance estimation approach to identify genes suited for normalization, applied to bladder and colon cancer data sets. *Cancer Res,* 64**,** 5245-50.

Andjelkovic, M., Alessi, D. R., Meier, R., Fernandez, A., Lamb, N. J., Frech, M., Cron, P., Cohen, P., Lucocq, J. M. & Hemmings, B. A. 1997. Role of translocation in the activation and function of protein kinase B. *J Biol Chem,* 272**,** 31515-24.

Andree, H. a. M., Reutelingsperger, C. P. M., Mann, R. H., Hemker, H. C., Hermens, W. T. & Willems, G. M. 1990. Binding of vascular

anticoagulant α (VACα) to planar phospholipid bilayers. *Journal of Biological Chemistry,* 265**,** 4923-4928.

Araki, N., Johnson, M. T. & Swanson, J. A. 1996. A role for phosphoinositide 3-kinase in the completion of macropinocytosis and phagocytosis by macrophages. *J Cell Biol,* 135**,** 1249-60.

Ariaans, M. P., Van De Haar, P. M., Hensen, E. J. & Vervelde, L. 2009. Infectious Bronchitis Virus induces acute interferon-gamma production through polyclonal stimulation of chicken leukocytes. *Virology,* 385**,** 68-73.

Armesto, M., Evans, S., Cavanagh, D., Abu-Median, A. B., Keep, S. & Britton, P. 2011. A recombinant avian infectious bronchitis virus expressing a heterologous spike gene belonging to the 4/91 serotype. *PLoS One,* 6**,** e24352.

Armstrong, J., Niemann, H., Smeekens, S., Rottier, P. & Warren, G. 1984. Sequence and topology of a model intracellular membrane protein, E1 glycoprotein, from a coronavirus. *Nature,* 308**,** 751-752.

Ashkenazi, A. & Dixit, V. M. 1998. Death receptors: signaling and modulation. *Science,* 281**,** 1305-8.

Bagchi, P., Dutta, D., Chattopadhyay, S., Mukherjee, A., Halder, U. C., Sarkar, S., Kobayashi, N., Komoto, S., Taniguchi, K. & Chawla-Sarkar, M. 2010. Rotavirus nonstructural protein 1 suppresses virus-induced cellular apoptosis to facilitate viral growth by activating the cell survival pathways during early stages of infection. *J Virol,* 84**,** 6834-45.

Batra, A., Maier, H. J. & Fife, M. S. 2016. Selection of reference genes for gene expression analysis by real-time qPCR in avian cells infected with infectious bronchitis virus. *Avian Pathology***,** 1-20.

Bellacosa, A., Chan, T. O., Ahmed, N. N., Datta, K., Malstrom, S., Stokoe, D., Mccormick, F., Feng, J. & Tsichlis, P. 1998. Akt activation by growth factors is a multiple-step process: the role of the PH domain. *Oncogene,* 17**,** 313-25.

Bellacosa, A., Testa, J. R., Staal, S. P. & Tsichlis, P. N. 1991. A retroviral oncogene, akt, encoding a serine-threonine kinase containing an SH2-like region. *Science,* 254**,** 274-7.

Belouzard, S., Chu, V. C. & Whittaker, G. R. 2009. Activation of the SARS coronavirus spike protein via sequential proteolytic cleavage at two distinct sites. *Proc Natl Acad Sci U S A,* 106**,** 5871-6.

Belouzard, S., Millet, J. K., Licitra, B. N. & Whittaker, G. R. 2012. Mechanisms of coronavirus cell entry mediated by the viral spike protein. *Viruses,* 4**,** 1011-33.

Belov, G. A., Nair, V., Hansen, B. T., Hoyt, F. H., Fischer, E. R. & Ehrenfeld, E. 2012. Complex Dynamic Development of Poliovirus Membranous Replication Complexes. *Journal of Virology,* 86**,** 302-312.

Benyeda, Z., Mató, T., Süveges, T., Szabó, É., Kardi, V., Abonyi-Tóth, Z., Rusvai, M. & Palya, V. 2009. Comparison of the pathogenicity of QX-like, M41 and 793/B infectious bronchitis strains from different pathological conditions. *Avian Pathology,* 38**,** 449-456.

Biondi, R. M., Cheung, P. C., Casamayor, A., Deak, M., Currie, R. A. & Alessi, D. R. 2000. Identification of a pocket in the PDK1 kinase domain that interacts with PIF and the C-terminal residues of PKA. *EMBO J,* 19**,** 979-88.

Blanchard, E. & Roingeard, P. 2015. Virus-induced double-membrane vesicles. *Cellular Microbiology,* 17**,** 45-50.

Bollo, M., Paredes, R. M., Holstein, D., Zheleznova, N., Camacho, P. & Lechleiter, J. D. 2010. Calcineurin interacts with PERK and dephosphorylates calnexin to relieve ER stress in mammals and frogs. *PLoS One,* 5**,** e11925.

Boltz, D. A., Nakai, M. & Bahra, J. M. 2004. Avian infectious bronchitis virus: a possible cause of reduced fertility in the rooster. *Avian Dis,* 48**,** 909-15.

Bonavia, A., Zelus, B. D., Wentworth, D. E., Talbot, P. J. & Holmes, K. V. 2003. Identification of a receptor-binding domain of the spike glycoprotein of human coronavirus HCoV-229E. *J Virol,* 77**,** 2530-8.

Bonni, A., Brunet, A., West, A. E., Datta, S. R., Takasu, M. A. & Greenberg, M. E. 1999. Cell Survival Promoted by the Ras-MAPK Signaling Pathway by Transcription-Dependent and -Independent Mechanisms. *Science,* 286**,** 1358-1362.

Boulbes, D. R., Shaiken, T. & Sarbassov Dos, D. 2011. Endoplasmic reticulum is a main localization site of mTORC2. *Biochem Biophys Res Commun,* 413**,** 46-52.

Bpc, B. P. C. 2016. *About the Poultry Industry* [Online]. http://www.britishpoultry.org.uk/how-the-sector-works/.

Bustin, S. A., Benes, V., Garson, J. A., Hellemans, J., Huggett, J., Kubista, M., Mueller, R., Nolan, T., Pfaffl, M. W., Shipley, G. L., Vandesompele, J. & Wittwer, C. T. 2009. The MIQE guidelines: minimum information for publication of quantitative real-time PCR experiments. *Clin Chem,* 55**,** 611-22.

Cain, K., Bratton, S. B. & Cohen, G. M. 2002. The Apaf-1 apoptosome: a large caspase-activating complex. *Biochimie,* 84**,** 203-214.

Calfon, M., Zeng, H., Urano, F., Till, J. H., Hubbard, S. R., Harding, H. P., Clark, S. G. & Ron, D. 2002. IRE1 couples endoplasmic reticulum load to secretory capacity by processing the XBP-1 mRNA. *Nature,* 415**,** 92-6.

Carlton, J., Bujny, M., Peter, B. J., Oorschot, V. M., Rutherford, A., Mellor, H., Klumperman, J., Mcmahon, H. T. & Cullen, P. J. 2004. Sorting nexin-1 mediates tubular endosome-to-TGN transport through coincidence sensing of high- curvature membranes and 3-phosphoinositides. *Curr Biol,* 14**,** 1791-800.

Casais, R., Davies, M., Cavanagh, D. & Britton, P. 2005. Gene 5 of the Avian Coronavirus Infectious Bronchitis Virus Is Not Essential for Replication. *Journal of Virology,* 79**,** 8065-8078.

Casais, R., Dove, B., Cavanagh, D. & Britton, P. 2003. Recombinant Avian Infectious Bronchitis Virus Expressing a Heterologous Spike Gene Demonstrates that the Spike Protein Is a Determinant of Cell Tropism. *Journal of Virology,* 77**,** 9084-9089.

Casais, R., Hodgson, T., Britton, P. & Cavanagh, D. 2004. Genetic manipulation of IBV: properties of recombinants with alterations to the spike protein gene and non-structural protein genes 3 and 5. *In:* HEFFELS-REDMANN, U. & KALETA, E. F. (eds.) *IV. International symposium on avian corona- and pneumovirus infections,*

*Rauischholzhausen, Germany, 20-23 June 2004.* Wettenberg: VVB Laufersweiler Verlag.

Casais, R., Thiel, V., Siddell, S. G., Cavanagh, D. & Britton, P. 2001. Reverse genetics system for the avian coronavirus infectious bronchitis virus. *J Virol,* 75**,** 12359-69.

Cavanagh, D. 2007. Coronavirus avian infectious bronchitis virus. *Vet Res,* 38**,** 281-97.

Cencic, R., Desforges, M., Hall, D. R., Kozakov, D., Du, Y., Min, J., Dingledine, R., Fu, H., Vajda, S., Talbot, P. J. & Pelletier, J. 2011. Blocking eIF4E-eIF4G Interaction as a Strategy To Impair Coronavirus Replication. *Journal of Virology,* 85**,** 6381-6389.

Chan, C. M., Ma, C. W., Chan, W. Y. & Chan, H. Y. 2007. The SARS-Coronavirus Membrane protein induces apoptosis through modulating the Akt survival pathway. *Arch Biochem Biophys,* 459**,** 197-207.

Chang, P., Kuchipudi, S. V., Mellits, K. H., Sebastian, S., James, J., Liu, J., Shelton, H. & Chang, K.-C. 2015. Early apoptosis of porcine alveolar macrophages limits avian influenza virus replication and pro-inflammatory dysregulation. *Scientific Reports,* 5**,** 17999.

Chen, D. L., Engle, J. T., Griffin, E. A., Miller, J. P., Chu, W., Zhou, D. & Mach, R. H. 2015. Imaging caspase-3 activation as a marker of apoptosis-targeted treatment response in cancer. *Mol Imaging Biol,* 17**,** 384-93.

Chen, W., Calvo, P. A., Malide, D., Gibbs, J., Schubert, U., Bacik, I., Basta, S., O'neill, R., Schickli, J., Palese, P., Henklein, P., Bennink, J. R. & Yewdell, J. W. 2001. A novel influenza A virus mitochondrial protein that induces cell death. *Nat Med,* 7**,** 1306-12.

Chhabra, R., Kuchipudi, S. V., Chantrey, J. & Ganapathy, K. 2016. Pathogenicity and tissue tropism of infectious bronchitis virus is associated with elevated apoptosis and innate immune responses. *Virology,* 488**,** 232-41.

Chinnaiyan, A. M. 1999. The apoptosome: heart and soul of the cell death machine. *Neoplasia,* 1**,** 5-15.

Cho, H., Mu, J., Kim, J. K., Thorvaldsen, J. L., Chu, Q., Crenshaw, E. B., 3rd, Kaestner, K. H., Bartolomei, M. S., Shulman, G. I. & Birnbaum, M. J. 2001a. Insulin resistance and a diabetes mellitus-like syndrome in mice lacking the protein kinase Akt2 (PKB beta). *Science,* 292**,** 1728-31.

Cho, H., Thorvaldsen, J. L., Chu, Q., Feng, F. & Birnbaum, M. J. 2001b. Akt1/PKBalpha is required for normal growth but dispensable for maintenance of glucose homeostasis in mice. *J Biol Chem,* 276**,** 38349-52.

Chung, L., Bailey, D., Leen, E. N., Emmott, E. P., Chaudhry, Y., Roberts, L. O., Curry, S., Locker, N. & Goodfellow, I. G. 2014. Norovirus Translation Requires an Interaction between the C Terminus of the Genome-linked Viral Protein VPg and Eukaryotic Translation Initiation Factor 4G. *The Journal of Biological Chemistry,* 289**,** 21738-21750.

Collisson, E. W., Williams, A. K., Vonder Haar, R., Li, W. & Sneed, L. W. 1990. Sequence comparisons of the 3' end of the genomes of five strains of avian infectious bronchitis virus. *Adv Exp Med Biol,* 276**,** 373-7.

Conner, S. D. & Schmid, S. L. 2003. Regulated portals of entry into the cell. *Nature,* 422**,** 37-44.

Connor, J. H. & Lyles, D. S. 2002. Vesicular stomatitis virus infection alters the eIF4F translation initiation complex and causes dephosphorylation of the eIF4E binding protein 4E-BP1. *J Virol,* 76**,** 10177-87.

Cook, J. K., Chesher, J., Baxendale, W., Greenwood, N., Huggins, M. B. & Orbell, S. J. 2001. Protection of chickens against renal damage caused by a nephropathogenic infectious bronchitis virus. *Avian Pathol,* 30**,** 423-6.

Cook, J. K., Jackwood, M. & Jones, R. C. 2012. The long view: 40 years of infectious bronchitis research. *Avian Pathol,* 41**,** 239-50.

Corse, E. & Machamer, C. E. 2000. Infectious bronchitis virus E protein is targeted to the Golgi complex and directs release of virus-like particles. *Journal of Virology,* 74**,** 4319-4326.

Corse, E. & Machamer, C. E. 2002. The Cytoplasmic Tail of Infectious Bronchitis Virus E Protein Directs Golgi Targeting. *Journal of Virology,* 76**,** 1273-1284.

Corse, E. & Machamer, C. E. 2003. The cytoplasmic tails of infectious bronchitis virus E and M proteins mediate their interaction. *Virology,* 312**,** 25-34.

Cottam, E. M., Maier, H. J., Manifava, M., Vaux, L. C., Chandra-Schoenfelder, P., Gerner, W., Britton, P., Ktistakis, N. T. & Wileman, T. 2011. Coronavirus nsp6 proteins generate autophagosomes from the endoplasmic reticulum via an omegasome intermediate. *Autophagy,* 7**,** 1335-47.

Cottam, E. M., Whelband, M. C. & Wileman, T. 2014. Coronavirus NSP6 restricts autophagosome expansion. *Autophagy,* 10**,** 1426-41.

Crinion, R. A. 1972. Egg quality and production following infectious bronchitis virus exposure at one day old. *Poult Sci,* 51**,** 582-5.

Darbyshire, J. H., Rowell, J. G., Cook, J. K. & Peters, R. W. 1979. Taxonomic studies on strains of avian infectious bronchitis virus using neutralisation tests in tracheal organ cultures. *Arch Virol,* 61**,** 227-38.

Daughenbaugh, K. F., Fraser, C. S., Hershey, J. W. & Hardy, M. E. 2003. The genome-linked protein VPg of the Norwalk virus binds eIF3, suggesting its role in translation initiation complex recruitment. *Embo j,* 22**,** 2852-9.

Davies, H. A., Dourmashkin, R. R. & Macnaughton, M. R. 1981. Ribonucleoprotein of avian infectious bronchitis virus. *J Gen Virol,* 53**,** 67-74.

De Haan, C. a. M., Vennema, H. & Rottier, P. J. M. 2000. Assembly of the coronavirus envelope: Homotypic interactions between the M proteins. *Journal of Virology,* 74**,** 4967-4978.

Dediego, M. L., Nieto-Torres, J. L., Jimenez-Guardeno, J. M., Regla-Nava, J. A., Alvarez, E., Oliveros, J. C., Zhao, J. C., Fett, C., Perlman, S. & Enjuanes, L. 2011. Severe Acute Respiratory Syndrome Coronavirus Envelope Protein Regulates Cell Stress Response and Apoptosis. *Plos Pathogens,* 7.

Dediego, M. L., Nieto-Torres, J. L., Regla-Nava, J. A., Jimenez-Guardeno, J. M., Fernandez-Delgado, R., Fett, C., Castano-Rodriguez, C., Perlman, S. & Enjuanes, L. 2014. Inhibition of NF-kappa B-Mediated

Inflammation in Severe Acute Respiratory Syndrome Coronavirus-Infected Mice Increases Survival. *Journal of Virology,* 88**,** 913-924.

Defra 2005. Economic assessment of livestock in Great Britain - ZZ0102. http://randd.defra.gov.uk/Default.aspx?Menu=Menu&Module=More&Location=None&Completed=0&ProjectID=9781: Department for Environment Food and Rural Affairs.

Denisova, O. V., Soderholm, S., Virtanen, S., Von Schantz, C., Bychkov, D., Vashchinkina, E., Desloovere, J., Tynell, J., Ikonen, N., Theisen, L. L., Nyman, T. A., Matikainen, S., Kallioniemi, O., Julkunen, I., Muller, C. P., Saelens, X., Verkhusha, V. V. & Kainov, D. E. 2014. Akt inhibitor MK2206 prevents influenza pH1N1 virus infection in vitro. *Antimicrob Agents Chemother*.

Diehl, N. & Schaal, H. 2013. Make yourself at home: viral hijacking of the PI3K/Akt signaling pathway. *Viruses,* 5**,** 3192-212.

Donnelly, G. M., Mckean, H. E., Heird, C. S. & Green, J. 1974. Ciliostasis as a Bioassay. *Archives of Environmental Health: An International Journal,* 28**,** 350-355.

Du, X., Kristiana, I., Wong, J. & Brown, A. J. 2006. Involvement of Akt in ER-to-Golgi Transport of SCAP/SREBP: A Link between a Key Cell Proliferative Pathway and Membrane Synthesis. *Molecular Biology of the Cell,* 17**,** 2735-2745.

Du, Y. F., Long, Q. Z., Shi, Y., Liu, X. G., Li, X. D., Zeng, J., Gong, Y. G., Wang, X. Y. & He, D. L. 2014. Downregulation of mTOR by lentivirus inhibits prostate cancer cell growth. *Int J Clin Exp Pathol,* 7**,** 923-31.

Dummler, B., Tschopp, O., Hynx, D., Yang, Z. Z., Dirnhofer, S. & Hemmings, B. A. 2006. Life with a single isoform of Akt: mice lacking Akt2 and Akt3 are viable but display impaired glucose homeostasis and growth deficiencies. *Mol Cell Biol,* 26**,** 8042-51.

Easton, R. M., Cho, H., Roovers, K., Shineman, D. W., Mizrahi, M., Forman, M. S., Lee, V. M. Y., Szabolcs, M., De Jong, R., Oltersdorf, T., Ludwig, T., Efstratiadis, A. & Birnbaum, M. J. 2005. Role for Akt3/Protein Kinase B in Attainment of Normal Brain Size. *Molecular and Cellular Biology,* 25**,** 1869-1878.

Ehrhardt, C., Marjuki, H., Wolff, T., Nurnberg, B., Planz, O., Pleschka, S. & Ludwig, S. 2006. Bivalent role of the phosphatidylinositol-3-kinase (PI3K) during influenza virus infection and host cell defence. *Cell Microbiol,* 8**,** 1336-48.

Ehrhardt, C., Wolff, T., Pleschka, S., Planz, O., Beermann, W., Bode, J. G., Schmolke, M. & Ludwig, S. 2007. Influenza A virus NS1 protein activates the PI3K/Akt pathway to mediate antiapoptotic signaling responses. *J Virol,* 81**,** 3058-67.

Eierhoff, T., Hrincius, E. R., Rescher, U., Ludwig, S. & Ehrhardt, C. 2010. The epidermal growth factor receptor (EGFR) promotes uptake of influenza A viruses (IAV) into host cells. *PLoS Pathog,* 6**,** e1001099.

Eifart, P., Ludwig, K., Bottcher, C., De Haan, C. A., Rottier, P. J., Korte, T. & Herrmann, A. 2007. Role of endocytosis and low pH in murine hepatitis virus strain A59 cell entry. *J Virol,* 81**,** 10758-68.

Elghazi, L., Rachdi, L., Weiss, A. J., Cras-Meneur, C. & Bernal-Mizrachi, E. 2007. Regulation of beta-cell mass and function by the Akt/protein kinase B signalling pathway. *Diabetes Obes Metab,* 9 Suppl 2**,** 147-57.

Ellis, H. M. & Horvitz, H. R. 1986. Genetic control of programmed cell death in the nematode C. elegans. *Cell,* 44**,** 817-29.

Emmott, E., Munday, D., Bickerton, E., Britton, P., Rodgers, M. A., Whitehouse, A., Zhou, E.-M. & Hiscox, J. A. 2013. The Cellular Interactome of the Coronavirus Infectious Bronchitis Virus Nucleocapsid Protein and Functional Implications for Virus Biology. *Journal of Virology,* 87**,** 9486-9500.

Enari, M., Sakahira, H., Yokoyama, H., Okawa, K., Iwamatsu, A. & Nagata, S. 1998. A caspase-activated DNase that degrades DNA during apoptosis, and its inhibitor ICAD. *Nature,* 391**,** 43-50.

English, L., Chemali, M., Duron, J., Rondeau, C., Laplante, A., Gingras, D., Alexander, D., Leib, D., Norbury, C., Lippe, R. & Desjardins, M. 2009. Autophagy enhances the presentation of endogenous viral antigens on MHC class I molecules during HSV-1 infection. *Nature Immunology,* 10**,** 480-487.

Fadok, V. A., Voelker, D. R., Campbell, P. A., Cohen, J. J., Bratton, D. L. & Henson, P. M. 1992. Exposure of phosphatidylserine on the surface of apoptotic lymphocytes triggers specific recognition and removal by macrophages. *J Immunol,* 148**,** 2207-16.

Fas, F. a. S. 2012. Livestock and Poultry: World Markets and Trade. *United States Department of Agriculture*.

Fayard, E., Tintignac, L. A., Baudry, A. & Hemmings, B. A. 2005. Protein kinase B/Akt at a glance. *J Cell Sci,* 118**,** 5675-8.

Fesq, H., Bacher, M., Nain, M. & Gemsa, D. 1994. Programmed cell death (apoptosis) in human monocytes infected by influenza A virus. *Immunobiology,* 190**,** 175-82.

Freeman, M. C., Peek, C. T., Becker, M. M., Smith, E. C. & Denison, M. R. 2014. Coronaviruses induce entry-independent, continuous macropinocytosis. *MBio,* 5**,** e01340-14.

Fung, T. S., Liao, Y. & Liu, D. X. 2014. The Endoplasmic Reticulum Stress Sensor IRE1 alpha Protects Cells from Apoptosis Induced by the Coronavirus Infectious Bronchitis Virus. *Journal of Virology,* 88**,** 12752-12764.

Ganapathy, K., Wilkins, M., Forrester, A., Lemiere, S., Cserep, T., Mcmullin, P. & Jones, R. C. 2012. QX-like infectious bronchitis virus isolated from cases of proventriculitis in commercial broilers in England. *Veterinary Record,* 171**,** 597.

Garcia-Perez, B. E., Mondragon-Flores, R. & Luna-Herrera, J. 2003. Internalization of Mycobacterium tuberculosis by macropinocitosis in non-phagocytic cells. *Microb Pathog,* 35.

Gingras, A. C., Gygi, S. P., Raught, B., Polakiewicz, R. D., Abraham, R. T., Hoekstra, M. F., Aebersold, R. & Sonenberg, N. 1999. Regulation of 4E-BP1 phosphorylation: a novel two-step mechanism. *Genes Dev,* 13**,** 1422-37.

Gingras, A. C., Kennedy, S. G., O'leary, M. A., Sonenberg, N. & Hay, N. 1998. 4E-BP1, a repressor of mRNA translation, is phosphorylated and inactivated by the Akt(PKB) signaling pathway. *Genes Dev,* 12**,** 502-13.

Gingras, A. C., Svitkin, Y., Belsham, G. J., Pause, A. & Sonenberg, N. 1996. Activation of the translational suppressor 4E-BP1 following infection

with encephalomyocarditis virus and poliovirus. *Proceedings of the National Academy of Sciences of the United States of America,* 93**,** 5578-5583.

Goodfellow, I., Chaudhry, Y., Gioldasi, I., Gerondopoulos, A., Natoni, A., Labrie, L., Laliberte, J. F. & Roberts, L. 2005. Calicivirus translation initiation requires an interaction between VPg and eIF 4 E. *EMBO Rep,* 6**,** 968-72.

Gough, R. E., Allan, W. H. & Nedelciu, D. 1977. Immune response to monovalent and bivalent Newcastle disease and infectious bronchitis inactivated vaccines. *Avian Pathol,* 6**,** 131-42.

Guertin, D. A., Stevens, D. M., Thoreen, C. C., Burds, A. A., Kalaany, N. Y., Moffat, J., Brown, M., Fitzgerald, K. J. & Sabatini, D. M. 2006. Ablation in Mice of the mTORC Components raptor, rictor, or mLST8 Reveals that mTORC2 Is Required for Signaling to Akt-FOXO and PKCα, but Not S6K1. *Developmental Cell,* 11**,** 859-871.

Haagmans, B. L., Al Dhahiry, S. H., Reusken, C. B., Raj, V. S., Galiano, M., Myers, R., Godeke, G. J., Jonges, M., Farag, E., Diab, A., Ghobashy, H., Alhajri, F., Al-Thani, M., Al-Marri, S. A., Al Romaihi, H. E., Al Khal, A., Bermingham, A., Osterhaus, A. D., Alhajri, M. M. & Koopmans, M. P. 2014. Middle East respiratory syndrome coronavirus in dromedary camels: an outbreak investigation. *Lancet Infect Dis,* 14**,** 140-5.

Han, S. C., Guo, H. C., Sun, S. Q., Jin, Y., Wei, Y. Q., Feng, X., Yao, X. P., Cao, S. Z., Xiang Liu, D. & Liu, X. T. 2016. Productive Entry of Foot-and-Mouth Disease Virus via Macropinocytosis Independent of Phosphatidylinositol 3-Kinase. *Sci Rep,* 6**,** 19294.

Harding, H. P., Novoa, I., Zhang, Y., Zeng, H., Wek, R., Schapira, M. & Ron, D. 2000. Regulated translation initiation controls stress-induced gene expression in mammalian cells. *Mol Cell,* 6**,** 1099-108.

Harding, H. P., Zhang, Y. & Ron, D. 1999. Protein translation and folding are coupled by an endoplasmic-reticulum-resident kinase. *Nature,* 397**,** 271-4.

Hawes, B. E., Luttrell, L. M., Van Biesen, T. & Lefkowitz, R. J. 1996. Phosphatidylinositol 3-kinase is an early intermediate in the G beta gamma-mediated mitogen-activated protein kinase signaling pathway. *J Biol Chem,* 271**,** 12133-6.

Haze, K., Yoshida, H., Yanagi, H., Yura, T. & Mori, K. 1999. Mammalian transcription factor ATF6 is synthesized as a transmembrane protein and activated by proteolysis in response to endoplasmic reticulum stress. *Mol Biol Cell,* 10**,** 3787-99.

Heidari, M., Fitzgerald, S. D. & Zhang, H. 2014. Marek's disease virus-induced transient cecal tonsil atrophy. *Avian Dis,* 58**,** 262-70.

Heierholzer & Killington 1996. *Virology Methods Manual*.

Hemida, M. G., Chu, D. K., Poon, L. L., Perera, R. A., Alhammadi, M. A., Ng, H. Y., Siu, L. Y., Guan, Y., Alnaeem, A. & Peiris, M. 2014. MERS coronavirus in dromedary camel herd, Saudi Arabia. *Emerg Infect Dis,* 20**,** 1231-4.

Hennion, R. M. & Hill, G. 2015. The Preparation of Chicken Kidney Cell Cultures for Virus Propagation. *In:* MAIER, H. J., BICKERTON, E. & BRITTON, P. (eds.) *Coronaviruses - Methods and Protocols.* Springer Protocols.

Herbert, T. P., Brierley, I. & Brown, T. D. 1997. Identification of a protein linked to the genomic and subgenomic mRNAs of feline calicivirus and its role in translation. *J Gen Virol,* 78 ( Pt 5)**,** 1033-40.

Hillebrand, F., Erkelenz, S., Diehl, N., Widera, M., Noffke, J., Avota, E., Schneider-Schaulies, S., Dabauvalle, M. C. & Schaal, H. 2014. The PI3K pathway acting on alternative HIV-1 pre-mRNA splicing. *J Gen Virol,* 95**,** 1809-15.

Himly, M., Foster, D. N., Bottoli, I., Iacovoni, J. S. & Vogt, P. K. 1998. The DF-1 chicken fibroblast cell line: transformation induced by diverse oncogenes and cell death resulting from infection by avian leukosis viruses. *Virology,* 248**,** 295-304.

Hiscox, J. A., Wurm, T., Wilson, L., Britton, P., Cavanagh, D. & Brooks, G. 2001. The coronavirus infectious bronchitis virus nucleoprotein localizes to the nucleolus. *Journal of Virology,* 75**,** 506-512.

Hodgson, T., Britton, P. & Cavanagh, D. 2006. Neither the RNA nor the Proteins of Open Reading Frames 3a and 3b of the Coronavirus Infectious Bronchitis Virus Are Essential for Replication. *Journal of Virology,* 80**,** 296-305.

Hodgson, T., Casais, R., Dove, B., Britton, P. & Cavanagh, D. 2004. Recombinant Infectious Bronchitis Coronavirus Beaudette with the Spike Protein Gene of the Pathogenic M41 Strain Remains Attenuated but Induces Protective Immunity. *Journal of Virology,* 78**,** 13804-13811.

Hofstad, M. S. & Yoder, H. W., Jr. 1966. Avian infectious bronchitis--virus distribution in tissues of chicks. *Avian Dis,* 10**,** 230-9.

Hsu, A. C., Starkey, M. R., Hanish, I., Parsons, K., Haw, T. J., Howland, L. J., Barr, I., Mahony, J. B., Foster, P. S., Knight, D. A., Wark, P. A. & Hansbro, P. M. 2015. Targeting PI3K-p110alpha Suppresses Influenza Virus Infection in Chronic Obstructive Pulmonary Disease. *Am J Respir Crit Care Med,* 191**,** 1012-23.

Huber, R., Schneider, M., Mayr, I., Römisch, J. & Paques, E.-P. 1990. The calcium binding sites in human annexin V by crystal structure analysis at 2.0 A resolution Implications for membrane binding and calcium channel activity. *FEBS Letters,* 275**,** 15-21.

Huigsloot, M., Tijdens, I. B., Mulder, G. J. & Van De Water, B. 2001. Differential regulation of phosphatidylserine externalization and DNA fragmentation by caspases in anticancer drug-induced apoptosis of rat mammary adenocarcinoma MTLn3 cells. *Biochem Pharmacol,* 62**,** 1087-97.

Icgsc 2004. Sequence and comparative analysis of the chicken genome provide unique perspectives on vertebrate evolution. *Nature,* 432**,** 695-716.

Igney, F. H. & Krammer, P. H. 2002. Death and anti-death: tumour resistance to apoptosis. *Nat Rev Cancer,* 2**,** 277-88.

Inoue, Y., Tanaka, N., Tanaka, Y., Inoue, S., Morita, K., Zhuang, M., Hattori, T. & Sugamura, K. 2007. Clathrin-dependent entry of severe acute respiratory syndrome coronavirus into target cells expressing ACE2 with the cytoplasmic tail deleted. *J Virol,* 81**,** 8722-9.

Itoh, N. & Nagata, S. 1993. A novel protein domain required for apoptosis. Mutational analysis of human Fas antigen. *Journal of Biological Chemistry,* 268**,** 10932-7.

Jacobs, K. M., Bhave, S. R., Ferraro, D. J., Jaboin, J. J., Hallahan, D. E. & Thotala, D. 2012. GSK-3beta: A Bifunctional Role in Cell Death Pathways. *Int J Cell Biol,* 2012**,** 930710.

Johnson, R. A., Wang, X., Ma, X. L., Huong, S. M. & Huang, E. S. 2001. Human cytomegalovirus up-regulates the phosphatidylinositol 3-kinase (PI3-K) pathway: inhibition of PI3-K activity inhibits viral replication and virus-induced signaling. *J Virol,* 75**,** 6022-32.

Josset, L., Menachery, V. D., Gralinski, L. E., Agnihothram, S., Sova, P., Carter, V. S., Yount, B. L., Graham, R. L., Baric, R. S. & Katze, M. G. 2013. Cell host response to infection with novel human coronavirus EMC predicts potential antivirals and important differences with SARS coronavirus. *MBio,* 4**,** e00165-13.

Jourdan, S. S., Osorio, F. A. & Hiscox, J. A. 2012. Biophysical characterisation of the nucleocapsid protein from a highly pathogenic porcine reproductive and respiratory syndrome virus strain. *Biochem Biophys Res Commun,* 419**,** 137-41.

Kan, X. Z., Yang, J. K., Li, X. F., Chen, L., Lei, Z. P., Wang, M., Qian, C. J., Gao, H. & Yang, Z. Y. 2010. Phylogeny of major lineages of galliform birds (Aves: Galliformes) based on complete mitochondrial genomes. *Genet Mol Res,* 9**,** 1625-33.

Kandun , I. N., Wibisono , H., Sedyaningsih , E. R., Yusharmen, Hadisoedarsuno , W., Purba , W., Santoso , H., Septiawati , C., Tresnaningsih , E., Heriyanto , B., Yuwono , D., Harun , S., Soeroso , S., Giriputra , S., Blair , P. J., Jeremijenko , A., Kosasih , H., Putnam , S. D., Samaan , G., Silitonga , M., Chan , K. H., Poon , L. L. M., Lim , W., Klimov , A., Lindstrom , S., Guan , Y., Donis , R., Katz , J., Cox , N., Peiris , M. & Uyeki , T. M. 2006. Three Indonesian Clusters of H5N1 Virus Infection in 2005. *New England Journal of Medicine,* 355**,** 2186-2194.

Kauffmann-Zeh, A., Rodriguez-Viciana, P., Ulrich, E., Gilbert, C., Coffer, P., Downward, J. & Evan, G. 1997. Suppression of c-Myc-induced apoptosis by Ras signalling through PI(3)K and PKB. *Nature,* 385**,** 544-8.

Kennedy, S. G., Kandel, E. S., Cross, T. K. & Hay, N. 1999. Akt/Protein Kinase B Inhibits Cell Death by Preventing the Release of Cytochrome c from Mitochondria. *Molecular and Cellular Biology,* 19**,** 5800-5810.

Kerr, J. F., Wyllie, A. H. & Currie, A. R. 1972. Apoptosis: a basic biological phenomenon with wide-ranging implications in tissue kinetics. *Br J Cancer,* 26**,** 239-57.

Kerr, M. C., Lindsay, M. R., Luetterforst, R., Hamilton, N., Simpson, F., Parton, R. G., Gleeson, P. A. & Teasdale, R. D. 2006. Visualisation of macropinosome maturation by the recruitment of sorting nexins. *J Cell Sci,* 119**,** 3967-80.

Kerr, M. C. & Teasdale, R. D. 2009. Defining Macropinocytosis. *Traffic,* 10**,** 364-371.

Khaleghpour, K., Pyronnet, S., Gingras, A. C. & Sonenberg, N. 1999. Translational homeostasis: eukaryotic translation initiation factor 4E

control of 4E-binding protein 1 and p70 S6 kinase activities. *Mol Cell Biol,* 19**,** 4302-10.

Kindrachuk, J., Ork, B., Hart, B. J., Mazur, S., Holbrook, M. R., Frieman, M. B., Traynor, D., Johnson, R. F., Dyall, J., Kuhn, J. H., Olinger, G. G., Hensley, L. E. & Jahrling, P. B. 2015. Antiviral Potential of ERK/MAPK and PI3K/AKT/mTOR Signaling Modulation for Middle East Respiratory Syndrome Coronavirus Infection as Identified by Temporal Kinome Analysis. *Antimicrobial Agents and Chemotherapy,* 59**,** 1088-1099.

Kint, J., Dickhout, A., Kutter, J., Maier, H. J., Britton, P., Koumans, J., Pijlman, G. P., Fros, J. J., Wiegertjes, G. F. & Forlenza, M. 2015a. Infectious bronchitis coronavirus inhibits STAT1 signalling and requires accessory proteins for resistance to type I interferon. *Journal of Virology*.

Kint, J., Fernandez-Gutierrez, M., Maier, H. J., Britton, P., Langereis, M. A., Koumans, J., Wiegertjes, G. F. & Forlenza, M. 2015b. Activation of the chicken type I interferon response by infectious bronchitis coronavirus. *J Virol,* 89**,** 1156-67.

Kint, J., Langereis, M. A., Maier, H. J., Britton, P., Van Kuppeveld, F. J., Koumans, J., Wiegertjes, G. F. & Forlenza, M. 2016. Infectious Bronchitis Coronavirus Limits Interferon Production by Inducing a Host Shutoff That Requires Accessory Protein 5b. *Journal of Virology,* 90**,** 7519-7528.

Kischkel, F. C., Hellbardt, S., Behrmann, I., Germer, M., Pawlita, M., Krammer, P. H. & Peter, M. E. 1995. Cytotoxicity-dependent APO-1 (Fas/CD95)-associated proteins form a death-inducing signaling complex (DISC) with the receptor. *Embo j,* 14**,** 5579-88.

Klumperman, J., Locker, J. K., Meijer, A., Horzinek, M. C., Gueze, H. J. & Rottier, P. J. M. 1994. Coronavirus M Proteins Accumulate in the Golgi Complex beyond the Site of Virion Budding. *Journal of Virology,* 68**,** 6523-6534.

Knipe, D. M. & Howley, P. M. E. 2013. Coronaviridae. *Fields Virology.* sixth ed. Philidelphia, PA: Lippincot Williams & Wilkins.

Knoops, K., Kikkert, M., Worm, S. H., Zevenhoven-Dobbe, J. C., Van Der Meer, Y., Koster, A. J., Mommaas, A. M. & Snijder, E. J. 2008. SARS-coronavirus replication is supported by a reticulovesicular network of modified endoplasmic reticulum. *PLoS Biol,* 6**,** e226.

Kopek, B. G., Perkins, G., Miller, D. J., Ellisman, M. H. & Ahlquist, P. 2007. Three-dimensional analysis of a viral RNA replication complex reveals a virus-induced mini-organelle. *PLoS Biol,* 5**,** e220.

Kothakota, S., Azuma, T., Reinhard, C., Klippel, A., Tang, J., Chu, K., Mcgarry, T. J., Kirschner, M. W., Koths, K., Kwiatkowski, D. J. & Williams, L. T. 1997. Caspase-3-generated fragment of gelsolin: effector of morphological change in apoptosis. *Science,* 278**,** 294-8.

Koyama, A. H., Irie, H., Fukumori, T., Hata, S., Iida, S., Akari, H. & Adachi, A. 1998. Role of virus-induced apoptosis in a host defense mechanism against virus infection. *J Med Invest,* 45**,** 37-45.

Krijnse-Locker, J., Ericsson, M., Rottier, P. J. & Griffiths, G. 1994. Characterization of the budding compartment of mouse hepatitis virus:

evidence that transport from the RER to the Golgi complex requires only one vesicular transport step. *J Cell Biol,* 124**,** 55-70.

Kulik, G., Klippel, A. & Weber, M. J. 1997. Antiapoptotic signalling by the insulin-like growth factor I receptor, phosphatidylinositol 3-kinase, and Akt. *Mol Cell Biol,* 17**,** 1595-606.

Lakadamyali, M., Rust, M. J. & Zhuang, X. 2004. Endocytosis of influenza viruses. *Microbes Infect,* 6**,** 929-36.

Lavi, E., Wang, Q., Weiss, S. R. & Gonatas, N. K. 1996. Syncytia formation induced by coronavirus infection is associated with fragmentation and rearrangement of the Golgi apparatus. *Virology,* 221**,** 325-334.

Lee, A. H., Iwakoshi, N. N. & Glimcher, L. H. 2003. XBP-1 regulates a subset of endoplasmic reticulum resident chaperone genes in the unfolded protein response. *Mol Cell Biol,* 23**,** 7448-59.

Lee, C. W., Brown, C. & Jackwood, M. W. 2002. Tissue distribution of avian infectious bronchitis virus following in ovo inoculation of chicken embryos examined by in situ hybridization with antisense digoxigenin-labeled universal riboprobe. *Journal of Veterinary Diagnostic Investigation,* 14**,** 377-381.

Lewis, W. H. 1931. Pinocytosis. *Bulletin of the Johns Hopkins Hospital,* 49**,** 17-27.

Li, F. Q., Tam, J. P. & Liu, D. X. 2007. Cell cycle arrest and apoptosis induced by the coronavirus infectious bronchitis virus in the absence of p53. *Virology,* 365**,** 435-45.

Li , Q., Zhou , L., Zhou , M., Chen , Z., Li , F., Wu , H., Xiang , N., Chen , E., Tang , F., Wang , D., Meng , L., Hong , Z., Tu , W., Cao , Y., Li , L., Ding , F., Liu , B., Wang , M., Xie , R., Gao , R., Li , X., Bai , T., Zou , S., He , J., Hu , J., Xu , Y., Chai , C., Wang , S., Gao , Y., Jin , L., Zhang , Y., Luo , H., Yu , H., He , J., Li , Q., Wang , X., Gao , L., Pang , X., Liu , G., Yan , Y., Yuan , H., Shu , Y., Yang , W., Wang , Y., Wu , F., Uyeki , T. M. & Feng , Z. 2014. Epidemiology of Human Infections with Avian Influenza A(H7N9) Virus in China. *New England Journal of Medicine,* 370**,** 520-532.

Li, W., Moore, M. J., Vasilieva, N., Sui, J., Wong, S. K., Berne, M. A., Somasundaran, M., Sullivan, J. L., Luzuriaga, K., Greenough, T. C., Choe, H. & Farzan, M. 2003. Angiotensin-converting enzyme 2 is a functional receptor for the SARS coronavirus. *Nature,* 426**,** 450-4.

Li, W., Shi, Z., Yu, M., Ren, W., Smith, C., Epstein, J. H., Wang, H., Crameri, G., Hu, Z., Zhang, H., Zhang, J., Mceachern, J., Field, H., Daszak, P., Eaton, B. T., Zhang, S. & Wang, L. F. 2005. Bats are natural reservoirs of SARS-like coronaviruses. *Science,* 310**,** 676-9.

Liao, Y., Fung, T. S., Huang, M., Fang, S. G., Zhong, Y. & Liu, D. X. 2013. Upregulation of CHOP/GADD153 during coronavirus infectious bronchitis virus infection modulates apoptosis by restricting activation of the extracellular signal-regulated kinase pathway. *J Virol,* 87**,** 8124-34.

Liao, Y., Yuan, Q., Torres, J., Tam, J. P. & Liu, D. X. 2006. Biochemical and functional characterization of the membrane association and membrane permeabilizing activity of the severe acute respiratory syndrome coronavirus envelope protein. *Virology,* 349**,** 264-275.

Lim, J. P. & Gleeson, P. A. 2011. Macropinocytosis: an endocytic pathway for internalising large gulps. *Immunol Cell Biol,* 89**,** 836-843.

Lim, J. P., Wang, J. T., Kerr, M. C., Teasdale, R. D. & Gleeson, P. A. 2008. A role for SNX5 in the regulation of macropinocytosis. *BMC Cell Biol,* 9**,** 58.

Lim, K. P. & Liu, D. X. 2001. The missing link in coronavirus assembly - Retention of the avian coronavirus infectious bronchitis virus envelope protein in the pre-Golgi compartments and physical interaction between the envelope and membrane proteins. *Journal of Biological Chemistry,* 276**,** 17515-17523.

Limon, J. J. & Fruman, D. A. 2012. Akt and mTOR in B Cell Activation and Differentiation. *Frontiers in Immunology,* 3**,** 228.

Lin, J. H., Li, H., Yasumura, D., Cohen, H. R., Zhang, C., Panning, B., Shokat, K. M., Lavail, M. M. & Walter, P. 2007. IRE1 signaling affects cell fate during the unfolded protein response. *Science,* 318**,** 944-9.

Lin, P.-Y., Liu, H.-J., Liao, M.-H., Chang, C.-D., Chang, C.-I., Cheng, H.-L., Lee, J.-W. & Shih, W.-L. 2010. Activation of PI 3-kinase/Akt/NF-κB and Stat3 signaling by avian reovirus S1133 in the early stages of infection results in an inflammatory response and delayed apoptosis. *Virology,* 400**,** 104-114.

Lindquist, M. E., Lifland, A. W., Utley, T. J., Santangelo, P. J. & Crowe, J. E., Jr. 2010. Respiratory syncytial virus induces host RNA stress granules to facilitate viral replication. *J Virol,* 84**,** 12274-84.

Liu, C., Xu, H. Y. & Liu, D. X. 2001. Induction of caspase-dependent apoptosis in cultured cells by the avian coronavirus infectious bronchitis virus. *J Virol,* 75**,** 6402-9.

Liu, D. X., Cavanagh, D., Green, P. & Inglis, S. C. 1991. A polycistronic mRNA specified by the coronavirus infectious bronchitis virus. *Virology,* 184**,** 531-44.

Liu, D. X. & Inglis, S. C. 1991a. Association of the Infectious-Bronchitis Virus-3c Protein with the Virion Envelope. *Virology,* 185**,** 911-917.

Liu, D. X. & Inglis, S. C. 1991b. Association of the infectious bronchitis virus 3c protein with the virion envelope. *Virology,* 185**,** 911-7.

Liu, D. X. & Inglis, S. C. 1992a. Identification of two new polypeptides encoded by mRNA5 of the coronavirus infectious bronchitis virus. *Virology,* 186**,** 342-7.

Liu, D. X. & Inglis, S. C. 1992b. Internal entry of ribosomes on a tricistronic mRNA encoded by infectious bronchitis virus. *J Virol,* 66**,** 6143-54.

Liu, Z., Tian, Y., Machida, K., Lai, M. M. C., Luo, G., Foung, S. K. H. & Ou, J.-H. J. 2012. Transient Activation of the PI3K-AKT Pathway by Hepatitis C Virus to Enhance Viral Entry. *Journal of Biological Chemistry,* 287**,** 41922-41930.

Locksley, R. M., Killeen, N. & Lenardo, M. J. 2001. The TNF and TNF receptor superfamilies: integrating mammalian biology. *Cell,* 104**,** 487-501.

Lokugamage, K. G., Narayanan, K., Huang, C. & Makino, S. 2012. Severe Acute Respiratory Syndrome Coronavirus Protein nsp1 Is a Novel Eukaryotic Translation Inhibitor That Represses Multiple Steps of Translation Initiation. *Journal of Virology,* 86**,** 13598-13608.

Lontok, E., Corse, E. & Machamer, C. E. 2004. Intracellular targeting signals contribute to localization of coronavirus spike proteins near the virus assembly site. *J Virol,* 78**,** 5913-22.

Lucio, B. & Fabricant, J. 1990. Tissue Tropism of 3 Cloacal Isolates and Massachusetts Strain of Infectious-Bronchitis Virus. *Avian Diseases,* 34**,** 865-870.

Ma, X. M. & Blenis, J. 2009. Molecular mechanisms of mTOR-mediated translational control. *Nat Rev Mol Cell Biol,* 10**,** 307-18.

Mader, S., Lee, H., Pause, A. & Sonenberg, N. 1995. The translation initiation factor eIF-4E binds to a common motif shared by the translation factor eIF-4 gamma and the translational repressors 4E-binding proteins. *Mol Cell Biol,* 15**,** 4990-7.

Maehama, T. & Dixon, J. E. 1998. The tumor suppressor, PTEN/MMAC1, dephosphorylates the lipid second messenger, phosphatidylinositol 3,4,5-trisphosphate. *J Biol Chem,* 273**,** 13375-8.

Mahajan, K. & Mahajan, N. P. 2012. PI3K-independent AKT activation in cancers: a treasure trove for novel therapeutics. *J Cell Physiol,* 227**,** 3178-84.

Maier, H. J., Cottam, E. M., Stevenson-Leggett, P., Wilkinson, J. A., Harte, C. J., Wileman, T. & Britton, P. 2013a. Visualizing the autophagy pathway in avian cells and its application to studying infectious bronchitis virus. *Autophagy,* 9**,** 496-509.

Maier, H. J., Hawes, P. C., Cottam, E. M., Mantell, J., Verkade, P., Monaghan, P., Wileman, T. & Britton, P. 2013b. Infectious bronchitis virus generates spherules from zippered endoplasmic reticulum membranes. *MBio,* 4**,** e00801-13.

Makino, S., Joo, M. & Makino, J. K. 1991. A system for study of coronavirus mRNA synthesis: a regulated, expressed subgenomic defective interfering RNA results from intergenic site insertion. *J Virol,* 65**,** 6031-41.

Maréchal, V., Prevost, M.-C., Petit, C., Perret, E., Heard, J.-M. & Schwartz, O. 2001. Human Immunodeficiency Virus Type 1 Entry into Macrophages Mediated by Macropinocytosis. *Journal of Virology,* 75**,** 11166-11177.

Mcdonnell, M. A., Wang, D., Khan, S. M., Vander Heiden, M. G. & Kelekar, A. 2003. Caspase-9 is activated in a cytochrome c-independent manner early during TNFalpha-induced apoptosis in murine cells. *Cell Death Differ,* 10**,** 1005-15.

Meir, R., Rosenblut, E., Perl, S., Kass, N., Ayali, G., Hemsani, E. & Perk, S. 2004. Identification of a Novel Nephropathogenic Infectious Bronchitis Virus in Israel. *Avian Diseases,* 48**,** 635-641.

Mercer, J. & Helenius, A. 2008. Vaccinia virus uses macropinocytosis and apoptotic mimicry to enter host cells. *Science,* 320**,** 531-5.

Mercer, J. & Helenius, A. 2009. Virus entry by macropinocytosis. *Nat Cell Biol,* 11**,** 510-20.

Mercer, J. & Helenius, A. 2012. Gulping rather than sipping: macropinocytosis as a way of virus entry. *Curr Opin Microbiol,* 15**,** 490-9.

Mercer, J., Knebel, S., Schmidt, F. I., Crouse, J., Burkard, C. & Helenius, A. 2010. Vaccinia virus strains use distinct forms of macropinocytosis for host-cell entry. *Proc Natl Acad Sci U S A,* 107**,** 9346-51.

Miguel, B., Pharr, G. T. & Wang, C. 2002. The role of feline aminopeptidase N as a receptor for infectious bronchitis virus. Brief review. *Arch Virol,* 147**,** 2047-56.

Miron, M., Lasko, P. & Sonenberg, N. 2003. Signaling from Akt to FRAP/TOR targets both 4E-BP and S6K in Drosophila melanogaster. *Mol Cell Biol,* 23**,** 9117-26.

Mitsuhashi, M. 1996a. Technical report: Part 1. Basic requirements for designing optimal oligonucleotide probe sequences. *J Clin Lab Anal,* 10**,** 277-84.

Mitsuhashi, M. 1996b. Technical report: Part 2. Basic requirements for designing optimal PCR primers. *J Clin Lab Anal,* 10**,** 285-93.

Moiseyeva, I. G., Romanov, M. N., Nikiforov, A. A., Sevastyanova, A. A. & Semyenova, S. K. 2003. Evolutionary relationships of Red Jungle Fowl and chicken breeds. *Genet Sel Evol,* 35**,** 403-23.

Mori, I., Komatsu, T., Takeuchi, K., Nakakuki, K., Sudo, M. & Kimura, Y. 1995. In vivo induction of apoptosis by influenza virus. *J Gen Virol,* 76 ( Pt 11)**,** 2869-73.

Nagata, S. & Golstein, P. 1995. The Fas death factor. *Science,* 267**,** 1449-56.

Nakase, I., Kobayashi, N. B., Takatani-Nakase, T. & Yoshida, T. 2015. Active macropinocytosis induction by stimulation of epidermal growth factor receptor and oncogenic Ras expression potentiates cellular uptake efficacy of exosomes. *Scientific Reports,* 5**,** 10300.

Narayanan, K., Huang, C. & Makino, S. 2008. SARS coronavirus accessory proteins. *Virus Res,* 133**,** 113-21.

Narayanan, K., Maeda, A., Maeda, J. & Makino, S. 2000. Characterization of the Coronavirus M Protein and Nucleocapsid Interaction in Infected Cells. *Journal of Virology,* 74**,** 8127-8134.

Nemeroff, M. E., Barabino, S. M., Li, Y., Keller, W. & Krug, R. M. 1998. Influenza virus NS1 protein interacts with the cellular 30 kDa subunit of CPSF and inhibits 3'end formation of cellular pre-mRNAs. *Mol Cell,* 1**,** 991-1000.

Neri, L. M., Borgatti, P., Capitani, S. & Martelli, A. M. 2002. The nuclear phosphoinositide 3-kinase/AKT pathway: a new second messenger system. *Biochim Biophys Acta,* 1584**,** 73-80.

Neuman, B. W., Kiss, G., Kunding, A. H., Bhella, D., Baksh, M. F., Connelly, S., Droese, B., Klaus, J. P., Makino, S., Sawicki, S. G., Siddell, S. G., Stamou, D. G., Wilson, I. A., Kuhn, P. & Buchmeier, M. J. 2011. A structural analysis of M protein in coronavirus assembly and morphology. *Journal of structural biology,* 174**,** 11-22.

Noah, D. L., Twu, K. Y. & Krug, R. M. 2003. Cellular antiviral responses against influenza A virus are countered at the posttranscriptional level by the viral NS1A protein via its binding to a cellular protein required for the 3' end processing of cellular pre-mRNAS. *Virology,* 307**,** 386-95.

Norbury, C. J. & Hickson, I. D. 2001. Cellular responses to DNA damage. *Annu Rev Pharmacol Toxicol,* 41**,** 367-401.

Ochs, K., Rust, R. C. & Niepmann, M. 1999. Translation initiation factor eIF4B interacts with a picornavirus internal ribosome entry site in both 48S and 80S initiation complexes independently of initiator AUG location. *J Virol,* 73**,** 7505-14.

Orvedahl, A., Macpherson, S., Sumpter, R., Talloczy, Z., Zou, Z. J. & Levine, B. 2010. Autophagy Protects against Sindbis Virus Infection of the Central Nervous System. *Cell Host & Microbe,* 7**,** 115-127.

Pause, A., Belsham, G. J., Gingras, A. C., Donze, O., Lin, T. A., Lawrence, J. C., Jr. & Sonenberg, N. 1994. Insulin-dependent stimulation of protein synthesis by phosphorylation of a regulator of 5'-cap function. *Nature,* 371**,** 762-7.

Pérez-Gil, G., Landa-Cardeña, A., Coutiño, R., García-Román, R., Sampieri, C. L., Mora, S. I. & Montero, H. 2015. 4EBP1 Is Dephosphorylated by Respiratory Syncytial Virus Infection. *Intervirology,* 58**,** 205-208.

Pernet, O., Pohl, C., Ainouze, M., Kweder, H. & Buckland, R. 2009. Nipah virus entry can occur by macropinocytosis. *Virology,* 395**,** 298-311.

Persad, S., Attwell, S., Gray, V., Delcommenne, M., Troussard, A., Sanghera, J. & Dedhar, S. 2000. Inhibition of integrin-linked kinase (ILK) suppresses activation of protein kinase B/Akt and induces cell cycle arrest and apoptosis of PTEN-mutant prostate cancer cells. *Proc Natl Acad Sci U S A,* 97**,** 3207-12.

Peter, B. J., Kent, H. M., Mills, I. G., Vallis, Y., Butler, P. J. G., Evans, P. R. & Mcmahon, H. T. 2004. BAR Domains as Sensors of Membrane Curvature: The Amphiphysin BAR Structure. *Science,* 303**,** 495.

Pfaffl, M. W., Tichopad, A., Prgomet, C. & Neuvians, T. P. 2004. Determination of stable housekeeping genes, differentially regulated target genes and sample integrity: BestKeeper--Excel-based tool using pair-wise correlations. *Biotechnol Lett,* 26**,** 509-15.

Planz, O. 2013. Development of cellular signaling pathway inhibitors as new antivirals against influenza. *Antiviral Res,* 98**,** 457-68.

Porta, C. & Figlin, R. A. 2009. Phosphatidylinositol-3-kinase/Akt signaling pathway and kidney cancer, and the therapeutic potential of phosphatidylinositol-3-kinase/Akt inhibitors. *J Urol,* 182**,** 2569-77.

Prentice, E., Jerome, W. G., Yoshimori, T., Mizushima, N. & Denison, M. R. 2004. Coronavirus replication complex formation utilizes components of cellular autophagy. *Journal of Biological Chemistry,* 279**,** 10136-10141.

Promkuntod, N., Van Eijndhoven, R. E., De Vrieze, G., Grone, A. & Verheije, M. H. 2014. Mapping of the receptor-binding domain and amino acids critical for attachment in the spike protein of avian coronavirus infectious bronchitis virus. *Virology,* 448**,** 26-32.

Pujhari, S., Kryvvoruchko, M. & Zakhartchouk, A. N. 2014. Role of phosphatidylinositol-3-kinase (PI3K) and the mammalian target of rapamycin (mTOR) signalling pathways in porcine reproductive and respiratory syndrome virus (PRRSV) replication. *Virus Research,* 194**,** 138-144.

Raj, G. D. & Jones, R. C. 1997. Infectious bronchitis virus: Immunopathogenesis of infection in the chicken. *Avian Pathol,* 26**,** 677-706.

Rajesh, K., Krishnamoorthy, J., Kazimierczak, U., Tenkerian, C., Papadakis, A. I., Wang, S., Huang, S. & Koromilas, A. E. 2015. Phosphorylation of the translation initiation factor eIF2alpha at serine 51 determines the cell fate decisions of Akt in response to oxidative stress. *Cell Death Dis,* 6**,** e1591.

Ratcliffe, M. J. 2006. Antibodies, immunoglobulin genes and the bursa of Fabricius in chicken B cell development. *Dev Comp Immunol,* 30**,** 101-18.

Ravindra, P. V., Tiwari, A. K., Ratta, B., Chaturvedi, U., Palia, S. K., Subudhi, P. K., Kumar, R., Sharma, B., Rai, A. & Chauhan, R. S. 2008a. Induction of apoptosis in Vero cells by Newcastle disease virus requires viral replication, de-novo protein synthesis and caspase activation. *Virus Res,* 133**,** 285-90.

Ravindra, P. V., Tiwari, A. K., Sharma, B., Rajawat, Y. S., Ratta, B., Palia, S., Sundaresan, N. R., Chaturvedi, U., Gangaplara, A., Chindera, K., Saxena, M., Subudhi, P. K., Rai, A. & Chauhan, R. S. 2008b. HN protein of Newcastle disease virus causes apoptosis in chicken embryo fibroblast cells. *Arch Virol,* 153**,** 749-54.

Ridley, A. J. 1994. Membrane ruffling and signal transduction. *BioEssays,* 16**,** 321-327.

Rodriguez-Viciana, P. & Downward, J. 2001. Ras activation of phosphatidylinositol 3-kinase and Akt. *Methods Enzymol,* 333**,** 37-44.

Rodriguez, A., Rodriguez, M., Cordoba, J. J. & Andrade, M. J. 2015. Design of primers and probes for quantitative real-time PCR methods. *Methods Mol Biol,* 1275**,** 31-56.

Romanov, M. N., Tuttle, E. M., Houck, M. L., Modi, W. S., Chemnick, L. G., Korody, M. L., Mork, E. M. S., Otten, C. A., Renner, T., Jones, K. C., Dandekar, S., Papp, J. C., Da, Y., Green, E. D., Magrini, V., Hickenbotham, M. T., Glasscock, J., Mcgrath, S., Mardis, E. R. & Ryder, O. A. 2009. The value of avian genomics to the conservation of wildlife. *BMC Genomics,* 10**,** 1-19.

Ron, D. & Walter, P. 2007. Signal integration in the endoplasmic reticulum unfolded protein response. *Nat Rev Mol Cell Biol,* 8**,** 519-29.

Rossman, J. S., Leser, G. P. & Lamb, R. A. 2012. Filamentous influenza virus enters cells via macropinocytosis. *J Virol,* 86**,** 10950-60.

Royall, E., Doyle, N., Abdul-Wahab, A., Emmott, E., Morley, S. J., Goodfellow, I., Roberts, L. O. & Locker, N. 2015. Murine Norovirus 1 (MNV1) Replication Induces Translational Control of the Host by Regulating eIF4E Activity during Infection. *Journal of Biological Chemistry,* 290**,** 4748-4758.

Ruch, T. R. & Machamer, C. E. 2011. The Hydrophobic Domain of Infectious Bronchitis Virus E Protein Alters the Host Secretory Pathway and Is Important for Release of Infectious Virus. *Journal of Virology,* 85**,** 675-685.

Ruch, T. R. & Machamer, C. E. 2012. The Coronavirus E Protein: Assembly and Beyond. *Viruses-Basel,* 4**,** 363-382.

Rupper, A., Lee, K., Knecht, D. & Cardelli, J. 2001. Sequential activities of phosphoinositide 3-kinase, PKB/Aakt, and Rab7 during macropinosome formation in Dictyostelium. *Mol Biol Cell,* 12**,** 2813-24.

Sable, C. L., Filippa, N., Hemmings, B. & Van Obberghen, E. 1997. cAMP stimulates protein kinase B in a Wortmannin-insensitive manner. *FEBS Lett,* 409**,** 253-7.

Saeed, M. F., Kolokoltsov, A. A., Albrecht, T. & Davey, R. A. 2010. Cellular Entry of Ebola Virus Involves Uptake by a Macropinocytosis-Like Mechanism and Subsequent Trafficking through Early and Late Endosomes. *PLoS Pathog,* 6**,** e1001110.

Saji, M. & Ringel, M. D. 2010. The PI3K-Akt-mTOR pathway in initiation and progression of thyroid tumors. *Mol Cell Endocrinol,* 321**,** 20-8.

Sanchez, E. G., Quintas, A., Perez-Nunez, D., Nogal, M., Barroso, S., Carrascosa, A. L. & Revilla, Y. 2012. African Swine Fever Virus Uses Macropinocytosis to Enter Host Cells. *Plos Pathogens,* 8.

Sarbassov, D. D., Guertin, D. A., Ali, S. M. & Sabatini, D. M. 2005. Phosphorylation and regulation of Akt/PKB by the rictor-mTOR complex. *Science,* 307**,** 1098-101.

Sawicki, S. G., Sawicki, D. L. & Siddell, S. G. 2007. A contemporary view of coronavirus transcription. *J Virol,* 81**,** 20-9.

Schaffer, F. L., Ehresmann, D. W., Fretz, M. K. & Soergel, M. I. 1980. A protein, VPg, covalently linked to 36S calicivirus RNA. *J Gen Virol,* 47**,** 215-20.

Schalk, A. F. & Hawn, M. C. 1931. An apparently new respiratory disease of baby chicks. *Journal of American Veterinary Medical Association,* 78**,** 413-422.

Schlegel, A., Giddings, T. H., Jr., Ladinsky, M. S. & Kirkegaard, K. 1996. Cellular origin and ultrastructure of membranes induced during poliovirus infection. *J Virol,* 70**,** 6576-88.

Schultze, B., Gross, H. J., Brossmer, R., Klenk, H. D. & Herrler, G. 1990. Hemagglutinating encephalomyelitis virus attaches to N-acetyl-9-O-acetylneuraminic acid-containing receptors on erythrocytes: comparison with bovine coronavirus and influenza C virus. *Virus Res,* 16**,** 185-94.

Schultze, B. & Herrler, G. 1992. Bovine coronavirus uses N-acetyl-9-O-acetylneuraminic acid as a receptor determinant to initiate the infection of cultured cells. *J Gen Virol,* 73 ( Pt 4)**,** 901-6.

Schulze-Osthoff, K., Ferrari, D., Los, M., Wesselborg, S. & Peter, M. E. 1998. Apoptosis signaling by death receptors. *Eur J Biochem,* 254**,** 439-59.

Sharma, N. R., Mani, P., Nandwani, N., Mishra, R., Rana, A. & Sarkar, D. P. 2010. Reciprocal Regulation of AKT and MAP Kinase Dictates Virus-Host Cell Fusion. *Journal of Virology,* 84**,** 4366-4382.

Shiozaki, E. N., Chai, J. & Shi, Y. 2002. Oligomerization and activation of caspase-9, induced by Apaf-1 CARD. *Proceedings of the National Academy of Sciences,* 99**,** 4197-4202.

Shukla, S., Maclennan, G. T., Hartman, D. J., Fu, P., Resnick, M. I. & Gupta, S. 2007. Activation of PI3K-Akt signaling pathway promotes prostate cancer cell invasion. *Int J Cancer,* 121**,** 1424-32.

Siu, Y. L., Teoh, K. T., Lo, J., Chan, C. M., Kien, F., Escriou, N., Tsao, S. W., Nicholls, J. M., Altmeyer, R., Peiris, J. S. M., Bruzzone, R. & Nal, B. 2008. The M, E, and N Structural Proteins of the Severe Acute Respiratory Syndrome Coronavirus Are Required for Efficient

Assembly, Trafficking, and Release of Virus-Like Particles. *Journal of Virology,* 82**,** 11318-11330.

Snijder, E. J., Van Der Meer, Y., Zevenhoven-Dobbe, J., Onderwater, J. J., Van Der Meulen, J., Koerten, H. K. & Mommaas, A. M. 2006. Ultrastructure and origin of membrane vesicles associated with the severe acute respiratory syndrome coronavirus replication complex. *J Virol,* 80**,** 5927-40.

Soares, J. a. P., Leite, F. G. G., Andrade, L. G., Torres, A. A., De Sousa, L. P., Barcelos, L. S., Teixeira, M. M., Ferreira, P. C. P., Kroon, E. G., Souto-Padrón, T. & Bonjardim, C. A. 2009. Activation of the PI3K/Akt Pathway Early during Vaccinia and Cowpox Virus Infections Is Required for both Host Survival and Viral Replication. *Journal of Virology,* 83**,** 6883-6899.

Spencer, K. A. & Hiscox, J. A. 2006. Characterisation of the RNA binding properties of the coronavirus infectious bronchitis virus nucleocapsid protein amino-terminal region. *FEBS Lett,* 580**,** 5993-8.

Staines, K., Batra, A., Mwangi, W., Maier, H. J., Van Borm, S., Young, J. R., Fife, M. & Butter, C. 2016. A Versatile Panel of Reference Gene Assays for the Measurement of Chicken mRNA by Quantitative PCR. *PLoS ONE,* 11**,** e0160173.

Stambolic, V. & Woodgett, J. R. 2006. Functional distinctions of protein kinase B/Akt isoforms defined by their influence on cell migration. *Trends Cell Biol,* 16**,** 461-6.

Stennicke, H. R., Jürgensmeier, J. M., Shin, H., Deveraux, Q., Wolf, B. B., Yang, X., Zhou, Q., Ellerby, H. M., Ellerby, L. M., Bredesen, D., Green, D. R., Reed, J. C., Froelich, C. J. & Salvesen, G. S. 1998. Pro-caspase-3 Is a Major Physiologic Target of Caspase-8. *Journal of Biological Chemistry,* 273**,** 27084-27090.

Stephens, L., Anderson, K., Stokoe, D., Erdjument-Bromage, H., Painter, G. F., Holmes, A. B., Gaffney, P. R., Reese, C. B., Mccormick, F., Tempst, P., Coadwell, J. & Hawkins, P. T. 1998. Protein kinase B kinases that mediate phosphatidylinositol 3,4,5-trisphosphate-dependent activation of protein kinase B. *Science,* 279**,** 710-4.

Sun, L., Lv, F., Guo, X. & Gao, G. 2012. Glycogen synthase kinase 3beta (GSK3beta) modulates antiviral activity of zinc-finger antiviral protein (ZAP). *J Biol Chem,* 287**,** 22882-8.

Surjit, M., Liu, B., Jameel, S., Chow, V. T. & Lal, S. K. 2004. The SARS coronavirus nucleocapsid protein induces actin reorganization and apoptosis in COS-1 cells in the absence of growth factors. *Biochem J,* 383**,** 13-8.

Sweeney, T. R., Abaeva, I. S., Pestova, T. V. & Hellen, C. U. 2014. The mechanism of translation initiation on Type 1 picornavirus IRESs. *Embo j,* 33**,** 76-92.

Tait, J. F., Gibson, D. F. & Smith, C. 2004. Measurement of the affinity and cooperativity of annexin V-membrane binding under conditions of low membrane occupancy. *Analytical Biochemistry,* 329**,** 112-119.

Takizawa, T., Matsukawa, S., Higuchi, Y., Nakamura, S., Nakanishi, Y. & Fukuda, R. 1993. Induction of programmed cell death (apoptosis) by influenza virus infection in tissue culture cells. *J Gen Virol,* 74 ( Pt 11)**,** 2347-55.

Takizawa, T., Tatematsu, C., Ohashi, K. & Nakanishi, Y. 1999. Recruitment of apoptotic cysteine proteases (caspases) in influenza virus-induced cell death. *Microbiol Immunol,* 43**,** 245-52.

Tay, F. P., Huang, M., Wang, L., Yamada, Y. & Liu, D. X. 2012. Characterization of cellular furin content as a potential factor determining the susceptibility of cultured human and animal cells to coronavirus infectious bronchitis virus infection. *Virology,* 433**,** 421-30.

Terregino, C., Toffan, A., Serena Beato, M., De Nardi, R., Vascellari, M., Meini, A., Ortali, G., Mancin, M. & Capua, I. 2008. Pathogenicity of a QX strain of infectious bronchitis virus in specific pathogen free and commercial broiler chickens, and evaluation of protection induced by a vaccination programme based on the Ma5 and 4/91 serotypes. *Avian Pathology,* 37**,** 487-493.

Thomas, C. C., Deak, M., Alessi, D. R. & Van Aalten, D. M. F. High-Resolution Structure of the Pleckstrin Homology Domain of Protein Kinase B/Akt Bound to Phosphatidylinositol (3,4,5)-Trisphosphate. *Current Biology,* 12**,** 1256-1262.

Tooze, J., Tooze, S. & Warren, G. 1984. Replication of coronavirus MHV-A59 in sac- cells: determination of the first site of budding of progeny virions. *Eur J Cell Biol,* 33**,** 281-93.

Tooze, J., Tooze, S. A. & Fuller, S. D. 1987. Sorting of progeny coronavirus from condensed secretory proteins at the exit from the trans-Golgi network of AtT20 cells. *J Cell Biol,* 105**,** 1215-26.

Tran, A. T., Cortens, J. P., Du, Q., Wilkins, J. A. & Coombs, K. M. 2013. Influenza Virus Induces Apoptosis via BAD-Mediated Mitochondrial Dysregulation. *Journal of Virology,* 87**,** 1049-1060.

Tresnan, D. B., Levis, R. & Holmes, K. V. 1996. Feline aminopeptidase N serves as a receptor for feline, canine, porcine, and human coronaviruses in serogroup I. *Journal of Virology,* 70**,** 8669-74.

Tsoi, H., Li, L., Chen, Z. S., Lau, K. F., Tsui, S. K. & Chan, H. Y. 2014. The SARS-coronavirus membrane protein induces apoptosis via interfering with PDK1-PKB/Akt signalling. *Biochem J,* 464**,** 439-47.

Ulasli, M., Verheije, M. H., De Haan, C. a. M. & Reggiori, F. 2010. Qualitative and quantitative ultrastructural analysis of the membrane rearrangements induced by coronavirus. *Cellular Microbiology,* 12**,** 844-861.

Van Der Most, R. G., De Groot, R. J. & Spaan, W. J. 1994. Subgenomic RNA synthesis directed by a synthetic defective interfering RNA of mouse hepatitis virus: a study of coronavirus transcription initiation. *J Virol,* 68**,** 3656-66.

Van Der Most, R. G. & Spaan, W. J. M. 1995. Coronavirus Replication, Transcription, and RNA Recombination. *In:* SIDDELL, S. G. (ed.) *The Coronaviridae.* Boston, MA: Springer US.

Van Vliet, A. L. W., Smits, S. L., Rottier, P. J. M. & De Groot, R. J. 2002. Discontinuous and non-discontinuous subgenomic RNA transcription in a nidovirus. *The EMBO Journal,* 21**,** 6571-6580.

Vandekerchove, D., De Herdt, P., Laevens, H. & Pasmans, F. 2004. Risk factors associated with colibacillosis outbreaks in caged layer flocks. *Avian Pathol,* 33**,** 337-42.

Vandesompele, J., De Preter, K., Pattyn, F., Poppe, B., Van Roy, N., De Paepe, A. & Speleman, F. 2002. Accurate normalization of real-time quantitative RT-PCR data by geometric averaging of multiple internal control genes. *Genome Biol,* 3**,** RESEARCH0034.

Vandesompele J., D. P. K., Pattyn F., Poppe B., Van Roy N., De Paepe A., Speleman F. 2002. Accurate normalization of real-time quantitative RT-PCR data by geometric averaging of multiple internal control genes. *Genome Biology,* 3**,** 1-12.

Vanhaesebroeck, B., Leevers, S. J., Panayotou, G. & Waterfield, M. D. 1997. Phosphoinositide 3-kinases: a conserved family of signal transducers. *Trends Biochem Sci,* 22**,** 267-72.

Veithen, A., Amyere, M., Van Der Smissen, P., Cupers, P. & Courtoy, P. J. 1998. Regulation of macropinocytosis in v-Src-transformed fibroblasts: cyclic AMP selectively promotes regurgitation of macropinosomes. *J Cell Sci,* 111 ( Pt 16)**,** 2329-35.

Vlahos, C. J., Matter, W. F., Hui, K. Y. & Brown, R. F. 1994. A specific inhibitor of phosphatidylinositol 3-kinase, 2-(4-morpholinyl)-8-phenyl-4H-1-benzopyran-4-one (LY294002). *J Biol Chem,* 269**,** 5241-8.

Vlasak, R., Luytjes, W., Spaan, W. & Palese, P. 1988. Human and bovine coronaviruses recognize sialic acid-containing receptors similar to those of influenza C viruses. *Proc Natl Acad Sci U S A,* 85**,** 4526-9.

Wanderley, J. L., Moreira, M. E., Benjamin, A., Bonomo, A. C. & Barcinski, M. A. 2006. Mimicry of apoptotic cells by exposing phosphatidylserine participates in the establishment of amastigotes of Leishmania (L) amazonensis in mammalian hosts. *J Immunol,* 176**,** 1834-9.

Wang, J. T., Teasdale, R. D. & Liebl, D. 2014a. Macropinosome quantitation assay. *MethodsX,* 1**,** 36-41.

Wang, J. T. H., Kerr, M. C., Karunaratne, S., Jeanes, A., Yap, A. S. & Teasdale, R. D. 2010. The SNX-PX-BAR Family in Macropinocytosis: The Regulation of Macropinosome Formation by SNX-PX-BAR Proteins. *PLoS ONE,* 5**,** e13763.

Wang, L. F. & Eaton, B. T. 2007. Bats, civets and the emergence of SARS. *Curr Top Microbiol Immunol,* 315**,** 325-44.

Wang, Q., Qi, J., Yuan, Y., Xuan, Y., Han, P., Wan, Y., Ji, W., Li, Y., Wu, Y., Wang, J., Iwamoto, A., Woo, P. C., Yuen, K. Y., Yan, J., Lu, G. & Gao, G. F. 2014b. Bat origins of MERS-CoV supported by bat coronavirus HKU4 usage of human receptor CD26. *Cell Host Microbe,* 16**,** 328-37.

Wang, X., Zhang, H., Abel, A. M., Young, A. J., Xie, L. & Xie, Z. 2014c. Role of phosphatidylinositol 3-kinase (PI3K) and Akt1 kinase in porcine reproductive and respiratory syndrome virus (PRRSV) replication. *Arch Virol,* 159**,** 2091-6.

Waskiewicz, A. J., Flynn, A., Proud, C. G. & Cooper, J. A. 1997. Mitogen-activated protein kinases activate the serine/threonine kinases Mnk1 and Mnk2. *The EMBO Journal,* 16**,** 1909-1920.

Watarai, M., Derre, I., Kirby, J., Growney, J. D., Dietrich, W. F. & Isberg, R. R. 2001. Legionella pneumophila Is Internalized by a Macropinocytotic Uptake Pathway Controlled by the Dot/Icm System and the Mouse Lgn1 Locus(✪). *The Journal of Experimental Medicine,* 194**,** 1081-1096.

Wei, L., Hou, L., Zhu, S., Wang, J., Zhou, J. & Liu, J. 2011. Infectious bursal disease virus activates the phosphatidylinositol 3-kinase (PI3K)/Akt signaling pathway by interaction of VP5 protein with the p85alpha subunit of PI3K. *Virology,* 417**,** 211-20.

Wei, M. C., Zong, W. X., Cheng, E. H. Y., Lindsten, T., Panoutsakopoulou, V., Ross, A. J., Roth, K. A., Macgregor, G. R., Thompson, C. B. & Korsmeyer, S. J. 2001. Proapoptotic BAX and BAK: A requisite gateway to mitochondrial dysfunction and death. *Science,* 292**,** 727-730.

Westneat, D. F. 1992. *Journal of Field Ornithology,* 63**,** 380-384.

Williams, R. K., Jiang, G. S. & Holmes, K. V. 1991. Receptor for mouse hepatitis virus is a member of the carcinoembryonic antigen family of glycoproteins. *Proceedings of the National Academy of Sciences of the United States of America,* 88**,** 5533-5536.

Winter, C., Schwegmann-Wessels, C., Cavanagh, D., Neumann, U. & Herrler, G. 2006. Sialic acid is a receptor determinant for infection of cells by avian Infectious bronchitis virus. *J Gen Virol,* 87**,** 1209-16.

Winterfield, R. W. & Albassam, M. A. 1984. Nephropathogenicity of infectious bronchitis virus. *Poult Sci,* 63**,** 2358-63.

Wojcechowskyj, J. A., Didigu, C. A., Lee, J. Y., Parrish, N. F., Sinha, R., Hahn, B. H., Bushman, F. D., Jensen, S. T., Seeholzer, S. H. & Doms, R. W. 2013. Quantitative phosphoproteomics reveals extensive cellular reprogramming during HIV-1 entry. *Cell Host Microbe,* 13**,** 613-23.

Wurzer, W. J., Planz, O., Ehrhardt, C., Giner, M., Silberzahn, T., Pleschka, S. & Ludwig, S. 2003. Caspase 3 activation is essential for efficient influenza virus propagation. *The EMBO Journal,* 22**,** 2717.

Yamada, Y., Liu, X. B., Fang, S. G., Tay, F. P. & Liu, D. X. 2009. Acquisition of cell-cell fusion activity by amino acid substitutions in spike protein determines the infectivity of a coronavirus in cultured cells. *PLoS One,* 4**,** e6130.

Yamaguchi, H. & Wang, H. G. 2001. The protein kinase PKB/Akt regulates cell survival and apoptosis by inhibiting Bax conformational change. *Oncogene,* 20**,** 7779-7786.

Yang, Z. Y., Huang, Y., Ganesh, L., Leung, K., Kong, W. P., Schwartz, O., Subbarao, K. & Nabel, G. J. 2004a. pH-dependent entry of severe acute respiratory syndrome coronavirus is mediated by the spike glycoprotein and enhanced by dendritic cell transfer through DC-SIGN. *J Virol,* 78**,** 5642-50.

Yang, Z. Z., Tschopp, O., Baudry, A., Dummler, B., Hynx, D. & Hemmings, B. A. 2004b. Physiological functions of protein kinase B/Akt. *Biochem Soc Trans,* 32**,** 350-4.

Yang, Z. Z., Tschopp, O., Hemmings-Mieszczak, M., Feng, J., Brodbeck, D., Perentes, E. & Hemmings, B. A. 2003. Protein kinase B alpha/Akt1 regulates placental development and fetal growth. *J Biol Chem,* 278**,** 32124-31.

Yano, S., Tokumitsu, H. & Soderling, T. R. 1998. Calcium promotes cell survival through CaM-K kinase activation of the protein-kinase-B pathway. *Nature,* 396**,** 584-7.

Yao, R. & Cooper, G. M. 1995. Requirement for phosphatidylinositol-3 kinase in the prevention of apoptosis by nerve growth factor. *Science,* 267**,** 2003-2006.

Yeager, C. L., Ashmun, R. A., Williams, R. K., Cardellichio, C. B., Shapiro, L. H., Look, A. T. & Holmes, K. V. 1992. Human aminopeptidase N is a receptor for human coronavirus 229E. *Nature,* 357**,** 420-2.

Yoganathan, T. N., Costello, P., Chen, X., Jabali, M., Yan, J., Leung, D., Zhang, Z., Yee, A., Dedhar, S. & Sanghera, J. 2000. Integrin-linked kinase (ILK): a "hot" therapeutic target. *Biochem Pharmacol,* 60**,** 1115-9.

Yonehara, S., Ishii, A. & Yonehara, M. 1989. A cell-killing monoclonal antibody (anti-Fas) to a cell surface antigen co-downregulated with the receptor of tumor necrosis factor. *J Exp Med,* 169**,** 1747-56.

Yoshida, H., Matsui, T., Yamamoto, A., Okada, T. & Mori, K. 2001. XBP1 mRNA is induced by ATF6 and spliced by IRE1 in response to ER stress to produce a highly active transcription factor. *Cell,* 107**,** 881-91.

Yoshida, S., Gaeta, I., Pacitto, R., Krienke, L., Alge, O., Gregorka, B. & Swanson, J. A. 2015. Differential signaling during macropinocytosis in response to M-CSF and PMA in macrophages. *Frontiers in Physiology,* 6**,** 8.

Youn, S., Collisson, E. W. & Machamer, C. E. 2005. Contribution of trafficking signals in the cytoplasmic tail of the infectious bronchitis virus spike protein to virus infection. *J Virol,* 79**,** 13209-17.

Yu, X., Bi, W. Z., Weiss, S. R. & Leibowitz, J. L. 1994. Mouse Hepatitis-Virus Gene 5b Protein Is a New Virion Envelope Protein. *Virology,* 202**,** 1018-1023.

Zhang, X. & Lai, M. M. 1994. Unusual heterogeneity of leader-mRNA fusion in a murine coronavirus: implications for the mechanism of RNA transcription and recombination. *Journal of Virology,* 68**,** 6626-6633.

Zhang, Y., Burke, C. W., Ryman, K. D. & Klimstra, W. B. 2007. Identification and characterization of interferon-induced proteins that inhibit alphavirus replication. *J Virol,* 81**,** 11246-55.

Zhirnov, O. P. & Klenk, H. D. 2007. Control of apoptosis in influenza virus-infected cells by up-regulation of Akt and p53 signaling. *Apoptosis,* 12**,** 1419-32.

Zhirnov, O. P., Konakova, T. E., Wolff, T. & Klenk, H.-D. 2002. NS1 Protein of Influenza A Virus Down-Regulates Apoptosis. *Journal of Virology,* 76**,** 1617-1625.

Zhong, Q., Hu, Y. X., Jin, J. H., Zhao, Y., Zhao, J. & Zhang, G. Z. 2016. Pathogenicity of virulent infectious bronchitis virus isolate YN on hen ovary and oviduct. *Vet Microbiol,* 193**,** 100-5.

Zhu, L., Ding, X. Y., Zhu, X. F., Meng, S. S., Wang, J. Y., Zhou, H., Duan, Q. D., Tao, J., Schifferli, D. M. & Zhu, G. Q. 2011a. Biphasic activation of PI3K/Akt and MAPK/Erk1/2 signaling pathways in bovine herpesvirus type 1 infection of MDBK cells. *Veterinary Research,* 42.

Zhu, Y., Chen, G., Lv, F., Wang, X., Ji, X., Xu, Y., Sun, J., Wu, L., Zheng, Y. T. & Gao, G. 2011b. Zinc-finger antiviral protein inhibits HIV-1 infection by selectively targeting multiply spliced viral mRNAs for degradation. *Proc Natl Acad Sci U S A,* 108**,** 15834-9.

Ziebuhr, J., Snijder, E. J. & Gorbalenya, A. E. 2000. Virus-encoded proteinases and proteolytic processing in the Nidovirales. *J Gen Virol,* 81**,** 853-79.

Zúñiga, S., Cruz, J. L. G., Sola, I., Mateos-Gómez, P. A., Palacio, L. & Enjuanes, L. 2010. Coronavirus Nucleocapsid Protein Facilitates Template Switching and Is Required for Efficient Transcription. *Journal of Virology,* 84**,** 2169-2175.

# Appendix 1

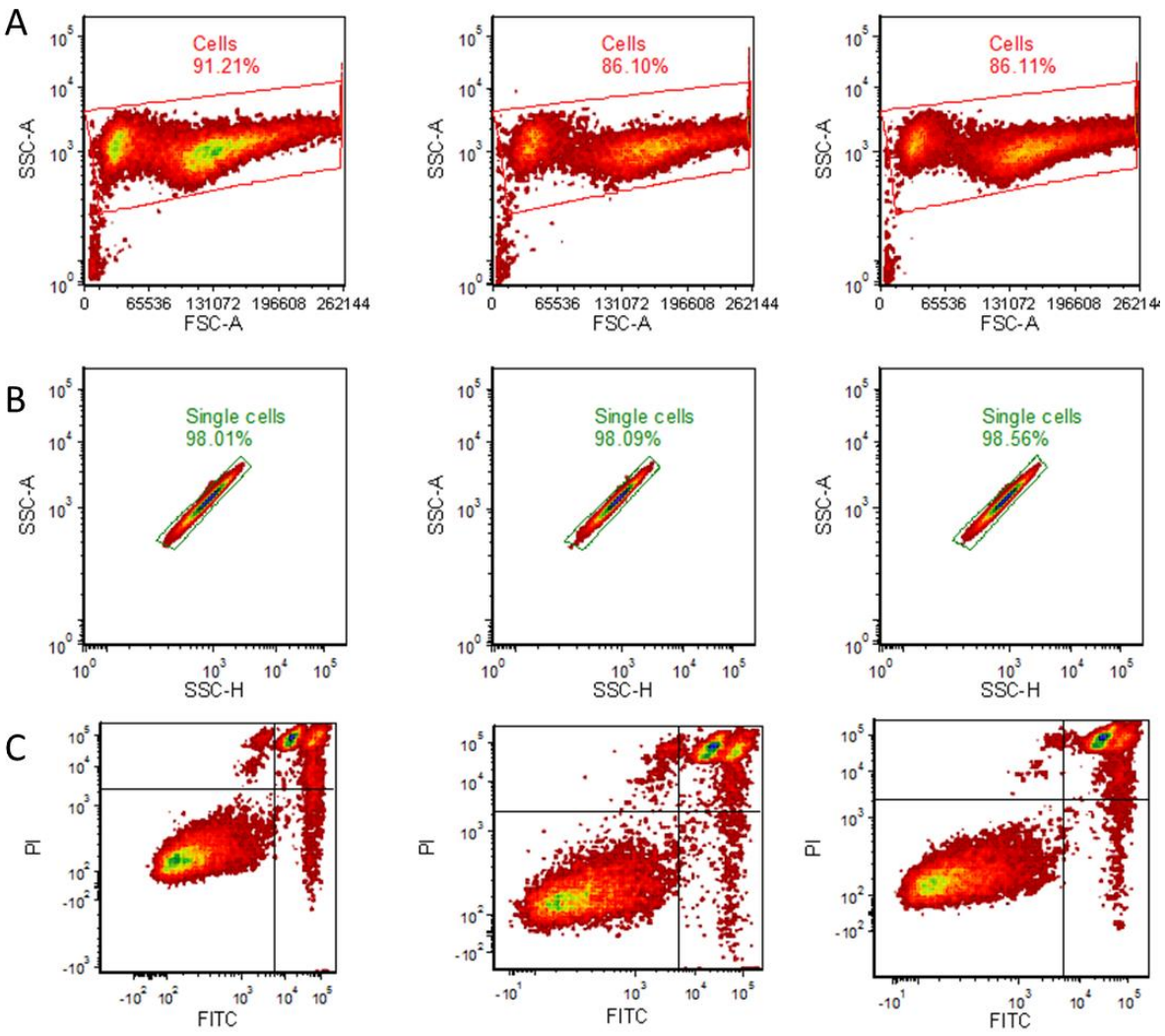


| Gate | # of Events | % of gated cells | % of all cells |
|---|---|---|---|
| UL | 324 | 3.42 | 3.06 |
| UR | 2239 | 23.63 | 21.12 |
| LL | 6136 | 64.75 | 57.89 |
| LR | 777 | 8.20 | 7.33 |

| Gate | # of Events | % of gated cells | % of all cells |
|---|---|---|---|
| UL | 192 | 3.18 | 2.68 |
| UR | 1541 | 25.49 | 21.53 |
| LL | 3964 | 65.56 | 55.37 |
| LR | 349 | 5.77 | 4.87 |

| Gate | # of Events | % of gated cells | % of all cells |
|---|---|---|---|
| UL | 198 | 1.98 | 1.68 |
| UR | 2539 | 25.36 | 21.52 |
| LL | 6689 | 66.81 | 56.70 |
| LR | 586 | 5.85 | 4.97 |

**Appendix 1. Flow cytometry data from mock infected DF1 cells labelled for cell death and apoptosis.** DF1 cells were mock infected and at 24 hpi labelled with Annexin V conjugated to FITC (to indicate apoptosis) or PI (to indicate cell death). Each column indicates a single experimental replicate. (A) Cells were gated for independently of cellular debris. (B) Single cells were gated for. (C) Annexin V FITC vs PI plots with quadrant gates and statistics in table. Upper left (UL) quadrant representative of necrotic cells negative for FITC. Upper right (UR) quadrant representative of necrotic or late apoptotic cells. Lower left (LL) quadrant representative of live Annexin V and PI negative cells. Lower right (LR) quadrant representative of early apoptotic cells and PI negative.

# Appendix 2

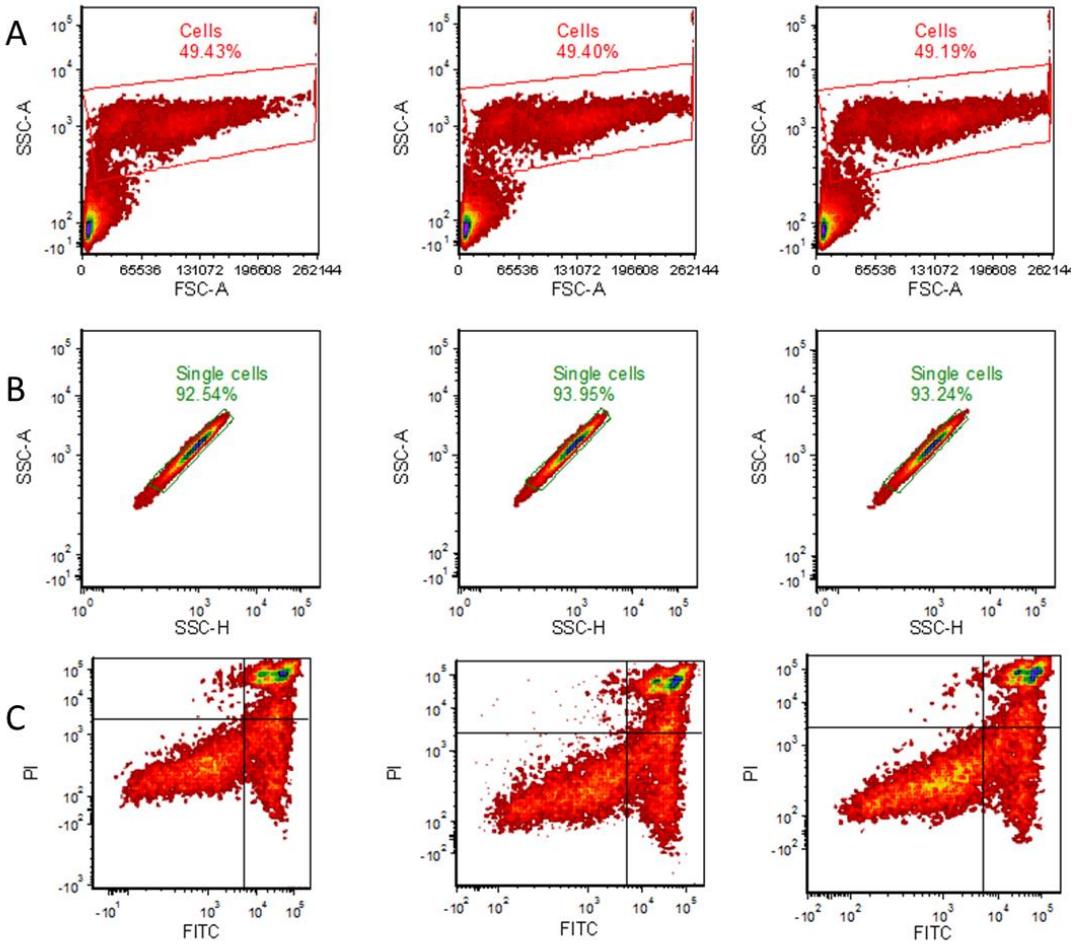


| Gate | # of Events | % of gated cells | % of all cells |
|---|---|---|---|
| UL | 148 | 2.29 | 1.05 |
| UR | 1954 | 30.18 | 13.81 |
| LL | 2708 | 41.83 | 19.13 |
| LR | 1664 | 25.70 | 11.76 |

| Gate | # of Events | % of gated cells | % of all cells |
|---|---|---|---|
| UL | 118 | 1.77 | 0.82 |
| UR | 1952 | 29.30 | 13.60 |
| LL | 2828 | 42.44 | 19.70 |
| LR | 1765 | 26.49 | 12.30 |

| Gate | # of Events | % of gated cells | % of all cells |
|---|---|---|---|
| UL | 105 | 1.63 | 0.75 |
| UR | 1701 | 26.34 | 12.08 |
| LL | 3082 | 47.72 | 21.89 |
| LR | 1571 | 24.32 | 11.16 |

**Appendix 2. Flow cytometry data from DF1 cells treated with staurosporine and labelled for cell death and apoptosis.** DF1 cells were treated with staurosporine and at 24 hpi labelled with Annexin V conjugated to FITC (to indicate apoptosis) or PI (to indicate cell death). Each column indicates a single experimental replicate. (A) Cells were gated for independently of cellular debris. (B) Single cells were gated for. (C) Annexin V FITC vs PI plots and statistics in table. Upper left (UL) quadrant representative of necrotic cells negative for FITC. Upper right (UR) quadrant representative of necrotic or late apoptotic cells. Lower left (LL) quadrant representative of live Annexin V and PI negative cells. Lower right (LR) quadrant representative of early apoptotic cells and PI negative.

# Appendix 3

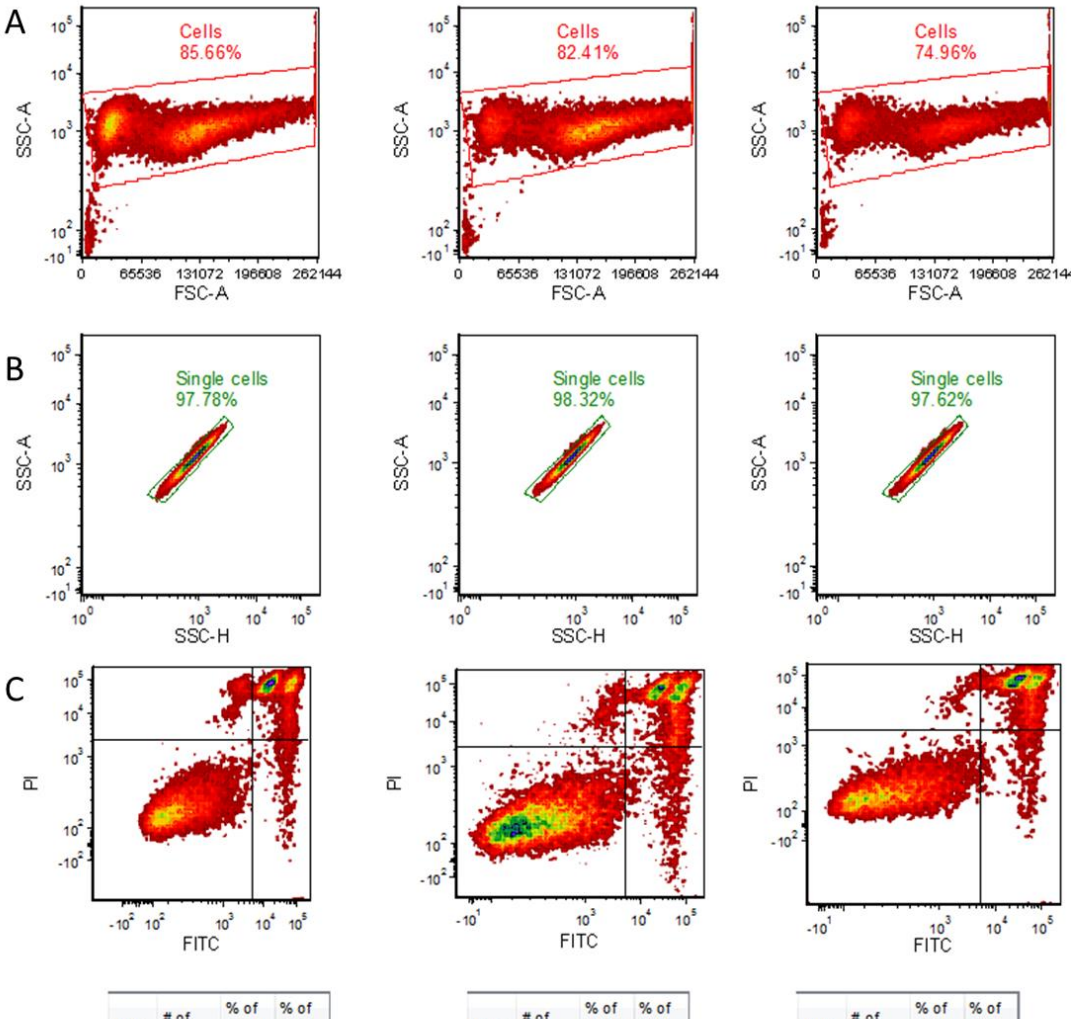


| Gate | # of Events | % of gated cells | % of all cells |
|---|---|---|---|
| UL | 548 | 4.83 | 4.04 |
| UR | 3464 | 30.51 | 25.56 |
| LL | 6585 | 58.00 | 48.58 |
| LR | 756 | 6.66 | 5.58 |

| Gate | # of Events | % of gated cells | % of all cells |
|---|---|---|---|
| UL | 263 | 3.10 | 2.51 |
| UR | 1761 | 20.73 | 16.79 |
| LL | 5899 | 69.43 | 56.26 |
| LR | 573 | 6.74 | 5.46 |

| Gate | # of Events | % of gated cells | % of all cells |
|---|---|---|---|
| UL | 180 | 2.78 | 2.04 |
| UR | 2078 | 32.13 | 23.51 |
| LL | 3762 | 58.16 | 42.56 |
| LR | 448 | 6.93 | 5.07 |

**Appendix 3. Flow cytometry data from IBV infected DF1 cells labelled for cell death and apoptosis.** DF1 cells were infected with IBV and at 24 hpi labelled with Annexin V conjugated to FITC (to indicate apoptosis) or PI (to indicate cell death). Each column indicates a single experimental replicate. (A) Cells were gated for independently of cellular debris. (B) Single cells were gated for. (C) Annexin V FITC vs PI plots and statistics in table. Upper left (UL) quadrant representative of necrotic cells negative for FITC. Upper right (UR) quadrant representative of necrotic or late apoptotic cells. Lower left (LL) quadrant representative of live Annexin V and PI negative cells. Lower right (LR) quadrant representative of early apoptotic cells and PI negative.

# Appendix 4 – Reference genes for qPCR in IBV studies, Batra et al (2016)

**Publisher:** Taylor & Francis & Houghton Trust Ltd
**Journal:** *Avian Pathology*
**DOI:** 10.1080/03079457.2016.1235258

**Selection of reference genes for gene expression analysis by real-time qPCR in avian cells infected with infectious bronchitis virus**

Ambalika Batra[1,2], Helena J. Maier[1], Mark S. Fife[1]

[1]Avian Viral Diseases, The Pirbright Institute, Ash Road, Pirbright, GU21 0NF, UK

[2] Institute of Infection and Global Health, University of Liverpool, 8 West Derby Street, Liverpool, L69 7BE, UK

Short title: Reference genes for qPCR in IBV studies

Corresponding Author: Mark Fife - mark.fife@pirbright.ac.uk

This work was supported by the BBSRC BB/J016837/1; BBSRC BB/L003996/1 and BBSRC Pirbright Institute core strategic grant studentship fund.

**Abstract (250 words max)**

Infectious bronchitis virus (IBV) causes infectious bronchitis in poultry, a respiratory disease that is a source of major economic loss to the poultry industry. Detection and the study of the molecular pathogenesis of the virus often involves the use of real-time quantitative PCR assays (qPCR). To account for error within the experiments, the levels of target gene transcription are normalised to that of suitable reference genes. Despite publication of the MIQE guidelines in 2009, single un-tested reference genes are often used for normalization of

qPCR assays in avian research studies. Here we use the geNorm algorithm to identify suitable reference genes in different avian cell types during infection with apathogenic and pathogenic strains of IBV. We discuss the importance of selecting an appropriate experimental sample subset for geNorm analysis, and show the effect that this selection can have on resultant reference gene selection. The effects of inappropriate normalization on the transcription pattern of a cellular signalling gene, *AKT1*, and the interferon-inducible, *MX1*, were studied. We identify the possibility of the misinterpretation of qPCR data when an inappropriate normalisation strategy is employed. This is most notable when measuring the transcription of *AKT1*, where changes are minimal during infection.

**Keywords**

Infectious bronchitis virus, reference gene selection, Real-time quantitative PCR, geNorm, normalisation

**Introduction**

Infectious bronchitis is one of the most economically detrimental diseases to the poultry industry. The infection, caused by the gammacoronavirus, infectious bronchitis virus (IBV), initially establishes itself within the respiratory tract and often leads to secondary bacterial infections. The emergence of new strains and the lack of cross protection between them mean that effective vaccines that fully protect against IBV are difficult to develop. Early and quick detection of the virus is therefore important for the control of the disease. IBV has historically been detected via various methods including virus isolation in embryonated eggs, tracheal organ cultures or immunoassays. These methods however are expensive and time consuming and therefore, the use of broadly targeted multi-probe qPCR assays are more often used (Hewson et al., 2009; Muradrasoli et al., 2009). In these assays the transcription of strain

specific viral genes are measured and the levels of viral RNA are normalised to host reference genes. The selection of the most stable reference genes is important to compensate for any errors in sample preparation and processing. The study of the replication of infectious bronchitis virus, like many other viruses infecting non-model species, is often hindered by the absence of molecular reagents. However, with the design of primer and probes, qPCR is often used for the study of the molecular basis of viral replication. In this study we investigate the effects of inaccurate normalisation on two host genes. The interferon-induced *MX1* gene and *AKT1*, encoding for a cellular signalling protein. The transcription profiles of both genes are predicted to be different during infection, with *MX1* transcription altered by viral infection. On the contrary, activity of AKT1 is known to be modulated by phosphorylation at the protein level and therefore gene transcription is unlikely to be altered due to virus infection.

In a previous study, *GAPDH* and *UB* were identified as suitable reference genes in IBV-M41 infected SPF chickens (Fan et al., 2012). In the study, Fan et al provide an indication of potentially suitable reference genes in IBV infected tissues. There is, however, a need to identify the most stable reference genes for each individual experimental condition by the use of algorithms such as geNorm (Vandesompele et al., 2002), Normfinder (Andersen et al., 2004) or BestKeeper (Pfaffl et al., 2004), this is discussed in the MIQE guidelines published in 2009 (Bustin et al., 2009). Several studies have also investigated the implications of inappropriate normalisation (Dheda et al., 2005; Tricarico et al., 2002). Staines et al (2016) discuss the importance of reference gene selection and compare the different normalization methods available. It is now widely accepted that multiple reference genes must be used to normalize data, however many recent studies have recommended a set of reference genes for the study of gene expression in avian species (Bages et al., 2015; Borowska et al., 2016; Chapman et al., 2016; Nascimento et al., 2015; Olias et al., 2014; Yin et al., 2011), or

particular avian viral infections (W. Q. Fan et al., 2012; Li et al., 2005; Yang et al., 2013; Yue et al., 2010). Yang et al. (2013) recommend the use of *RPL30* and *SDHA* as reference genes for mRNA transcription analysis in chicken embryo fibroblasts (CEF) infected with avian leucosis virus. The stability of reference genes in CEFs infected with Newcastle disease virus was also investigated and *ACTB*, *HPRT1* and *HMBS* were recommended for use in such studies (Yin et al., 2011) . Whilst the majority of these publications discuss the implications of inappropriate normalisation methods, they recommend a set of reference genes identified as being suitable for a particular set of experimental data. These studies may give an indication as to appropriate reference genes for certain experimental conditions. However, these genes should be used as candidate reference genes only, and their stability be measured for each experimental condition independently. This strategy is not often employed in avian viral research. The present study discusses the design of geNorm analysis studies and the implications of inappropriate normalization on the measurement of host gene transcription during IBV infection of avian cells.

**Materials and Methods**

**Cell culture and virus strains.** Chick kidneys were prepared from 2 to 3 week old specific pathogen free (SPF) Rhode Island Red chickens. Primary chick kidney cells (CK cells) were prepared as described previously (Hennion & Hill, 2015). DF1 cells (Himly et al., 1998) were maintained in 1x DMEM (Sigma) supplemented with 10% FCS and 100U Pen/Strep.
IBV Beau-R is an apathogenic molecular clone of Beaudette-CK described previously (Casais et al., 2001). M4-CK is a pathogenic strain of IBV adapted to grow in CK cells, here referred to as M41(Darbyshire et al., 1979).

**Sample preparation and experimental design.** CK cells were infected with IBV-Beau-R (MOI 1), IBV-M41 (MOI 1) or mock infected. At 12 and 24 hours post infection the RNA was

extracted using RNeasy Mini kit (Qiagen). RNA was quantified using a Nanodrop (Thermo Scientific). One µg of RNA was reverse transcribed using Superscript III (Invitrogen) according to manufacturer's protocol including a DNase step and using random primers (Promega).

**Selection of appropriate reference genes.** SYBR Green qPCR was performed using Power SYBR Green Master Mix (ThermoFisher Scientific). Primers were used at a final concentration of 0.8 µM and sequences are shown in Table 1 (Staines et al., 2016). The qPCR was run on a 7500 Fast Real Time System (Applied Biosystems) with the following cycle profile: 95 °C for 10 mins and then 40 cycles at 95 °C for 15 sec and 60 °C for 30 sec. A dissociation step was included for melt curve analysis. The raw CT values were analyzed using the geNorm algorithm through the qbase+ software (Biogazelle).

**Measurement of gene transcription by qPCR.** TaqMan qPCR was performed using TaqMan® Fast Universal PCR 2x Master Mix (ThermoFisher Scientific). Primers were used at 500nM and hydrolysis probes at 125nM final concentrations (primer and probe sequences are shown in Table 2 (Staines et al., 2016)). The qPCR was run on a 7500 Fast Real Time System (Applied Biosystems) with the following cycle profile: 95 °C for 1 mins and then 40 cycles at 95 °C for 10 sec and 60 °C for 30 sec. IBV 5′UTR primer and hydrolysis probe sequences were as follows: IBV5′ Forward, 5′-GCTTTTGAGCCTAGCGTT-3′; IBV5′ Reverse 5′-GCCATGTTGTCACTGTCTATTG-3′; and IBV 5′ probe, 5′ (FAM)-CACCACCAGAACCTGTCACCTC-(TAMRA)-3′ (Maier et al., 2013).



## Results

**Selection of samples for geNorm analysis.** CK cells were infected with a pathogenic (M41) and apathogenic (Beau-R) strain of IBV and RNA collected at 12 and 24 hpi. The viral genome copy number was quantitated by qPCR using a standard curve (Figure 1). Viral

genome copy number was normalised to a mock infected sample at each time point. An increase in genome copies can be seen from 12 to 24 hpi with similar levels of Beau-R and M41 genome being produced at each time point. A SYBR green qPCR was then performed using primer sets previously described by Staines et al (2016). The stability factors of candidate reference genes were established by imputing CT values of gene transcription into the geNorm algorithm. Of the three replicates, one from each experimental subset was chosen for testing. The relative stability of 9 candidate genes was ranked by geNorm M value, with the more stable genes having the lowest value. The stability of the candidate reference genes in CK cells infected with Beau-R and M41 are shown (Figure 2 (a)). The reference genes were ranked according to their stability, from lowest to highest as; *28s rRNA*, *TBP*, *RPLP0*, *RPL13*, *GAPDH*, *HPRT1*, *PGK1*, *HMBS* and *ACTB*. The geNorm V values (not shown) recommend the optimal number of reference genes to be used. In this case the results of the algorithm suggest that the addition of the third most stable reference gene, *PGK1*, to *ACTB* and *HMBS* does not significantly increase the stability of the reaction. Therefore it is recommended that *ACTB* and *HMBS* be used as reference genes in this experimental set up.

The importance of using an appropriate subset of data was investigated by removing sections of data from the analysis. Figure 2 (b) and (c) show the candidate reference genes ranked according to stability in CK cells infected with Beau-R and M41 at 12 hpi or 24 hpi, respectively. The stability of the reference genes changes depending on which subset of data is used. The most suitable reference genes at 12 hpi are *HMBS* and *RPL13* whereas at 24 hpi they are *ACTB* and *HPRT1*. Differences in the stability of reference genes when CK cells were infected with the different strains of IBV, Beau-R (Figure 2 (d)) and M41 (Figure 2 (e)) were investigated. Here again, the most appropriate reference genes are different between the different experimental setups with *HMBS* and *ACTB* being more stable in CK cells infected

with Beau-R and *HPRT1* and *TBP* being the most suitable genes in CK cells infected with M41.

In addition to the primary CK cells, the apathogenic strain Beau-R is able to infect the continuous avian cell line, DF1 cells. DF1 cells were infected with Beau-R and RNA extracted at 12 and 24 hpi. Viral genome copy number was quantified by qPCR and an increase in viral genome copy number can be seen between 12 and 24 hpi (Figure 3). SYBR green qPCR assays were performed using the primer sets described in Table 1, and the raw data analyzed using the geNorm algorithm. The reference genes in order of stability in DF1 cells infected with Beau-R at 12 and 24 hpi were; *28s rRNA*, *GAPDH*, *ACTB*, *TBP*, *RPLP0*, *PGK1*, *HPRT1*, *HMBS* and *RPL13* (Figure 4 (a)). The geNorm V values (not shown) recommend the use of the first two reference genes for these experimental samples, *HMBS* and *RPL13*. Once more, the effect of selecting a smaller subset of the data was investigated. The two most suitable reference genes in the 12 hpi samples of DF1 cells infected with Beau-R were *HPRT1* and *HMBS* where as *ACTB* was the least stable (Figure 4 (b)). At 24 hpi the most stable reference genes were *PGK1* and *GAPDH* (Figure 4 (c)). The variation in the stability of reference genes is consistent across the cell types, virus strain and time points examined.

**Effect of inappropriate normalisation.** The selection of appropriate reference genes has been discussed at length as being important for the accurate analysis of gene expression levels. The two genes with the highest stability measure in DF1 cells infected with Beau-R at 12 and 24 hpi were found to be *HMBS* and *RPL13*. The effect of inappropriate normalisation on studies of gene transcription was investigated. The transcription of avian *AKT1* was compared to that of the interferon-inducible avian *MX1* when normalised using different reference genes (Figure 5). The most suitable reference genes as identified by geNorm (*RPL13* and *HMBS*)

were compared to the use of single, commonly used, reference genes with low stability values, *ACTB* and *28s rRNA*. Figure 5a and b respectively show a significant change, calculated by unpaired t-test, in transcription of both *AKT1* ($P$=0.0025) and *MX1* ($P$ =0.0382) over time during infection, when normalised to *RPL13* and *HMBS*. The use of a single reference gene changes the significance of the data. This is most notably different in the *AKT1* data where changes in transcription are smaller than those of *MX1* during infection. For example changes *AKT1* transcription normalised to *RPL13* and *HMBS* has $P$ =0.0025 (Figure 5 (a)) whereas, when the same Ct values are normalised to *ACTB*, $P$ =0.3170 (Figure 5 (b)). However, the change in the significance of *MX1* transcription is not as different, where $P$ =0.0382 when normalised to *RPL13* and *HMBS* (Figure 5 (b)) compared to $P$ =0.0903 when normalised to *ACTB* (Figure 5 (d)). The use of *28s rRNA* as a single reference gene was also investigated. The change in significance of *AKT1* gene expression (from $P$ =0.0025 to 0.0213) was seen (Figures 5 (a) and 5 (e)), however this change is less notable for *MX1* transcription (Figures 5 (b) and 5 (f)).

**Discussion**

Limitations that prevent the use of reference gene stability analysis include lack of sufficient sample, time and cost of reagent. A cross sectional subset of samples is therefore often used, and the choice of samples has an impact on the outcome of the calculation of reference gene stability. In this study the transcription of candidate reference genes in one batch of three replicates was analyzed, as viral genome copy number had previously been found to be consistent throughout the samples. We were interested to investigate whether selecting a smaller subset of the samples would have had an effect on the stability measure of the reference genes. The stability changed depending on the cell type, strain of virus and the time at which the RNA was collected (Figures 2 and 4). Most notably the stability of *TBP* was

found to be low in CK infected samples except in CK cells infected with M41 at 12 and 24 hpi. Also, a commonly used reference gene, *ACTB*, was found to be one of the more stable genes in CK cells however, that stability was not observed in DF1 cells. Ribosomal RNA has historically been used in avian studies as a reference gene. However, in this study we have found it to be the least stable reference gene out of the candidates in both CK and DF1 cells infected with IBV. This suggests that the selection of an appropriate subset of experimental samples is an important step in accurate normalisation of mRNA transcription levels.

There has been a recent surge in the publication of reference gene stability papers, most of which recommend a set of four to six reference genes for use in a particular experimental setup. Whilst the importance of using multiple reference genes is recognized in these studies, the suggestion that these reference genes may have uniform transcription across different experimental samples performed in different laboratories is misleading. Despite significant improvement in the design and publication of qPCR studies in model species, single reference genes are still used for normalisation of target genes in non-model species such as *Gallus gallus*. We therefore investigated variations in the transcription of two avian genes when normalised to geNorm selected reference genes, *HMBS* and *RPL13* and also *ACTB* and *28s rRNA*. The mRNA expression of *AKT1* was measured along with that of *MX1*, which is known to change during infection with IBV (Cong et al., 2013). We found a significant change in transcription levels of both *AKT1* and *MX1* mRNA during infection from 12 to 24 hpi when normalised correctly to the selected reference genes (Figures 5 (a) and 5 (b)). This correlated with an increase in copies of IBV genome present (Figure 3). When the same raw data was normalised to *ACTB* the statistical significance of the variation was lost and the transcription of mRNA would be interpreted as not changing over time during IBV infection (Figures 5 (c) and 5 (d)). The most notable changes were in the transcription of *AKT1* mRNA (Figures 5(a),

(c), (e)). This highlights that data sets showing small changes in mRNA levels are more susceptible to inappropriate normalisation strategies than those with large changes, such as in the case of *MX1*. Nonetheless, our study clearly demonstrates the importance of correct selection of reference genes for robust analysis of experimental data.

**Acknowledgements**

We thank Simon Gubbins for discussion of the statistical analysis of qPCR data.

**Disclosure statement**

The authors declare no conflict of interest.

**References**

Bages, S., Estany, J., Tor, M., & Pena, R. N. (2015). Investigating reference genes for quantitative real-time PCR analysis across four chicken tissues. *Gene, 561*, 82-87. doi: 10.1016/j.gene.2015.02.016

Borowska, D., Rothwell, L., Bailey, R. A., Watson, K., & Kaiser, P. (2016). Identification of stable reference genes for quantitative PCR in cells derived from chicken lymphoid organs. *Vet Immunol Immunopathol, 170*, 20-24. doi: 10.1016/j.vetimm.2016.01.001

Bustin, S. A., Benes, V., Garson, J. A., Hellemans, J., Huggett, J., Kubista, M., Mueller, R., Nolan, T., Pfaffl, M. W., Shipley, G. L., Vandesompele, J., & Wittwer, C. T. (2009). The MIQE guidelines: minimum information for publication of quantitative real-time PCR experiments. *Clin Chem, 55*, 611-622. doi: 10.1373/clinchem.2008.112797

Casais, R., Thiel, V., Siddell, S. G., Cavanagh, D., & Britton, P. (2001). Reverse genetics system for the avian coronavirus infectious bronchitis virus. *J Virol, 75*, 12359-12369. doi: 10.1128/jvi.75.24.12359-12369.2001

Chapman, J. R., Helin, A. S., Wille, M., Atterby, C., Jarhult, J. D., Fridlund, J. S., & Waldenstrom, J. (2016). A Panel of Stably Expressed Reference Genes for Real-Time qPCR Gene Expression Studies of Mallards (Anas platyrhynchos). *PLoS ONE, 11*, e0149454. doi: 10.1371/journal.pone.0149454

Cong, F., Liu, X., Han, Z., Shao, Y., Kong, X., & Liu, S. (2013). Transcriptome analysis of chicken kidney tissues following coronavirus avian infectious bronchitis virus infection. *BMC Genomics, 14*, 743. doi: 10.1186/1471-2164-14-743

Darbyshire, J. H., Rowell, J. G., Cook, J. K., & Peters, R. W. (1979). Taxonomic studies on strains of avian infectious bronchitis virus using neutralisation tests in tracheal organ cultures. *Arch Virol, 61*, 227-238.

Dheda, K., Huggett, J. F., Chang, J. S., Kim, L. U., Bustin, S. A., Johnson, M. A., Rook, G. A., & Zumla, A. (2005). The implications of using an inappropriate reference gene for real-time reverse transcription PCR data normalization. *Anal Biochem, 344*, 141-143. doi: 10.1016/j.ab.2005.05.022

Fan, W., Wang, H., Zhang, Y., Zhang, A., Fan, W. Q., Wang, H. N., Zhang, Y., & Zhang, A. Y. (2012). Evaluation of the suitability of five housekeeping genes as internal control for quantitative real-time RT-PCR assays in chickens acutely infected with IBV M41 strain. *Journal of Animal and Veterinary Advances, 11*, 3064-3067.

Fan, W. Q., Wang, H. N., Zhang, Y., & Zhang, A. Y. (2012). Evaluation of the Suitability of Five Housekeeping Genes as Internal Control for Quantitative Real-Time RT-PCR Assays in Chickens Acutely Infected with IBV M41 Strain. *Journal of Animal and Veterinary Advances, 11*, 3064-3067.

Hennion, R. M., & Hill, G. (2015). The Preparation of Chicken Kidney Cell Cultures for Virus Propagation. In H. J. Maier, E. Bickerton & P. Britton (Eds.), *Coronaviruses - Methods and Protocols*: Springer Protocols.

Hewson, K., Noormohammadi, A. H., Devlin, J. M., Mardani, K., & Ignjatovic, J. (2009). Rapid detection and non-subjective characterisation of infectious bronchitis virus isolates using high-resolution melt curve analysis and a mathematical model. *Arch Virol, 154*, 649-660. doi: 10.1007/s00705-009-0357-1

Himly, M., Foster, D. N., Bottoli, I., Iacovoni, J. S., & Vogt, P. K. (1998). The DF-1 chicken fibroblast cell line: transformation induced by diverse oncogenes and cell death resulting from infection by avian leukosis viruses. *Virology, 248*, 295-304. doi: 10.1006/viro.1998.9290

Li, Y. P., Bang, D. D., Handberg, K. J., Jorgensen, P. H., & Zhang, M. F. (2005). Evaluation of the suitability of six host genes as internal control in real-time RT-PCR assays in chicken embryo cell cultures infected with infectious bursal disease virus. *Vet Microbiol, 110*, 155-165. doi: 10.1016/j.vetmic.2005.06.014

Maier, H. J., Hawes, P. C., Cottam, E. M., Mantell, J., Verkade, P., Monaghan, P., Wileman, T., & Britton, P. (2013). Infectious bronchitis virus generates spherules from zippered endoplasmic reticulum membranes. *MBio, 4*, e00801-00813. doi: 10.1128/mBio.00801-13

Muradrasoli, S., Mohamed, N., Hornyak, A., Fohlman, J., Olsen, B., Belak, S., & Blomberg, J. (2009). Broadly targeted multiprobe QPCR for detection of coronaviruses: Coronavirus is common among mallard ducks (Anas platyrhynchos). *J Virol Methods, 159*, 277-287. doi: 10.1016/j.jviromet.2009.04.022

Nascimento, C. S., Barbosa, L. T., Brito, C., Fernandes, R. P. M., Mann, R. S., Pinto, A. P. G., Oliveira, H. C., Dodson, M. V., Guimaraes, S. E. F., & Duarte, M. S. (2015). Identification of Suitable Reference Genes for Real Time Quantitative Polymerase Chain Reaction Assays on Pectoralis major Muscle in Chicken (Gallus gallus). *PLoS ONE, 10*. doi: ARTN e012793510.1371/journal.pone.0127935

Olias, P., Adam, I., Meyer, A., Scharff, C., & Gruber, A. D. (2014). Reference genes for quantitative gene expression studies in multiple avian species. *PLoS ONE, 9*, e99678. doi: 10.1371/journal.pone.0099678

Staines, K., Batra, A., Mwangi, W., Maier, H. J., Van Borm, S., Young, J. R., Fife, M., & Butter, C. (2016). A Versitile Panel of Reference Gene Assays for the Measurement of Chicken mRNA by Quantitative PCR. *PLoS ONE* (*in press*)

Tricarico, C., Pinzani, P., Bianchi, S., Paglierani, M., Distante, V., Pazzagli, M., Bustin, S. A., & Orlando, C. (2002). Quantitative real-time reverse transcription polymerase chain reaction: normalization to rRNA or single housekeeping genes is inappropriate for human tissue biopsies. *Anal Biochem, 309*, 293-300.

Yang, F., Lei, X., Rodriguez-Palacios, A., Tang, C., & Yue, H. (2013). Selection of reference genes for quantitative real-time PCR analysis in chicken embryo fibroblasts

infected with avian leukosis virus subgroup J. *BMC Res Notes, 6*, 402. doi: 10.1186/1756-0500-6-402

Yin, R., Liu, X., Liu, C., Ding, Z., Zhang, X., Tian, F., Liu, W., Yu, J., Li, L., Hrabe de Angelis, M., & Stoeger, T. (2011). Systematic selection of housekeeping genes for gene expression normalization in chicken embryo fibroblasts infected with Newcastle disease virus. *Biochem Biophys Res Commun, 413*, 537-540. doi: 10.1016/j.bbrc.2011.08.131

Yue, H., Lei, X. W., Yang, F. L., Li, M. Y., & Tang, C. (2010). Reference gene selection for normalization of PCR analysis in chicken embryo fibroblast infected with H5N1 AIV. *Virol Sin, 25*, 425-431. doi: 10.1007/s12250-010-3114-4

**Table 1.** Primer sequences and accession numbers of candidate reference genes used for geNorm analysis (Staines et al., 2016)

| Gene | | Sequence | Accession Number |
|---|---|---|---|
| *ACTB* | Forward | 5'-CAGGTCATCACCATTGGCAAT-3' | NM_205518 |
| | Reverse | 5'-GCATACAGATCCTTACGGATATCCA-3' | |
| *HMBS* | Forward | 5'-GGTTGAGATGCTCCGTGAGTTT-3' | XM_417846 |
| | Reverse | 5'-GGCTCTTCTCCCCAATCTTAGAA-3' | |
| *HPRT1* | Forward | 5'-TGGTCAAAAGAACTCCTCGAAGT-3' | NM_204848 |
| | Reverse | 5'-TGTAATCGAGGGCGTATCCAA-3' | |
| *PGK1* | Forward | 5'-GTTTATGTCAATGATGCTTTTGGAA-3' | NM_204985 |
| | Reverse | 5'-GCCTTTGCAAAATAATCCAGTTCT-3' | |
| *RPL13* | Forward | 5'-TCGTGCTGGCAGAGGATTC-3' | NM_204999 |
| | Reverse | 5'-TCGTCCGAGCAAACCTTTTG-3' | |
| *RPLP0* | Forward | 5'-TTGTTCATCACCACAAAGATT-3' | NM_204987 |
| | Reverse | 5'-CCCACTTTGTCTCCGGTCTTAA-3' | |
| *TBP* | Forward | 5'-CTTCGTGCCCGAAATGCT-3' | NM_205103 |
| | Reverse | 5'-GCGCAGTAGTACGTGGTTCTCTT-3' | |
| *28s rRNA* | Forward | 5'-GGCGAAGCCAGACCAAACT-3' | X59733 |
| | Reverse | 5'-GACGACCGATTTGCACGTC-3' | |
| *GAPDH* | Forward | 5'-GGTGGTGCTAAGCGTGTTA-3' | X01578 |
| | Reverse | 5'-CCCTCCACAATGCCAA-3' | |

**Table 2.** Primer and probe sequences and accession numbers of *AKT1* and *MX1* genes as well as reference genes.

| Gene | | Sequence | Accession Number |
|---|---|---|---|
| ***AKT1***[a] | Forward | 5'-TCACGGCATCCATTCTTAAACA-3' | NM_205055 |
| | Reverse | 5'-CTTCAGAAAATACACACTCTCTC-3' | |
| | Probe | 5'-AAAACAACTCCCCTCCGTTAGCATACTCCA(BHQ)-3' | |
| ***MX1***[b] | Forward | 5'-CACTGCAACAAGCAAAGAAGGA-3' | NM_204609.1 |
| | Reverse | 5'-TGATCAACCCCACAAGGAAAA-3' | |
| | Probe | 5'(FAM)-ACAAAGCACACACCCAACTGTCAGCG-(TAMRA)-3' | |
| ***HMBS*** | Forward | 5'-GGTTGAGATGCTCCGTGAGTTT-3' | XM_417846 |
| | Reverse | 5'-GGCTCTTCTCCCCAATCTTAGAA-3' | |
| | Probe | 5'-(FAM)-CCTGACCTCTGCTTTGAGATTGTTGCCA-(TAMRA)-3' | |
| ***RPL13*** | Forward | 5'-TCGTGCTGGCAGAGGATTC-3' | NM_204999 |
| | Reverse | 5'-TCGTCCGAGCAAACCTTTTG-3' | |
| | Probe | 5'-(FAM)-TAATGCCCGCCAGTTTAAGCTCTTCTAGGC-(TAMRA)-3' | |
| ***ACTB*** | Forward | 5'-CAGGTCATCACCATTGGCAAT-3' | NM_205518 |
| | Reverse | 5'-GCATACAGATCCTTACGGATATCCA-3' | |
| | Probe | 5'-(FAM)-CACAGGACTCCATACCCAAGAAAGATGGC-(TAMRA)-3' | |
| ***28s rRNA*** | Forward | 5'-GGCGAAGCCAGACCAAACT-3' | X59733 |
| | Reverse | 5'-GACGACCGATTTGCACGTC-3' | |
| | Probe | 5'-(FAM)-AGGACCGCTACGGACCTCCACCA-(TAMRA)-3' | |

[a]AKT1 primers and probe designed and produced by Primerdesign Ltd., UK
[b]MX1 primer and probe designed by William Mwangi, The Pirbright Institute, UK

**Figure Captions**

**Figure 1**. Viral genome copy number in CK cells infected with IBV. CK cells were infected with IBV Beau-R and M41 strains and at 12 and 24 hpi cells were lysed and RNA extracted. Viral genome was amplified by qPCR of the 5′UTR region of the genome. CT values were compared to a standard curve to calculate genome copy number. Copy number was normalised to control mock levels and the average of three replicates is plotted as viral genome copy number (±SEM).

**Figure 2.** Transcriptional stability of candidate reference genes in IBV infected CK cells. CK cells were infected with IBV Beau-R and M41 and at 12 and 24 hpi cells were lysed and RNA extracted. Candidate reference gene mRNA was amplified by SYBRgreen qPCR. The transcriptional stability of the candidate reference genes is calculated by inputting CT values into the geNorm algorithm. The geNorm algorithm calculates the M value, a representation of the stability of the reference genes. The lower the M value, the more stable the gene between the experimental samples. (a) The geNorm M values of candidate reference genes in CK cells infected with mock, BeauR or M41 at 12 and 24 hpi. GeNorm M values of candidate reference gene transcription in CK cells infected with Beau-R and M41 at 12 hpi (b) or 24 hpi (c). M values of candidate reference gene transcription in CK cells infected with Beau-R (d) or M41 (e) at 12 and 24 hpi.

**Figure 3.** Viral genome copy number in DF1 cells infected with Beau-R. DF1 cells were infected with IBV Beau-R and at 12 and 24 hpi cells were lysed and RNA extracted. Viral genome present was amplified by qPCR of the 5′UTR region of the genome. CT values were compared to a standard curve to calculate genome copy number. Copy number was normalised to control mock levels and the average of three replicates is plotted as viral genome copy number (±SEM).

**Figure 4.** Transcriptional stability of candidate reference genes in IBV infected DF1 cells. DF1 cells were mock infected or infected with IBV Beau-R and at 12 and 24 hpi cells were lysed and RNA extracted. Candidate reference gene mRNA was amplified by SYBRgreen qPCR. The transcriptional stability of the candidate reference genes is calculated by entering CT values into the geNorm algorithm. The geNorm algorithm calculates the M value which is a representation of the transcriptional stability of the candidate reference genes. The lower the M value, the more stable the gene. (a) The M values of candidate reference genes in DF1 cells infected with mock and Beau-R at 12 and 24 hpi. The M values of candidate reference gene transcription in DF1 cells infected with mock or Beau-R at 12 (b) or 24 hpi (c).

**Figure 5.** Transcription of *AKT1* and *MX1* genes normalised to various reference genes. DF1 cells were infected with mock or Beau-R and at 12 and 24 hpi cells were lysed and RNA extracted. *AKT1* and *MX1* mRNA was amplified by qPCR and transcription calculated using ΔΔCT and normalising to *RPL13* and *HMBS*, *ACTB* or *28s rRNA*. (a) *AKT1* transcription normalised to *RPL13* and *HMBS*. (b) *MX1* transcription normalised to *RPL13* and *HMBS*. (c) *AKT1* transcription normalised to *ACTB*. (d) *MX1* transcription normalised to *ACTB*. (e) *AKT1* transcription normalised to *28s rRNA*. (f) *MX1* transcription normalised to *28s rRNA*. *P* values calculated by two-tailed t-test.

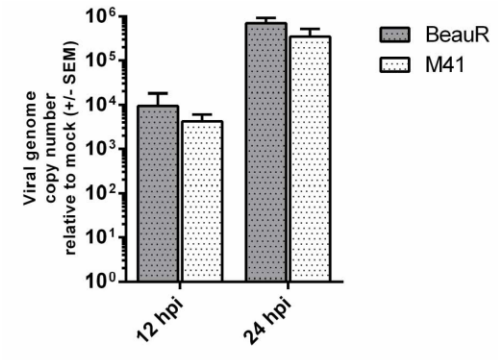

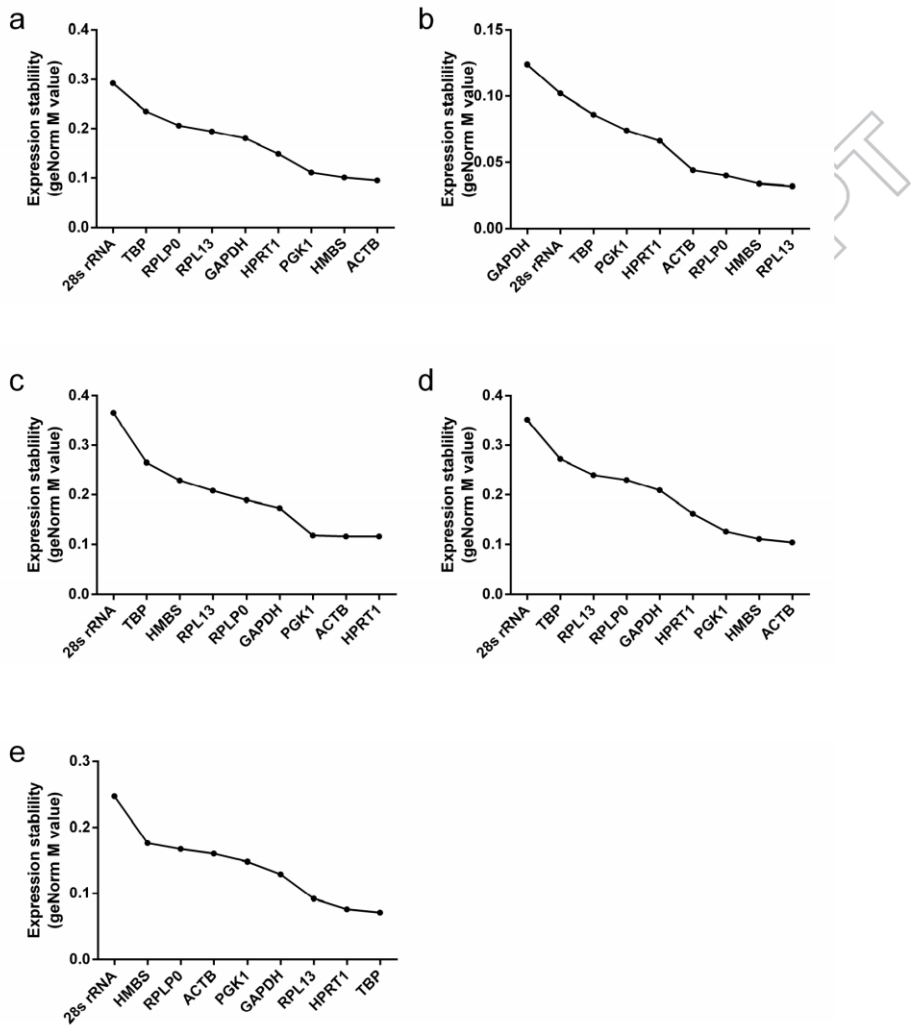
a
Expression stability (geNorm M value)
0.4
0.3
0.2
0.1
0.0
28s rRNA
TBP
RPLP0
RPL13
GAPDH
HPRT1
PGK1
HMBS
ACTB
b
Expression stability (geNorm M value)
0.15
0.10
0.05
0.00
GAPDH
28s rRNA
TBP
PGK1
HPRT1
ACTB
RPLP0
HMBS
RPL13
c
Expression stability (geNorm M value)
0.4
0.3
0.2
0.1
0.0
28s rRNA
TBP
HMBS
RPL13
RPLP0
GAPDH
PGK1
ACTB
HPRT1
d
Expression stability (geNorm M value)
0.4
0.3
0.2
0.1
0.0
28s rRNA
TBP
RPL13
RPLP0
GAPDH
HPRT1
PGK1
HMBS
ACTB
e
Expression stability (geNorm M value)
0.3
0.2
0.1
0.0
28s rRNA
HMBS
RPLP0
ACTB
PGK1
GAPDH
RPL13
HPRT1
TBP

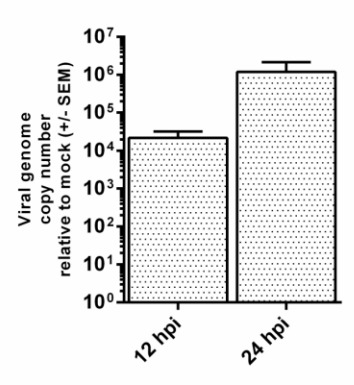

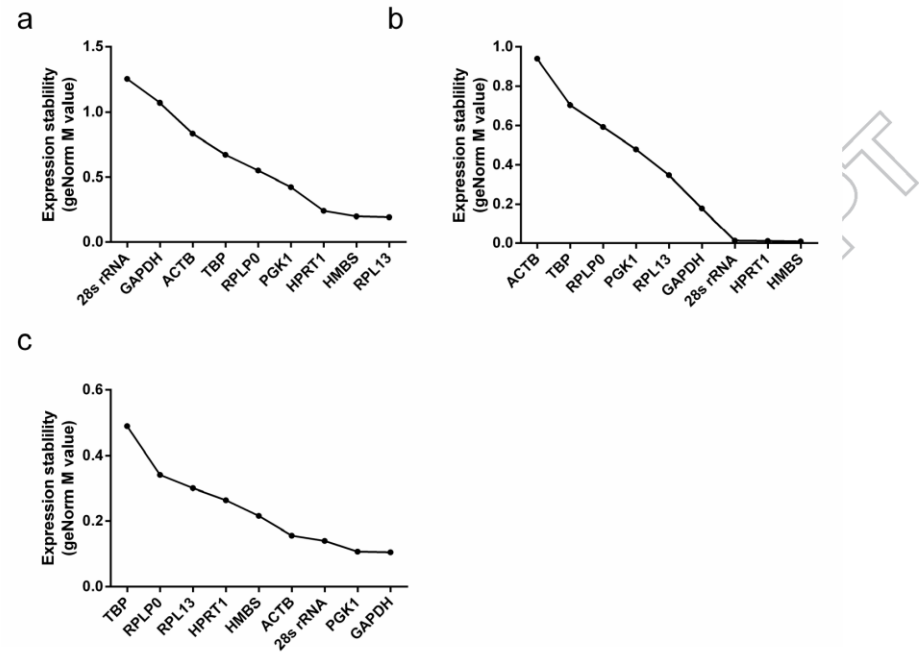
a
Expression stability (geNorm M value)
1.5
1.0
0.5
0.0
28s rRNA
GAPDH
ACTB
TBP
RPLP0
PGK1
HPRT1
HMBS
RPL13
b
Expression stability (geNorm M value)
1.0
0.8
0.6
0.4
0.2
0.0
ACTB
TBP
RPLP0
PGK1
RPL13
GAPDH
28s rRNA
HPRT1
HMBS
c
Expression stability (geNorm M value)
0.6
0.4
0.2
0.0
TBP
RPLP0
RPL13
HPRT1
HMBS
ACTB
28s rRNA
PGK1
GAPDH

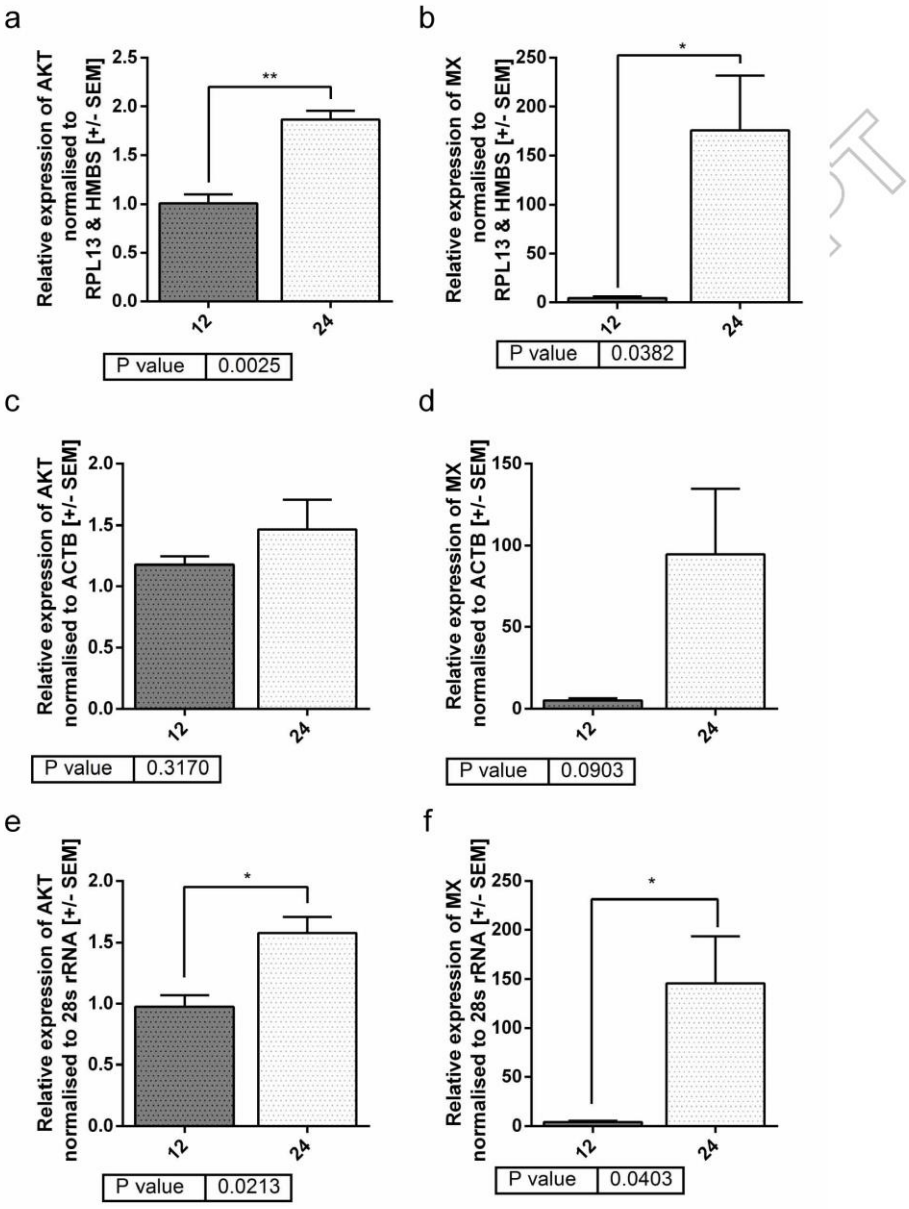
a
Relative expression of AKT normalised to RPL13 & HMBS [+/- SEM]
2.5
2.0
1.5
1.0
0.5
0.0
**
12
24
P value
0.0025
b
Relative expression of MX normalised to RPL13 & HMBS [+/- SEM]
250
200
150
100
50
0
*
12
24
P value
0.0382
c
Relative expression of AKT normalised to ACTB [+/- SEM]
2.0
1.5
1.0
0.5
0.0
12
24
P value
0.3170
d
Relative expression of MX normalised to ACTB [+/- SEM]
150
100
50
0
12
24
P value
0.0903
e
Relative expression of AKT normalised to 28s rRNA [+/- SEM]
2.0
1.5
1.0
0.5
0.0
*
12
24
P value
0.0213
f
Relative expression of MX normalised to 28s rRNA [+/- SEM]
250
200
150
100
50
0
*
12
24
P value
0.0403

20